WIDEBAND MODELLING AND PARAMETER ESTIMATION OF TWO-WINDING TRANSFORMERS

C. C. Brozio

Dissertation presented for the Degree of Doctor of Philosophy (Electrical Engineering) at the University of Stellenbosch.

Promoter: Dr. H. J. Vermeulen

December 1999

Declaration

I, the undersigned, hereby declare that the work contained in this dissertation is my own original work and that I have not previously in its entirety or in part sumitted it at any university for a degree.

Cornel Cristan Brozio

Stellenbosch, December 1999

Abstract

This dissertation proposes a new wideband, lumped-parameter equivalent-circuit transformer model that is suitable for parameter estimation applications, while reflecting the internal electromagnetic behaviour of the transformer in its structure. Frequency-dependence of the resistive and inductive model elements is investigated experimentally and provision is made for these effects in the model structure. A procedure by which the parameters of the proposed model structure can be estimated directly from terminal frequency response measurements is developed and applied to a 16 kVA, 22 kV / 220 V single-phase distribution transformer and a 11 kV / 110 V single-phase voltage transformer. The transformer model is validated by applying it to frequency-domain and time- domain simulations in the frequency range between 10 Hz and 100 kHz. The results show that the proposed model is able to accurately predict transformer responses in this frequency range, including all prominent winding resonances. The physical significance of the model structure is validated by comparing the frequency response of the voltage induced in a search coil around the core of the 11 kV / 110 V voltage transformer to the magnetizing branch voltage predicted by the model. From this comparison it could be concluded that the proposed transformer model correctly represents the magnetic coupling between the transformer windings.

Keywords: Transformer, Wideband modelling, Parameter estimation

Opsomming

In hierdie proefskrif word 'n nuwe wyeband, saamgevoegde-parameter, ekwivalente stroombaan transformator-modelstruktuur voorgestel. Hierdie modelstruktuur is geskik vir die toepassing van parameter afskattingsmetodes en weerspieël die interne elektromagnetiese gedrag van die transformator. Frekwensieafhanklikheid van die resistiewe en induktiewe modelelemente word eksperimenteel ondersoek en voorsiening vir hierdie effekte word in die modelstruktuur gemaak. 'n Metodiek waardeur die parameters van die voorgestelde model vanaf terminaal frekwensieweergawe-metings afgeskat kan word, is ontwikkel en word toegepas op 'n 16 kVA, 22 kV / 220 V enkelfase distribusietransformator en 'n 11 kV / 110 V enkelfase spanningstransformator. Die geldigheid van die transformatormodel word bevestig deur dit in die frekwensiebereik tussen 10 Hz en 100 kHz toe te pas, in frekwensiegebied- en tydgebied-simulasies. Die resultate toon dat die voorgestelde model akkurate voorspellings van transformatorweergawes in hierdie frekwensiebereik lewer, insluitende alle prominente windingsresonansies. Die geldigheid van die modelstruktuur, ten opsigte van die interne elektromagnetiese gedrag van die transformator, is ondersoek deur die frekwensieweergawe van die spanning wat in 'n soekspoel om die kern van die 11 kV / 110 V spanningstransformator geïnduseer word, te vergelyk met die magnetiserings-takspanning wat deur die model voorspel word. Hieruit kon die gevolgtrekking bereik word dat die voorgestelde transformator modelstruktuur die magnetiese koppeling tussen die transformatorwindings korrek verteenwoordig.

Sleutelwoorde: Transformator, Wyeband modellering, Parameter afskatting

Acknowledgements

I would like to thank the following individuals and institutions for their contributions and support:

- My promotor, Dr. Johan Vermeulen, for his encouragement and support throughout this project. Our many informal discussions were especially helpful and constructive.
- The University of Stellenbosch and the FRD/Eskom Tertiary Education Support Programme for providing the facilities and financial assistance that made this project possible.
- Karel Cornelissen, who was responsible for the development and implementation of the PRBS source, Sven Ladewig, who conducted the stepped-frequency transformer response measurements and Jacques Germishuizen, who performed the low-voltage impulse response measurements.
- NEI Transformers, formerly Power Engineers, for providing the 16 kVA distribution transformer.

A special word of appreciation to my wife Heather and my daughters Sarah and Liesl, for their unfailing support, constant encouragement and understanding.

Cornel Brozio
December 1998

Table of Contents

Nomenclature

Symbols

a	Transformer turns ratio
B	Magnetic flux density
$\mathcal{E}$	Cost function
ε	Error term
f_C	Low-pass filter -3 dB cutoff frequency
f_{clock}	PRBS clock frequency
f_s	Sampling frequency
$\mathbf{\Gamma}$	Inverse inductance matrix, $\mathbf{\Gamma} = \boldsymbol{L}^{-1}$
$\mathbf{G}(j\omega)$	Frequency response, $\mathbf{G}(j\omega) \in \mathcal{G}_\mathbf{T}$
$\mathcal{G}_\mathbf{T}$	Set of frequency responses: $\mathcal{G}_\mathbf{T} = \{\mathbf{Z}_{Loc}(j\omega), \mathbf{Z}_{Lsc}(j\omega), \mathbf{Z}_{Hoc}(j\omega), \mathbf{Z}_{Hsc}(j\omega), \mathbf{H}_{LH}(j\omega), \mathbf{H}_{HL}(j\omega)\}$
$\mathbf{H}_{HL}$	HV–LV voltage transformation ratio
$\mathbf{H}_{LH}$	LV–HV voltage transformation ratio
k_{ij}	Mutual coupling coefficient for L_i and L_j
$\boldsymbol{L}$	Inductance matrix
m_s	PRBS shift-register feedback tapping point
N_k	Number of turns on winding k
N_s, n_s	PRBS length and shift-register length: $N_s = 2^{n_s} - 1$
Φ_c, ϕ_c	Core flux
$\mathfrak{R}_c$	Reluctance of core magnetic path
μ	Permeability
$x(t)$, $\mathbf{X}(j\omega)$	System input (or excitation) signal

$y(t)$, $\mathbf{Y}(j\omega)$	System output (or response) signal
$\mathbf{Z}_{Hoc}$	Open-circuit HV input impedance
$\mathbf{Z}_{Hsc}$	Short-circuit HV input impedance
$\mathbf{Z}_{Loc}$	Open-circuit LV input impedance
$\mathbf{Z}_{Lsc}$	Short-circuit LV input impedance

Abbreviations and Acronyms

ATP	Alternative Transients Program (EMTP implementation)
DFT	Discrete Fourier Transform
EMTP	Electromagnetic Transients Program
FACTS	Flexible AC Transmission System
FFT	Fast Fourier Transform
FRA	Frequency Response Analysis
HV	High Voltage
LV	Low Voltage
MLBS	Maximum-Length Binary Sequence
MMF	Magnetomotive Force
PRBS	Pseudo-Random Binary Sequence
SQP	Sequential Quadratic Programming

Notational Conventions

Instantaneous values: lowercase italic letters, e.g. $v_e(t)$ or $\phi_c(t)$.
RMS or scalar quantities: uppercase italic letters, e.g. V_e, I_1 or Φ_c.
Phasors: Boldface uppercase letters, e.g. $\mathbf{V}_e$, $\mathbf{I}_1$ or $\mathbf{Z}_{Loc}(j\omega)$.
Matrices and Vectors: Boldface uppercase, italic letters, e.g. $\boldsymbol{Y}_n$ or $\boldsymbol{\theta}$.
Superscript T denotes matrix or vector transpose, e.g. $\boldsymbol{A}^T$.
Asterisk (*) denotes complex conjugate, e.g. $\mathbf{Z}^*$.

Estimated quantities: A response predicted by a model (with estimated parameters) is indicated by single caret accent, e.g. $\hat{\mathbf{G}}(j\omega)$. A double inverted caret accent, e.g. $\breve{\breve{\mathbf{G}}}(j\omega)$, is used to denote the empirical transfer function estimate obtained from measured data. A (smoothed) response estimate, based on measured data (usually obtained by applying a spectral estimation algorithm to the empirical estimate), is denoted by a single inverted caret accent, e.g. $\check{\mathbf{G}}(j\omega)$.

Chapter 1

Introduction

This dissertation discusses the development of a wideband lumped-parameter, equivalent-circuit transformer model and the development of a technique by which its parameters can be estimated. The following section presents an overview of the factors that motivated this study and formulates the basic specifications of the transformer model, with reference to particular application areas. The remainder of this introductory chapter is devoted to a summary of the methodology that was followed during this project and the boundaries within which the research was carried out.

1.1 Project Motivation

The electromagnetic behaviour of power transformers working under steady-state sinusoidal conditions and within their normal operational limits, can generally be approximated adequately by considering the transformer as a simple low-loss voltage-changer [1]. However, during transient conditions or during operation at frequencies below or above its nominal frequency, the behaviour of a transformer can be complex and difficult to predict [1]. The response of a transformer under such operating conditions is affected by the non-linear nature of the core and by capacitances distributed throughout the winding structure [1, 2]. A variety of transformer model structures which allow for these effects are available and usually take the form of lumped-parameter equivalent-circuit representations. For most applications, this is the preferred model structure, as such a representation is easily included in data files for network analysis programs such as the EMTP. By ex-

pressing an equivalent-circuit model in terms of its state-space representation, or in terms of transfer functions, it can be implemented in most general-purpose simulation programs such as MATLAB [3]. Another important advantage of equivalent-circuit models is that they can provide a great deal of physical insight regarding the processes that take place inside the device under consideration. However, this is only true if the equivalent-circuit elements correspond to physically meaningful components or processes in the device that is being modelled.

For condition monitoring applications, the physical significance of the elements of a transformer equivalent-circuit model are of particular interest. The application of the so-called Frequency Response Analysis (FRA) method as a diagnostic tool has been the topic of several research projects [4, 5, 6, 7, 8, 9]. The method requires that the frequency-response characteristics of a transformer are measured regularly during its service life. Any internal damage, such as permanent mechanical deformation of the windings, will lead to changes in the magnetising and leakage inductances of the transformer as well as changes in the distribution and magnitude of the winding capacitances. Depending on the severity of the damage, such changes are thus detectable as changes in the frequency-response characteristics of the transformer. While measurement methods for FRA have been extensively researched and several transformer manufacturers and utilities have FRA measurement programs in place [10], little is known regarding the interpretation of FRA measurement data. A number of researchers have attempted to address the problem by relating changes in the transformer frequency-response characteristics to changes in the parameters of an equivalent-circuit model, by using the measured response data to estimate the parameters of the model [6, 11, 12, 13]. By observing which model parameters are most sensitive to a change in the frequency-response characteristics, conclusions regarding the nature and severity of any internal changes in the transformer can be reached; provided that the model parameters (i.e. the equivalent-circuit elements) can be directly related to the physical structure of the transformer.

Such parameter estimation procedures have been carried out for relatively simple fourth or fifth order equivalent-circuit transformer models [14, 15, 16, 13]. A reasonably good prediction of the transformer frequency-response characteristics can be obtained with a simple low-order equivalent circuit model, such as the circuit proposed by Douglass [17]. This is illustrated by figure 1.1, which shows the measured Low-Voltage (LV) open-circuit input-impedance frequency response of a 16 kVA, 22 kV / 240 V single-phase distribution transformer and a simulation of the same response obtained by applying the fourth-order model developed by Douglass. It is clear that the model is able to predict the locations of

the major resonant frequencies of the response (at 100 Hz and at 4.5 kHz) and the amount of damping associated with these resonances. However, at frequencies above 5 kHz, the model does little more than predict the general trend of the frequency response. The order of the model is too low to make provision for the 'minor' resonances that are evident in figure 1.1 at the higher frequencies.

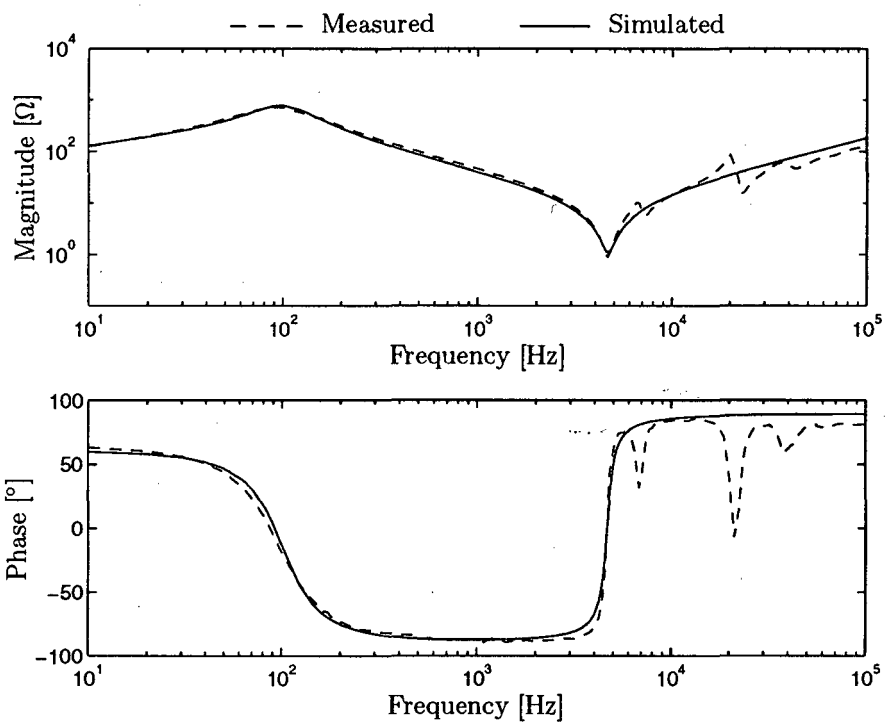

Figure 1.1: Measured and simulated LV open-circuit input-impedance frequency responses of a 16 kVA distribution transformer. The simulated response was obtained by applying the equivalent-circuit model proposed by Douglass [17].

A number of equivalent-circuit model structures that are able to predict the 'minor' winding resonances have been developed [18, 19, 20], mainly with time-domain applications in mind. The structures of these models are complex and often rely on arbitrarily synthesized networks to account for secondary resonances and other frequency-dependent effects, so that the physical significance of the model elements is greatly reduced or non-existent. In addition, such model structures have a large number of parameters, which complicates the parameter estimation procedure. Thus, for condition monitoring applications there exists a clear need for an improved equivalent-circuit transformer model structure with the following characteristics:

- The equivalent-circuit elements of the model structure must represent the physical

construction of the transformer as closely as possible.

- The order of the model structure must be high enough to make it possible to predict the 'minor' resonances of the transformer frequency-response characteristics (see figure 1.1).
- The complexity of the model, and the number of parameters that it requires, must be low enough to make parameter estimation from a number of terminal response measurements possible.

The application area of such a model is not limited to transformer condition monitoring. A number of research projects have been devoted to the frequency-domain characteristics of voltage transformers and high-voltage test transformers for wideband measurement and testing applications [17, 14, 21, 22, 23, 24, 25, 26]. These projects concentrated mainly on the prediction of the voltage transfer functions, either to correct the transformation ratio for harmonic measurements (or other wideband measurements), or to predict the response of the transformer when it is employed as part of an excitation system for wideband, high-voltage testing. One approach to the problem is to model the transformer by a transfer function [21, 23]. The drawback of this method is that the model is not able to account for changes in the frequency response due to changes in the load impedance, i.e. the transformer model is only valid at the load impedance at which the transfer-function coefficients were determined. This problem is overcome if an equivalent-circuit model is applied, as proposed by a number of authors [17, 14, 22, 24, 26]. Third or fourth order equivalent-circuit models are generally applied, which again results in poor prediction of any secondary resonant effects in the transformer windings. While the physical significance of the model structure is of lesser importance in this application, more accurate transformer response predictions could be obtained from an improved model structure.

The same argument applies to transformer models for use in power system simulations in the harmonic frequency range or in the carrier band. For large-scale system simulations, complex model structures are not desirable and simple impedance-branch equivalent-circuit models are normally employed [27, 28, 29]. Such models can be derived directly from data which is usually available from the transformer manufacturer and generally provide an adequate estimate of the impedance presented to the system by the transformer. However, in many cases this approach is not satisfactory. Transformers normally form part of large static drive systems and are also employed as part of Flexible AC Transmission System (FACTS) devices. As the capability of power electronic switching elements increases, the switching frequencies employed in such systems increase. Accu-

rate analysis of large power electronic systems, or accurate analysis of the propagation of harmonics and noise generated by such systems, thus requires a wideband transformer model with a bandwidth that extends beyond the switching frequency of the device in question. A suitable transformer model would have to cover a frequency band ranging from the power system frequency up to at least 100 kHz [30], which is not possible with a low-order equivalent-circuit model. Specifying this bandwidth as a minimum requirement for an improved model structure would make such a model suitable for a large number of applications in the harmonic- and carrier-frequency ranges.

1.2 Project Description

The research described in this dissertation is based on the hypotheses that:

(a) A structure for an improved wideband transformer model can be found that adheres to the requirements defined in section 1.1, i.e.
   - the model must take the form of a lumped-parameter equivalent circuit that represents the physical transformer as closely as possible,
   - the order of the model must be high enough to predict 'minor' winding resonances up to 100 kHz, and
   - it must be possible to estimate the model parameters from terminal response measurements.

(b) That a practical procedure can be developed to estimate the parameters of such a transformer model structure from terminal frequency response measurements.

This project thus takes the form of a system identification problem, as illustrated in figure 1.2 [31, 32]. Within this framework provision is made, not only for the development of a suitable model structure and the estimation of its parameters, but also for the development and execution of steps to acquire data from which the model parameters can be estimated and for validation of the model.

Following the outline of figure 1.2, the component tasks of this project are:

(a) *Establishment of prior knowledge.* In order to provide a basis for the development of an improved transformer model, the first part of this project concentrates on an

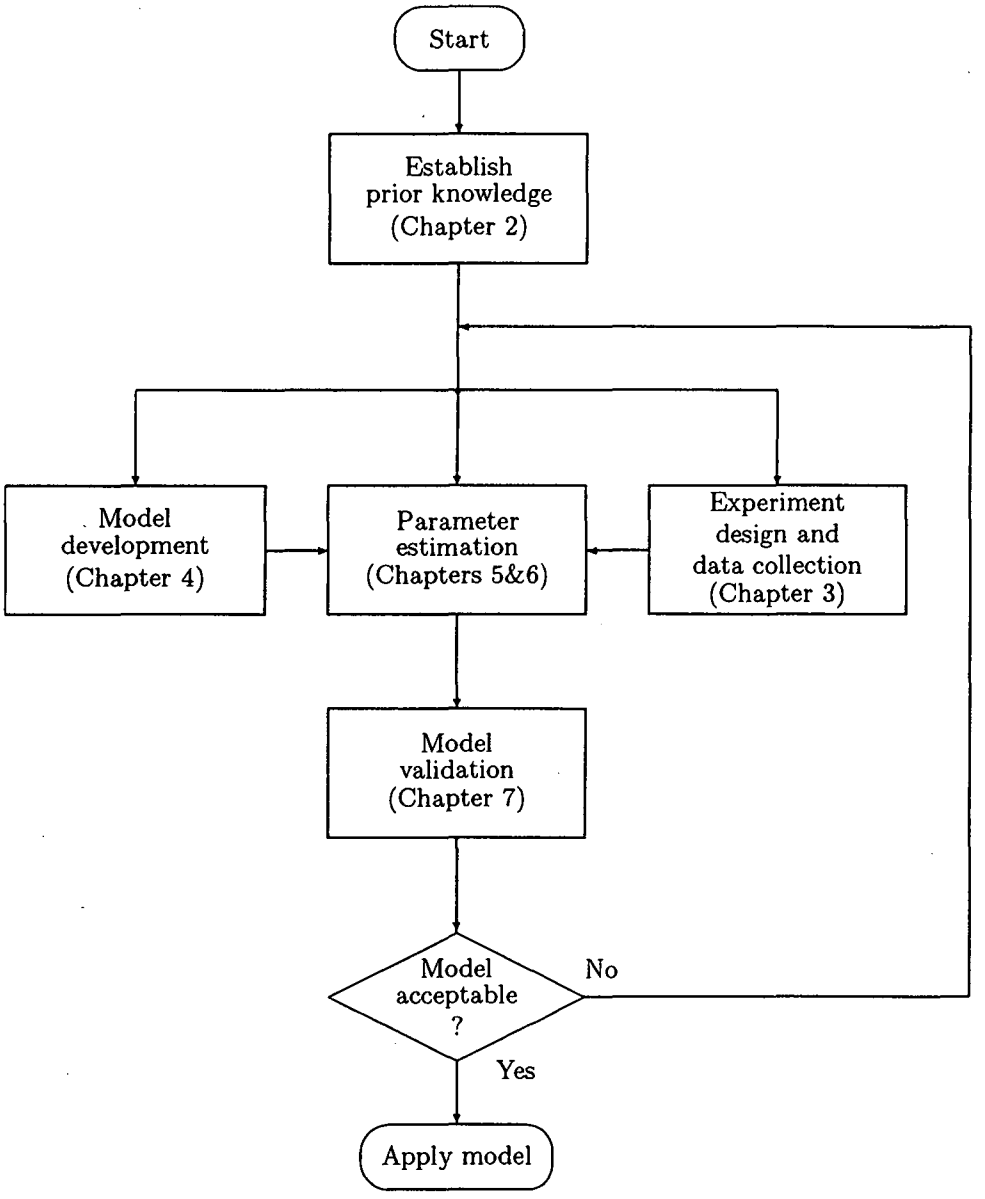

Figure 1.2: The system identification loop and its relation to the structure of this project.

overview of transformer models that have been developed to date. This takes the form of a detailed literature survey, which also serves to confirm the need for the development of a new transformer model. Techniques for the measurement of transformer frequency-response characteristics are also investigated as well as methods by which the parameters of transformer models can be estimated from such measurements. The literature survey is presented in chapter 2 of this dissertation.

(b) *Experiment design and data collection.* Accurate and reliable frequency-response data is required to implement a frequency-domain transformer model parameter estimation procedure and to guide the transformer model development process. A number of methods exist by which the frequency-response characteristics of transformers can be obtained experimentally. The comparative merits and disadvantages of the use of stepped-frequency (sinusoidal) excitation, impulse excitation and Pseudo-Random Binary Sequence (PRBS) excitation for transformer frequency response measurements are investigated.

A 16 kVA, 22 kV / 240 V single-phase distribution transformer was available for laboratory testing. Following the development of suitable experimental arrangements and signal processing procedures, the frequency-response characteristics of this transformer were measured using stepped-frequency and PRBS excitation signals. The effects of the transformer non-linearities on the measured frequency responses are investigated experimentally. The experimental component of this project is discussed in chapter 3.

(c) *Model development.* The resonant behaviour of individual transformer windings is investigated and an equivalent-circuit representation of a winding is established, forming the basis for the construction of a full transformer equivalent-circuit model structure. Subsequently, an improved wideband lumped-parameter equivalent-circuit transformer model structure, adhering to the requirements outlined in section 1.1, is proposed. Frequency-dependence of the equivalent-circuit model elements is investigated and methods are defined by which these effects can be represented for frequency-domain application of the transformer model. The development of the transformer model is presented in chapter 4 of this dissertation.

(d) *Parameter estimation.* A procedure by which the transformer equivalent-circuit model parameters can be estimated directly from the transformer terminal frequency responses, is developed and implemented using MATLAB [3]. Attention is given to the representation of the transformer model within the parameter estimation procedure and to the conditions under which a consistent and unique set of parameters is obtained. The parameter estimation procedure is applied to the proposed

model structure for the 16 kVA experimental transformer, followed by an evaluation of the results. Application of the estimation procedure to other lumped-parameter equivalent-circuit model structures, such as the one proposed by Douglass [17], is also investigated. Chapter 5 deals with the development of the parameter estimation procedure, while chapter 6 focuses on its application to the proposed transformer model structure.

(e) *Model validation.* To ensure that the identified model will yield accurate transformer response predictions when applied within its limitations, the model has to be validated by using it to simulate a variety of responses which can be compared to measurements of the same response. A number of such simulations are carried out, using the identified model of the 16 kVA transformer, in the frequency-domain as well as in the time-domain.

The proposed model structure and the parameter estimation procedure are then applied to an 11 kV / 110 V voltage transformer so that the entire model identification process is validated for a transformer other than the 16 kVA test transformer. Correct prediction of the magnetizing branch voltage is verified by comparing the frequency responses of the simulated magnetizing branch voltage and the voltage induced in a search coil wound around the 11 kV / 110 V voltage transformer core. Validation of the transformer model is discussed in chapter 7 of this dissertation.

The project tasks discussed above will be carried out within the following boundaries, so that the scope of this research is clearly defined and limited to manageable proportions:

- Only two-winding transformers are considered.
- Measurements and simulations are limited to the frequency range between 10 Hz and 100 kHz. There are two reasons for establishing this limitation. Firstly, the frequency ranges associated with power system harmonics [28], noise from power electronic drive systems [33], power system carrier frequencies [30] and a wide range of power system transients, including slower lightning impulses [33], are covered. Secondly, the data acquisition system that was available for this work has a maximum -3 dB bandwidth of 200 kHz when its anti-aliasing filters are in use. As wideband excitation signals are used for the experimental work, the use of anti-aliasing filters is mandatory, leading to the decision to limit the work presented in this dissertation to the frequency range below 100 kHz.
- Voltage- and frequency-dependent effects resulting from the transformer non-linearities will only be represented in the frequency-domain, i.e. time-domain representation of

non-linear effects will not be attempted.

The project is concluded by reviewing and evaluating the success of the various transformer model identification steps in chapter 8. Conclusions that can be drawn from the results of this research, and suggestions for further research are presented.

Chapter 2

Literature Survey

This chapter provides an overview of transformer models and transformer model structures that have been developed and applied to date and investigates the application of parameter estimation techniques to these transformer model structures. The aim is to motivate the need for an improved lumped-parameter, equivalent-circuit transformer model and to provide a basis for the development of such a model and an accompanying parameter estimation procedure.

2.1 Power Transformer Models

2.1.1 The Basic Transformer Model and its Limitations

In principle, a two-winding transformer consists of two mutually coupled inductors. By forming a T-equivalent circuit of such mutually coupled inductors, a simple transformer equivalent circuit can be formed, as shown in figure 2.1 [34]. The leakage inductances of the primary and secondary windings are explicitly represented and are given by $L_1 - M$ and $L_2 - M$ respectively, where L_1 and L_2 are the self-inductances of each of the windings. The mutual inductance (or the magnetizing inductance of the transformer) is represented by M, and is related to L_1 and L_2 by [34]:

$$M = k_{12}\sqrt{L_1 L_2}\,, \tag{2.1}$$

where k_{12} is the coefficient of coupling of the transformer windings. This T-equivalent allows the transformer to be represented in terms of circuit elements that are not magnetically coupled, but is subject to the restriction that the 'bottom' terminals of the two inductors have to be connected as shown in figure 2.1 [34]. By adding resistances to represent the primary and secondary winding resistances (R_1 and R_2 respectively), and the core losses (R_m), the transformer equivalent-circuit model shown in figure 2.2 is obtained. The transformer T-equivalent circuit model is commonly employed in steady-state simulations and performance calculations [1, 2, 35].

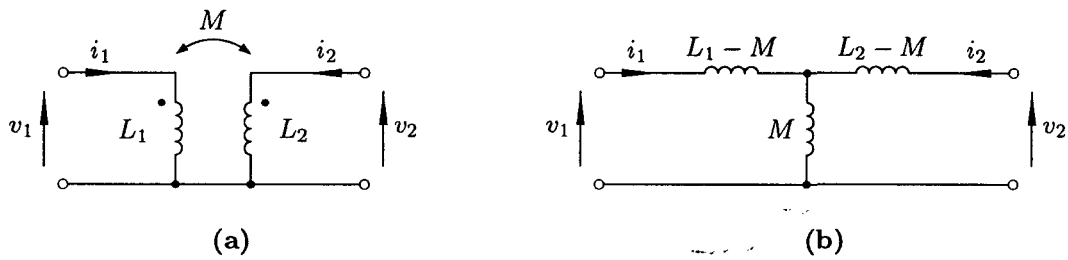

Figure 2.1: Two mutually coupled inductors (a) and their T-equivalent circuit representation (b).

Referring to equation 2.1, it can be seen that the situation where $L_1 < M$ or $L_2 < M$ arises when $L_2 < k_{12}^2 L_1$ or $L_1 < k_{12}^2 L_2$, resulting in a negative inductance value for one of the leakage inductances in figure 2.1 (b). In practical transformers, k_{12} is close to unity and the magnitudes of L_1 and L_2 can differ by an order of magnitude or more (approximately by the square of the winding ratio). This leads to a negative value for one of the leakage inductances in most practical cases where the transformer turns ratio is not close to unity. To avoid this problem and to eliminate the need for a common reference node for both windings, an ideal transformer is usually added to the T-equivalent circuit model, as shown in figure 2.2. The ideal transformer has the same ratio, a, as the winding ratio of the practical transformer under consideration, thus providing the correct voltage transformation ratio without including a negative inductance in the equivalent circuit. For clarity and ease of analysis, all equivalent-circuit parameters are typically referred to either the primary or secondary side of the ideal transformer. For a specific transformer, these parameters are easily estimated by performing an open-circuit test and a short-circuit test [35]. In many cases the basic equivalent-circuit parameters can be obtained directly from the transformer manufacturer.

It is important to note that the representation of the magnetizing branch by linear circuit elements, L_m and R_m, is an approximation. In practical transformers the magnetizing

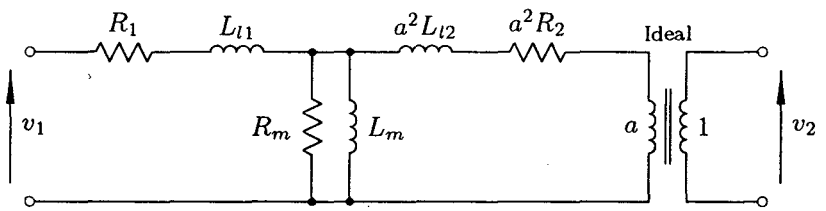

Figure 2.2: Basic transformer equivalent-circuit model.

current is determined by the characteristics of the core material, which is saturable and exhibits hysteretic properties. The permeability of the core material, μ, is thus dependent on the applied magnetomotive force (MMF) and is time-varying due to the hysteresis curve of the material. If it is assumed that μ is constant, the self-inductance of a transformer winding can be expressed as [35]

$$L = \frac{N^2}{\mathfrak{R}_c}, \tag{2.2}$$

where N is the number of turns on the winding and $\mathfrak{R}_c$ represents the reluctance of the core, which is given by

$$\mathfrak{R}_c = \frac{l_c}{\mu A_c}, \tag{2.3}$$

where A_c is the cross-sectional area of the core and l_c is the mean length of the magnetic flux path. Thus, to apply a linear magnetizing inductance in a transformer equivalent circuit, an 'effective' value of μ, and thus L_m, has to be found. The value of such an 'effective' magnetizing inductance will depend largely on the excitation voltage applied to the transformer as this will determine the extremes traversed by the hysteresis loop.

The resistive component of the magnetizing branch, R_m, accounts for hysteresis losses and eddy-current losses in the core, both of which are frequency dependent. Assuming a sinusoidal flux density, B, the hysteresis losses, P_h, are given by the empirical relationship [1, 2]

$$P_h = c_h f B^x. \tag{2.4}$$

The factor c_h and the exponent x depend on the properties of the core material; x lies between 0.8 and 2.3 and is often taken as $x \approx 2$ [1]. The eddy-current losses, P_e, can be

determined from [1, 2]

$$P_e = c_e f^2 B^2 , \tag{2.5}$$

where c_e depends on the properties of the core material and the thickness of the core laminations. By combining the loss components of equations 2.4 and 2.5 and assuming that $x = 2$, the following expression for R_m as a function of frequency can be obtained [15]:

$$R_m = \frac{kf}{c_e f + c_h} , \tag{2.6}$$

where k is a factor dependent on the number of turns of the winding and the cross-sectional area of the core.

A number of methods have been proposed to incorporate the effects of core saturation and hysteresis into transformer simulation models. Saturation is commonly represented by applying a piecewise-linear approximation of the transformer magnetizing curve [36, 37]. Representation of the hysteretic behaviour of the core is more complicated. Especially under transient conditions, the trajectory of the hysteresis loop is not static, but changes as the core excitation conditions change. For simulations such as inrush-current calculations, the remanent core flux at the time that the transformer is energized, will also affect the trajectory followed by the hysteresis loop during the transient. Simple backlash elements [38], hyperbolic functions [38] or polynomial approximations [39] can be applied to model the hysteretic behaviour of the core and to make provision for the associated hysteresis losses.

In some cases, a series magnetizing branch is preferred to the parallel combination of L_m and R_m shown in figure 2.2. In this case, both the inductive and resistive components of the magnetizing branch are frequency dependent and can be represented as second-order functions of frequency [15].

From the above discussion it is clear that the basic transformer model is only valid at the voltage and frequency at which its parameters were determined. However, the model is appropriate for most applications which involve operation of the transformer at, or near, rated frequency and rated voltage.

2.1.2 Modification of the Basic Transformer Model for Wideband Applications

This section considers a class of lumped-parameter equivalent-circuit transformer models which are derived from the basic transformer model discussed in section 2.1.1. In particular, the models discussed in this section were developed to increase the relatively narrow frequency range over which the basic transformer model can be applied. Essentially, this is achieved by the addition of winding capacitances to the basic transformer equivalent-circuit model, as shown in figure 2.3.

The model structure shown in figure 2.3 is commonly applied to model transformers in the harmonic frequency range [29, 23, 25, 24, 40, 28]. Capacitances C_1' and C_2' are lumped representations of the primary and secondary inter-turn and winding-to-ground capacitances respectively, while C_{12}' represents the inter-winding capacitance. Arrilaga *et al.* [28] have included a further capacitance (C_m) across the magnetizing branch of the transformer model, but do not offer any explanation as to its physical origin or purpose. This capacitance is generally omitted by other authors.

Slemon [41] discusses a similar transformer model and deals extensively with the transformation of capacitances across the ideal transformer. Note that all capacitances in figure 2.3 have been referred to the primary side of the ideal transformer, mainly to facilitate analysis of the equivalent circuit. Figure 2.4 shows the transformer equivalent-circuit model with the winding resistances and leakage inductances referred to the primary, but with the winding capacitances in their original locations. The relationships between the referred capacitances (C_1', C_2' and C_{12}') and the original capacitances (C_1, C_2 and C_{12}

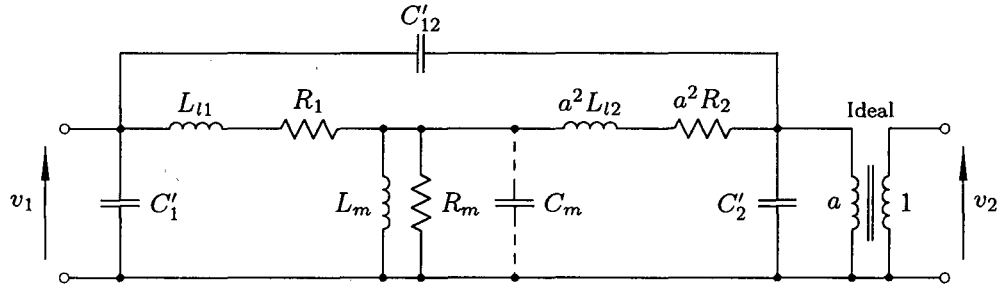

Figure 2.3: Basic transformer model adapted for wideband application by the addition of winding capacitances.

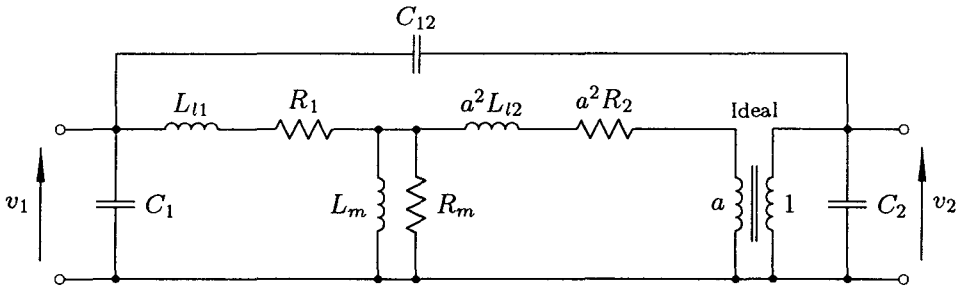

Figure 2.4: Basic transformer model with additional capacitances for wideband applications, before capacitances have been referred to primary.

shown in figure 2.4) are derived by Slemon [41], leading to the following results:

$$C_1' = C_1 + C_{12}\left(\frac{a-1}{a}\right), \tag{2.7}$$

$$C_2' = \frac{C_2}{a^2} + C_{12}\left(\frac{1-a}{a^2}\right) \quad \text{and} \tag{2.8}$$

$$C_{12}' = \frac{C_{12}}{a}. \tag{2.9}$$

The conclusion that can be drawn from the results given in equations 2.7, 2.8 and 2.9 is that care must be taken when applying the model of figure 2.3. The model capacitances do not directly reflect the physical transformer capacitances, as C_1' and C_2' include components related to C_{12}. If the physical significance of the model capacitances is to be preserved, transformation of C_2 and C_{12} across the ideal transformer must be avoided.

While the model structure of figure 2.3 is often referred to in the literature [29, 23, 25, 24, 40, 28], not many authors have reported on the validity of the model or the frequency range over which it can be successfully applied. Vermeulen *et al.* [23, 25] used the model as a basis to predict the voltage transformation ratio frequency responses of a 220 V / 100 kV high-voltage test transformer and a 11 kV / 110 V voltage transformer, under no-load conditions. They reported good results in the frequency range between 100 Hz and 10 kHz. Olivier *et al.* [26] used the model to predict the frequency response of a cascade connection of 440 V / 100 kV high-voltage test transformers and reported good results up to 1500 Hz by making provision only for the capacitance of the high-voltage winding, i.e. all capacitances except C_2' were ignored.

The basic linear transformer equivalent-circuit model of figure 2.3 becomes more useful when it is adapted to allow for the non-linear behaviour of the core. Significant work in

this regard was done by Douglass [17, 42], who investigated the accuracy of voltage- and current transformers in the harmonic frequency range. Douglass proposed the fourth-order transformer equivalent-circuit model shown in figure 2.5 [17]. The model is essentially identical to the model of figure 2.3, the main differences are that the magnetizing branch is represented by a non-linear impedance, Z_e, and that the primary and secondary leakage inductances and winding resistances have been lumped as L_{ps} and R_{ps} respectively. Z_b is the burden impedance of the voltage transformer. All circuit elements have been referred to the secondary side of the ideal transformer.

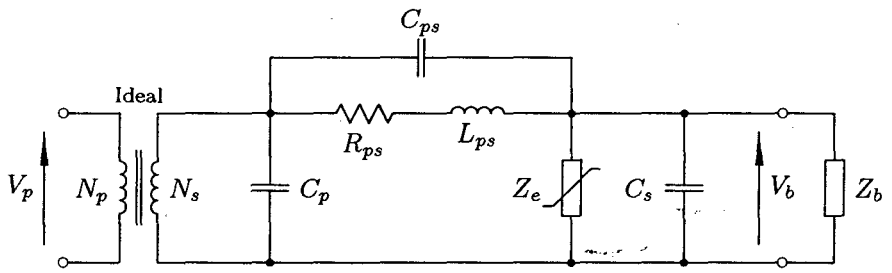

Figure 2.5: Voltage transformer equivalent-circuit model proposed by Douglass [17].

Douglass [17] evaluates his model by showing how it can be used to calculate the frequency response of the primary to secondary voltage transformation ratio of two voltage transformers. The frequency responses of the primary and secondary open-circuit and short-circuit input impedances were measured for each transformer, from which the equivalent-circuit parameters were estimated. The equivalent-circuit model could then be used to predict the voltage transformation ratio of both transformers (with an arbitrary burden impedance) for frequencies between 60 Hz and 30 kHz with reasonable accuracy. The effect of excitation voltage on the (non-linear) magnetizing impedance is investigated carefully. Measurements at 60 Hz with excitation levels below the rated voltage, show an increase in the magnitude of Z_e as the excitation voltage increases. Douglass found that the latter effect reduces as the frequency increases above 60 Hz. For this reason (and due to the mathematical complications that would be introduced), the effect of excitation voltage is not included in the model. However, allowance is made for the strong frequency-dependence of Z_e, by introducing the following expression [17]:

$$Z_e = k_R\sqrt{f} + jk_X\sqrt{f}\ , \tag{2.10}$$

where k_R and k_X are constant parameters. No physical basis is provided for the result given in equation 2.10. An important conclusion reached by Douglass is that the

frequency-dependence of Z_e becomes negligible at frequencies above 1 kHz.

The lumped-parameter equivalent-circuit model developed by Douglass [17] has been successfully applied by a number of authors [14, 22, 43, 13]. Bak-Jensen, *et al.* [14] and Van Rooijen [22] applied the model to predict the frequency-response characteristics of voltage transformers. Good results were reported for frequencies ranging from 50 Hz to over 100 kHz. Similar results were reported by Ladewig [43], who applied the model to a 16 kVA, 22 kV / 240 V single-phase distribution transformer. The model is able to predict the general trend of the transformer frequency responses, but it is clear from the reported results that the order of the model is too low to predict any of the 'minor' winding resonances that are evident in the transformer frequency responses, especially in the transformer input-impedance responses (see figure 1.1).

A number of extensions to the transformer model structure of figure 2.3 have been proposed, in order to cater for the 'minor' winding resonances. Ladewig [43] suggested the equivalent-circuit model shown in figure 2.6 and shows how the model can be applied to predict the frequency-response characteristics of a 16 kVA single-phase distribution transformer. From results presented by Ladewig, it is clear that the order of the model is high enough to predict the 'minor' resonances of the transformer frequency responses, but a good fit was not obtained, as only a manual parameter-fitting procedure was applied. The physical significance of the equivalent-circuit elements is not fully explained by Ladewig, and inspection of the model structure reveals a poor representation of the physical transformer windings. The primary and secondary leakage inductances and winding resistances have each been split into two sections, but any mutual coupling between the respective sections has been ignored. In a practical transformer winding, the leakage inductances, winding resistances and winding capacitances are distributed throughout the

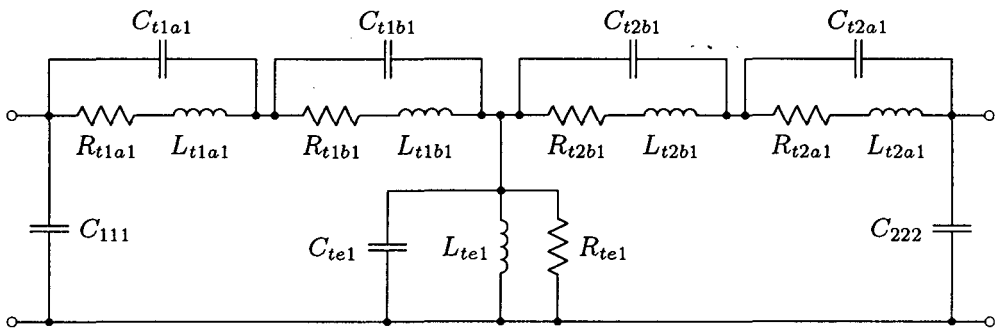

Figure 2.6: Transformer equivalent-circuit model proposed by Ladewig [43].

winding. For this reason, the validity of isolating several 'leakage' sections, each with its own parallel lumped representation of the winding capacitances (C_{t1a1}, C_{t1b1}, C_{t2a1} and C_{t2b1}), is questionable.

A similar approach is followed by Van Rooijen [22], who proposed the model structure shown in figure 2.7. The leakage branches and the magnetizing branch are each divided into two sections, after which stray capacitances are added to the circuit. Van Rooijen motivates his model structure with a discussion of the resonant behaviour of the circuit, but like Ladewig [43], ignores mutual coupling between the inductive branches. Also, a sound physical basis is not provided for the location of the lumped representation of the winding capacitances.

An important contribution made by Van Rooijen was to investigate the ability of his model to predict the frequency response of the 'core voltage' ($\mathbf{V}_e$ in figure 2.7). A search coil was placed on the core of an 11 kV / 110 V voltage transformer and the frequency response of the 'core voltage' obtained in this manner was measured together with the other frequency responses. Thus, if the model proposed by Van Rooijen is able to give a good prediction of $\mathbf{V}_e$, it would reinforce the physical reasoning underlying the model structure, as Faraday's law states that:

$$v_e(t) = N_c \frac{d\phi_c}{dt} , \tag{2.11}$$

where ϕ_c is the core flux and N_c represents the number of turns on the search coil. In turn, ϕ_c is proportional to the current flowing through the magnetizing inductance and thus, if the model is correct, the measured response of the search coil voltage should be similar to the response of the sum of the voltages across L_{Tea1} and L_{Teb1}, as given by

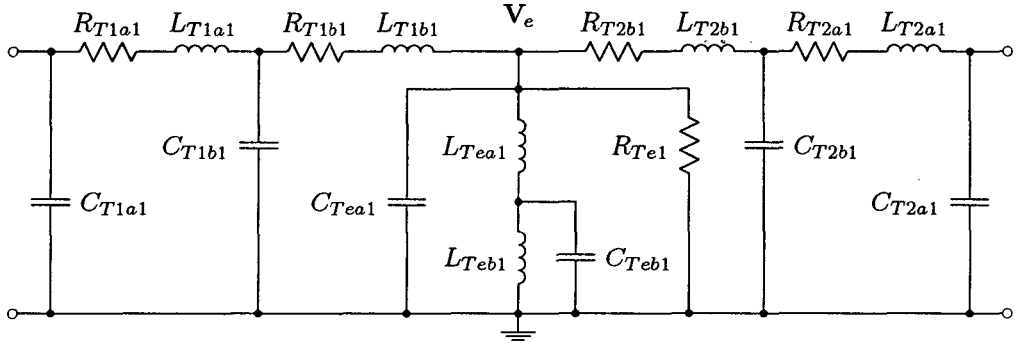

Figure 2.7: Voltage transformer equivalent-circuit model proposed by Van Rooijen [22].

$\mathbf{V}_e$ in figure 2.7. While Van Rooijen demonstrated that his model is able to produce a reasonable prediction of the transformer terminal frequency responses, it failed to provide an adequate prediction of $\mathbf{V}_e$, leading to the conclusion that the physical basis of the model is not sound.

The basic wideband transformer equivalent-circuit model of figure 2.3 also forms the basis of the model structure proposed by Chimklai and Martí [20]. Their model is intended for use in transient simulations, but is based on frequency-domain considerations. As shown in figure 2.8, the location of the winding capacitances is retained, but the leakage and magnetizing branches are replaced by RLC networks which synthesize the frequency-dependent branches $Z_{winding}$ and Z_m. Capacitances $C_{w\text{-}g}$ are lumped representations of the winding-to-ground capacitances and make provision for the case where none of the transformer terminals are earthed. (Cf. the circuit of figure 2.3, which assumes that at least one terminal of the transformer is earthed and as a consequence the lumped representation of the winding-to-ground capacitances is included in C_1' and C_2'.)

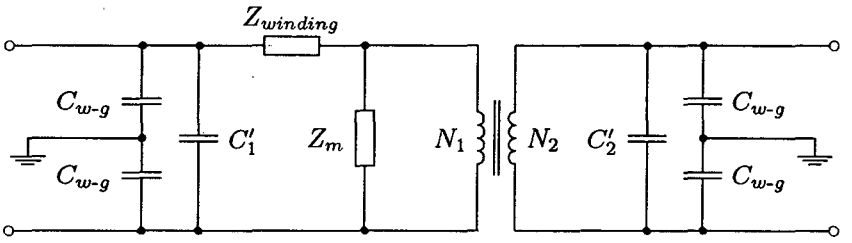

Figure 2.8: Transformer model for electromagnetic transient studies proposed by Chimklai and Martí [20].

Chimklai and Martí [20] do not provide details on the synthesis of Z_m, but the network that was used to approximate $Z_{winding}$ is shown in figure 2.9. The parameters of this network are obtained by fitting the network to a short-circuit input-impedance frequency response measurement of the transformer.

Chimklai and Martí [20] show that good results can be obtained in a frequency band ranging from 100 Hz to over 100 kHz using their model, by comparing measured and predicted short-circuit input-impedance frequency responses. The model has an order that is high enough to provide for the 'minor' resonances of the frequency responses, but has been validated for only one of the transformer frequency responses. The use of the network of figure 2.9 to synthesize $Z_{winding}$ suggests that none of the model parameters, except the winding capacitances, have any physical significance.

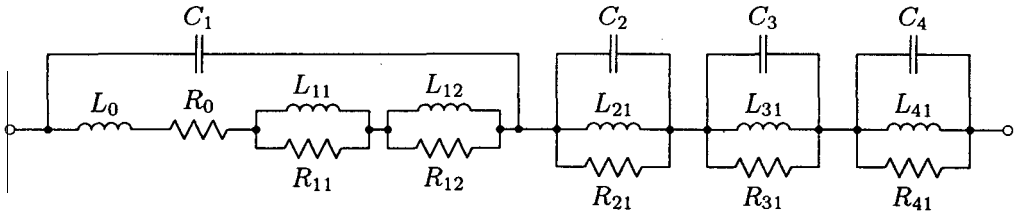

Figure 2.9: *RLC* network used by Chimklai and Martí [20] to synthesize $Z_{winding}$ shown in figure 2.8.

Thus far, this section has considered transformer equivalent-circuit models that are intended for, or applicable to, frequency-domain applications and that have been formulated as wideband extensions of the basic T-equivalent transformer model of figure 2.2. In some cases the T-equivalent model structure is not desirable, especially where a more explicit representation of the winding capacitances is required. In this case, a model structure which considers a two-winding transformer as two mutually coupled inductors, as shown in figure 2.1 (a), can be applied. Such a model structure has been proposed by Keyhani *et al.* [44] and in an extended form by Bak-Jensen [15], as shown in figure 2.10.

The circuit parameters L_p, R_p, L_s and R_s represent the leakage inductances and winding resistances of the primary and secondary windings respectively. The mutual coupling between the windings is represented by current-controlled voltage sources v_{mp} and v_{ms},

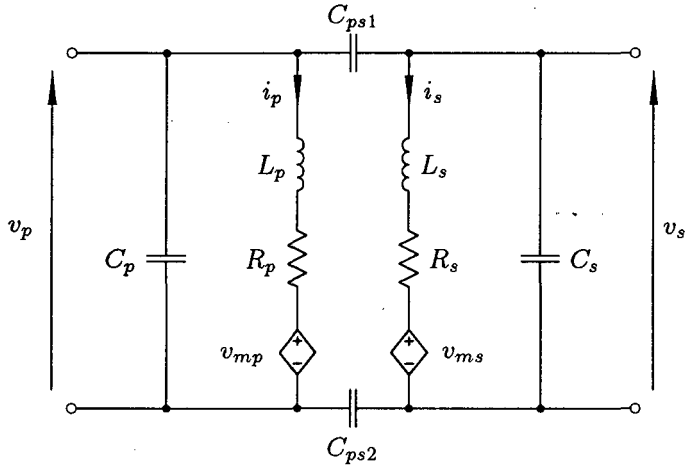

Figure 2.10: Wideband transformer model proposed by Keyhani *et al.* [44] and Bak-Jensen [15].

which also account for the core-losses [15]. The voltages of v_{mp} and v_{ms} are given by:

$$v_{mp} = L_m \frac{d}{dt}(i_p + ai_s) + R_m(i_p + ai_s) \tag{2.12}$$

$$v_{ms} = a^2 L_m \frac{d}{dt}\left(\frac{i_p}{a} + i_s\right) + a^2 R_m \left(\frac{i_p}{a} + i_s\right) , \tag{2.13}$$

where a is the turns-ratio of the transformer windings, given by:

$$a = \frac{N_p}{N_s} . \tag{2.14}$$

Keyhani *et al.* [44] used the model to predict the frequency-response characteristics of a 15 kVA, 7620 V / 240 V, single-phase distribution transformer and reported good results up to 100 kHz.

2.1.3 Winding-section Based Transformer Models

The transformer models discussed in this section consider a single transformer winding as a starting point, recognizing the distributed nature of the inductive, capacitive and resistive components that constitute such a winding, as shown in figure 2.11 [1, 45, 46, 4, 47, 48, 49].

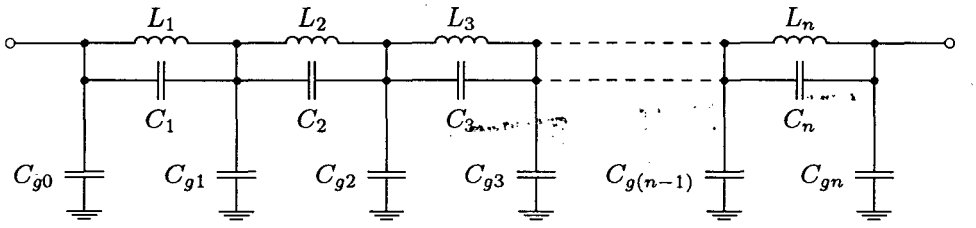

Figure 2.11: Cascade equivalent circuit of a transformer winding.

In its most basic form, the circuit of figure 2.11 describes the winding on a turn-to-turn basis. Each inductance represents one turn of the winding and provision is made for the inter-turn capacitance and the capacitance between turns and ground. The individual turns are mutually coupled. A transformer winding with N turns would thus be represented by a circuit with N mutually coupled sections. This is usually impractical, and methods by which the number of sections can be reduced have to be found [50, 51, 52, 53]. The simplest manner in which this can be achieved is by assuming that the winding is completely uniform. Based on this assumption, all the sections of the circuit in figure 2.11 would be equivalent and could thus be lumped into a single section. Practical transformer

windings, however, are not uniform and are made up of a set of disks or layers [1, 50, 2]. Within such a winding structure it is usually possible to identify uniform winding sections, each of which can then be represented by an equivalent-circuit section. Consider, for example, the cross-sectional view of a layered winding shown in figure 2.12. Each rectangular box represents a layer of uniformly wound turns. Also note that there is capacitive coupling between adjacent layers and between each layer and ground (the transformer core or its tank).

If it is now assumed that each layer is uniformly wound, the equivalent circuit of figure 2.13 can be formed [50, 45, 54]. In figure 2.13 each parallel LC combination, such as L_A-C_A, thus represents one (uniform) winding layer. The inter-layer capacitances are represented by C_{AB}, C_{BC}, etc. and the winding-to-ground capacitances are represented by C_g.

By assuming the existence of an equipotential surface between adjacent winding layers, a further circuit reduction step is possible [45, 50]. In figure 2.14, such equipotential surfaces are represented by x-x', y-y' and z-z'. For example, consider the inter-layer capacitance C_{AB} shown in figure 2.13. The equipotential surface x-x' makes it possible to divide C_{AB} into two capacitances (C'_{AB}), as shown in figure 2.14. The magnitude of C'_{AB} is twice that of C_{AB} [50]. As the node between the two newly formed capacitances C'_{AB} (x) has the same potential as node x', these two capacitances can now be added to the inter-winding capacitances C_A and C_B, yielding a transformer-winding equivalent circuit similar to the circuit of figure 2.11, with a number of sections that correspond to the number of winding layers.

While the above discussion concentrated on the derivation of a winding model for layered transformer windings, the procedure is equally applicable to other winding types such as disc-windings or bobbin-coil (pancake) windings [50]. The parameters for a lumped-parameter winding-section model are typically derived from the turn-to-turn parameters of a transformer winding. The latter are usually obtained from calculations based on the physical construction of the transformer winding [53, 52, 51, 55, 56, 57, 58, 59]. The turn-to-turn winding model is then reduced to the desired number of sections by a mathematical reduction technique [52, 53, 51, 60].

By combining two or more winding-section equivalent circuits and introducing inter-winding capacitances, a lumped-parameter transformer equivalent circuit can be formed, as shown in figure 2.15 [61, 44, 62, 63]. This circuit represents the transformer windings in terms of mutually coupled winding sections and makes provision for inter-turn, inter-

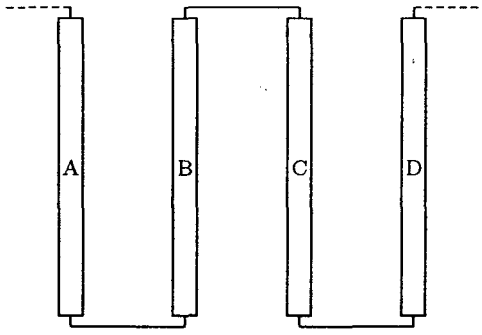

Figure 2.12: Cross-sectional view of a layered transformer winding. Each labeled rectangle represents one winding layer.

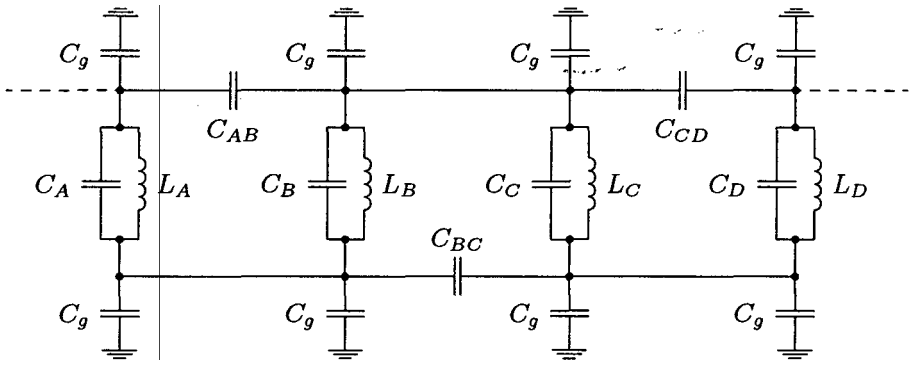

Figure 2.13: Equivalent-circuit representation of the winding layers shown in figure 2.12 [50].

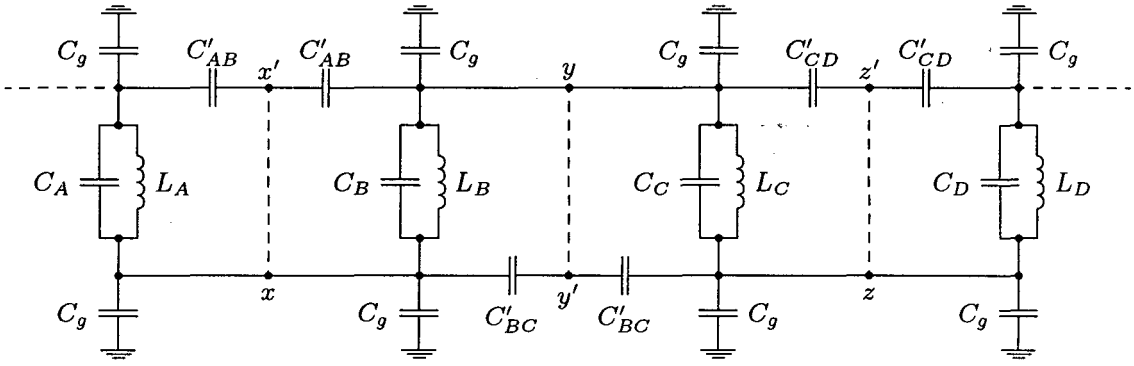

Figure 2.14: Simplification of the winding-layer model by the introduction of inter-layer equipotential surfaces [50].

winding and winding-to-ground capacitances. When the model of figure 2.15 is applied to very high frequency simulations, the effects of the core losses and core non-linearities are generally ignored, as the core-flux is inversely proportional to the applied frequency and thus has a very small effect at high frequencies [19]. A number of methods have however been proposed to include the effect of the core in the model structure of figure 2.15. This is usually done by complementing the electrical equivalent circuit of figure 2.15 with a representation of the magnetic circuit of the core.

By applying the principle of duality, the MMF attributed to each winding section and the voltages induced in that section due to the MMF's applied by all the other winding sections, can be related via an electrical equivalent of the magnetic circuit of the core [64, 18]. In this manner, core non-linearities can be represented and provision can be made for core loss-components (and their voltage- and frequency-dependence) in the electrical equivalent of the core magnetic circuit [64, 18, 51]. An adequate representation of the core non-linearities and losses can generally not be obtained by the direct representation of the windings as a system of mutually coupled inductors, which is based on the assumption that the coupling mechanism is linear [64]. The application of the duality principle has the advantage that the resulting equivalent-circuit elements can be related to the physical characteristics of the transformer core.

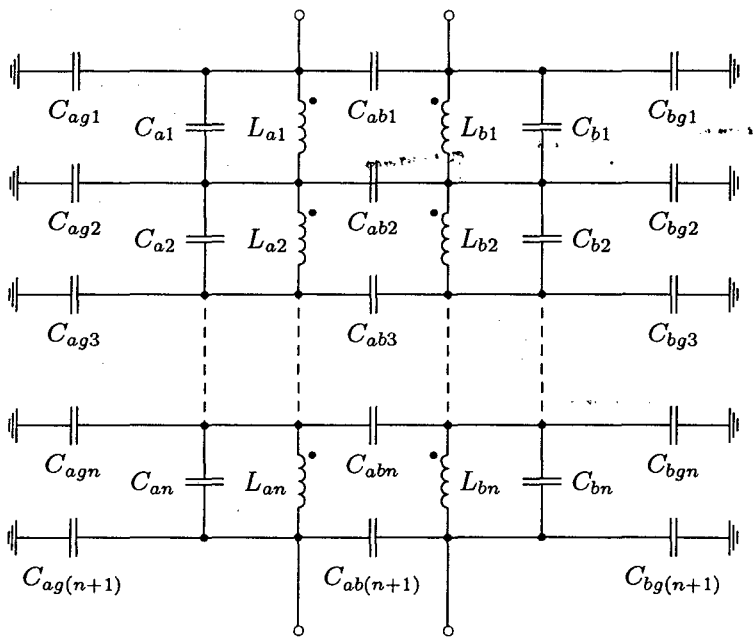

Figure 2.15: Lumped-parameter two-winding transformer equivalent circuit formed by combining two winding-section equivalent circuits [61, 44, 62, 63].

Heuck *et al.* [54] and Kegel *et al.* [65] proposed a winding-layer based voltage transformer model which provides for the magnetizing inductance and the core losses by coupling each winding section to a common magnetizing branch via ideal transformers, as shown in figure 2.16. A similar approach is followed by Dettmann *et al.* [66] to model the frequency-response characteristics of high-inductance coils. Each winding layer is represented by a winding-resistance and a leakage inductance component, together with a lumped representation of the inter-turn capacitance of each layer. Inter-layer and inter-winding capacitances are also included, but have not been shown in figure 2.16. Each winding is represented by n equal sections, which differ only in the values assigned to the various capacitances. Coupling between the leakage inductances is ignored, except the coupling of leakage-flux components between adjacent layers of the primary and secondary windings, which is represented by current controlled voltage sources. The model parameters were determined by performing open-circuit and short-circuit frequency-response measurements on a specially constructed voltage transformer, which made it possible to access the windings at various points for the connection of instruments.

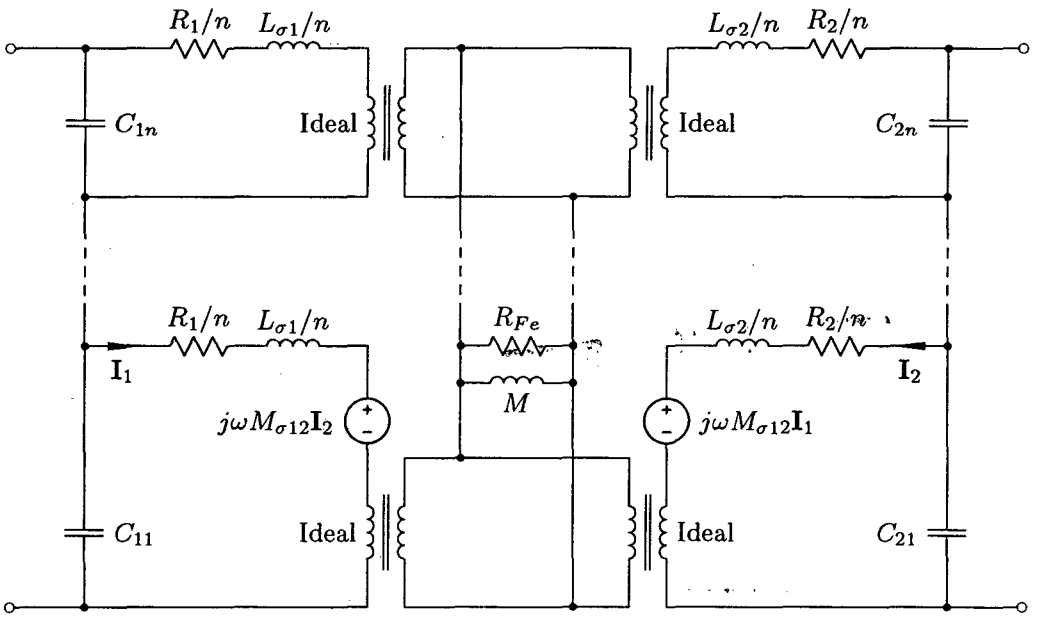

Figure 2.16: Voltage transformer equivalent-circuit model proposed by Heuck *et al.* [54] and Kegel *et al.* [65].

Heuck *et al.* [54] and Kegel *et al.* [65] applied the model structure of figure 2.16 to frequency-domain simulations of voltage transformers and reported good results for the frequency range between 100 Hz and 100 kHz. The assumptions made by them are restrictive if their model structure is to be applied on a winding-section basis (where one section would represent several layers), as the inductances of the various winding sections

will not necessarily be equal. This problem can be overcome by allowing different leakage inductances and differing ideal transformer ratios for the various winding sections, although this would lead to a significant increase in the number of model parameters. The use of ideal transformers in the model structure makes it possible to represent the magnetizing inductance and the core losses in a manner which is related to the electromagnetic behaviour of the physical transformer. However, this complicates mathematical representation of the model (such as a state-space or nodal admittance matrix formulation), or its representation in data files for simulation programs such as the EMTP.

An alternative approach is proposed by Wilcox *et al.* [67, 62, 68, 63] by which the mutually coupled winding sections are represented by independent (uncoupled) modal networks. In this way, frequency-dependent core effects are taken into account, but saturation (or hysteresis) can not be represented. Modal analysis techniques are useful in that they make it possible to represent the frequency-dependent parameters of the transformer in the time-domain and the frequency-domain. In this way, modal networks can be used to represent frequency-dependent branches in the transformer equivalent circuit. Vaessen [69] suggested a transformer model based entirely on modal networks and reported good correlation between measured and simulated time-domain transformer responses for frequencies up to 5 MHz. While the application of modal analysis techniques can yield some useful insights into the resonant behavior of transformer windings [70], the use of modal techniques or modal networks in the modelling of transformers is not a direct representation of the transformer in terms of its physical construction.

2.1.4 Black-box Transformer Models

A black-box model is defined as a model whose parameters are treated as a means to fit the model characteristics to the available data, but do not reflect the physical considerations underlying the system that is being modelled [31]. In the context of this dissertation, a black-box model structure is not desirable, as a transformer model structure that reflects the physical properties of the device is required. Of interest, however, are the parameter fitting techniques applied to such models and the data that is required to obtain a satisfactory fit. Black-box transformer models are generally applied to reduce the complexities associated with wideband transformer modelling and have the distinct advantage that their parameters can be determined from terminal measurements alone.

The structure of a black-box transformer model often takes the form of a Laplace-domain

(s-domain) transfer function

$$H(s) = \frac{a_0 + a_1 s + a_2 s^2 + \cdots + a_n s^n}{b_0 + b_1 s + b_2 s^2 + \cdots + b_m s^m}, \tag{2.15}$$

or a discrete frequency-domain (z-domain) transfer function of the form

$$H(z) = \frac{c_1 z^{-1} + c_2 z^{-2} + \cdots + c_n z^{-n}}{1 + d_1 z^{-1} + d_2 z^{-2} + \cdots + d_m z^{-m}}. \tag{2.16}$$

Such a transfer function can be used to describe the relationship between transformer input and output terminal voltages or, in the case where the input impedance of a winding is of interest, the relationship between the current flowing through a transformer winding and the voltage across that winding. The transfer-function approach has been applied to transformer modeling by Soysal [71], by Soysal and Semlyen [72] and by Vermeulen *et al.* [23, 25]. Soysal [71] and also Soysal and Semlyen [72] used input-impedance frequency response measurements to estimate the transfer-function coefficients, while Vermeulen *et al.* [23, 25] carried out the parameter estimation in the time domain. The transfer-function approach has the advantage that the order of the model can be increased to improve the fit of the model, although this increases the number of transfer-function coefficients, thus complicating the parameter estimation process. The model orders that are typically employed range from 4 to 8. Soysal and Semlyen [72] show that a sixth-order transfer function could be used to provide a good description of the winding impedances of a 500 VA single-phase transformer and a 75 kVA, three-phase transformer up to the MHz range. Vermeulen *et al.* [25] reported good predictions of the voltage transformation ratio frequency responses up to 10 kHz; for a 110 V / 11 kV single-phase transformer using a fourth-order transfer function and for a 33 kV / 110 V single-phase transformer, using a sixth-order transfer function.

A problematic aspect of transfer-function models, especially those designed to model voltage transformation ratios, is the inability to interact with any circuitry external to the transformer. The frequency response of the voltage transformation ratio of a transformer is dependent on its load [17]. Clearly, the transfer-function approach is not able to account for any load changes and is thus only valid at the loading conditions for which the transfer-function coefficients were estimated.

This problem is overcome by a second type of black-box transformer model, which essentially represents the transformer as an n-port network with no internal nodes. Morched *et al.* [19] formulated such a network by interconnecting each of the terminal nodes with

frequency-dependent admittance branches, each of which is expressed in terms of a rational function approximation or an equivalent *RLC* network. A similar approach is followed by Caldecott *et al.* [73] and LaForest *et al.* [30], who used impedance functions to interconnect the transformer terminal nodes. In all cases the admittance or impedance functions are estimated from frequency-domain terminal impedance measurements and the bandwidth of the model structure is only limited by the bandwidth of these measurements and the desired complexity of the approximation functions. All the authors report good results up to 100 kHz. The model structure accounts for all frequency-dependent effects, but can not be used to account for non-linear effects such as saturation [19].

2.2 Parameter Estimation Applied to Transformer Models

2.2.1 Overview

Once a transformer model structure has been defined, the parameters of that model structure have to be determined before the model can be applied. In the case of transformer models, the parameters are often obtained from calculations based on detailed knowledge of the physical construction of the transformer. An alternative approach is to estimate the model parameters from measured response data. In some cases this is not feasible, as the required measurements can only be carried out with great difficulty (e.g. measurement of quantities that are only available at points inside the transformer tank). However, many model structures are suitable for parameter estimation based on terminal response measurements.

The principle underlying parameter estimation techniques is shown in figure 2.17. X^N and Y^N are sets containing N observations of the system input signal, X, and the system response, Y, respectively. Note that noise can be introduced into the system from a variety of sources, so that the observations X^N and Y^N inevitably contain noise components. The observed response of the system (Y^N) is now compared to the response predicted by a model of that system ($\hat{Y}^N$), with the observed input signal, X^N, applied to the model. A quantitative comparison between Y^N and $\hat{Y}^N$ is made by defining a cost function in terms of Y^N and $\hat{Y}^N$. The value of the cost function reduces as the ability of the model to predict Y improves. The idea is now to minimize the cost function by adjusting the parameters

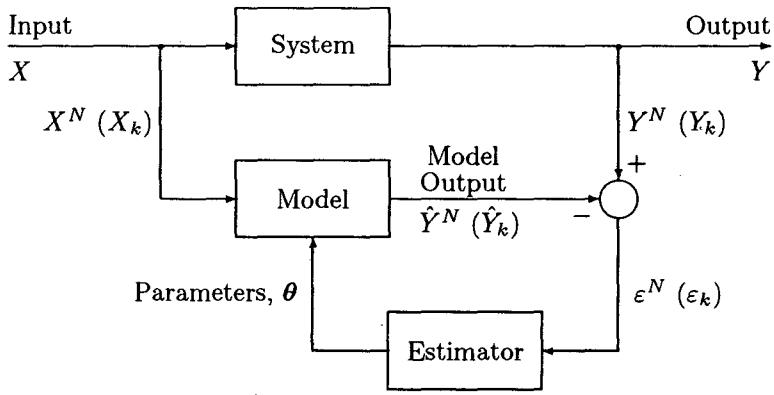

Figure 2.17: Parameter estimation principle.

of the model ($\theta_1, \theta_2, \ldots \theta_n$ for a model with n parameters). The relationship between the parameters of a model and the cost function is seldom linear and the minimization of the cost function becomes a non-linear optimization problem which has to be solved by an iterative procedure.

Thus far it has been assumed that observations X and Y are available as complete sets of previously measured data (X^N and Y^N) and that the cost function is formulated in terms of all the observations contained in X^N and Y^N (non-recursive parameter estimation). The parameter estimation scheme of figure 2.17 is equally applicable to cases where the parameters are updated from one observation of X and Y to the next (recursive parameter estimation) [74]. In this case an error signal (ε_k) is generated from current observation Y_k and model output $\hat{Y}_k$ which is then used to recursively adjust the model parameters, thus producing $\hat{Y}_{(k+1)}$ which can then be compared to the next observation of the system output, $Y_{(k+1)}$.

A variety of methods by which the estimator of figure 2.17 can be formulated are available [75, 32, 74]. The choice of an estimation method for a particular application depends on the model structure, the statistical properties of the noise signals (if these are known) and the nature of the available measured data [75, 32, 74].

2.2.2 Transformer Model Parameter Estimation

The need to derive parameters for transformer models from terminal response measurements, rather than by deriving the parameters from detailed physical knowledge of the

transformer construction, has prompted a number of researchers to investigate the application of parameter estimation techniques to transformer models. A transfer-function model structure is preferred, as parameter estimation techniques for such a model structure are widely applied and well documented in the literature [75, 32, 74]. The use of a transfer-function model structure also makes it possible to directly apply existing parameter estimation software, such as the MATLAB System Identification Toolboxes [75, 76].

Vermeulen *et al.* [25] and Koch [21] investigated the use of least-squares parameter estimation techniques to determine the parameters of a transfer function describing the voltage transformation ratio of voltage transformers. The transformer is excited by a Pseudo-Random Binary Sequence (PRBS) wideband excitation signal while the excitation signal and the transformer response are sampled using a digital data-acquisition system. The sampled time-domain waveforms are then used to estimate the parameters of fourth-order and sixth-order discrete frequency-domain transfer functions. The resulting models are shown to give good simulations of the secondary to primary voltage transformation ratio of an 11 kV / 110 V voltage transformer and the voltage transformation ratio of a 33 kV / 110 V voltage transformer, up to about 10 kHz.

The lumped-parameter equivalent-circuit transformer model proposed by Douglass [17] forms the basis of the investigation conducted by Bak-Jensen *et al.* [14] (also see figure 2.5). The aim of the investigation was to determine the parameters of the Douglass equivalent-circuit model, rather than the parameters of a transfer-function model, by applying parameter estimation techniques. The full equivalent-circuit model is subdivided into a number of sub-models, by omitting elements that are not expected to have an influence in a particular frequency range, as shown in figure 2.18.

Each sub-circuit is used to estimate a different subset of the transformer equivalent-circuit parameters. In each case an s-domain transfer function is derived in terms of the sub-circuit parameters. The s-domain transfer function is then mapped to the z-domain where the transfer-function coefficients are estimated using a least-squares technique. The relevant equivalent-circuit parameters can now be determined from the estimated transfer-function coefficients. Data for the estimation procedures is obtained from transformer response measurements using square-wave excitation signals.

At low frequencies, where C_{ps} and C_s are assumed to have a negligible influence, the sub-circuit of figure 2.18(b) is used to estimate Z_e and C_p. The transformer is excited from the secondary side and the excitation signal, $v_{in}(t)$, and the input current, $i_{in}(t)$, are

measured. Noting that Z_e represents a frequency-dependent series RL-branch consisting of L_e and R_e, the measured quantities can be related by an s-domain expression of the secondary open-circuit input admittance:

$$Y(s) = \frac{I_{in}(s)}{V_{in}(s)} = \frac{L_e C_p s^2 + R_e C_p s + 1}{L_e L_{ps} C_p s^3 + (R_e C_p L_{ps} + L_e R_{ps} C_p) s^2 + L_e s + R_e}, \tag{2.17}$$

from which R_e, L_e and C_p can be determined once the coefficients of equation 2.17 have been estimated. The frequency-dependence of R_e and L_e is found from several estimations, each obtained by applying a square-wave excitation signal with a different fundamental frequency in the range between 50 Hz and 500 Hz.

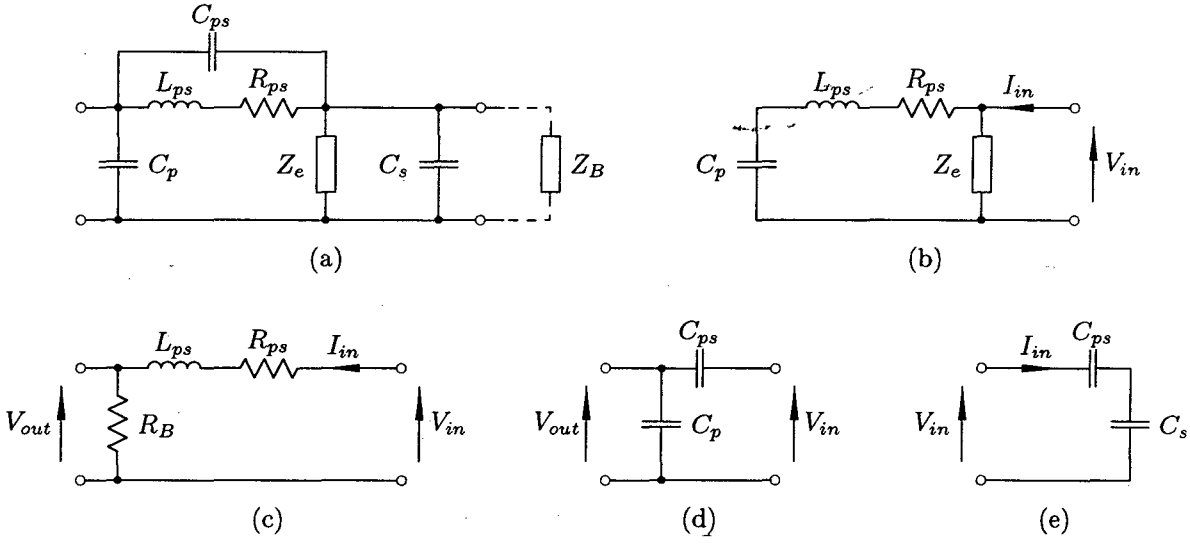

(a) Full transformer equivalent circuit.
(b) Estimation of Z_e and C_p at low frequencies.
(c) Estimation of L_{ps} and R_{ps} at frequencies below 1250 Hz.
(d) High-frequency estimation of C_{ps}.
(e) High-frequency estimation of C_s.

Figure 2.18: Sub-circuits used by Bak-Jensen *et al.* [14] to estimate the parameters of the transformer equivalent circuit proposed by Douglass [17].

The transformer subcircuit of figure 2.18(c) is used to estimate L_{ps} and R_{ps}. The effect of Z_e is largely obscured by loading the primary side of the transformer with a known, relatively low-valued resistance. The transformer is excited from the secondary side and the input signal, V_{in}, input current, I_{in}, and primary voltage, V_{out} are measured. A square-wave excitation signal with a fundamental frequency below 1 250 Hz is used. R_{ps} and L_{ps}

can now be found from estimates of the coefficients of:

$$Y(s) = \frac{I_{in}(s)}{V_{in}(s)} = \frac{1}{R'_B + R + L_{ps}s} , \tag{2.18}$$

or

$$H(s) = \frac{V_{out}(s)}{V_{in}(s)} = \frac{R'_B}{R'_B + R + L_{ps}s} , \tag{2.19}$$

where R'_B is the primary burden resistance referred to the secondary.

At high frequencies (above 500 kHz), the response of the transformer is dominated by the stray capacitances, leading to the sub-circuits of figure 2.18(d) and figure 2.18(e). Figure 2.18(d) shows how C_{ps} is determined by exciting the transformer from the secondary side and measuring the excitation signal, V_{in}, and the primary response signal, V_{out}. Using the previously estimated value of C_p, C_{ps} is estimated from:

$$H(s) = \frac{V_{out}(s)}{V_{in}(s)} = \frac{C_{ps}}{C_p + C_{ps}} . \tag{2.20}$$

Finally, by short-circuiting the transformer, C_s is estimated from primary input voltage and current measurements, V_{in} and I_{in}, as shown in figure 2.18(e), by estimating the coefficients of the primary input impedance:

$$Z(s) = \frac{V_{in}(s)}{I_{in}(s)} = \frac{1}{(C_s + C_{ps})s} \tag{2.21}$$

Using the above procedure, parameters were obtained for a $\frac{20}{\sqrt{3}}$ kV / $\frac{110}{\sqrt{3}}$ V voltage transformer. The estimated parameters were close to parameter values obtained by using the parameter measurement method originally described by Douglass [17]. It is shown that simulations of the frequency responses of the secondary open-circuit input impedance and the secondary short-circuit input impedance match the measured frequency responses quite well up to 1 MHz. Further results are described by Bak-Jensen [15], demonstrating the validity of the parameter estimates by showing good correlation between a number of measured and simulated transformer frequency responses, under loaded and unloaded conditions.

Islam *et al.* [13] describe a simpler method by which the parameters of the equivalent-circuit model proposed by Douglass [17] can be estimated. Similar to Bak-Jensen *et al.* [14, 15], the use of three sub-circuits of the full equivalent-circuit model is proposed, by defining

low-, medium- and high-frequency circuits. An s-domain transfer function is then written for each sub-circuit in terms of the primary to secondary voltage transformation ratio. The transfer-function coefficients are then estimated by the least-squares method, from which the equivalent-circuit parameters are determined. The parameter estimates are based on a single stepped-frequency measurement of the frequency response of the primary to secondary voltage transformation ratio. However, the resulting model is only validated by comparing the measured and simulated responses of the voltage transformation ratio, i.e. it is not clear whether the estimated model is able to accurately predict any of the other transformer frequency responses. It is also unclear whether the frequency-dependence of Z_e was considered.

A method by which the parameters of the lumped-parameter transformer model shown in figure 2.10 (p. 20) can be estimated, is proposed by Keyhani *et al.* [44]. The estimation procedure is based on frequency response measurements of the voltage transformation ratio and the short-circuit input impedance of the transformer. The time-constants of a transfer function describing the short-circuit input impedance are estimated using the non-linear least-squares method, from which the short-circuit step-response of the transformer is obtained. This data is now used to estimate the low-frequency parameters of the transformer model, using the maximum likelihood parameter estimation method (see [31, 32, 74, 77]). At low frequencies the basic transformer T-equivalent circuit is applied. The same procedure is followed to estimate the parameters of the high-frequency model, with good estimates of the low-frequency parameters being available. The method was applied to a 15 kVA, 7 620 V / 240 V single-phase distribution transformer and the measured and predicted frequency responses of the short-circuit input impedance and the voltage transformation ratio agree well up to 100 kHz. In another paper, Keyhani *et al.* [78] describe a similar procedure to estimate the parameters of a cascade transformer-winding model, such as the one shown in figure 2.11. Good results were reported for a six-section transformer-winding model, but were not based on practical measurements. The parameter estimation procedures described by Keyhani *et al.* [78, 44] are lengthy and require several estimation steps. Further, from the discussion of the estimation procedures it is clear that very good initial parameter values have to be supplied for the estimation procedures to succeed (within 10% to 20% of the final value).

2.3 Transformer Condition Monitoring Based on Frequency Response Measurements

In recent years, the use of terminal frequency response measurements has emerged as a condition monitoring and diagnostic tool for power transformers and is gaining acceptance amongst utilities and transformer manufacturers [10, 79]. The so-called Frequency Response Analysis (FRA) method relies on the fact that an internal fault or mechanical deformation will cause changes in the electromagnetic parameters of the transformer, which are detectable by comparing the frequency-response characteristics of a (suspected) faulty transformer to the same response characteristics obtained at an earlier stage, when the transformer was known to be healthy. The method was first proposed by Dick and Erven [4], who used a frequency-sweep network analyser to measure the frequency responses of the transformer voltage transformation ratio and the open-circuit input impedance. By using the high-voltage impulse applied during insulation testing of transformers as a wideband signal source, Malewski and Poulin [7] measured the frequency response of the transformer winding input impedance by digitising the applied impulse signal and the winding ground current. The frequency response of the winding impedance is obtained in the frequency-domain, by first applying the Fast Fourier Transform (FFT) to both signals. The technique was further refined by Vaessen and Hanique [5], who applied a low-voltage impulse to the HV windings of the transformer under test. The impulse excitation signal and the response at the LV winding terminals are digitized and transformed to the frequency domain by FFT processing. From the resulting data, the frequency response of the voltage transformation ratio is found.

While a number of authors have demonstrated that transformer frequency responses are sensitive to a variety of mechanical deformations and faults inside the transformer (e.g. [4, 7, 5, 8, 6, 13]), little is known about the interpretation of FRA data. In other words, it is difficult to determine the nature and location of internal transformer faults based only on the available FRA data. If the measured FRA data can be related to a transformer model based on physical considerations, further information would be made available, as the suspected transformer fault can now be related to changes in the model parameters. This approach was investigated theoretically by Dick and Erven [4], Prabhakar *et al.* [80] and Islam and Ledwich [12] who modelled the sensitivity of transformer-winding frequency responses to changes in the parameters of a cascade winding equivalent-circuit model. More reliable information is made available when FRA data is used to directly estimate the parameters of a transformer model. In this way, a change in FRA data can be related

to a change in the model parameters, which will aid in diagnosing the nature and location of a suspected fault.

Significant work in this regard was carried out by Mikkelsen [16] and Bak-Jensen *et al.* [6, 11, 81]. The secondary input-impedance frequency responses of three $\frac{20}{\sqrt{3}}$ kV / $\frac{110}{\sqrt{3}}$ V voltage transformers were measured at various stages during accelerated ageing tests and with simulated faults applied to the transformer windings and core. In each case the transformer is excited from the secondary side by a PRBS signal and the applied voltage and the winding input current are measured. The measured results are then used to estimate the parameters of the equivalent-circuit transformer model shown in figure 2.10. The estimation process is simplified somewhat by further lumping the representation of the winding resistances, the leakage inductances and the stray capacitances. The input impedance is thus represented by a third-order transfer function with six coefficients from which five equivalent-circuit parameters have to be determined. Clear changes in these parameters due to ageing and internal faults are demonstrated, but too few parameters were estimated to yield a precise description of the transformer condition from those parameters [16]. However, it was shown that the FRA approach can be applied to detect the gradual appearance of ageing phenomena. An interesting aspect of the research carried out by Mikkelsen [16] and Bak-Jensen *et al.* [6] is that the most pronounced effects of ageing and short-circuited winding turns were noticeable in the low-frequency range of the measured input-impedance frequency responses (up to about 10 kHz). Most other researchers consider only the high-frequency responses of a transformer when performing FRA measurements (typically above 100 kHz).

Islam *et al.* [13] estimated the parameters of the equivalent circuit proposed by Douglass [17] and report significant parameter changes due to internal transformer faults. Parameters for the equivalent circuit were estimated from voltage transformation ratio frequency response measurements obtained from two faulted transformers. A further set of parameter estimates was obtained from measurements taken after these transformers had been repaired. The results presented by Islam *et al.* [13] are less conclusive than those obtained by Mikkelsen [16] and Bak-Jensen *et al.* [6], but do highlight the relationship between internal transformer faults and changes in the transformer model parameters estimated from terminal frequency response measurements.

2.4 Discussion

The previous sections presented an overview of existing transformer models, with particular attention to the degree by which a model represents the physical transformer and the methods by which the model parameters are determined. A brief overview of the FRA transformer diagnostic and condition monitoring technique has also been provided to establish the current status of the method, especially with regard to the estimation of transformer equivalent-circuit parameters from FRA data.

With the aims of this dissertation in mind, the following conclusions can be drawn from the literature presented in the previous sections:

(a) The bandwidth of wideband transformer models based on the T-equivalent circuit of a transformer is limited and the order of such models is too low to adequately describe all the winding resonances that occur in practical transformers. Where attempts have been made to extend the bandwidth or order of the basic T-equivalent circuit, the physical significance of the model elements is lost. Wideband transformer models based on the T-equivalent circuit have the advantage that it is relatively easy to account for frequency-dependent effects and core non-linearities. It has also been demonstrated that the parameters of such transformer models can be estimated from terminal response measurements.

(b) By representing transformer windings in terms of a finite number of (uniform) winding sections, high-order, wideband transformer models can be constructed. The accuracy and bandwidth of such models is generally determined by the number of sections chosen to represent the transformer windings. The frequency-dependence and non-linearities of the core can be included in the model by providing a representation of the core magnetic circuit. This type of transformer model has a large number of parameters, which are usually derived from the physical construction parameters of the transformer or from a known turn-to-turn representation of the windings. To date, it has not been shown that the parameters of such models can be estimated successfully from terminal response measurements alone.

(c) Black-box transformer models are characterized by a lack of physical significance of the model parameters. Black-box models are however used to provide a further abstraction of transformer equivalent-circuit models. This makes it possible to apply existing parameter estimation techniques to determine the parameters of the black-box model from which, in turn, the parameters of an equivalent-circuit model can be

solved. Practically, this is only possible for reasonably simple systems, as the black-box parameters are usually lengthy, non-linear expressions in terms of the equivalent-circuit parameters, making solution of the equivalent-circuit parameters difficult.

(d) The use of the transformer 'core-voltage' frequency response (measured via a search coil wound on the transformer core) provides an excellent method by which the physical significance of a transformer model can be validated [22]. In cases where the transformer core is accessible during measurements, it is worth measuring the 'core-voltage' frequency response to provide an additional response for model validation.

(e) The parameter estimation techniques that have been proposed to date for lumped-parameter transformer models (using terminal response measurements) are lengthy and require a number of estimation steps. Generally, the equivalent-circuit model is sub-divided into two or more sub-circuits, based on frequency bands where certain parameters are known to dominate the transformer response. These sub-circuits are then represented by a transfer function, or a state-space formulation, to which a parameter estimation procedure is applied. Finally, the equivalent-circuit parameters are determined from the estimated transfer-function (or state-space) coefficients. Such procedures have only been demonstrated for relatively simple transformer models.

(f) While the FRA technique for transformer condition monitoring is gaining acceptance, an accurate assessment of the condition of a transformer (or diagnosis of a transformer fault) from FRA data is not yet possible. It has been shown that transformer equivalent-circuit parameters can be estimated from FRA data to assist in the interpretation of that data, but this has only been proven for very simple models. To make more accurate interpretation of FRA data possible, an improved model and an associated parameter estimation technique is required.

Chapter 3

Transformer Frequency Response Measurement

In the context of this dissertation, the frequency-response characteristics of a practical two-winding transformer have to be known, to serve as part of the knowledge-base from which a suitable transformer model structure can be developed and to provide data from which the parameters of such a model structure can be estimated. A single-phase 22 kV / 240 V, 16 kVA distribution transformer was used for most of the experimental work discussed in this dissertation and the measurement of its frequency-response characteristics is discussed in this chapter. Procedures for the measurement of the transformer frequency responses are developed, focusing on the choice of excitation signal, the experimental arrangements and the signal processing techniques that are required to extract accurate frequency-response data from sampled time-domain signals. Further, the nature and severity of voltage- and frequency-dependent effects that arise from the non-linear properties of the transformer core are investigated experimentally to establish their influence on the frequency responses of the 22 kV / 240 V, 16 kVA test transformer.

3.1 Overview

The frequency response, or transfer function, between an input and an output of a linear system can be determined by exciting the system with an excitation signal, $x(t)$, and measuring the response, $y(t)$, of the system to the excitation signal, as shown in figure 3.1.

If $\mathbf{X}(j\omega)$ and $\mathbf{Y}(j\omega)$ are the Fourier transforms of $x(t)$ and $y(t)$ respectively, the frequency response is given by [34]:

$$\mathbf{G}(j\omega) = \frac{\mathbf{Y}(j\omega)}{\mathbf{X}(j\omega)}. \tag{3.1}$$

In the case of power transformers, the system under consideration is, strictly speaking, non-linear. However, under certain operating conditions the behaviour of the transformer can be approximated as linear, and the relationship of figure 3.1 can be applied. The transformer non-linearities introduce noise to the system, which will also be present in the response signal, $y(t)$. If the transformer is excited at a single frequency, the non-linear behaviour of the system causes responses at frequencies other than the excitation frequency. As long as these 'unwanted' responses are small in comparison to the response at the excitation frequency, the approximation that the system is linear, is acceptable [74].

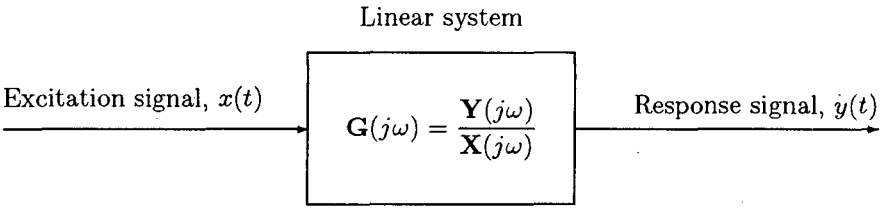

Figure 3.1: Frequency response determination of a linear system.

Noise can also be introduced into the system from other sources, such as electromagnetically coupled noise. Further, the input and output signals are measured with a digital data acquisition system which represents the signals in terms of a finite number of discrete levels. The inaccuracies introduced by this process are another source of noise, which is usually referred to as quantization noise [82].

Accurate frequency response measurements require that the combined effect of the various noise sources is reduced as far as possible. Firstly, a suitable excitation signal has to be chosen, so that the signal-to-noise ratio of the measured signals is high enough to yield acceptable frequency response results. Correct design of the experimental arrangement will ensure minimal coupling of electromagnetic noise from external sources and the analog-to-digital converter that is used to sample the excitation and response signals must have a sufficient number of bits to ensure sampling of the signals at an acceptable level of accuracy. The use of anti-aliasing filters is usually required, especially if the excitation signal is a wideband signal, to prevent aliasing when the sampled time-domain data is transformed to the frequency domain. The sampled data will still contain a noise

component, which can be dealt with by suitable signal processing techniques, provided that the noise component is relatively low and that the statistical properties of the noise component are known [31, 83].

3.2 Choice of Excitation Signal

A wide variety of techniques are available by which the frequency-response characteristics of power transformers can be measured. In principle, these methods differ only in the type of excitation signal that is applied to the transformer during a frequency response measurement [84, 85]. The type of signal that is chosen can have a large influence on the accuracy and validity of frequency response measurements. Several excitation signals, commonly applied to transformer frequency response measurements, are evaluated in this section, with reference to their frequency-domain properties and the excitation levels that can be obtained practically.

During frequency response measurements, it is desirable to excite the transformer under test at a reasonably high excitation level, in order to excite the transformer at a level at which non-power-frequency excitation signals are likely to occur in practice. In this way, the effects that the non-linear properties of the transformer have on its frequency-response characteristics will be similar to the non-linearities encountered e.g. by power system harmonic voltages [86, 84, 85]. Increasing the excitation level has the added benefit of increasing the signal-to-noise ratio of the frequency response measurements [74], provided that an increase in the signal level does not disproportionately increase the noise resulting from the non-linear characteristics of the transformer (as is likely to be the case if the transformer is driven into saturation).

Stepped-frequency sinusoidal signals, impulse signals and Pseudo-Random Binary Sequences (PRBS) were considered as excitation signals for the power transformer frequency response measurements:

(a) *Stepped-frequency Sinusoidal Excitation.* The most straight-forward method of measuring the frequency-response characteristics of a transformer is to excite the transformer with a sinusoidal signal. The frequency of the sinusoidal signal is stepped across the frequency range of interest and the magnitudes and relative phase of the excitation- and response signals are measured at each frequency. Especially at freq-

uencies below about 1 kHz, the response waveform is likely to be distorted as a result of the non-linear behaviour of the transformer [86]. A linearized frequency response measurement is obtained by considering only the fundamental component of the excitation- and response signals [43]. Stepped-frequency sinusoidal excitation is known to provide consistent, accurate transformer frequency response measurements [6, 43, 84, 85]. One of the main benefits of applying stepped-frequency sinusoidal excitation is that the non-linear behaviour of the transformer can be analysed at each frequency, as the non-linearities cause harmonic distortion which is directly visible in the measured response signal [74, 84, 85].

The primary disadvantage of stepped-frequency sinusoidal excitation is the time required to perform a complete frequency response measurement. In most cases the measurements are performed by manually adjusting the excitation frequency across the frequency range of interest, resulting in a tedious, time-consuming measurement procedure.

(b) *Impulse Excitation.* The use of an impulse as a wideband excitation signal for power transformer frequency response measurements is very popular, especially for condition monitoring applications using the FRA method [5, 7, 8, 87, 84, 85]. For FRA measurements, a low-voltage impulse with a peak voltage of a few 100 V is typically used [5, 8]. Reasonably simple circuitry is required to implement a suitable low-voltage impulse generator, as shown in figure 3.2. An impulse is formed by discharging capacitor C_1 via a pulse-shaping circuit by closing switch S_2, after C_1 has been charged via S_1 (with S_2 open). The shape of the impulse, and hence its frequency-domain properties, depends on the values of C_1, C_2, R_1 and R_2, but is also affected by the input impedance of the transformer under test [84, 85].

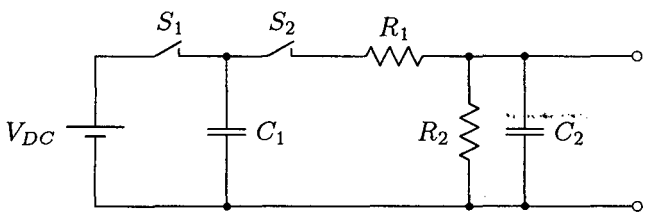

Figure 3.2: Impulse generator.

Although the power spectral density of a low-voltage impulse signal is low compared to e.g. a sinusoidal excitation signal, good frequency response measurement results have been reported up to frequencies of 10 MHz [5, 7, 8, 87]. However, Germishuizen [88] investigated the use of impulse excitation for power transformer frequency response measurements, with particular reference to the performance of

the method in the low-frequency range (below 1 kHz). Germishuizen found that impulse excitation yielded very poor frequency response measurements in this frequency range, due to the non-linear characteristics of the transformer under test. (The reason for this is also briefly investigated in section 3.7.) This poor performance in the low frequency range is the reason why impulse excitation is not applied in this investigation.

(c) *PRBS Excitation.* PRBS signals, also known as Maximum Length Binary Sequences (MLBS), are usually generated with a shift-register inside a feedback loop as shown in figure 3.3 [89, 74, 90]. The choice of the number of shift-register stages n_s and the feedback tapping-point m_s is not arbitrary, but a number of combinations exist, making it possible to generate a variety of PRBS signals with different frequency-domain properties [89, 90, 86]. The length of the generated PRBS increases with n_s and is given by $N_s = 2^{n_s} - 1$. When the shift register has been clocked N_s times the sequence repeats, i.e. after a time $T_s = N_s/f_{clock}$, where f_{clock} is the frequency at which the shift-register is clocked. The digital output of the shift-register is usually shifted in level and amplified, so that the PRBS assumes levels of $+a$ or $-a$, corresponding to a digital 1 or 0, respectively.

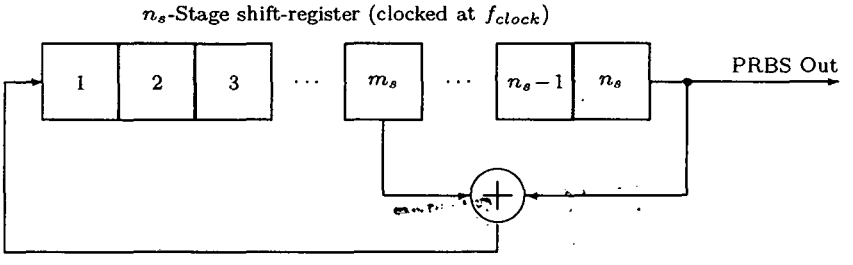

Figure 3.3: Generation of a PRBS signal using a shift-register

A periodic (repeating) PRBS is a binary signal with an auto-correlation function, $r_{xx}(\tau)$, which is an optimal approximation of a Dirac pulse for given values of n_s and f_{clock} [74], as shown in figure 3.4. Of all the possible sequences which can be generated with an n_s-stage shift register, the PRBS has the longest period and the shortest correlation length, which means that its power spectral density, $P_{xx}(\omega)$, is as flat as possible, as the auto-correlation function and the power spectral density are related to each other by the Fourier transform [74, 89, 82]. The power spectral density of a repeating PRBS is a discrete function of frequency, consisting of lines spaced at frequency intervals of f_{clock}/N_s, bordered by the envelope shown in figure 3.5. The power spectral density remains reasonably flat up to its -3 dB point at $\frac{1}{3}f_{clock}$.

For a single (non-repetitive) PRBS, the auto-correlation function also drops to a low

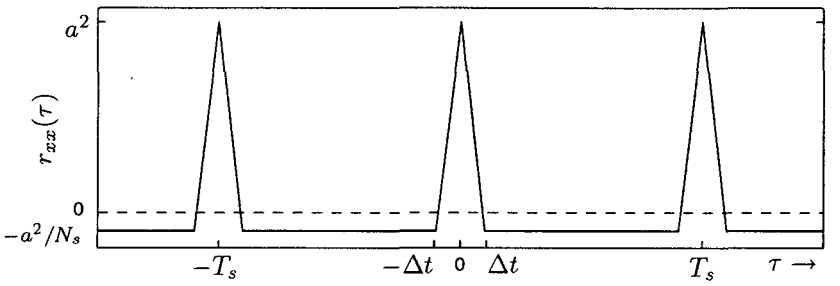

Figure 3.4: Auto-correlation, $r_{xx}(\tau)$, of a repetitive PRBS signal.

value for $|\tau| > \Delta t = 1/f_{clock}$ but becomes equal to zero for $|\tau| \geq T_s$, so that only the pulse at $\tau = 0$ in figure 3.4 is retained. Thus, the power spectral density follows the same function as the repetitive case, but is a continuous function of frequency as shown in figure 3.5.

As its name implies, a PRBS is a binary signal, i.e. it only assumes one of two signal levels ($+a$ or $-a$). This suggests that high-level PRBS excitation signals can be generated by amplifying a digital PRBS signal with power-electronic switching elements. Such PRBS generators have been described by Van Rooijen and Vermeulen [91] and by Cornelissen *et al.* [92, 90]. The generator developed by Cornelissen [90] consists of a programmable digital PRBS source which drives MOSFET switching elements and can supply PRBS signals with current levels up to 5 A or voltage levels up to 700 V. The flat power spectral density of a PRBS over a wide frequency range and the ability to generate PRBS signals at high current- or voltage-levels, makes it an excellent choice of wideband excitation signal for transformer frequency response measurements.

For the reasons discussed above, PRBS excitation was selected as the preferred excitation method for transformer frequency response measurements. However, as some uncertainty existed as to the accuracy of PRBS frequency response measurements, especially at frequencies below 1 kHz, it was decided to also obtain a set of stepped-frequency response measurements to validate the PRBS measurements. Once the validity of frequency response measurements with PRBS excitation had been established, this method could be applied to obtain transformer frequency response measurements within a very short time.

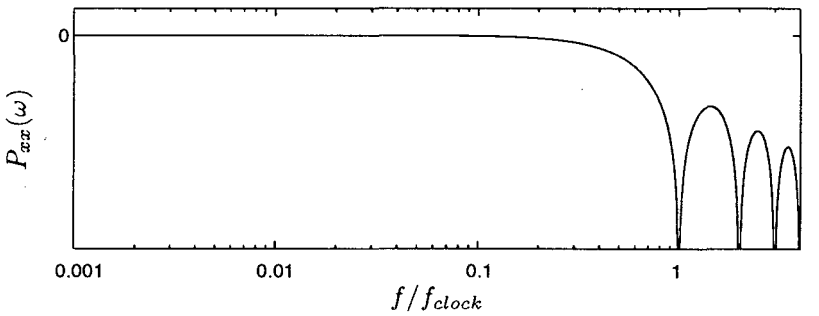

Figure 3.5: Power spectral density, $P_{xx}(\omega)$, of a non-repetitive PRBS signal. Note that the frequency-axis has been normalized with respect to f_{clock}.

3.3 Instrumentation

3.3.1 Data Acquisition System

An overview of the instrumentation arrangement for the transformer frequency response measurements is shown in figure 3.6. The transformer excitation and response signals are sampled by a Yokogawa Model 3656 Analysing Recorder, which has the following specifications:

Analog sub-system

Number of channels:	2
Input voltage range:	±60 mV to ±60 V (peak).
Input impedance:	Standard 1 MΩ ‖ 13 pF.
Anti-aliasing filters	
Cut-off frequency, f_C:	Adjustable from 10 Hz to 200 kHz in 1–2–5 steps.
Stop-band roll-off:	-40 dB @ $1.27f_C$, -60 dB @ $1.4f_C$
Pass-band ripple:	up to ±1.5 dB.

Digital sub-system

Sampling rate:	Adjustable from 0.01 Hz to 5 MHz in 1–2–5 steps.
Resolution:	10 bits (60.2 dB dynamic range).
Memory:	8000 Samples per channel.

The Yokogawa 3656 data acquisition system is connected to a host computer via an IEEE–488 (GPIB) parallel interface. The sampled time-domain data is downloaded to the host computer via this interface for processing and frequency response calculation.

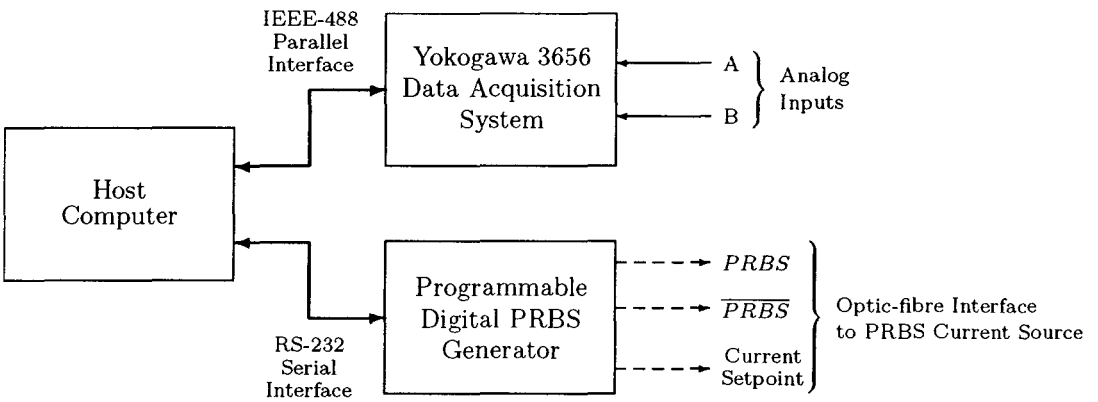

Figure 3.6: Computer-based instrumentation system for the transformer frequency response measurements.

The use of anti-aliasing filters is mandatory to avoid aliasing, especially when a PRBS signal is used to excite the transformer under test, as the power spectral density of these signals will normally contain energy above the Nyquist frequency of the sampling system. Practical anti-aliasing filters are not ideal, i.e. the sampled signals will be distorted by the magnitude and phase responses of the filter, which results in measurement errors. Two signals are sampled by the Yokogawa 3656 instrument during frequency response measurements. Provided that the amplitude and phase responses of the two filters are identical, errors introduced by the anti-aliasing filters are effectively cancelled when the frequency response is calculated, as the relative magnitude and phase angle of the two sampled signals is determined. However, it can not be assumed that the two filters are identical, as some difference is inevitable due to the tolerances of the components that were used to construct the filters. By applying the same wideband signal to both inputs and comparing the sampled signals in the frequency domain, it was found that the magnitude responses of the filters differed by up to 1 dB across the pass-band width of the filter, while the maximum difference in the phase responses was 3°. These errors are reduced by compensating measured frequency response data with the transfer function that is obtained by sampling the same wideband signal with both channels. Such a compensation response is required for each set of filters (i.e. each cut-off frequency) that will be used during frequency response measurements.

At the excitation levels that were used during the transformer frequency response measurements, the input currents to the transformer under test were very low (compared to the transformer rating); typically in the range between 0.1 mA and 500 mA. Specially designed low-inductance shunt resistors, with a measurement bandwidth of several MHz, were used to measure these currents [43]. Shunt resistor values (R_{shunt}) between 11 Ω and 1 125 Ω were used. Depending on the frequency response measurement that was being carried out, R_{shunt} was selected to be high enough to ensure a high signal-to-noise ratio in the shunt-resistor output voltage, but low enough not to affect the excitation level at the transformer terminals. Voltage measurements were always carried out with 10:1 or 100:1 probes, calibrated and matched to the input impedance of the Yokogawa 3656 instrument.

3.3.2 PRBS Excitation Source

The PRBS excitation source that is used in this investigation is described in detail by Cornelissen [90, 92]. The PRBS source is controlled from the host computer, via an RS 232 serial interface and consists of two sub-systems. The digital sub-system (shown in figure 3.6) contains a programmable PRBS generator which drives the PRBS output stage via a fibre-optic interface to ensure galvanic isolation between the two sub-systems. The parameters of the PRBS signal can be set from the host computer, including the length of the sequence, N_s, the clock frequency, f_{clock}, and the amplitude setpoint, I_a.

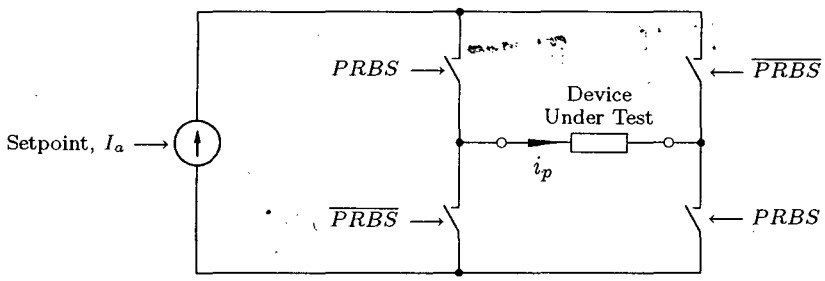

Figure 3.7: Topology of the PRBS current source.

Two digital control signals, $PRBS$ and its complement $\overline{PRBS}$, are used to control the state of semiconductor switching elements so that a PRBS source with high output levels is realized, as shown in figure 3.7. The device under test is connected to a DC current source via a MOSFET H-bridge, thus causing a PRBS current with levels $\pm I_a$ to be forced through the device. The current source is realized by a fast current limiter, designed to supply a constant current from a voltage source of up to 700 V. The output current setpoint of the current controller can be adjusted from the host computer via the digital

sub-system of the PRBS generator. The current source can supply a maximum current of 5 A, but is subject to a maximum power dissipation capability of 150 W. The frequency range over which the PRBS source can be applied is limited by the maximum switching frequency of the MOSFET switches and the dynamic response of the current source. However, PRBS clock frequencies in excess of 200 kHz could be obtained, which was found to be sufficient for power transformer frequency response measurements up to 100 kHz.

3.3.3 Stepped-frequency Excitation Source

A Meguro MCR-4031 signal generator was used to provide a sinusoidal excitation signal. The maximum output voltage of this signal generator is limited to 1 V RMS and an additional power amplifier was used to increase the excitation voltage, as shown in figure 3.8 [22, 43]. A separate frequency counter was used to provide an accurate reading of the signal generator output frequency (which is adjusted manually).

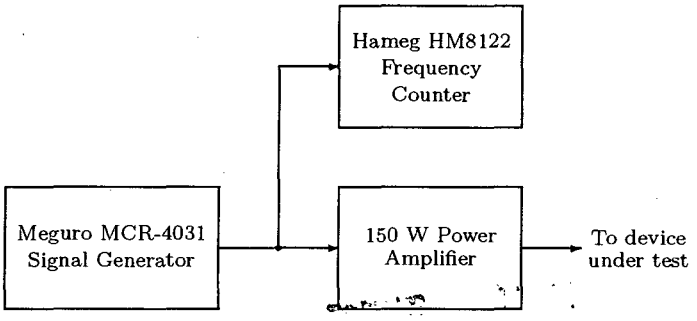

Figure 3.8: Instrumentation for stepped-frequency excitation.

The arrangement is limited by the capabilities of the power amplifier, which has a power bandwidth of DC to ≈60 kHz. In practice, the useful bandwidth is also affected by the varying load impedance presented to the amplifier by the transformer under test.

3.4 Frequency Response Measurements Using Stepped-frequency Excitation

3.4.1 Experimental Arrangements

Three transformer frequency responses were measured by exciting the transformer from the LV terminals:

- LV open-circuit input impedance, $\mathbf{Z}_{Loc}(j\omega)$.
- LV short-circuit input impedance, $\mathbf{Z}_{Lsc}(j\omega)$.
- LV–HV voltage transformation ratio, $\mathbf{H}_{LH}(j\omega)$.

A similar experimental arrangement was employed for the measurement of each of these three responses and is shown in figure 3.9. Note that one terminal of each winding, as well as the transformer tank (and core) are earthed. All voltage measurements were carried out with respect to the earthing point. In figure 3.9, the LV terminals are designated by LV_1 and LV_2, while the HV terminals are labelled HV_1 and HV_2.

As discussed in section 3.3.3, the transformer was excited from a sine-wave generator, using a power amplifier to increase the excitation voltage to a reasonable level. The bandwidth of the power amplifier extends to approximately 60 kHz, which means that its output voltage drops considerably beyond this point. However, the terminal voltage of the transformer can be increased by series-resonating the transformer input reactance with an external, variable inductor or capacitor, X_r, depending on whether the transformer input impedance is capacitive or inductive at the test frequency (figure 3.9). Using this technique, it was possible to maintain an excitation level of 4.5 % of the transformer LV voltage rating across the required 10 Hz to 100 kHz frequency range for the open-circuit measurements and an excitation level of 2.3 % for the short-circuit measurements. In the case of the short-circuit measurements, the excitation system is limited by the maximum output current capability of the power amplifier. The disadvantage of increasing the excitation level by forming a series-resonant circuit with the transformer winding is that additional time is required to adjust X_r at each frequency, so that several hours were required to complete one frequency response measurement.

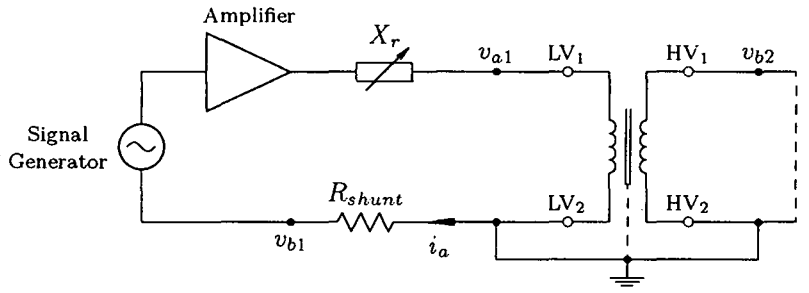

Figure 3.9: Experimental arrangement for stepped-frequency measurement of the transformer frequency response characteristics with excitation applied to the LV terminals.

The LV input-impedance frequency responses, $\mathbf{Z}_{Loc}(j\omega)$ and $\mathbf{Z}_{Lsc}(j\omega)$, were measured with the HV terminals open-circuit and short-circuit respectively. In each case, $v_{a1}(t)$ (see figure 3.9) was measured as the response voltage, $y(t)$, while the excitation signal, $x(t)$, i.e. the input current to the winding, $i_a(t)$, is given by:

$$x(t) = i_a(t) = \frac{-v_{b1}(t)}{R_{shunt}}. \tag{3.2}$$

For both responses a shunt resistance of $R_{shunt} = 11\,\Omega$ was used. The LV–HV voltage transformation ratio, $\mathbf{H}_{LH}(j\omega)$, was measured with R_{shunt} short-circuited and with the HV winding open-circuit. For $\mathbf{H}_{LH}(j\omega)$, the excitation and response signals were v_{a1} and v_{b2} respectively. A summary of the details of the LV frequency response measurements is given in table 3.1.

Table 3.1: Instrumentation and signal details for stepped-frequency response measurement with excitation applied to the LV terminals.

Frequency response	R_{shunt} [Ω]	Input signal, $x(t)$	Response signal, $y(t)$	Excitation level	HV Terminals
$\mathbf{Z}_{Loc}(j\omega)$	11	$-v_{b1}(t)/R_{shunt}$	$v_{a1}(t)$	10 V (4.2 %)	Open-circuit
$\mathbf{Z}_{Lsc}(j\omega)$	11	$-v_{b1}(t)/R_{shunt}$	$v_{a1}(t)$	5 V (2.1 %)	Short-circuit
$\mathbf{H}_{LH}(j\omega)$	0	$v_{a1}(t)$	$v_{b2}(t)$	10 V (4.2 %)	Open-circuit

Similar to the frequency responses that were measured by exciting the transformer from the LV terminals, three frequency responses were measured by exciting the transformer from the HV terminals:

- HV open-circuit input impedance, $\mathbf{Z}_{Hoc}(j\omega)$.

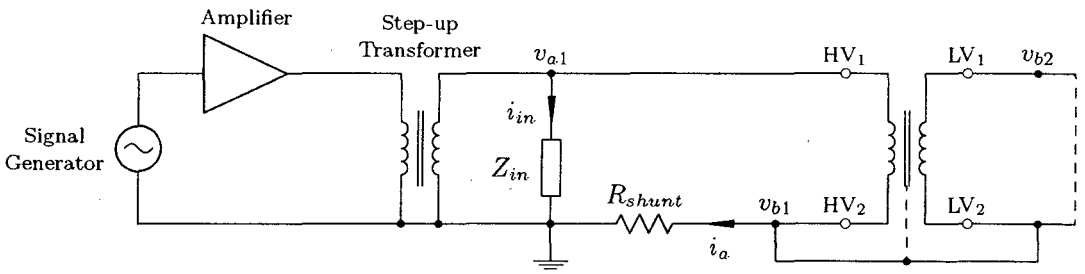

Figure 3.10: Stepped-frequency response measurement with the transformer excited from the HV terminals, using a step-up transformer to increase the terminal voltage.

- HV short-circuit input impedance, $\mathbf{Z}_{Hsc}(j\omega)$.
- HV–LV voltage transformation ratio, $\mathbf{H}_{HL}(j\omega)$.

The experimental arrangement that was used to measure these responses is shown in figure 3.10. A step-up transformer was used to raise the output voltage of the power amplifier to about 1 % of the rated HV terminal voltage. This arrangement was found to work well up to about 10 kHz; at frequencies above 10 kHz the limited bandwidth of the step-up transformer resulted in a rapid reduction of the maximum attainable excitation level as a function of frequency (also see [23]). At frequencies above 10 kHz, the open-circuit and short-circuit HV terminal input impedance of the 16 kVA transformer is capacitive and it was possible to form a series resonance between the transformer input impedance and an external, adjustable inductance, X_r, to increase the excitation voltage. The resulting resonant circuit was lightly damped, so that the 1 % excitation level could be maintained, for frequencies above 10 kHz, without the use of the step-up transformer, as shown in figure 3.11.

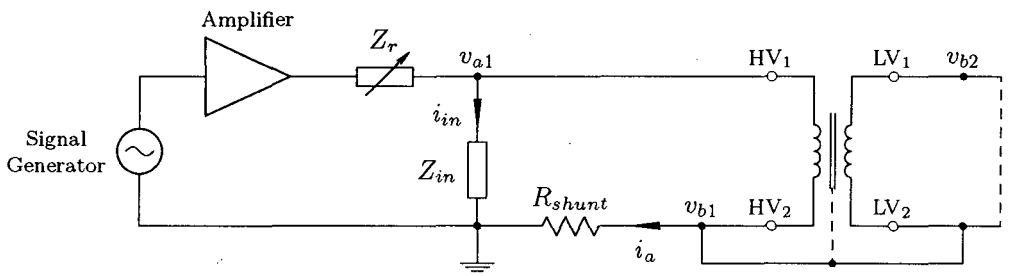

Figure 3.11: Stepped-frequency response measurement with the transformer excited from the HV terminals, using a series-resonant circuit to increase the terminal voltage.

At the main parallel resonant frequencies of the HV input-impedance frequency responses, the input impedance of the 16 kVA transformer is in the order of 10 MΩ. This is in the same order of magnitude as the input impedance presented by the digitising instrument via a 10:1 probe. Thus, if the HV terminal voltage, v_{a1}, is measured with respect to an earthing point at the connection of terminals HV_2 and LV_2 (as in figure 3.9), the current flowing through R_{shunt} would be the sum of the currents flowing through the instrument input impedance and the transformer input impedance respectively. This would cause unacceptable errors in the measured frequency responses. The problem was eliminated by moving the earthing point to the position shown in figures 3.10 and 3.11. The current, i_{in}, flowing through the input impedance, Z_{in}, of the data acquisition system is now confined to a loop that will not affect the transformer terminal current measurements. The voltage signal v_{a1} is now the sum of the transformer terminal voltage and the voltage across R_{shunt}, so that the response signal, $y(t)$, is given by:

$$y(t) = v_{a1}(t) - v_{b1}(t), \tag{3.3}$$

while the input signal, $x(t)$, i.e. the transformer input current, i_a, is:

$$x(t) = i_a = \frac{v_{b1}(t)}{R_{shunt}}. \tag{3.4}$$

Details of the stepped-frequency response measurements, with excitation applied to the HV terminals, are summarized in table 3.2.

Table 3.2: Instrumentation and signal details for stepped-frequency response measurement with excitation applied to the HV terminals.

Frequency response	R_{shunt} [Ω]	Input signal, $x(t)$	Response signal, $y(t)$	Excitation level	HV Terminals
$\mathbf{Z}_{Hoc}(j\omega)$	1250	$v_{b1}(t)/R_{shunt}$	$v_{a1}(t) - v_{b1}(t)$	110 V (0.5 %)	Open-circuit
$\mathbf{Z}_{Hsc}(j\omega)$	1250	$v_{b1}(t)/R_{shunt}$	$v_{a1}(t) - v_{b1}(t)$	110 V (0.5 %)	Short-circuit
$\mathbf{H}_{HL}(j\omega)$	0	$v_{a1}(t)$	$v_{b2}(t)$	110 V (0.5 %)	Open-circuit

3.4.2 Signal Processing

During the stepped-frequency transformer frequency response measurements, the excitation signal, $x(t)$, and the response signal, $y(t)$, were sampled by the data acquisition system at each frequency of interest. These signals are corrupted by noise and are often distorted due to the non-linear characteristics of the transformer or due to harmonic distortion introduced by the excitation system. Only the magnitudes and relative phase of the fundamental components of $x(t)$ and $y(t)$ are of interest. This information can be extracted by obtaining the Fourier transform of $x(t)$ and $y(t)$, so that the frequency response at the fundamental frequency, ω_f, is given by:

$$\mathbf{G}(j\omega_f) = \frac{\mathbf{Y}(j\omega_f)}{\mathbf{X}(j\omega_f)}, \tag{3.5}$$

where $\mathbf{X}(j\omega_f)$ and $\mathbf{X}(j\omega_f)$ are the Fourier transforms of $x(t)$ and $y(t)$ at ω_f. Practically, this procedure has a number of possible sources of error [28]. Signals $x(t)$ and $y(t)$ are each sampled at a sampling interval of T_s to yield M discrete data points, $x(kT_s)$ and $y(kT_s)$, where $k = 1 \ldots M$. Taking the Discrete Fourier Transform (DFT) of $x(kT_s)$ and $y(kT_s)$ yields the following estimate of the frequency response spectrum:

$$\check{\mathbf{G}}(j\omega_k) = \frac{\check{\mathbf{Y}}(j\omega_k)}{\check{\mathbf{X}}(j\omega_k)}, \tag{3.6}$$

where

$$\omega_k = \frac{2\pi k}{T_s M}. \tag{3.7}$$

Because the sampling clock and the excitation frequency are derived from separate sources, the sampling frequency is unlikely to be an exact integer multiple of the excitation frequency, so that there is no ω_k that coincides exactly with ω_f. Thus, $\check{\mathbf{G}}(j\omega)$ is not evaluated at ω_f, but at the closest value of ω_k. The resulting error can be reduced by truncating $x(kT_s)$ and $y(kT_s)$ so that M samples represent, as closely as possible, an integer number of cycles of the excitation frequency [28]. Further, the sampling interval should be increased as far as possible, without violating the Nyquist criterion and the original sampled record length must be as long as possible. In this way the spacing, $\Delta\omega_k$, between successive values of ω_k can be decreased, as

$$\Delta\omega_k = \frac{2\pi}{T_s M}. \tag{3.8}$$

The sampled signals $x(kT_s)$ and $y(kT_s)$ must be truncated at the same point to preserve their relative phase. Due to their finite record lengths, discontinuities exist at either end of $x(kT_s)$ and $y(kT_s)$ which leads to leakage in their respective frequency spectra [28]. Spectral leakage is reduced by applying a suitable time-domain windowing function to the sampled data. A Hanning window [83, 28] was applied for the transformer frequency response measurements.

3.5 Frequency Response Measurements Using PRBS Excitation

The stepped-frequency transformer response measurements, discussed in section 3.4, require the excitation- and response signals to be sampled at each frequency of interest. Using PRBS wideband excitation, frequency response measurements can be carried out within a much shorter time, as only one or two measurements of the excitation and response signals are required to calculate an estimate of a frequency response.

3.5.1 Experimental Arrangements

The experimental arrangement that was used to measure the 16 kVA transformer frequency responses with a PRBS excitation signal applied to the LV terminals ($\mathbf{Z}_{Loc}(j\omega)$, $\mathbf{Z}_{Lsc}(j\omega)$ and $\mathbf{H}_{LH}(j\omega)$) is shown in figure 3.12. Typically, a PRBS signal, with a signal level of I_a=0.4 A and a clock frequency up to 200 kHz was applied to the transformer LV terminals. For the LV input impedance frequency responses, the excitation and response signals are:

$$\begin{aligned} x(t) &= i_p(t) = \frac{-v_{b1}(t)}{R_{shunt}} \qquad \text{and} \\ y(t) &= v_{a1}(t) \end{aligned} \tag{3.9}$$

respectively, with all voltage signals measured with respect to the earthing point. For the LV–HV voltage transformation ratio, the excitation and response signals are given by $x(t) = v_{a1}(t)$ and $y(t) = v_{b2}(t)$ respectively (also see table 3.3).

Figure 3.13 shows the arrangement that was used to obtain the transformer frequency responses that are measured with the PRBS excitation signal applied to the HV terminals ($\mathbf{Z}_{Hoc}(j\omega)$, $\mathbf{Z}_{Hsc}(j\omega)$ and $\mathbf{H}_{HL}(j\omega)$). As discussed in section 3.4.1, the earthing point is moved to the source-side of R_{shunt}, so that the current, i_{in}, flowing through the data acquisition instrument input impedance, Z_{in}, does not result in erroneous transformer terminal current measurements. Thus, for the input-impedance frequency responses with excitation applied to the HV terminals, the excitation and response signals are given by:

$$x(t) = \frac{v_{b1}(t)}{R_{shunt}} \qquad \text{and}$$
$$y(t) = v_{a1}(t) - v_{b1}(t) \tag{3.10}$$

respectively, with all voltage signals measured with respect to the earthing point. For the HV–LV voltage transformation ratio, the excitation and response signals are given by $x(t) = v_{a1}(t)$ and $y(t) = v_{b2}(t)$ respectively, with R_{shunt} short-circuited. A summary of the relevant arrangement and signal details is provided in table 3.3.

The PRBS current source is not ideal, i.e. it can not deliver the full setpoint current if its load impedance is too high. The input impedance presented between the HV terminals of the 16 kVA transformer is in the order of several MΩ across most of the frequency range between 10 Hz and 100 kHz. Even with the PRBS current setpoint at a very low value (100 mA is the minimum value), the transformer input impedance is too high for the full PRBS current to flow. Instead, a PRBS voltage signal with an amplitude equal to the PRBS current controller source voltage is applied, while the maximum current is limited to the PRBS current setpoint. The PRBS source voltage was typically set to 200 V during the HV terminal frequency response measurements. Practically it was found that the non-ideal behaviour of the PRBS source does not noticeably affect the frequency response measurement results or the frequency range over which excitation is obtained.

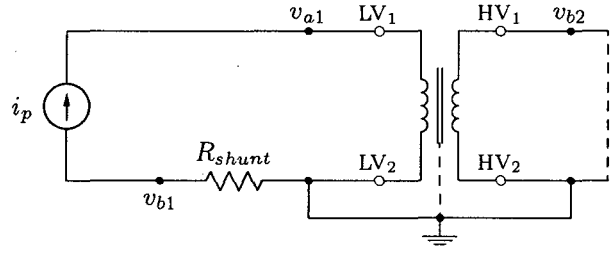

Figure 3.12: Experimental arrangement for frequency response measurements with PRBS excitation applied to the LV terminals.

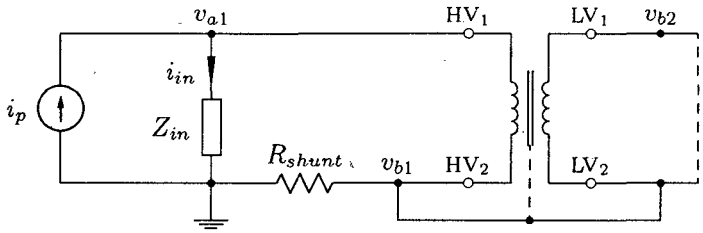

Figure 3.13: Experimental arrangement for frequency response measurements with PRBS excitation applied to the HV terminals.

Because the length of the time-domain data records that can be sampled with the data acquisition system is limited to 8000 samples per channel, it is impractical to sample one set of time-domain data in order to calculate a transformer frequency response over the full 10 Hz to 100 kHz frequency range, as the spacing between the frequency-domain data points is too high in the lower frequency range. E.g. if the time-domain data is sampled at 500 kHz, the spacing between the frequency-domain data points is 62.5 Hz, which is sufficient above 1 kHz, but yields only two or three frequency response points in the vicinity of the first parallel resonance of the open-circuit input impedances. In practice, two frequency decades were spanned by one measurement, so that two sets of response measurements were required for each frequency response. The resulting two frequency responses are then joined in the frequency-domain to form the required frequency response over the full 10 Hz to 100 kHz range. Details of the PRBS signals and the excitation levels that were used to obtain the frequency responses of the 16 kVA transformer are given in table 3.4. The sampling rates and the anti-aliasing filter cut-off frequencies that were used, are also shown.

Table 3.3: Instrumentation and signal details for transformer frequency response measurements using PRBS excitation.

Frequency response	R_{shunt} [Ω]	Input signal, $x(t)$	Response signal, $y(t)$	Transformer terminals	Figure
$\mathbf{Z}_{Loc}(j\omega)$	11	$-v_{b1}(t)/R_{shunt}$	$v_{a1}(t)$	HV open-circuit	3.12
$\mathbf{Z}_{Lsc}(j\omega)$	11	$-v_{b1}(t)/R_{shunt}$	$v_{a1}(t)$	HV short-circuit	3.12
$\mathbf{H}_{LH}(j\omega)$	0	$v_{a1}(t)$	$v_{b2}(t)$	HV open-circuit	3.12
$\mathbf{Z}_{Hoc}(j\omega)$	1250	$v_{b1}(t)/R_{shunt}$	$v_{a1}(t) - v_{b1}(t)$	LV open-circuit	3.13
$\mathbf{Z}_{Hsc}(j\omega)$	1250	$v_{b1}(t)/R_{shunt}$	$v_{a1}(t) - v_{b1}(t)$	LV short-circuit	3.13
$\mathbf{H}_{HL}(j\omega)$	0	$v_{a1}(t)$	$v_{b2}(t)$	LV open-circuit	3.13

Table 3.4: PRBS signals used to determine the frequency response characteristics of the 16 kVA test transformer.

Frequency response	PRBS Signal			Data Acquisition	
	n_s	f_{clock} [kHz]	a	Filter f_C [kHz]	f_s [kHz]
$\mathbf{Z}_{Loc}(j\omega)$	11	2	0.4 A	1	5
	11	200	0.4 A	100	500
$\mathbf{Z}_{Lsc}(j\omega)$	9	4	0.4 A	10	50
	11	200	0.4 A	100	500
$\mathbf{H}_{LH}(j\omega)$	9	4	0.4 A	10	50
	11	200	0.4 A	100	500
$\mathbf{Z}_{Hoc}(j\omega)$	11	2	200 V	1	5
	11	200	200 V	100	500
$\mathbf{Z}_{Hsc}(j\omega)$	9	4	100 V	10	50
	11	200	100 V	100	500
$\mathbf{H}_{HL}(j\omega)$	9	4	200 V	10	50
	11	200	200 V	100	500

3.5.2 Signal Processing

During a frequency response measurement, the transformer under test is excited by a PRBS signal while the excitation signal, $x(t)$, and the required response signal, $y(t)$, are sampled by the data acquisition system. Typical excitation and response signals are shown in figure 3.14; in this case the first 4 ms of the PRBS input current and the terminal response voltage, that were used to determine the transformer LV open-circuit input-impedance frequency response, are shown. The PRBS excitation current shown in figure 3.14 was clocked at 40 kHz, with $n_s = 9$, and excitation level a=0:4 A. The full sequence is 12.8 ms in length and occupies 6 400 sample points when sampled at 500 kHz.

The power spectral density of the PRBS excitation signal is shown in figure 3.15. It can be seen that the applied PRBS signal provides excitation energy over a wide frequency range. In practice it was found that the signal energy contained in the first sidelobe was high enough to allow frequency response estimation in its frequency range (40 kHz to 80 kHz for the power spectral density shown in figure 3.15). Note that the measured power

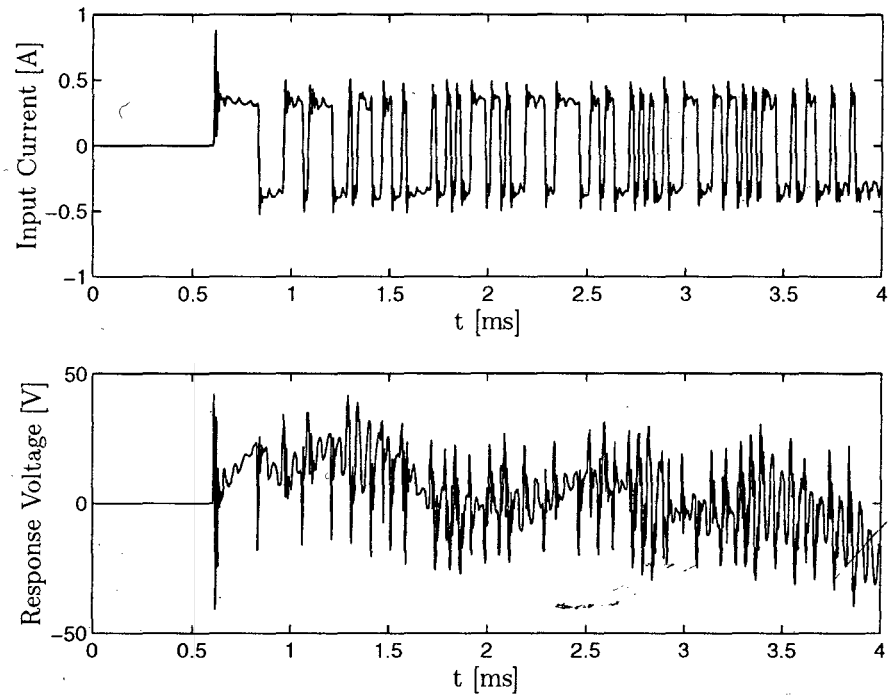

Figure 3.14: Typical excitation and response signals during measurement of the transformer LV open-circuit input impedance.

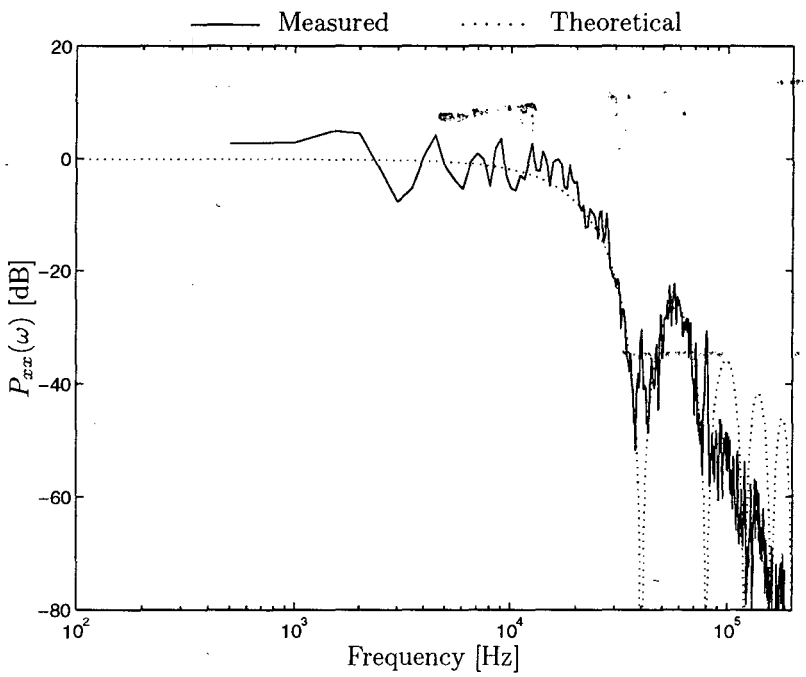

Figure 3.15: Measured and theoretical power density spectrum of the excitation signal shown in figure 3.14.

spectral density agrees well with the theoretical prediction, which is given by [74, 89]:

$$P_{xx}(\omega_k) = \frac{a^2(N_s+1)}{N_s^2}\left[\frac{\sin(k\pi/N_s)}{k\pi/N_s}\right]^2, \tag{3.11}$$

where $\omega_k = 2\pi k f_{clock}/N_s$. Above 80 kHz, the measured power spectral density drops more rapidly than predicted, due to the anti-aliasing filter (f_c=100 kHz) that was used when sampling the PRBS signal.

Given the sampled excitation and response signals, $x(kT_s)$ and $y(kT_s)$, the so-called empirical estimate of one of the transformer frequency responses can be found [31]:

$$\check{\mathbf{G}}(j\omega_k) = \frac{\check{\mathbf{Y}}(j\omega_k)}{\check{\mathbf{X}}(j\omega_k)}, \tag{3.12}$$

where $\check{\mathbf{X}}(j\omega_k)$ and $\check{\mathbf{Y}}(j\omega_k)$ are estimates of the spectra of $x(kT_s)$ and $y(kT_s)$ respectively (obtained by applying the DFT). By applying equation 3.12 to the signals of figure 3.14, the empirical estimate of the LV open-circuit input-impedance frequency response, $\check{\mathbf{Z}}_{Loc}(j\omega_k)$, is found as shown in figure 3.16. The same frequency response, obtained by stepped-frequency excitation is also shown in figure 3.16 for comparison. It is clear that $\check{\mathbf{Z}}_{Loc}(j\omega_k)$ is corrupted by noise, showing some variance around the stepped-frequency reference response, but is virtually unbiased with respect to the reference response. One method of reducing the variance of the empirical frequency response estimate is to average several similar responses in the frequency domain. In practice, this yields good results, but involves the sampling and manipulation of large amounts of data and it was found to be more convenient to smooth the frequency response estimate by applying a spectral estimation algorithm.

A spectral estimator, that is simple to implement and was found to yield excellent results when applied to the empirical estimates of the transformer frequency responses, is described by Kay [83] and by Koopmans [93]. This estimator performs frequency-domain averaging within a rectangular frequency-window, centered around a frequency ω_k and is given by:

$$\bar{\mathbf{G}}(j\omega_k) = \frac{1}{2M+1}\sum_{n=-M}^{M}\check{\mathbf{G}}(j\omega_{k+n}), \tag{3.13}$$

where M is the width of the frequency window to either side of ω_k (the total window width is thus $2M+1$). The estimator of equation 3.13 can be refined by introducing

a weighted frequency window, $W_\gamma(\omega)$, so that response values close to ω_k have a larger influence on $\check{\mathbf{G}}(j\omega_k)$ than values that are further away:

$$\check{\mathbf{G}}(j\omega_k) = \sum_{n=-M}^{M} W_\gamma(n)\breve{\breve{\mathbf{G}}}(j\omega_{k+n}) \,. \tag{3.14}$$

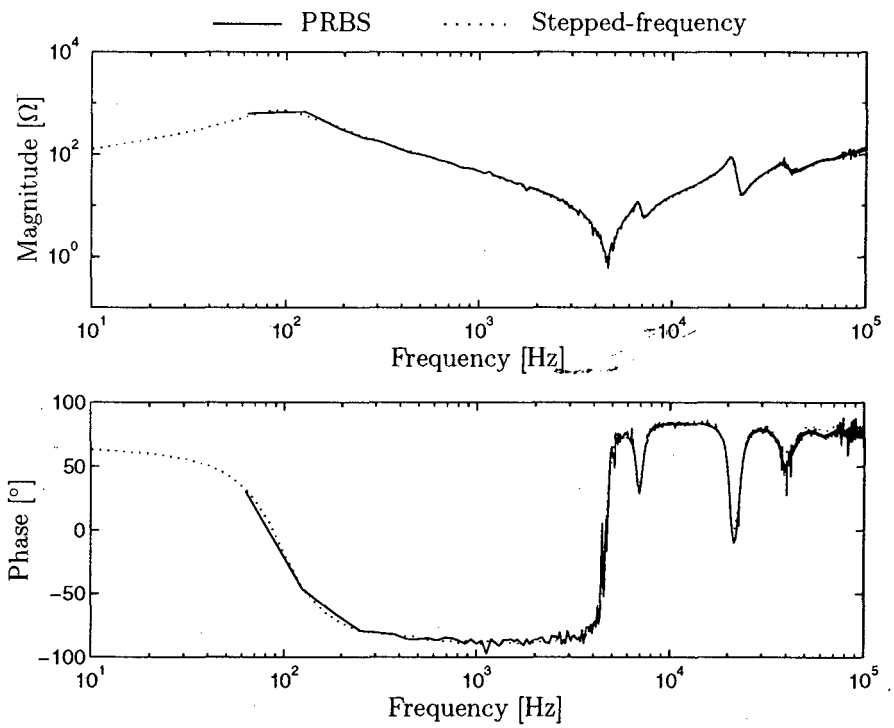

Figure 3.16: Empirical estimate of the transformer LV open-circuit input-impedance frequency response, $\breve{\breve{\mathbf{Z}}}_{Loc}(j\omega_k)$, obtained by applying PRBS excitation and the same response measured by applying stepped-frequency excitation.

A wide variety of weighting functions can be used in equation 3.14. For the transformer frequency responses, the Bartlett frequency window [31, 83] was applied as follows:

$$W_\gamma(n) = \frac{1}{\gamma}\left[\frac{\sin(\gamma\frac{n\pi}{2M})}{\sin(\frac{n\pi}{2M})}\right]^2 , \tag{3.15}$$

where γ controls the width of the frequency window within the frequency range bounded by ω_{k-M} and ω_{k+M}; a value of $\gamma = 2$ was generally used and the overall frequency window width was adjusted by changing M. An optimum value for M is found by trial and error, as it depends on the nature and severity of the noise components in $\breve{\breve{\mathbf{G}}}(j\omega_k)$ as well as

the nature of the frequency response itself [31]. In general, large values of M will reduce the variance of the estimated frequency response while increasing its bias, especially at frequencies where the response changes rapidly.

For the transformer frequency responses obtained with PRBS excitation, the estimator of equation 3.14 was found to give good results. Calculation of the transformer frequency response estimates required very little computing time compared to the time required to calculate a response estimate using e.g. the spa estimator provided by the MATLAB System Identification Toolbox [75], which is a variation of the Blackman-Tukey spectral estimator [31, 83]. The complete set of estimated frequency responses of the 16 kVA transformer are presented in section 3.6 below.

3.6 Frequency Response Measurement Results for the 16 kVA Transformer

This section presents the full set of measured frequency responses, $\check{\mathbf{G}}_{\mathbf{T}}$, of the 16 kVA test transformer, as obtained by using stepped-frequency excitation and by PRBS excitation. From figures 3.17 to 3.22 it can be seen that very good agreement is obtained between the responses measured with stepped-frequency excitation and those obtained by applying PRBS excitation. This validates the accuracy of the frequency response measurements across the 10 Hz to 100 kHz frequency range. At frequencies below 1 kHz, there is some disagreement between the stepped-frequency and PRBS versions of the open-circuit input-impedance frequency responses, $\mathbf{Z}_{Loc}(j\omega)$ and $\mathbf{Z}_{Hoc}(j\omega)$. This disagreement results from the fact that different excitation levels were applied for the stepped-frequency and PRBS measurements. The non-linear effects, which cause this voltage-dependence in the transformer frequency responses, are explored in more detail in section 3.7.

The stepped-frequency and PRBS amplitude responses of $\mathbf{H}_{LH}(j\omega)$, shown in figure 3.21, disagree at the first resonance of the response (4.5 kHz). This error is due to some bias introduced by the spectral estimator that was used to smooth the PRBS frequency response (see section 3.5.2).

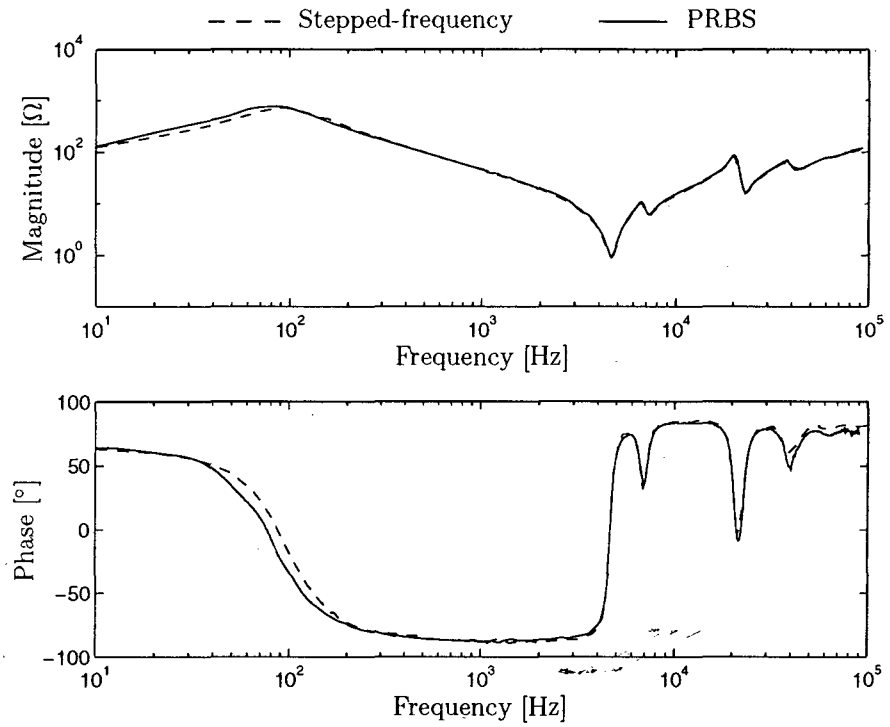

Figure 3.17: Measured LV open-circuit input-impedance frequency response, $\mathbf{Z}_{Loc}(j\omega)$.

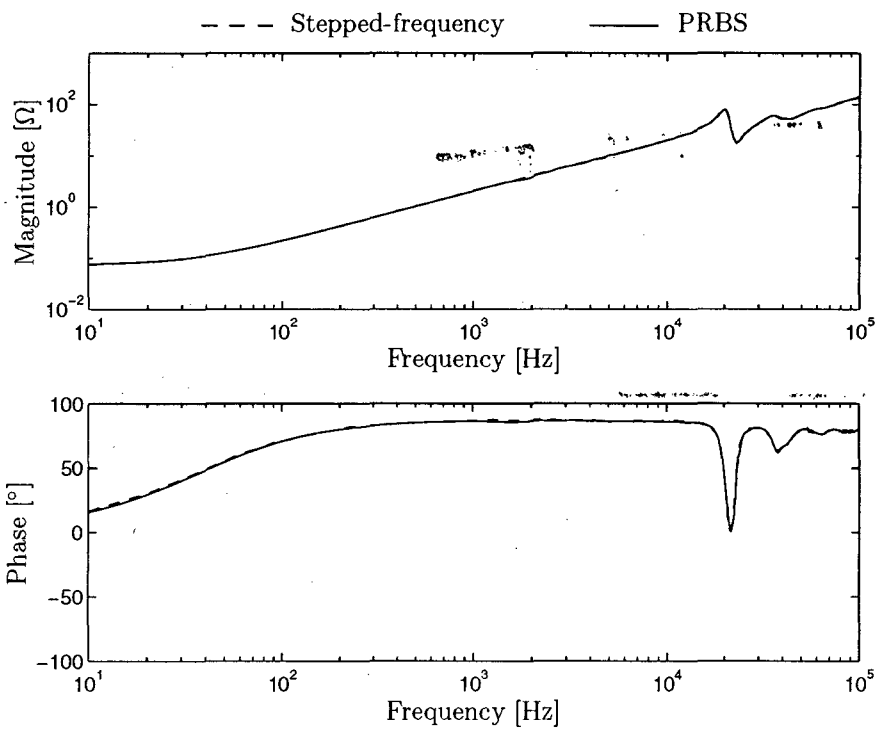

Figure 3.18: Measured LV short-circuit input-impedance frequency response, $\mathbf{Z}_{Lsc}(j\omega)$.

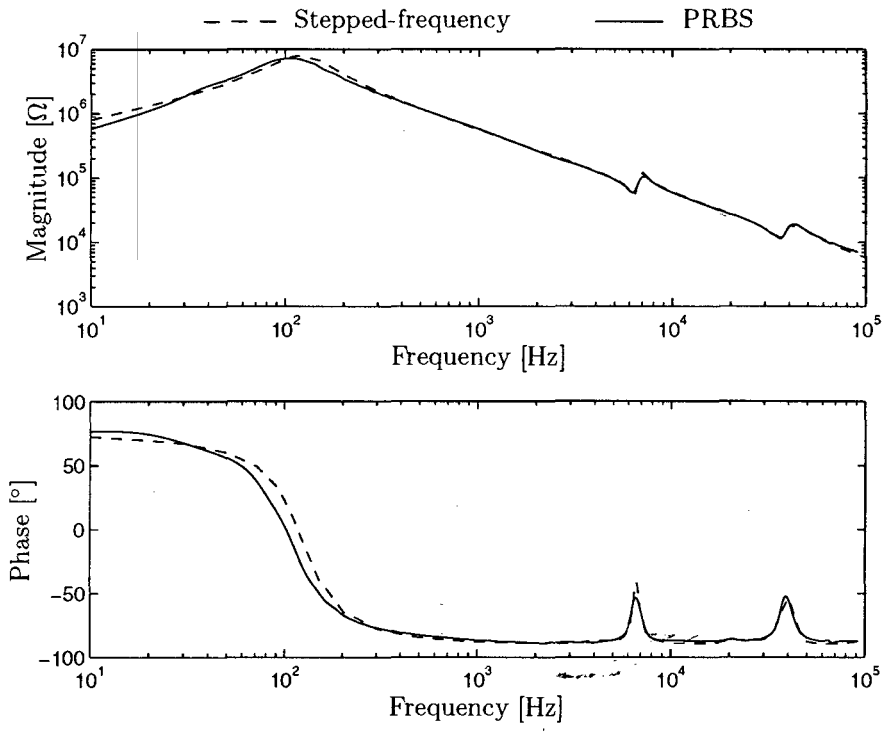

Figure 3.19: Measured HV open-circuit input-impedance frequency response, $\mathbf{Z}_{Hoc}(j\omega)$.

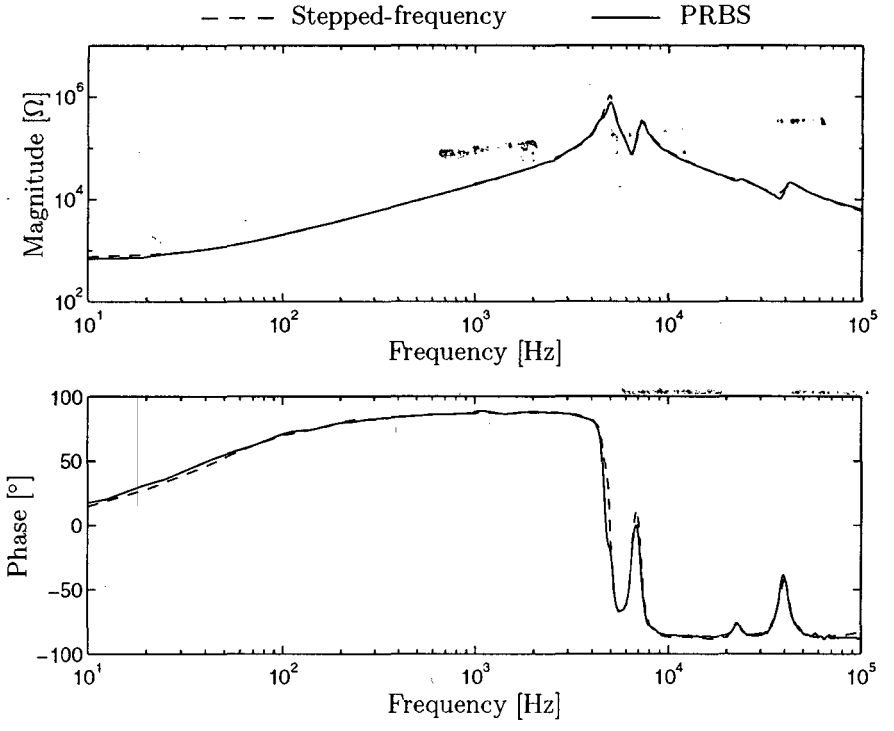

Figure 3.20: Measured HV short-circuit input-impedance frequency response, $\mathbf{Z}_{Hsc}(j\omega)$.

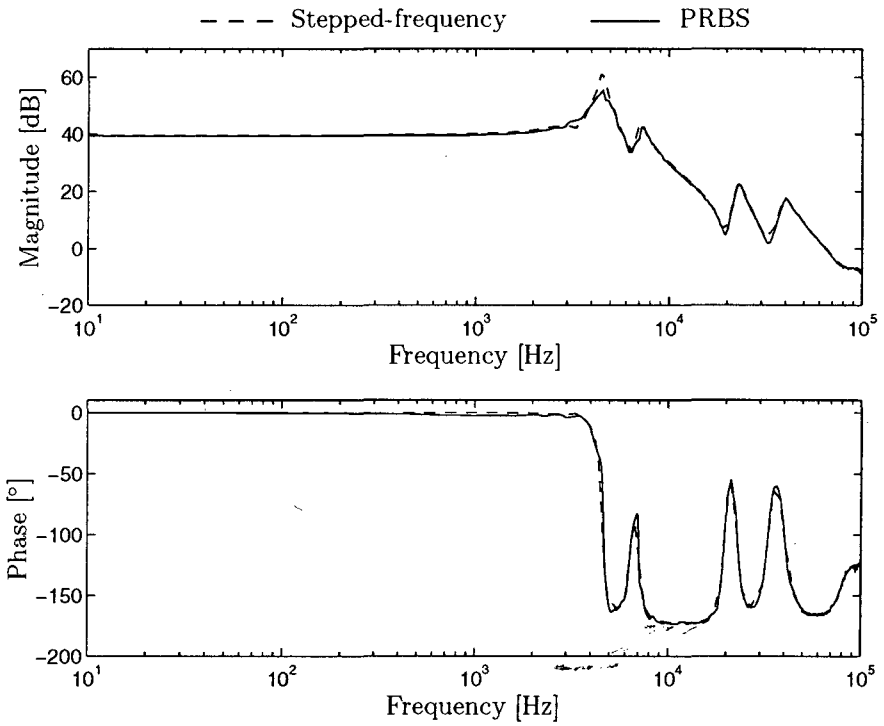

Figure 3.21: Measured LV–HV voltage transformation ratio frequency response, $\mathbf{H}_{LH}(j\omega)$.

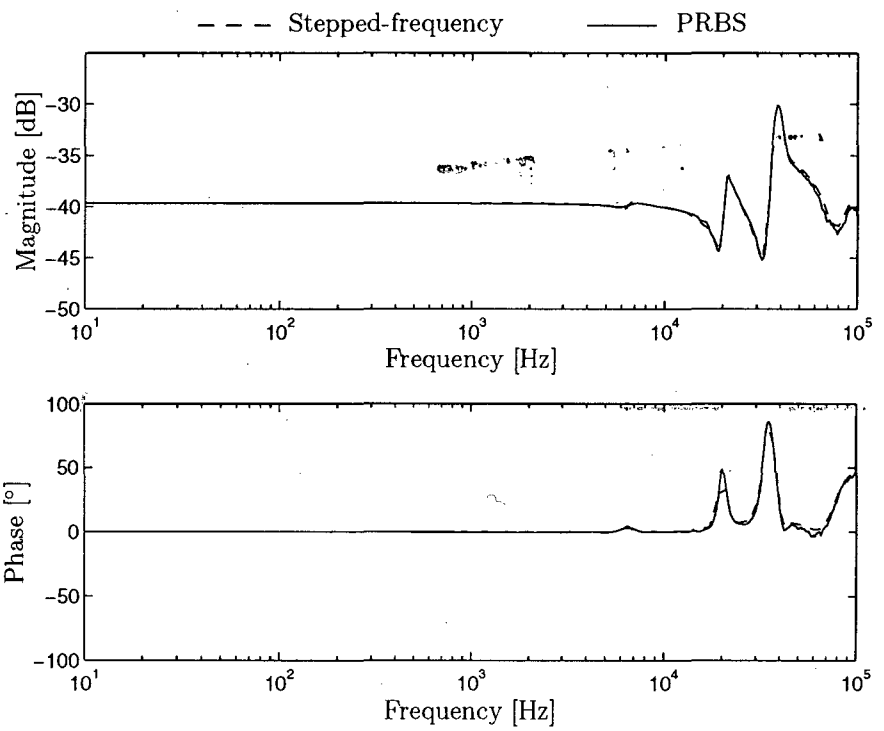

Figure 3.22: Measured HV–LV voltage transformation ratio frequency response, $\mathbf{H}_{HL}(j\omega)$.

3.7 Frequency- and Voltage-dependent Effects

The results presented in section 3.6 show a mismatch, at low frequencies, between the transformer open-circuit input-impedance frequency responses measured by the stepped-frequency and PRBS excitation methods respectively. It was suggested that this mismatch is due to the different excitation levels that were used during the measurements. To confirm this, the HV open-circuit input-impedance frequency response of the transformer was measured at a number of excitation levels, in the low-frequency range. The transformer was excited at 220 V, using stepped-frequency sinusoidal excitation, and also with a PRBS signal, using excitation levels of 1 kV and 2.5 kV. The high PRBS excitation levels were obtained by applying the PRBS signal via a step-up transformer, as shown in figure 3.23. The results of these measurements are presented in figure 3.24 and show that the first parallel resonant frequency of the HV open-circuit input-impedance decreases as the excitation level increases.

In the frequency range around the first parallel resonance of the transformer open-circuit input impedances, the simple parallel RLC circuit shown in figure 3.25 can be used to approximate the open-circuit input impedance [94]. The equivalent RLC circuit shown in figure 3.25 is a simplification of the basic wideband T-equivalent transformer model shown in figure 2.3 (p. 14). The parallel RLC circuit is formed by assuming that the leakage-branch components (L_{l1}, L_{l2}, R_1 and R_2 in figure 2.3) are very small compared to the magnetizing-branch elements (L_m and R_m in figure 2.3) and can thus be replaced by zero-impedance branches. The inter-winding capacitance, C'_{12} in figure 2.3 is not expected to have an effect at frequencies in the vicinity of the first parallel resonance of the open-circuit input impedance [14], and can thus be ignored.

In figure 3.25, L_e represents the magnetizing inductance of the transformer and the value

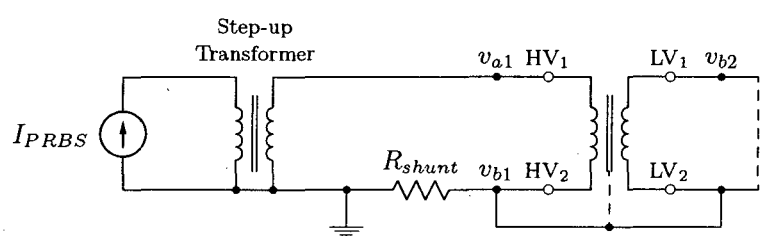

Figure 3.23: PRBS excitation applied to the transformer HV terminals via a step-up transformer.

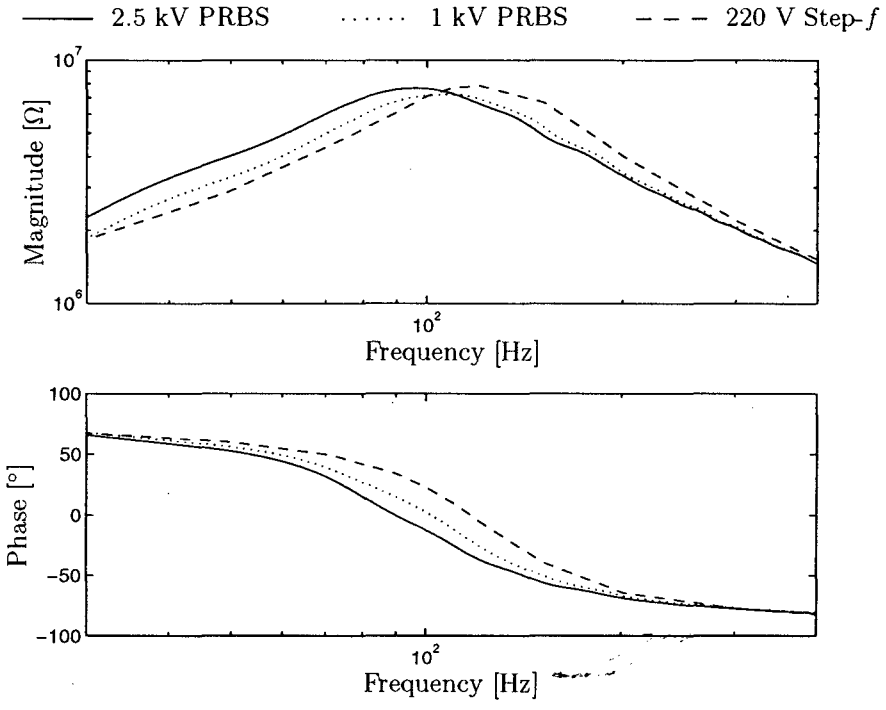

Figure 3.24: HV open-circuit input-impedance frequency response measured at different excitation levels.

of R_e is related to the hysteresis and eddy-current losses in the core. The capacitance C_e is a lumped representation of the winding inter-turn capacitances and the capacitances between the windings and earth. Referring to the equivalent circuit shown in figure 2.3, C_e can be considered as a lumped representation of capacitances C_1' and C_2'. The first parallel resonance of the input impedance then occurs at:

$$\omega_1 = \frac{1}{\sqrt{L_e C_e}}. \tag{3.16}$$

Capacitance C_e is a function of the geometrical arrangement of the various components from which the transformer is constructed, as well as the permittivity of the materials that form the dielectric of C_e. Under normal operating conditions, none if these parameters are likely to change significantly as a function of the voltage or the frequency of a signal applied to the transformer terminals. Thus, it can be assumed that C_e is constant [95]. Therefore, the shift in the location of the resonant frequency of the open-circuit input impedance (shown in figure 3.24), has to be due to an increase in the equivalent value of L_e as the excitation voltage, V_e, increases.

The value of C_e can be estimated from the LV open-circuit input impedance frequency response of the transformer. At frequencies sufficiently greater than the first resonant

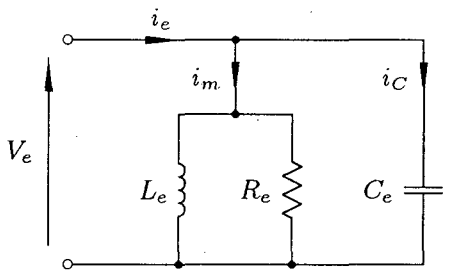

Figure 3.25: Equivalent circuit to simulate the transformer open-circuit input impedance at frequencies in the vicinity of the first parallel resonant frequency.

frequency of the open-circuit input impedance, $\mathbf{Z}_{Loc}(j\omega)$ becomes capacitive, so that an estimate of C_e can be found from [94]:

$$C_e = \frac{1}{2\pi f_a \, |\mathbf{Z}_{Loc}(j2\pi f_a)|}, \tag{3.17}$$

where f_a is the frequency at which $\mathbf{Z}_{Loc}(j\omega)$ is evaluated to determine C_e. From figure 3.17 it can be seen that $\mathbf{Z}_{Loc}(j\omega)$ is essentially purely capacitive at frequencies in the vicinity of 1 kHz, which is 10 times higher than the first resonant frequency of the open-circuit input impedance. By applying equation 3.17 at $f_a = 1$ kHz, the value of C_e was found from the stepped-frequency measurement of $\mathbf{Z}_{Loc}(j\omega)$ as 3.6 μF.

To investigate the voltage-dependence of L_e, the LV open-circuit input impedance of the 16 kVA transformer was measured as a function of the excitation voltage, at a fixed frequency of 50 Hz. If a constant value is assumed for C_e, the values L_e and R_e can be determined at each voltage level from:

$$R_e(V_e) = \frac{1}{\mathrm{Re}\{\mathbf{Y}^{50}_{Loc}(V_e)\}} \tag{3.18}$$

and

$$L_e(V_e) = \frac{-1}{\omega^2 C_e - \omega \, \mathrm{Im}\{\mathbf{Y}^{50}_{Loc}(V_e)\}}, \tag{3.19}$$

where $\mathbf{Y}^{50}_{Loc}(V_e) = \{\mathbf{Z}^{50}_{Loc}(V_e)\}^{-1}$ is the LV open-circuit input admittance as a function of the excitation voltage V_e at 50 Hz. Note that only the fundamental components of V_e and the transformer input current were considered when determining $\mathbf{Z}^{50}_{Loc}(V_e)$, using the procedure described in section 3.4.2. The results are shown in figure 3.26 and it can be seen that L_e increases considerably as V_e increases, for $V_e < 100$ V. Over the same voltage

range, the value of R_e shows a relatively small percentage increase. The knee-point of the transformer magnetization curve is reached when $V_e \approx 110$ V and core saturation occurs as V_e is increased further. The reversal in the trend of R_e and L_e for $V_e > 100$ V, shown in figure 3.26, corresponds to the value of V_e at which the knee-point is reached.

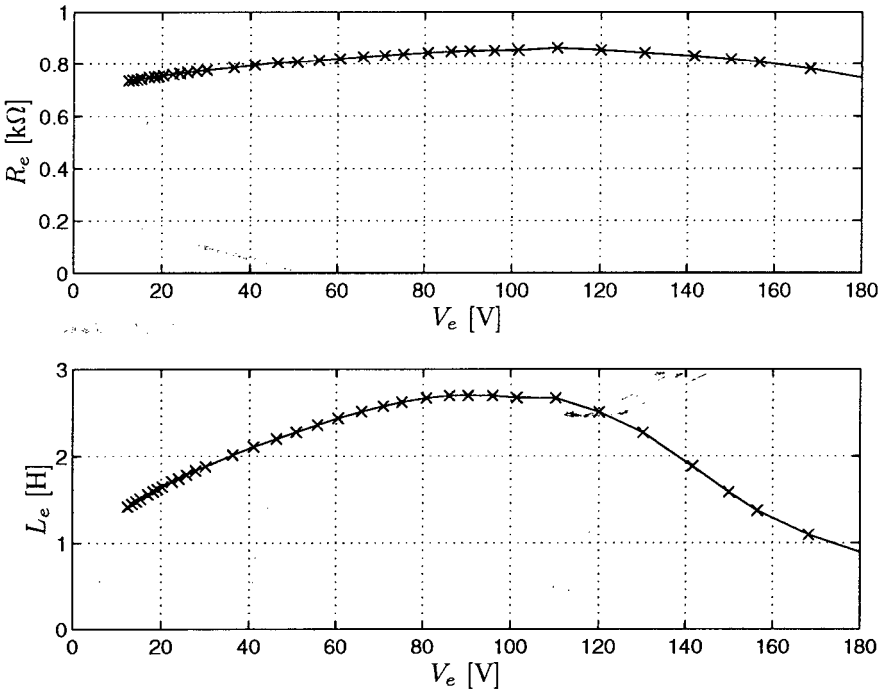

Figure 3.26: Voltage-dependence of R_e and L_e.

The voltage-dependence of L_e is related to the non-linear characteristics of the transformer core, which is hysteretic and is subject to saturation effects. The remainder of this section aims to investigate the voltage- and frequency-dependence of L_e and R_e, by relating L_e to the core flux, which is a function of the applied voltage and frequency.

Letting the equivalent circuit shown in figure 3.25 represent the transformer as seen from the LV terminals, with the HV terminals open-circuit, L_e can be expressed as [35]:

$$L_e = N\frac{d\phi_c(t)}{di_m(t)}, \tag{3.20}$$

where N represents the number of turns on the LV winding and $\phi_c(t)$ is the core flux. The instantaneous current flowing in the winding is $i_m(t)$, ignoring the effects of the winding capacitances. Due to the non-linear characteristics of the transformer core, the relationship between $\phi_c(t)$ and $i_m(t)$ is not linear (i.e. $\frac{d\phi}{di}$ is not a constant), which implies that L_e is time-varying. However, if L_e is defined in terms of the fundamental components

of $\phi_c(t)$ and $i_m(t)$, it will be a constant representing an 'effective' inductance, which is valid at the fundamental frequency and at the magnitude of V_e that was used during its measurement. (L_e was defined in this way to obtain the measurements of figure 3.26.) Using Faraday's law, $\phi_c(t)$ can be found as a function of $v_e(t)$, assuming that all the flux linked by the winding is confined to the core:

$$\phi_c(t) = \frac{1}{N}\int v_e(t)\,dt\,. \tag{3.21}$$

Note that equation 3.21 implies that if L_e is voltage-dependent, it will also be frequency-dependent, as the magnitude of Φ_c will decrease as the frequency of V_e is increased (assuming that the amplitude of V_e remains constant).

In figure 3.25, i_m is shown as the sum of the currents flowing in L_e and R_e, i.e. i_m is the magnetizing current of the transformer. The mechanism responsible for the voltage- and frequency-dependence of L_e can be visualized by plotting $\phi_c(t)$ as a function of $i_m(t)$ at a number of frequencies, which essentially represents the core hysteresis loop at a number of operating points. Neither $\phi_c(t)$ or $i_m(t)$ can be measured directly, but can be derived from measurements of $v_e(t)$ and $i_e(t)$. The number of turns on the LV winding of the 16 kVA test transformer is known ($N = 89$), so that $\phi_c(t)$ can be found from equation 3.21. Using the value of C_e estimated above, the magnetizing-branch current can be found from measurements of $v_e(t)$ and $i_e(t)$ by:

$$\begin{aligned} i_m(t) &= i_e(t) - i_C(t) \\ &= i_e(t) - C_e\frac{dv_e(t)}{dt} \end{aligned} \tag{3.22}$$

To measure i_e and v_e, the 16 kVA transformer was excited from the LV terminals, using a sinusoidal excitation signal, at frequencies of 5 Hz, 10 Hz, 40 Hz and 80 Hz. An excitation voltage of 14 V was used for all the measurements. Practically, this was the maximum voltage that could be applied at all the required frequencies with the available excitation equipment. In each case, signals v_e and i_e were sampled simultaneously and ϕ_c and i_m were calculated by applying equations 3.21 and 3.22 numerically. The integration of equation 3.21 was performed by applying trapezium-rule integration [74] and the differentiation in equation 3.22 was performed by applying the first-order forward-difference approximation method [74]. The resulting plots of ϕ_c as a function of i_m, measured at the same excitation voltage, are shown in figure 3.27.

It is interesting to note that the peak flux reached by the 5 Hz loop ($\approx$ 6.5 mWb) is

similar to the peak flux reached when the transformer is operating normally. According to the manufacturer, the 16 kVA test transformer peak core flux density, B_{peak}, is 1.1 T at 50 Hz and rated voltage. The core has a cross-sectional area, A, of 62 cm^2, which translates to a peak flux of:

$$\phi_{peak} = B_{peak}A = 1.1 \times 6.2 \times 10^{-3} = 6.8 \text{ mWb}. \tag{3.23}$$

This result provides a degree of validation for the (approximated) hysteresis-loop measurements shown in figure 3.27, as the estimated core-flux levels are realistic, considering the applied excitation levels and frequencies.

A crude approximation of the relative values of L_e, for the cases shown in figure 3.27, can be made by letting L_e be proportional to the slope of a straight line which passes through the extremes of each hysteresis loop. A reduction in the slope of such a line, as a function of frequency, can be seen in figure 3.27 for the hysteresis loops measured at 10 Hz, 40 Hz and 80 Hz. When the core is driven into saturation (as for the 5 Hz loop), the straight-line approximation predicts a reduction in L_e with increased excitation voltage or reduced frequency. Although the 5 Hz loop was measured at a low excitation level, it

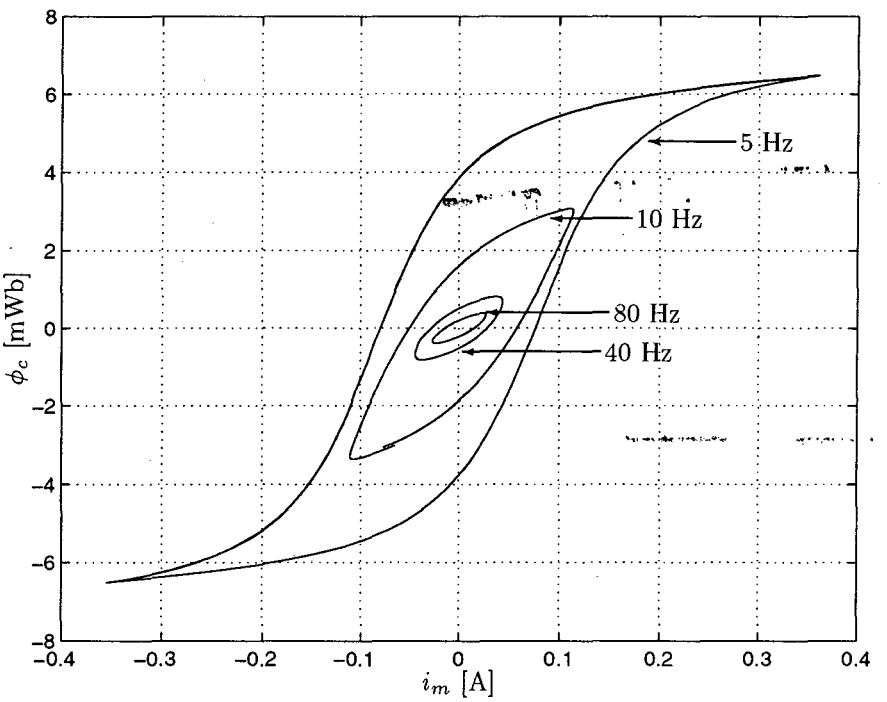

Figure 3.27: Approximated hysteresis loops for the 16 kVA transformer, excited at different frequencies, but at constant voltage magnitude.

can be related to the drop in L_e that can be seen in figure 3.26 for $V_e > 100$ V, if it is considered that it was measured at a much lower frequency than the results of figure 3.26.

The straight-line approximation can also be used to show why very poor low-frequency response measurements are obtained when an impulse excitation signal is applied to the transformer. Unlike sinusoidal and PRBS excitation signals, an impulse is a unipolar signal, so that a complete, closed hysteresis loop is never traversed while the impulse is applied. Thus, an approximation of L_e can never be formed, as the signal-to-noise ratio at low frequencies is simply too poor.

The hysteresis-loop measurements were repeated, maintaining a constant ratio of V_e/f so that the magnitude of Φ_c is expected to remain constant. Figure 3.28 shows the results of these measurements. A similar hysteresis loop is obtained at each frequency, i.e. all the hysteresis loops in figure 3.28 extend to similar extremes and the slopes of straight lines drawn through the extremes have similar slopes. According the arguments presented above, the value of L_e should remain constant as a function of frequency if a constant V_e/f ratio is maintained during the measurements. It can also be seen in figure 3.28 that the area enclosed by the loops increases with frequency. The hysteresis-loop area

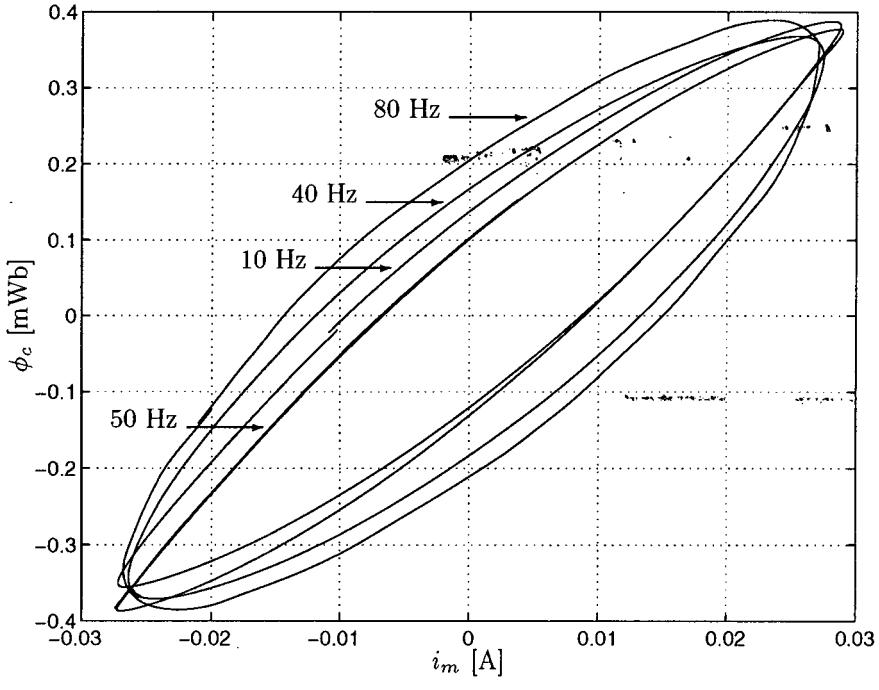

Figure 3.28: Approximate hysteresis loops for the 16 kVA transformer, measured at different frequencies, maintaining a constant V_e/f ratio.

is proportional to the hysteresis and eddy-current losses [35, 1, 2], so that the increase in area can be attributed to an increase in these losses with frequency, as predicted by equations 2.4 and 2.5.

Using the equivalent circuit shown in figure 3.25, values for L_e and R_e (as a function of frequency) can be found from the LV open-circuit input-impedance frequency response, for the constant V_e case and for the constant V_e/f case. $\mathbf{Z}_{Loc}(j\omega)$ was measured for each case, up to 80 Hz using sinusoidal excitation. L_e and R_e can be found from:

$$R_e(\omega) = \frac{1}{\mathrm{Re}\{\mathbf{Y}_{Loc}(j\omega)\}} \tag{3.24}$$

and

$$L_e(\omega) = \frac{-1}{\omega^2 C_e - \omega\,\mathrm{Im}\{\mathbf{Y}_{Loc}(j\omega)\}}, \tag{3.25}$$

where $\mathbf{Y}_{Loc}(j\omega) = \{\mathbf{Z}_{Loc}(j\omega)\}^{-1}$ is the LV open-circuit input admittance. The results of both sets of measurements are shown in figure 3.29. It can be seen that L_e remains constant for a constant V_e/f frequency response, while the constant V_e measurement of L_e shows the expected decrease in the value of L_e as the frequency is increased. From the results presented above, it can thus be concluded that L_e is dependent on the magnitude of the transformer core flux Φ_c, so that it is a strong function of the applied terminal voltage and of frequency.

As shown in figure 3.29, there is very little difference in the values of R_e obtained for the constant V_e/f and constant V_e cases. From this result and the result of figure 3.26, it can thus be concluded that R_e is a strong function of frequency, but varies only by a small amount if the excitation voltage is changed. This supports the approximate expression for R_e that is given by equation 2.6 [15], in which R_e is expressed as a function of frequency only.

From the above results it is clear that the frequency response characteristics of practical transformers are strong functions of the excitation voltage that was used to obtain the frequency response measurements. These results also highlight the importance of maintaining a constant excitation level while performing transformer frequency response measurements. It could be argued that a constant V_e/f ratio should be maintained, so that the equivalent value of L_e remains constant. However, in practice this is difficult to

achieve over a wide frequency range, complicates the measurement procedure and excludes the use wideband excitation signals such as PRBS signals.

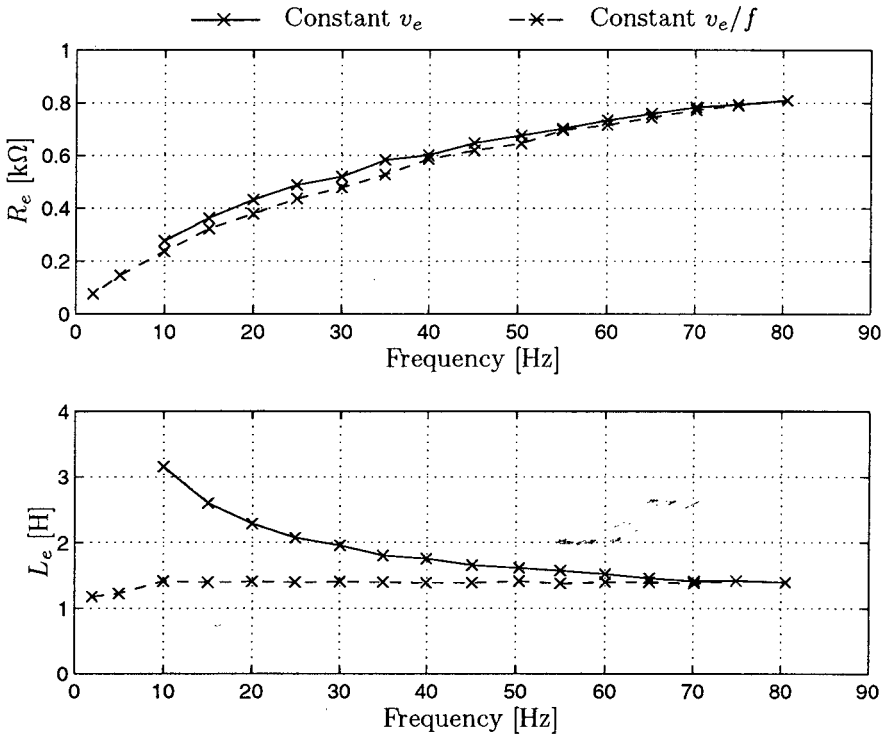

Figure 3.29: Frequency-dependence of L_e and R_e.

Chapter 4

Transformer Model Development

The development of a wideband two-winding transformer model is described in this chapter. As a starting point, the resonant behaviour of an isolated transformer winding is investigated and an equivalent-circuit model to represent such an isolated winding is established. By combining two such winding models, a two-winding transformer equivalent-circuit model is formed. At this point, inter-winding, turn-to-turn and winding-to-ground capacitances are added to the model, based on physical considerations. Finally, provision is made for the core losses and for the frequency-dependence of the inductive and resistive components of the transformer model.

During the model development process, it has to be kept in mind that the model parameters are to be found from terminal response measurements by a parameter estimation procedure. Care must thus be taken not to 'over-model' the transformer by introducing too many model parameters. This would increase the uncertainty of the parameter estimates or could cause the model to become unidentifiable [74]. Considering the constraints imposed by the parameter estimation process, an optimum transformer model structure has to be defined which will also meet the following requirements (see section 1.1):

- The order of the model structure must be high enough to predict the 'minor' resonances of the transformer frequency response characteristics in the frequency range between 10 Hz and 100 kHz, while keeping the number of parameters as low as possible.
- The model structure must take the form of a lumped-parameter equivalent circuit with elements that represent the internal structure of the transformer.

4.1 The Resonant Behaviour of Individual Transformer Windings

The approach that was followed in the transformer model development process was to first investigate the resonant behaviour of an isolated transformer winding and then to combine two or more winding models to form a transformer model. The resonant behaviour of transformer windings has been investigated and modelled by a number of researchers [46, 47, 96, 97, 98]. In all cases the winding is sub-divided into a finite number of sections, each of which is assumed to be homogeneous. This leads to an n-section, cascade equivalent-circuit model such as the one shown in figure 4.1. It is important to note that all the winding sections are mutually coupled. The mutual coupling of the winding sections complicates analysis of the equivalent circuit, but can not be ignored as this would lead to an inaccurate representation of the physical winding system [98].

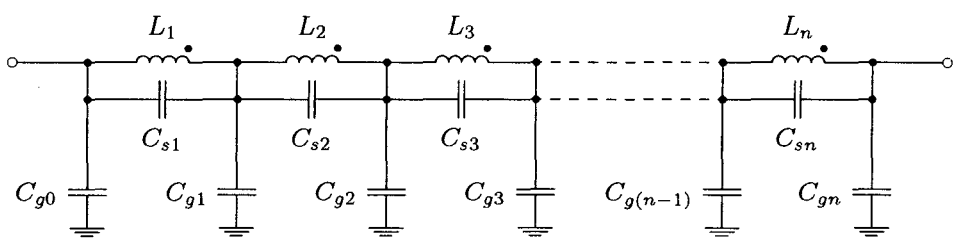

Figure 4.1: n-Section cascade representation of a transformer winding. Note that all inductances are mutually coupled.

In figure 4.1, capacitances C_g represent the capacitance between the winding and ground, while capacitances C_s are a lumped representation of the inter-turn capacitances. For most practical transformer windings it is expected that $C_g \ll C_s$, as the spacing between the winding and the transformer core, or the transformer tank, is usually large due to insulation requirements. Further, turns not located on the outer or inner layer of the winding are shielded by the outer and inner winding layers and are thus not expected to have a significant capacitance to ground, compared to the values of the lumped inter-turn capacitances, C_s. However, this is a strong function of the construction of the winding, e.g. Abetti and Maginniss [98] found that $C_g \gg C_s$ in their analysis of a specially constructed single-layer, helical transformer winding with an inner and an outer grounded electrostatic shield. To simplify the following analysis of a transformer winding it will be assumed that $C_g \ll C_s$ and therefore capacitances C_g will be ignored. Note that the omission of these capacitances does not reduce the order of the resulting model, as all these capacitances form part of loops consisting only of capacitances, thus not adding state variables to

the system (i.e. if the voltages across capacitances C_s are known, the voltages across capacitances C_g can be found, assuming that one end of the winding is grounded) [99]. The analysis is further simplified by the omission of lumped representations of the winding resistance, as this has only a small effect on the resonant frequencies of the winding [47, 97, 98, 49], but will result in incorrect prediction of the damping associated with each resonance.

The resonant behaviour of the n-section transformer winding equivalent circuit can be examined by determining the number and location of the poles and zeros of a frequency-domain expression for the total winding impedance [46, 98]. If the winding resistances are omitted, the winding impedance will tend to infinity at the location of a parallel resonance and to zero at the location of a series resonance. Figure 4.2 shows the simplified transformer-winding equivalent circuit. Choosing loop-currents as shown in figure 4.2, the Laplace-domain loop-equations for the equivalent circuit, in the form $\boldsymbol{ZI} = \boldsymbol{V}$, are given by:

$$\begin{bmatrix} sL_1 + \frac{1}{sC_1} & sM_{12} & \dots & sM_{1n} & \frac{1}{sC_1} \\ sM_{12} & sL_2 + \frac{1}{sC_2} & \dots & sM_{2n} & \frac{1}{sC_2} \\ \vdots & & \ddots & & \vdots \\ sM_{1n} & sM_{2n} & \dots & sL_n + \frac{1}{sC_n} & \frac{1}{sC_n} \\ \frac{1}{sC_1} & \frac{1}{sC_2} & \dots & \frac{1}{sC_n} & \sum_{m=1}^{n} \frac{1}{sC_m} \end{bmatrix} \begin{bmatrix} \mathbf{I}_1 \\ \mathbf{I}_2 \\ \vdots \\ \mathbf{I}_n \\ \mathbf{I}_a \end{bmatrix} = \begin{bmatrix} 0 \\ 0 \\ \vdots \\ 0 \\ \mathbf{V}_a \end{bmatrix}. \tag{4.1}$$

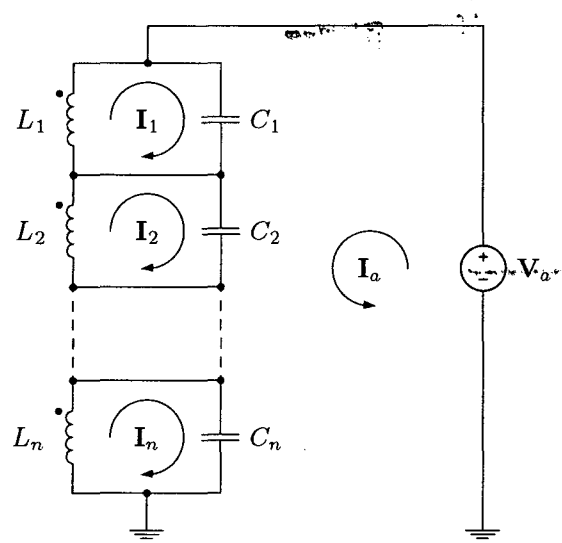

Figure 4.2: n-Section representation of a transformer winding, showing the loop-currents used in the analysis of the circuit. All inductances are mutually coupled and the capacitances to ground are not included.

The total impedance of the winding, $\mathbf{Z}_w(s)$, can now be found from equation 4.1:

$$\mathbf{Z}_w(s) = \frac{\mathbf{V}_a(s)}{\mathbf{I}_a(s)} = \frac{\Delta_Z}{\Delta_a}, \tag{4.2}$$

where Δ_Z is the determinant of the coefficient matrix $\boldsymbol{Z}$ and Δ_a is the $(n+1, n+1)$-th cofactor of $\boldsymbol{Z}$.

The simplest case (except representing the winding by a single, lumped inductance) is obtained when choosing $n = 2$. For this case, expansion of equation 4.2 yields the following expression for the winding impedance:

$$\mathbf{Z}_w(s) = \frac{(C_1 + C_2)(L_1L_2 - M^2)s^3 + (L_1 + L_2 + 2M)s}{C_1C_2(L_1L_2 - M^2)s^4 + (C_1L_1 + C_2L_2)s^2 + 1}. \tag{4.3}$$

For practical transformer windings $L_1L_2 > M^2$, leading to the conclusion that the coefficients of s in equation 4.3 will always be positive and real. The numerator has one trivial root at zero and the other two numerator roots are found as:

$$s = \pm\sqrt{\frac{-(L_1 + L_2 + 2M)}{(C_1 + C_2)(L_1L_2 - M^2)}}, \tag{4.4}$$

which are purely imaginary complex conjugates. By now setting $s = j\omega$, the location of the impedance zeros in the frequency domain can be found. The zero at 0 Hz is expected, as L_1 and L_2 present no impedance at DC. Only one positive numerator root remains, indicating one series resonance in the winding impedance for all positive frequencies.

The roots of the denominator of equation 4.3 can be found from:

$$s^2 = \frac{-(C_1L_1 + C_2L_2) \pm \sqrt{(C_1L_1 + C_2L_2)^2 - 4C_1C_2(L_1L_2 - M^2)}}{2C_1C_2(L_1L_2 - M^2)}. \tag{4.5}$$

For a practical, closely-coupled transformer winding:

$$(C_1L_1 + C_2L_2)^2 > 4C_1C_2(L_1L_2 - M^2), \tag{4.6}$$

indicating that the denominator of equation 4.3 has two pairs of purely imaginary, complex conjugate roots. Setting $s = j\omega$, two frequencies at which the winding impedance tends to infinity, or parallel resonant frequencies, are found for all positive frequencies.

The following example illustrates the properties of a two-section winding equivalent-circuit

model and the ability of the circuit to represent a practical transformer winding. Consider the two-section equivalent circuit shown in figure 4.3. Resistances R_1 and R_2 have been added to introduce some damping to the system. Ignoring the effect of R_1 and R_2 and substituting the element values shown in figure 4.3 into equation 4.3, the following expression is found for the frequency response of the input impedance of the example winding:

$$\mathbf{Z}_w(s) = \frac{2 \times 10^{-7} s^3 + 1\,700 s}{1 \times 10^{-16} s^4 + 1.1 \times 10^{-7} s^2 + 1}. \tag{4.7}$$

The numerator of equation 4.7 has roots at $s = 0$ and at $s = \pm j29\,155$. Thus, the example winding has a series resonance at 4 640 Hz. The roots of the denominator are at $s = \pm j3\,028$ and at $s = \pm j33\,028$, which means that the example winding impedance exhibits parallel resonances at 482 Hz and at 5 257 Hz. The frequency response of the example winding input impedance is shown graphically in figure 4.4 (including the effect of the winding resistances). The two parallel resonances and the single series resonance can clearly be seen. At this point it is interesting to note the close agreement between the trend of the response shown in figure 4.4 and the trend of the HV open-circuit input-impedance response measured for the 16 kVA, single-phase experimental transformer (see figure 3.19). The latter response also exhibits a 'main' parallel resonance, beyond which the winding input impedance is predominantly capacitive, followed by a number of 'smaller' resonance pairs. Each such resonance pair consists of a series resonance, followed almost immediately by a parallel resonance. One such resonance pair is also evident in figure 4.4, characterized by the series resonance at 4 640 Hz, followed by the parallel resonance at 5 256 Hz.

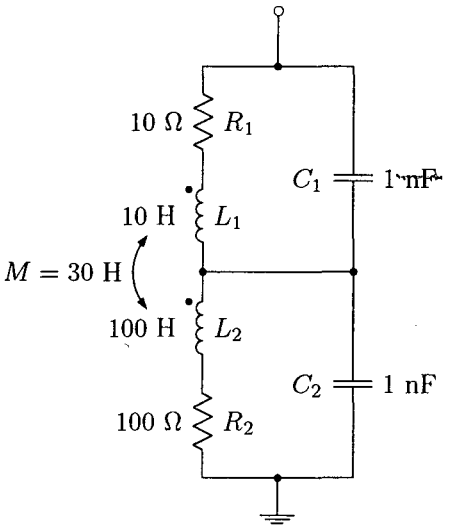

Figure 4.3: Two-section representation of a transformer winding.

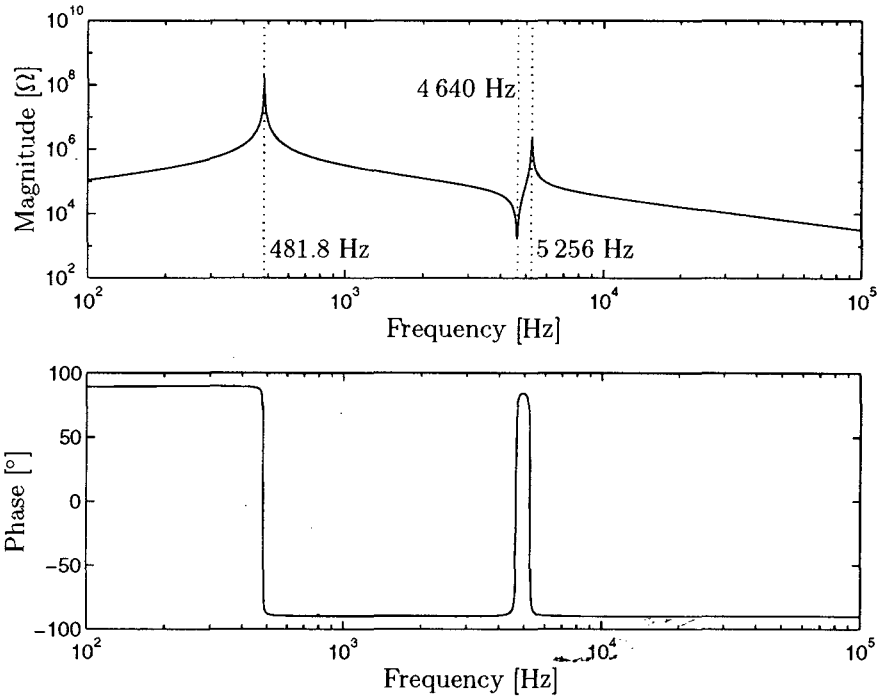

Figure 4.4: Input-impedance frequency response of the winding equivalent circuit shown in figure 4.3.

A further interesting result can be derived from equation 4.3. If it is assumed that the coupling between L_1 and L_2 is ideal, then $L_1L_2 - M^2 = 0$. In this case, equation 4.3 reduces to

$$\mathbf{Z}_w(s) = \frac{(L_1 + L_2 + 2M)s}{(C_1L_1 + C_2L_2)s^2 + 1}. \tag{4.8}$$

Using this simplified expression for the winding input impedance, a single parallel resonance is found at

$$\omega_1 = \frac{1}{\sqrt{C_1L_1 + C_2L_2}}. \tag{4.9}$$

In the case of the example winding discussed above, equation 4.9 yields $\omega_1 = 3\,015$ rad/s (480 Hz), which is very close to the frequency at which the 'main' parallel resonance in the winding occurs. Equation 4.9 can thus be used to approximate the location of the first parallel winding resonance, provided that the coupling factor between L_1 and L_2 is close to unity. This result also shows that the series-parallel resonance pair beyond the first parallel resonant frequency are related to the leakage components of L_1 and L_2, as this series-parallel resonance pair disappears when the coupling between L_1 and L_2 is ideal, i.e. when the inductances have no leakage components.

By increasing the number of sections that are used to represent a transformer winding, it should be possible to increase the number of series-parallel resonance pairs following the main parallel resonance of the input impedance. By increasing n to 3, the following expression is found for $\mathbf{Z}_w(s)$:

$$\mathbf{Z}_w(s) = \frac{a_5 s^5 + a_3 s^3 + a_1 s}{b_6 s^6 + b_4 s^4 + b_2 s^2 + 1}, \tag{4.10}$$

where

$$\begin{aligned}
a_5 &= (C_1C_2 + C_1C_3 + C_2C_3)(L_1L_2L_3 - L_3M_{12}^2 - L_2M_{13}^2 - L_1M_{23}^2 + 2M_{12}M_{13}M_{23}), \\
a_3 &= C_1(L_1L_2 + L_1L_3 - M_{12}^2 - 2M_{12}M_{13} - M_{13}^2 + 2L_1M_{23}) + \\
&\quad C_2(L_1L_2 + L_2L_3 - M_{12}^2 - 2M_{12}M_{23} - M_{23}^2 + 2L_2M_{13}) + \\
&\quad C_3(L_1L_3 + L_2L_3 - M_{13}^2 - 2M_{13}M_{23} - M_{23}^2 + 2L_3M_{12}), \\
a_1 &= L_1 + L_2 + L_3 + 2M_{12} + 2M_{13} + 2M_{23}, \\
b_6 &= C_1C_2C_3(L_1L_2L_3 - L_3M_{12}^2 - L_2M_{13}^2 - L_1M_{23}^2 + 2M_{12}M_{13}M_{23}), \\
b_4 &= C_1C_2(L_1L_2 - M_{12}^2) + C_1C_3(L_1L_3 - M_{13}^2) + C_2C_3(L_2L_3 - M_{23}^2) \quad \text{and} \\
b_2 &= C_1L_1 + C_2L_2 + C_3L_3.
\end{aligned} \tag{4.11}$$

Examination of equation 4.10 reveals that the numerator and the denominator have five and six roots respectively. The numerator has a root at $s = 0$, indicating zero winding input impedance at DC. The remaining four roots of the numerator are two complex conjugate pairs, leading to the interpretation that the winding input impedance has two series resonant frequencies. In a similar manner it can be deduced that the winding impedance has three parallel resonant frequencies as the denominator has three pairs of complex conjugate roots. As was the case where $n = 2$, an approximate expression for the location of the first parallel resonant frequency can be found, based on the assumption that L_1, L_2 and L_3 are tightly coupled (cf. equation 4.9):

$$\omega_1 = \frac{1}{\sqrt{C_1L_1 + C_2L_2 + C_3L_3}}. \tag{4.12}$$

From equations 4.3 and 4.10 it would thus seem that the input impedance of an n-section transformer equivalent circuit has n series resonant frequencies, including the impedance minimum at DC, and n parallel resonant frequencies. Proof of this statement will not be attempted here, but it is supported by the work of Popović [47], Abetti and Maginniss [97, 98] and Keyhani *et al.* [78], whose results show that n series resonances

and n parallel resonances are presented by an n-section winding equivalent circuit.

From the above discussion it can be concluded that an n-section lumped-parameter equivalent circuit is suitable for the representation of a practical transformer winding, provided that n is large enough to represent all the resonances in the frequency range of interest. It is clear that general expressions for $\mathbf{Z}_w(s)$ for $n > 3$ become increasingly more difficult and tedious to derive as n increases, and a variety of methods have been proposed by which an n-section winding model can be analysed [96, 47, 46, 98]. Common to these analysis methods is the assumption that the parameters of an n-section lumped-parameter winding equivalent circuit can be calculated from the physical parameters of the winding in question. Of interest to the present work is the feasibility of estimating the parameters of an n-section transformer winding model from terminal response measurements. A large number of parameters are involved: n capacitances (ignoring capacitances to ground or to other parts of the transformer), n self-inductances, $\frac{n}{2}(n-1)$ mutual inductances and n resistances, if the winding resistances are to be included.

Keyhani *et al.* [78] proposed a method by which these parameters can be estimated from terminal response measurement data and illustrate their method by estimating the parameters of a 6-section transformer winding model. The number of parameters to be estimated was reduced by assuming that the self-inductances of all the sections are equal. The same assumption was made for the values of the lumped inter-turn capacitances and the winding resistances. Further, it was assumed that the magnetic coupling between all winding sections that have the same geometrical location with respect to each other is equal. In this way the number of parameters to be estimated was reduced to 11 (compared to a total of 39 equivalent-circuit parameters, including capacitances to ground).

Despite the assumptions that were made, Keyhani *et al.* [78] found that it was not possible to obtain a unique solution for the parameters based on a terminal response measurement alone. The parameters to which the estimation algorithm converged, depended very strongly on the initial values chosen for those parameters. However, if the voltage responses across each winding model section were included in the estimation procedure, a unique solution for the model parameters was possible.

From the preceding discussion it would seem that it is not possible to uniquely estimate the parameters of an n-section transformer winding model based on a terminal response measurement alone. A requirement of the work discussed in this dissertation is, however, that only terminal response measurements can be used to estimate the parameters of a

transformer model. Measurements of the response of individual winding sections will not be available, as these are very difficult to obtain in practice. Even if the transformer windings were accessible, the point in the winding at which a sectional response measurement is to be taken would be difficult to determine. It must, however, be remembered that a transformer consists of at least two windings, each of which can be represented by a cascade winding model and that the number of sections used for each winding need not necessarily be equal. This also means that more than one terminal response measurement is possible, as shown in chapter 3, where a total of six responses were measured for a two-winding transformer. Provided that an optimal value of n is chosen to model each winding in the frequency range of interest, it should be possible to estimate a unique set of parameters for each winding model, as the resonant behaviour of a particular winding will be reflected in response measurements conducted at the terminals of the other winding(s).

4.2 Two-winding Transformer Model

By combining two n-section winding equivalent circuits, the basis of a model for a two-winding transformer can be formed. The construction of such a model is presented in this section, with reference to the 16 kVA, 22 kV / 240 V, single-phase transformer used in most of the experimental work discussed in this dissertation. Firstly, the number of sections to be used in the representation of each winding has to be determined. The location (in the equivalent circuit) of capacitances between individual winding sections and other parts of the transformer can now be determined. A method by which the core losses can be accounted for also has to be found.

The number of sections that will be used to represent each winding is determined by examining the measured frequency-response characteristics of the experimental transformer. The measurement of the open-circuit input impedance of the HV winding was discussed in chapter 3 and is shown in figure 3.19. This response shows a 'main' parallel resonance in the winding between 100 Hz and 200 Hz, followed by two clearly visible series-parallel resonance pairs at 6 500 Hz and 40 kHz. Following the arguments presented in section 4.1, this suggests a minimum of $n = 3$ for the HV winding. The resonances at 6 500 Hz and at 40 kHz are also visible on the response of the LV open-circuit input impedance, as parallel-series resonance pairs (see figure 3.17). A further such resonance is present at 20 kHz, which can also be identified on the HV open-circuit input-impedance response, although here it appears highly damped. The experimental transformer has a turns ratio of approximately 100, which means that the total self-inductance of the HV winding is

$100^2 = 10^4$ times higher than that of the LV winding. Further, due to the larger number of turns and the higher coil diameter, the lumped value of the HV winding inter-turn capacitance is expected to be higher than that of the LV winding. The resonant frequencies of the HV winding are thus expected to lie at much lower frequencies than the resonant frequencies of the LV winding. Thus, the response of the LV open-circuit input impedance for the measured frequency range of 10 Hz to 100 kHz (as shown in figure 3.17), is expected to show the resonant behaviour of the HV winding, as seen from the LV terminals, rather than the resonances of the LV winding itself, which occur at frequencies beyond the measured range. Four winding sections will thus be used to represent the HV winding of the experimental transformer up to 100 kHz, catering for the three resonance-pairs at 6 500 Hz, 20 kHz and 40 kHz. The LV winding will be represented by a single section, as its resonant frequencies are expected to lie above 100 kHz. During the frequency response measurements (chapter 3), one terminal of each winding was earthed, which simplified the measurement procedures. This configuration will be retained for the transformer model, eliminating some of the capacitances which would be required to connect the windings to ground. Based on the above discussion, the equivalent-circuit model shown in figure 4.5 can now be constructed for the experimental transformer.

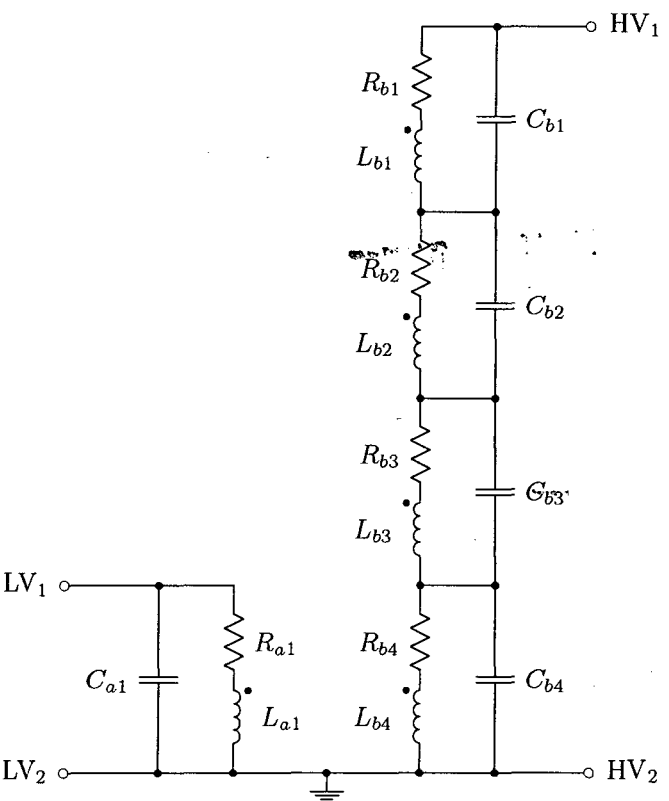

Figure 4.5: Basic two-winding equivalent-circuit model of the 16 kVA experimental transformer.

Not included in figure 4.5 are capacitances between the two windings or capacitances between the windings and ground. The location of these capacitances is derived from the physical layout of the transformer windings, which is shown in figure 4.6. The LV winding of the experimental transformer consists of two 4-layer coils, one wound on each leg of the core. These two coils are connected in parallel to form the LV winding. The HV winding consists of two series-connected 21-layer coils (one per leg), wound over the outside of the LV coils. The largest portion of the inter-winding capacitance is therefore found between the outer layers of the LV coils and the inner layers of the two HV coils. The lumped representation of the inter-winding capacitance, C_{ab1}, will thus be placed between the LV winding and the central node of the HV winding equivalent circuit, as shown in figure 4.7. The lumped inter-winding capacitance is not expected to be very large (relative to the inter-turn capacitances) as the spacing between the LV and HV winding is quite high, due to insulation and cooling requirements.

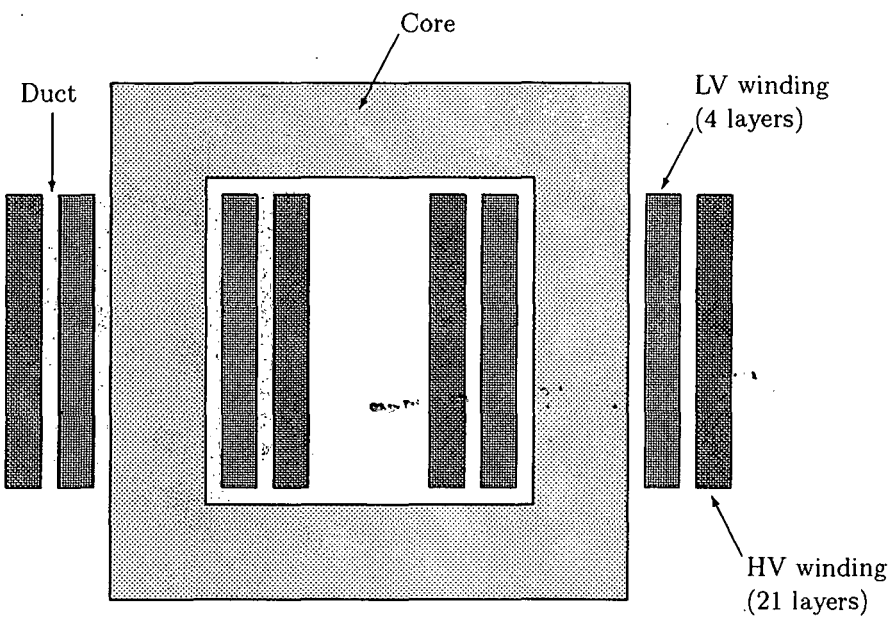

Figure 4.6: Winding layout of the 16 kVA experimental transformer.

In the present form of the transformer model, one terminal of each winding is connected to earth, which means that any capacitance between the earthed end of the windings and earth is effectively short-circuited. Lumped representations of the capacitance between the HV winding and earth are included in capacitances C_{b10} and C_{b34}, as shown in figure 4.7. C_{b34} and C_{b12} are lumped representations of the capacitance between adjacent layers of the HV winding, in addition to the lumped inter-turn capacitances C_{b1} to C_{b4}. C_{a10}, which is primarily intended as a representation of the LV winding inter-turn capacitance,

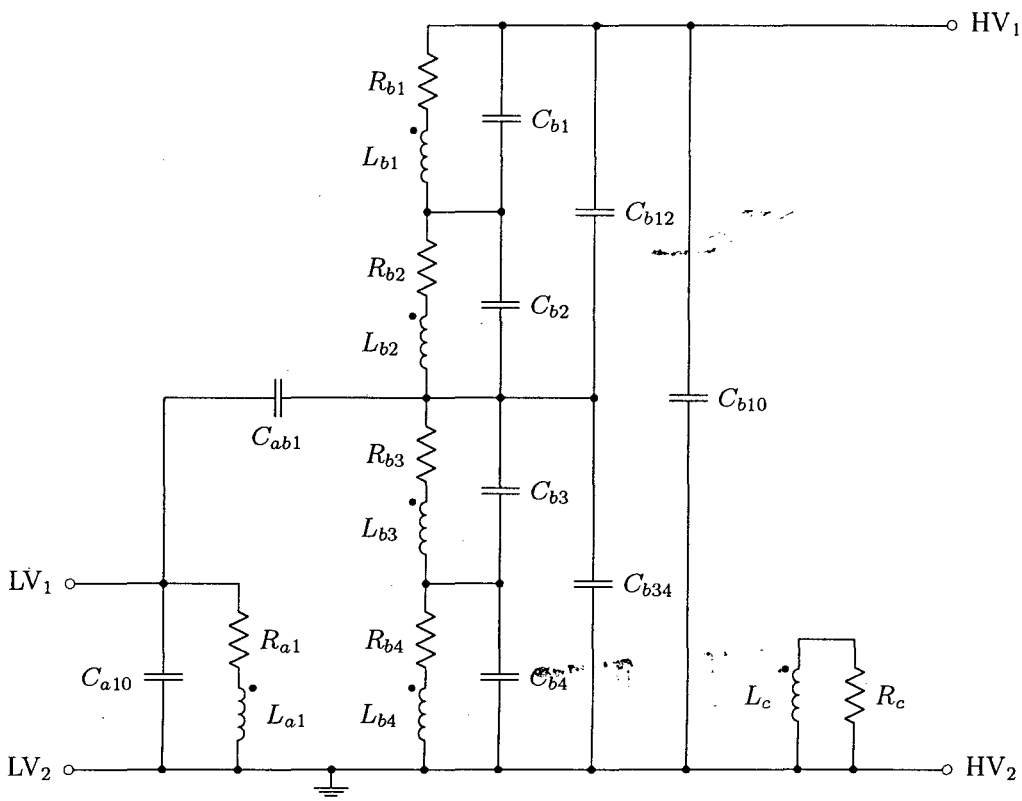

Figure 4.7: Lumped-parameter equivalent-circuit model of the 16 kVA experimental transformer. All inductances are mutually coupled.

will include a small component that can be attributed to the capacitance between the LV winding and earth.

Thus far, the transformer core losses have not been included in the transformer model. The core losses are often ignored when only the high-frequency behaviour of a transformer is under investigation [47]. However, the model of figure 4.7 must be able to predict the transformer frequency-response characteristics over the frequency range from 10 Hz to 100 kHz. A reasonably accurate representation of the core losses is thus required, especially at the lower frequencies where the core losses will have a significant influence on the damping associated with the transformer winding resonances. Ideally, the core losses would be represented by separating the leakage-flux components, associated with each lumped inductance in the equivalent circuit, from the main flux. The main flux is confined entirely to the core and can thus be used to determine the transformer core losses. The complexities of this approach (and the addition of a large number of model parameters) are avoided by assuming that all flux components, including leakage fluxes, that are linked by the lumped winding inductances are confined to the core and thus contribute to the core losses. The core losses can now be represented by tightly coupling an inductance L_c to all the lumped winding inductances. The current through L_c is proportional to the core flux and the power dissipated by resistance R_c, forming a loop with L_c, would thus be proportional to the core losses (see figure 4.7). This representation of the core losses also makes it possible to obtain the 'core voltage' directly from the transformer equivalent circuit. The voltage across L_c will be proportional in magnitude and will have the same phase as the voltage measured between the terminals of a search coil placed around the transformer core. This voltage provides an additional response measurement that can be used to validate the transformer model (if the core is accessible).

4.3 Frequency-dependence of the Transformer Model Parameters

The model structure of figure 4.7 does not explicitly represent the core of the transformer, which makes it difficult to include non-linear effects such as core saturation, hysteresis or eddy-current losses in the model. The model of figure 4.7 is intended primarily for frequency-domain applications and therefore accurate time-domain representations of the transformer non-linearities are not required. However, the frequency-dependence of the inductive and resistive equivalent-circuit elements will have a significant effect on the

transformer frequency-response characteristics, especially at low frequencies, as shown experimentally in chapter 3. In the following sections, expressions by which the frequency-dependence can be included in the transformer model structure, are established.

4.3.1 Magnetizing-branch Frequency-dependence

In section 3.7 the frequency-dependence of the magnetizing branch of the 16 kVA experimental transformer was investigated by representing the LV open-circuit input impedance by a simple parallel RLC equivalent circuit, as shown in figure 4.8. It was found that the resistance representing the core losses, R_e, is frequency dependent, while the magnetizing inductance, L_e, is a function of the transformer excitation voltage and of frequency. If the excitation voltage, V_e, is increased linearly with frequency, i.e. if a constant V_e/f ratio is maintained, the magnetizing inductance remains constant. However, a constant excitation voltage is usually used during transformer frequency response measurements, and the magnetizing inductance thus tends to decrease with increasing frequency.

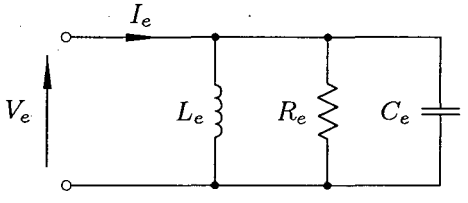

Figure 4.8: Simple parallel RLC equivalent circuit to represent the LV open-circuit input impedance at low frequencies (below 100 Hz).

To incorporate these effects into the transformer model (in the frequency domain), functions which describe the frequency-dependence of R_e and L_e have to be found. In section 2.1.1 the following expression for $R_e(f)$ was derived (also see [15]):

$$R_e(f) = \frac{k\,f}{c_e\,f + c_h}, \tag{4.13}$$

where k, c_e and c_h are constants depending on the core material and the constructional parameters of the transformer. Equation 4.13 can be rewritten as:

$$R_e(f) = \frac{a_{Re}\,f}{f + b_{Re}}, \tag{4.14}$$

with $a_{Re} = k/c_e$ and $b_{Re} = c_h/c_e$. In this way, the frequency-dependence of R_e is expressed

in terms of two parameters (a_{Re} and b_{Re}). To demonstrate that equation 4.13 yields an acceptable description of the frequency-dependence of R_e, consider the measured values of $R_e(f)$, obtained for the experimental transformer in section 3.7. By applying a non-linear least-squares curve-fitting routine, values for a_{Re} and b_{Re} can be estimated from the measured data (the `fmins` function provided by MATLAB [3, 100] was applied here). The result is shown in figure 4.9, from which it can be seen that equation 4.14 provides a good approximation of the measured values of $R_e(f)$, with $a_{Re} = 1\,144.9$ and $b_{Re} = 33.9$. The above result is applied to the transformer equivalent circuit of figure 4.7 by using equation 4.14 to represent R_c. Parameters a_{Re} and b_{Re} can now be estimated along with the other equivalent-circuit elements. Note that only one additional parameter is introduced due to the frequency-dependence of R_c, as R_c is completely described by a_{Re} and b_{Re}.

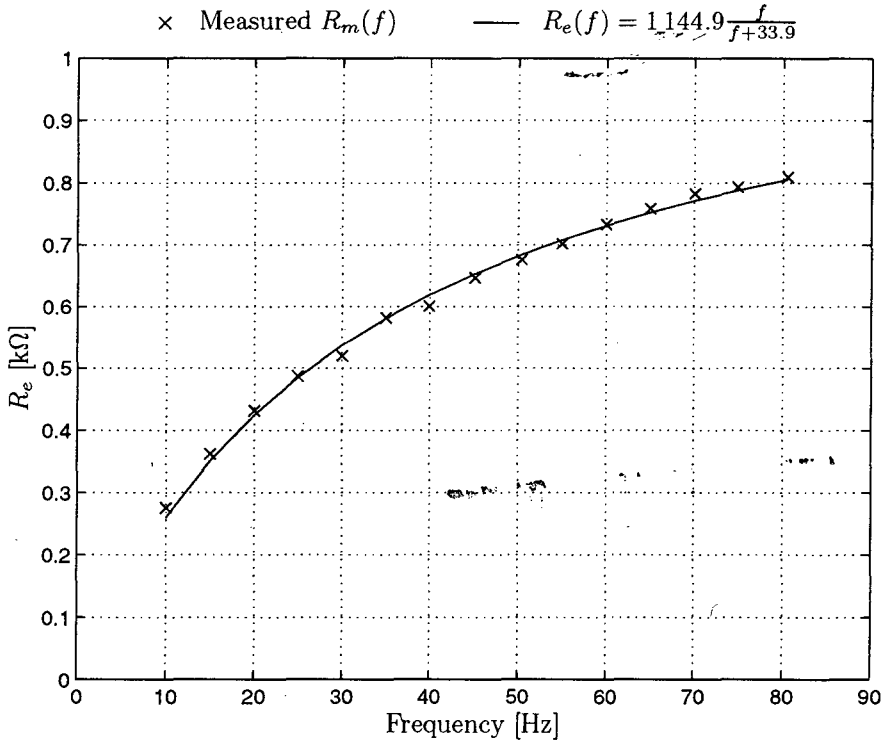

Figure 4.9: Frequency-dependence of R_e in the simplified equivalent circuit shown in figure 4.8, showing measured values and the approximation of those values by equation 4.14.

As shown in section 3.7, L_e is primarily a function of the excitation voltage used during a frequency response measurement, thus a general expression for L_e would be a function of both excitation voltage and frequency. To simplify the transformer model, it will be assumed that the transformer excitation voltage remains constant over the frequency range of interest. For this case it was found that the following expression, proposed by

Funk and Hantel [95], can be used to approximate the frequency-dependence of L_e:

$$L_e(f) = a_{Le}\, f^{-b_{Le}}. \tag{4.15}$$

Measured values of $L_e(f)$, discussed in section 3.7, will be used to test equation 4.15. The parameters of equation 4.15 are estimated from the measured data using a non-linear least-squares curve-fitting procedure, leading to the result shown in figure 4.10. It can be seen that equation 4.15 provides a good approximation of the measured values of L_e with $a_{Le} = 7.7798$ and $b_{Le} = 0.4026$.

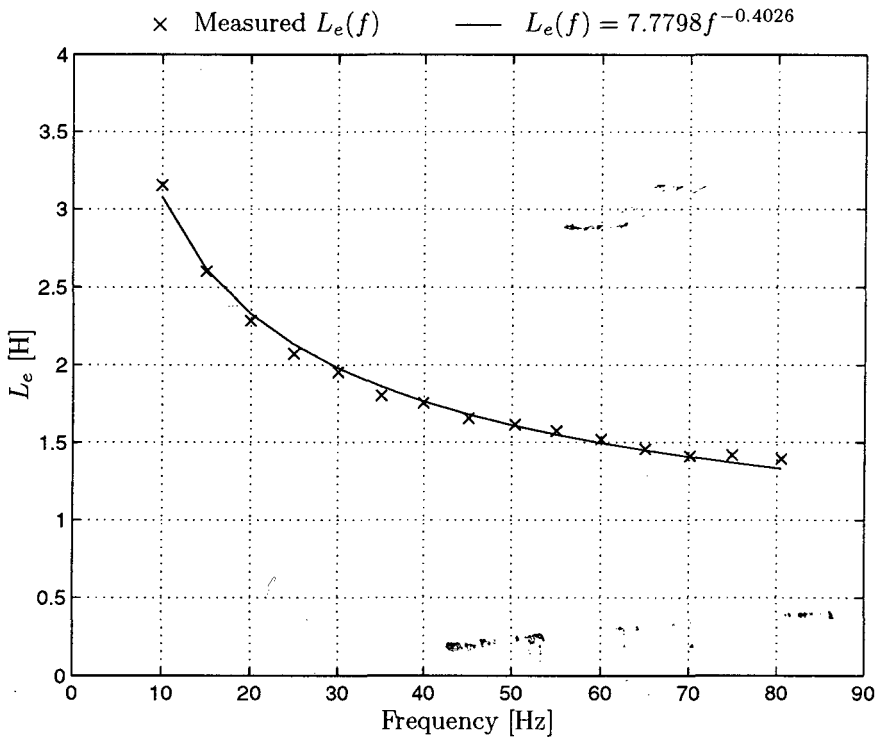

Figure 4.10: Frequency-dependence of L_e in the simplified equivalent circuit shown in figure 4.8, showing measured values and the approximation of those values by equation 4.15.

The frequency-dependence of the magnetizing inductance affects all the winding self-inductances of the transformer model (figure 4.7), as the magnetizing inductance is not represented by a single element. By adjusting L_{a1} and L_{b1} to L_{b4} according to equation 4.7, the frequency-dependence is taken into account. Because the self-inductances of the transformer equivalent-circuit are frequency-dependent, the mutual inductances between all the inductors, including L_c, will also be frequency-dependent. If the assumption is made that the coupling coefficients of the various inductance pairs does not change with

frequency, the mutual inductances can be determined from

$$M_{ij} = k_{ij}\sqrt{L_i L_j}\,, \quad (i \neq j) \tag{4.16}$$

at each frequency, where M_{ij} is the mutual inductance between L_i and L_j and k_{ij} is the coupling coefficient for L_i and L_j (i and j refer to subscripts contained in the set $\{a1, b1, b2, b3, b4, c\}$). The frequency-dependence of the magnetizing branch can be included in the transformer model of figure 4.7 by the introduction of one additional parameter (b_{Le}), if it is assumed that b_{Le} is the same for all the inductances (the existing self-inductances are each replaced by an expression like equation 4.15). This assumption is valid, considering that the same main flux is linked by all the inductances.

4.3.2 Leakage-branch Frequency-dependence

An acceptable representation of the frequency-dependence of the transformer leakage-branch elements, i.e. the winding resistances and the leakage components of the winding-section inductances, is considered important in transformer models for harmonic penetration studies [28, 27]. The following results will show that the frequency-dependence of the leakage-branch elements has to be considered to accurately represent the frequency-response characteristics of transformers under short-circuit conditions. The frequency-dependence of the leakage components can be attributed mainly to skin-effect, which causes an increase in the winding resistance with frequency [28]. A small decrease of the leakage inductances as frequency increases is also found [28, 95], and is caused by the non-linear behaviour of the transformer core, as the core often forms part of the leakage-flux paths. Figure 4.12 shows the measured frequency response of the LV short-circuit input impedance of the 16 kVA experimental transformer in terms of an equivalent RL series branch, as shown in figure 4.11. The LV short-circuit input impedance shows no resonances below 10 kHz and therefore this representation can be considered a valid approximation.

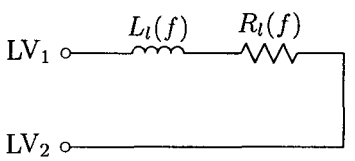

Figure 4.11: Simple series RL equivalent circuit to represent the LV short-circuit input impedance.

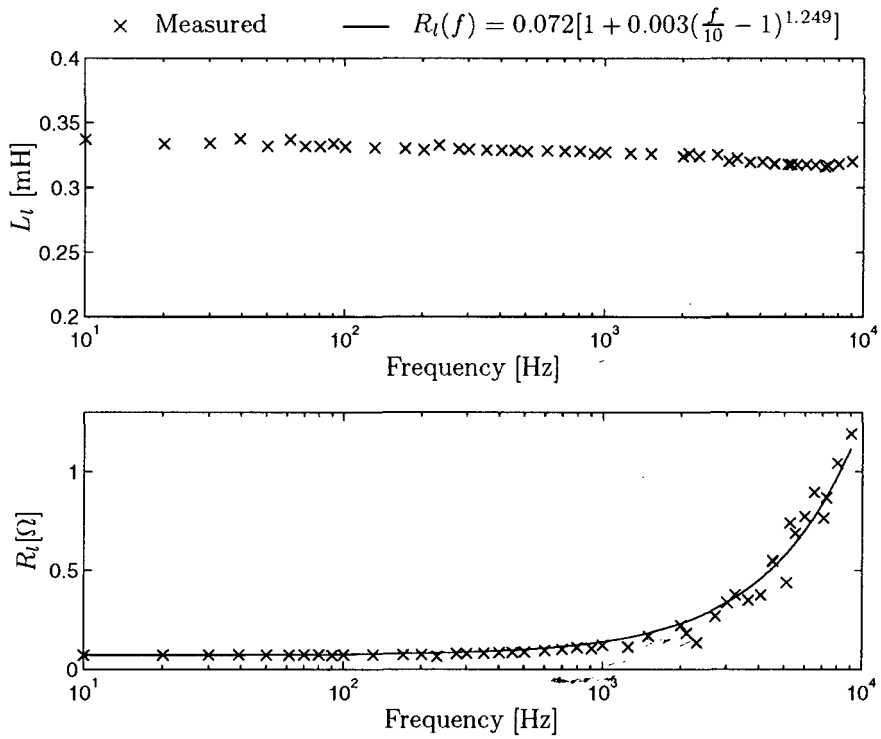

Figure 4.12: Frequency-dependence of the leakage-branch elements.

Although a decrease in the leakage inductance with increasing frequency can be seen in figure 4.12, the decrease is small and will be ignored, i.e. the leakage inductance will be assumed to be constant. The increase of the winding resistance with frequency is significant and can not be ignored. Funk and Hantel [95] suggested the following equation to model the frequency dependence of the winding resistances:

$$R_l(f) = R_{50}\left[1 + a_{Rl}\left(\frac{f}{50} - 1\right)^{b_{Rl}}\right]. \tag{4.17}$$

R_{50} is the winding resistance at 50 Hz and a_{Rl} and b_{Rl} are constants which are adjusted to obtain the best fit of $R_l(f)$ for a particular transformer. Rather than basing equation 4.17 on the winding resistance at 50 Hz, the winding resistance at the lowest measured frequency will be used (10 Hz in this case). Using a non-linear least-squares method, values of a_{Rl} and b_{Rl} can be found to fit equation 4.17 to the measured data shown in figure 4.12. With the winding resistance at 10 Hz, $R_{10} = 0.072\,\Omega$, the following expression for $R_l(f)$ is obtained:

$$R_l(f) = 0.072\left[1 + 0.003\left(\frac{f}{10} - 1\right)^{1.249}\right]. \tag{4.18}$$

From figure 4.12 it can be seen that a good approximation of the measured values of

$R_l(f)$ is obtained. To include the frequency-dependence of the winding resistances in the transformer equivalent circuit of figure 4.7, the values of R_{a1} and R_{b1}–R_{b4} are adjusted according to equation 4.17. As the same type of wire is used to wind the entire HV winding, it can be assumed that a_{Rl} and b_{Rl} are the same for all R_b. Four additional parameters are thus introduced to account for the frequency-dependence of the winding resistances, as separate expressions have to be used for the HV and LV winding resistances respectively. The implications of using the same values of a_{Rl} and b_{Rl} for both the HV and LV winding resistances, thereby reducing the number of additional parameters to two, will be investigated in chapter 6.

Chapter 5

Estimator Development and Implementation

Having established a suitable transformer model structure, the next step in the modelling process is to estimate the parameters of that model structure, based on measured response data and on the available *a priori* knowledge regarding the model parameters. This chapter discusses the development of a parameter estimation method for the transformer model and the representation of the model structure within that estimation procedure.

5.1 Estimator Structure

An overview of the transformer model parameter estimation procedure is shown in figure 5.1 and is typical of non-recursive parameter estimation methods [32, 31, 74]. An estimate of the transformer model responses, $\hat{\mathcal{G}}_{\mathbf{T}}$, is calculated from an estimate of the transformer model parameters, $\hat{\boldsymbol{\theta}}$. The estimated model responses are then compared to measurements of the same responses, $\check{\mathcal{G}}_{\mathbf{T}}$, by the cost function which reduces in value as the correlation between the measured and estimated responses improves. An optimization procedure is used to minimize the cost function, by iteratively adjusting the parameter estimates until a minimum value of the cost function is found.

It was already shown in chapter 4 that the estimation procedure will have to consider more than one transformer response in order to produce unique estimates of the model

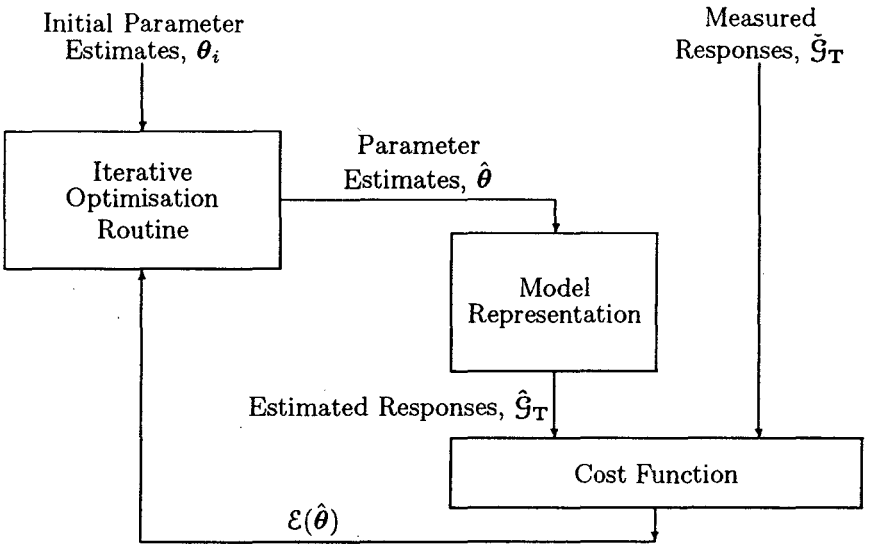

Figure 5.1: Overview of the transformer model parameter estimation procedure.

parameters. At this point, it will be assumed that all six terminal frequency responses in the set $\mathcal{G}_T$ will be considered, i.e. $\mathbf{Z}_{Loc}(j\omega)$, $\mathbf{Z}_{Lcc}(j\omega)$, $\mathbf{Z}_{Hoc}(j\omega)$, $\mathbf{Z}_{Hsc}(j\omega)$, $\mathbf{H}_{LH}(j\omega)$ and $\mathbf{H}_{HL}(j\omega)$. The reasons for using frequency-domain responses, rather than time-domain responses, will be discussed in section 5.2 below.

A mathematical representation of the transformer model is required to calculate estimates of the model responses from parameter estimates. This representation must be computationally efficient, as the model responses have to be evaluated many times during the parameter estimation procedure. The development of a suitable mathematical representation of the model structure is complicated by the relatively high complexity of the model structure and the frequency-dependence of some of the equivalent-circuit elements. The method that was applied to calculate the estimated transformer responses is discussed in section 5.3. The formulation of the cost function is described in section 5.4 and the choice of a suitable optimization algorithm is discussed in section 5.5. The cost function is defined in terms of quadratic error terms, so that a non-recursive, least-squares parameter estimator is established for the transformer model.

5.2 Reasons for Frequency-domain Estimation

Generally, the parameters of a model can be estimated either in the time-domain or in the frequency-domain. In the case of the transformer model, there are several reasons why frequency-domain estimation is used:

(a) The frequency-dependence of the inductances and resistances of the equivalent-circuit transformer model are represented by simple functions in the frequency domain. An accurate representation these frequency-dependencies in the time domain would require detailed modelling of the transformer core and of the electromagnetic characteristics of the windings. The resulting model would have a higher complexity than the present equivalent-circuit model and more parameters would be required to fully describe it.

(b) Frequency-domain estimation of the transformer model parameters makes it possible to estimate parameters that give the best representation of the transformer across the full 10 Hz to 100 kHz frequency range. A single PRBS signal, that contains information across this frequency range, would require $n_s \geq 15$ at a clock frequency of 300 kHz. Sampling such a PRBS signal at 500 kHz would yield in the order of 50 000 data points. Apart from the fact that this amount of data can not be sampled with the available equipment, the processing of such a high number of data points represents a significant computing overhead. Typically, it was found that the frequency responses only needed to be calculated at ± 200 frequency points to yield satisfactory results.

(c) As discussed in section 5.1, several transformer responses, i.e. $\mathbf{Z}_{Loc}(j\omega)$, $\mathbf{Z}_{Lsc}(j\omega)$, $\mathbf{Z}_{Hoc}(j\omega)$, $\mathbf{Z}_{Hsc}(j\omega)$, $\mathbf{H}_{LH}(j\omega)$ and $\mathbf{H}_{HL}(j\omega)$, are evaluated simultaneously during the parameter estimation process. To estimate the model parameters in the time domain, output responses for all these configurations would have to be evaluated from the relevant input signals. However, for frequency-domain estimation, no input data is required to evaluate the response characteristics of the transformer model.

(d) Time-domain evaluation of the transformer responses requires a separate state-space or transfer-function representation of the model for each response. It will be shown in section 5.3 that all the required model frequency responses can be evaluated from a single construction of the nodal admittance matrix of the equivalent circuit, resulting in a simpler and more efficient representation of the model.

5.3 Mathematical Representation of the Transformer Model

An s-domain transfer function is typically used to represent the frequency-response characteristics of a model within a parameter estimation routine. In most cases, only an input-output response prediction is required of the model structure, i.e. the physical significance of the model parameters is of secondary importance, and it is sufficient to estimate the coefficients of the transfer function. However, in the case of this investigation, estimates of the equivalent-circuit element values are required.

Generally, one of two routes can be followed when formulating a representation of an equivalent-circuit model structure in terms of its parameters. The first possibility is to derive (symbolic) expressions for the required transfer functions in terms of the network parameters. Manual derivation of such expressions is time-consuming and prone to errors, even for networks of modest complexity. Vermeulen [94] developed a software tool that is able to symbolically derive a state-space and a transfer-function representation of an *RLCM* network, i.e. a network consisting of resistances, inductances, capacitances and mutually coupled inductances, using the symbolic math capabilities of *Mathematica* [101]. Similar programs are described by Vermeulen and Brozio [102, 103] and Alderson and Lin [104]. Although it seems attractive, this approach is not feasible in the case of the transformer model. At the heart of the transformer model is a 6×6 inductance matrix, $\boldsymbol{L}$, describing the self-inductances and mutual coupling of the winding-sections. The determination of a state-space representation, and the associated transfer-function representation, requires inversion of matrices that contain $\boldsymbol{L}$ and $\boldsymbol{L}^{-1}$. The resulting symbolic manipulation is too complex to be handled by the software within a reasonable amount of time and the results are very complex expressions in terms of the circuit parameters.

The second approach to representing the equivalent-circuit model is to numerically determine the required frequency responses from a topological description of the network each time the responses have to be evaluated. E.g. the transfer-function coefficients for the required responses can be derived (numerically) by first formulating a numerical state-space representation of the transformer network [99] from its topological description. The task is computationally intensive, as the coefficients have to be re-evaluated for each evaluation of the frequency responses. The problem is compounded when the frequency-dependence of the equivalent-circuit elements is included. In this case, the transfer-function coefficients

have to be re-evaluated at each frequency at which a response calculation is required.

Direct calculation of the transformer model frequency responses from the nodal admittance matrix representation of the network was found to give the most satisfactory results, particularly if the frequency-dependence of the network elements is included. First, a symbolic representation of the nodal admittance matrix, $\boldsymbol{Y}_n$, is formed in terms of the resistive and capacitive network elements and the inverse of the inductance matrix, $\boldsymbol{\Gamma}$. The resulting expressions for the elements of $\boldsymbol{Y}_n$ are much simpler than expressions for a state-space or transfer-function representation of the network. This symbolic representation of $\boldsymbol{Y}_n$ is obtained to avoid numerical reconstruction of the nodal admittance matrix from a topological description of the network at each evaluation of the frequency responses. An auxiliary PASCAL program was written to formulate a symbolic nodal admittance matrix from a simple topological description of a network. An overview of the algorithm employed in this program and the results obtained for the transformer model are given in appendix A.

In general, the nodal equations of a network are given by:

$$\boldsymbol{Y}_n \boldsymbol{V}_n = \boldsymbol{J}_n \,, \tag{5.1}$$

where $\boldsymbol{V}_n$ is the nodal voltage vector and $\boldsymbol{J}_n$ is the equivalent nodal current source vector. As the transformer equivalent-circuit model is passive, the only entries in $\boldsymbol{J}_n$ are currents due to external excitation sources. In the following discussion, it will be assumed that the nodes of the transformer equivalent circuit are numbered as shown in figure 5.2, i.e. the un-earthed terminal of the LV winding is connected to node 1 and the un-earthed

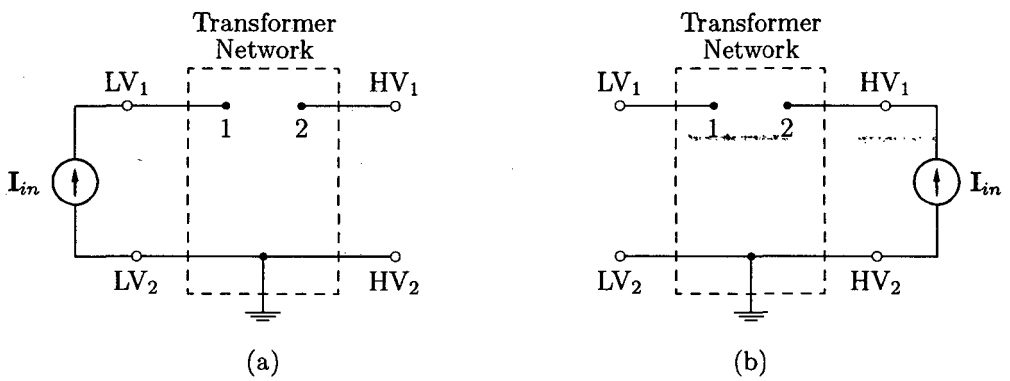

Figure 5.2: Node numbering used in nodal analysis of the transformer equivalent-circuit model, with excitation applied to the LV terminals (a) and to the HV terminals (b).

terminal of the HV winding is connected to node 2 of the equivalent network. (The transformer equivalent circuit has 11 nodes. The full node number assignments are shown in appendix A.) If the transformer is now excited from the LV terminals by a current source with $\mathbf{I}_{in} = 1\angle 0°$ A as shown in figure 5.2(a), the nodal equations are:

$$\boldsymbol{Y}_n \begin{bmatrix} \mathbf{V}_1 \\ \mathbf{V}_2 \\ \vdots \\ \mathbf{V}_{11} \end{bmatrix} = \begin{bmatrix} 1 \\ 0 \\ \vdots \\ 0 \end{bmatrix}. \tag{5.2}$$

After solving for the nodal voltages in equation 5.2, the following expressions can be obtained for the LV open-circuit input impedance and the LV-HV voltage transformation ratio, at the frequency for which $\boldsymbol{Y}_n$ was constructed:

$$\mathbf{Z}_{Loc} = \frac{\mathbf{V}_1}{\mathbf{I}_{in}} = \frac{\mathbf{V}_1}{1} = \mathbf{V}_1 \tag{5.3}$$

and

$$\mathbf{H}_{LH} = \frac{\mathbf{V}_2}{\mathbf{V}_1}. \tag{5.4}$$

The same procedure can be repeated to determine the HV open-circuit input impedance and the HV-LV voltage transformation ratio. With the network excited by a 1 A current source at the HV terminals (figure 5.2(b)), the nodal equations are:

$$\boldsymbol{Y}_n \begin{bmatrix} \mathbf{V}_1 \\ \mathbf{V}_2 \\ \mathbf{V}_3 \\ \vdots \\ \mathbf{V}_{11} \end{bmatrix} = \begin{bmatrix} 0 \\ 1 \\ 0 \\ \vdots \\ 0 \end{bmatrix}. \tag{5.5}$$

Having solved for the nodal voltages, $\mathbf{Z}_{Hoc}$ and $\mathbf{H}_{HL}$ are given by:

$$\mathbf{Z}_{Hoc} = \frac{\mathbf{V}_2}{\mathbf{I}_{in}} = \frac{\mathbf{V}_2}{1} = \mathbf{V}_2 \quad \text{and} \tag{5.6}$$

and

$$\mathbf{H}_{HL} = \frac{\mathbf{V}_1}{\mathbf{V}_2}. \tag{5.7}$$

The four open-circuit terminal responses of the transformer model (at one frequency) can thus be found from the solutions of two sets of nodal equations. The LV and HV short-circuit input impedances can be found without reconstructing the nodal admittance matrix. To short-circuit the HV terminals, row 2 and column 2 of $\boldsymbol{Y}_n$ are simply deleted to form the nodal admittance matrix $\boldsymbol{Y}_n^{sc2}$ of the resulting network. With current-source excitation at the LV terminals, the new set of nodal equations is given by:

$$\boldsymbol{Y}_n^{sc2} \begin{bmatrix} \mathbf{V}_1 \\ \mathbf{V}_3 \\ \mathbf{V}_4 \\ \vdots \\ \mathbf{V}_{11} \end{bmatrix} = \begin{bmatrix} 1 \\ 0 \\ 0 \\ \vdots \\ 0 \end{bmatrix}. \tag{5.8}$$

The LV short-circuit input impedance is now given by:

$$\mathbf{Z}_{Lsc} = \frac{\mathbf{V}_1}{\mathbf{I}_{in}} = \frac{\mathbf{V}_1}{1} = \mathbf{V}_1. \tag{5.9}$$

By deleting row 1 and column 1 from $\boldsymbol{Y}_n$, and exciting the resulting network with a 1 A current source at node 2, the nodal equations for the network with the LV terminals short-circuited are found as:

$$\boldsymbol{Y}_n^{sc1} \begin{bmatrix} \mathbf{V}_2 \\ \mathbf{V}_3 \\ \mathbf{V}_4 \\ \vdots \\ \mathbf{V}_{11} \end{bmatrix} = \begin{bmatrix} 1 \\ 0 \\ 0 \\ \vdots \\ 0 \end{bmatrix}, \tag{5.10}$$

and the HV short-circuit input impedance can subsequently be found:

$$\mathbf{Z}_{Hsc} = \frac{\mathbf{V}_2}{\mathbf{I}_{in}} = \frac{\mathbf{V}_2}{1} = \mathbf{V}_2. \tag{5.11}$$

Thus, to calculate the transformer frequency responses, the nodal equations of the transformer equivalent circuit have to be solved four times at each frequency of interest. The complete procedure is outlined in figure 5.3. Gaussian elimination is applied to solve the nodal equations as this is the computationally most efficient method [99, p. 171]. The frequency-dependence of the network elements is included by simply evaluating each frequency-dependent element, in terms of the relevant model parameters, before substitution in the nodal admittance matrix.

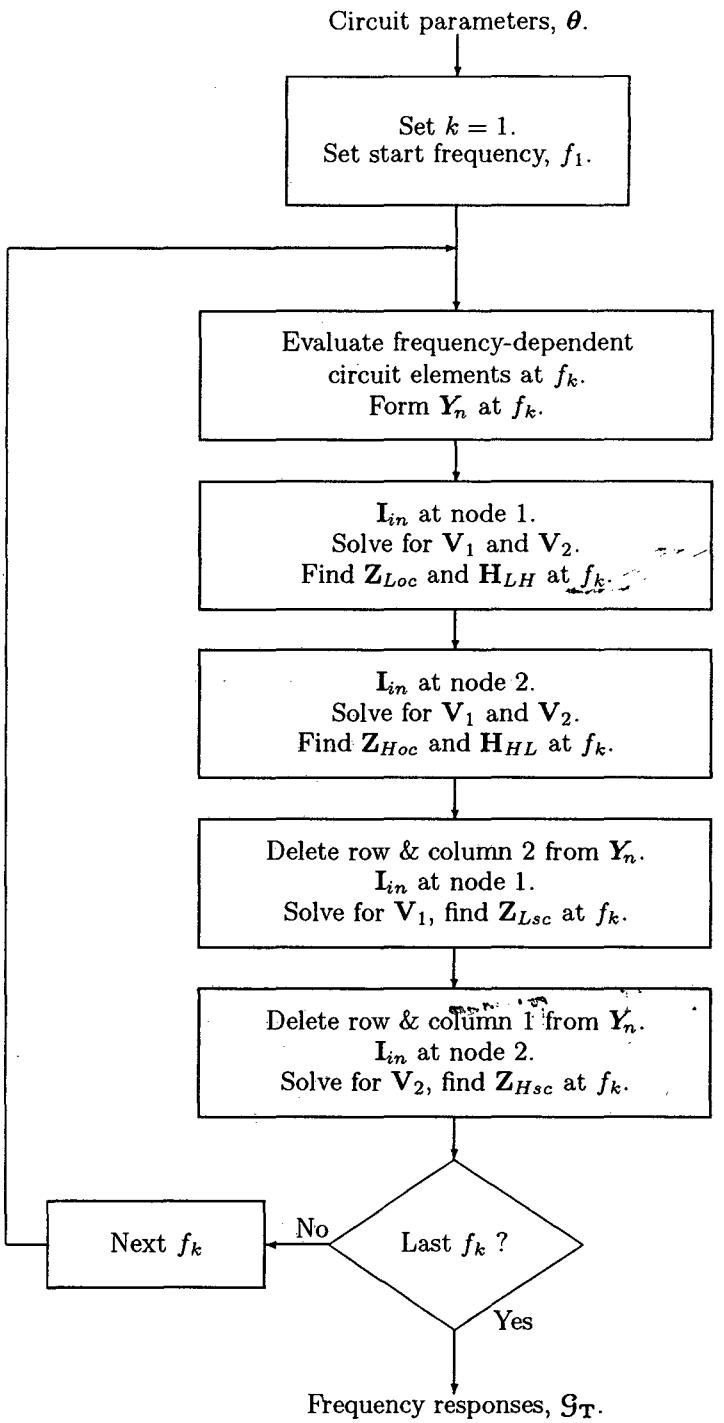

Figure 5.3: Determination of the transformer model frequency responses using a nodal admittance matrix description of the equivalent circuit.

5.4 Formulation of the Cost Function

The estimated and measured frequency responses of the transformer ($\hat{\mathfrak{G}}_\mathbf{T}$ and $\check{\mathfrak{G}}_\mathbf{T}$ respectively) are compared by the cost function, which calculates a norm defining the quality of the fit of the estimated frequency responses to the measured responses (see figure 5.1). The result, which is a function of the current parameter estimates, $\mathcal{E}(\hat{\boldsymbol{\theta}})$, reduces in magnitude as the quality of the estimates improves. $\mathcal{E}(\hat{\boldsymbol{\theta}})$ is fed back to the optimization algorithm, which bases its choice of $\hat{\boldsymbol{\theta}}$ on a number of evaluations of the cost function (which implies the same number of evaluations of the model responses).

By writing an error term, ε_r, for each frequency response $\mathbf{G}_r \in \mathfrak{G}_\mathbf{T}$ at frequency ω_k, as:

$$\varepsilon_r(\omega_k) = \check{\mathbf{G}}_r(j\omega_k) - \hat{\mathbf{G}}_r(j\omega_k)\,, \tag{5.12}$$

a quadratic cost function, including all frequency responses, can be defined as follows:

$$\mathcal{E} = \sum_{k=1}^{N_f} \left[\sum_{r=1}^{6} \varepsilon_r(\omega_k)\varepsilon_r^*(\omega_k) \right]\,, \tag{5.13}$$

where subscript r refers to one of the six responses in $\mathfrak{G}_\mathbf{T}$ and N_f is the number of frequencies at which each error term is evaluated. A problematic aspect of the cost function of equation 5.13 lies in the relative scale of the response function values across the frequency range. This is especially true of the input-impedance responses, which typically have impedance magnitudes ranging over three orders of magnitude across the 10 Hz to 100 kHz frequency range. Thus, a small percentage difference between the estimated and measured responses, at a frequency where the impedance magnitude is high, will have a much larger effect on the value of $\mathcal{E}$ than the same percentage error at a frequency where the impedance magnitude is low. A solution to this problem is to redefine the cost function in terms of the logarithm of the response magnitudes and the respective phase angles, rather than separately considering the real and imaginary parts of the frequency responses as implied by equation 5.13. Defining the following equation errors (at a frequency ω_k), in terms of the magnitude and phase angle of the measured and estimated frequency responses:

$$\varepsilon_{Mr}(\omega_k) = \log|\check{\mathbf{G}}_r(j\omega_k)| - \log|\hat{\mathbf{G}}_r(j\omega_k)| \qquad \text{and} \tag{5.14}$$

$$\varepsilon_{Ar}(\omega_k) = \angle\check{\mathbf{G}}_r(j\omega_k) - \angle\hat{\mathbf{G}}_r(j\omega_k)\,, \tag{5.15}$$

the following expression is obtained for the cost function:

$$\mathcal{E} = \sum_{r=1}^{6} \left[w_{Mr} \sum_{k=1}^{N_f} \varepsilon_{Mr}^2(\omega_k) + w_{Ar} \sum_{k=1}^{N_f} \varepsilon_{Ar}^2(\omega_k) \right] . \tag{5.16}$$

Weighting factors w_{Mr} and w_{Ar} are introduced to adjust the relative effect that the magnitude and phase information of each response has on the final value of $\mathcal{E}$. These weighting factors also make it possible to adjust the relative importance of a particular frequency response in the parameter estimation procedure.

5.5 Optimization Procedure

For typical parameter estimation applications, an unconstrained optimization algorithm is employed to minimize the cost function, which is normally a non-linear function of the model parameters [31, 32, 74]. A wide variety of optimization algorithms are available. Popular choices for parameter estimation are the Gauss-Newton method [105, 106, 107, 75], or the method of Levenberg-Marquardt [105, 106, 74]. These algorithms are computationally efficient and offer rapid convergence rates [105, 106].

An unconstrained optimization algorithm inherently has no regard for any physical constraints that apply to the model parameters. For instance, it is known *a priori* that all the equivalent circuit elements have positive values. If reasonable initial parameter values are available, the latter constraint was not found to be a practical problem. However, for any two coupled inductances, L_i and L_j, in the equivalent-circuit model, the following must hold [34]:

$$M_{ij}^2 < L_i L_j \, , \tag{5.17}$$

At the beginning of the estimation process, only fairly poor initial estimates of the model parameters will be available, including estimates of the elements of the inductance matrix, $\boldsymbol{L}$. In practice it was found that the physical constraint of (5.17) is violated by unconstrained optimization routines, unless a very good initial estimate of the elements of the inductance matrix is available. Similar problems were reported by Keyhani *et al.* [78] while estimating the parameters of a 6-section cascade transformer winding model, who found that initial parameter estimates within 20 % of the final values were required to obtain a unique and consistent solution for the model parameters.

The knowledge that the coupling coefficient between any two inductors in the transformer model must be less than unity, constitutes *a priori* information that can only be included in the estimation process by applying a constrained optimization algorithm. The Sequential Quadratic Programming (SQP) method is such an algorithm and is considered to be one of the most efficient and accurate constrained optimization algorithms currently available [107, 100]. The SQP method is implemented by the `constr` function of the MATLAB Optimization Toolbox [100] and was applied to the transformer parameter estimation problem. The method allows boundaries to be placed on the range of values that a parameter may assume and provides for the inclusion of inequality constraints.

The constraint of (5.17) is imposed by representing $\boldsymbol{L}$ in terms of the coupling coefficients between the various self-inductances, so that mutual inductance between L_i and L_j is given by:

$$M_{ij} = M_{ji} = k_{ij}\sqrt{L_i L_j}\,, \tag{5.18}$$

where k_{ij} is the coupling coefficient. Using the SQP optimization method, k_{ij} can now be limited to a very narrow physically feasible range.

5.6 Parameter Estimation Software

An interactive program was written for MATLAB to facilitate the transformer model parameter estimation process. The program consists of an interface which displays current parameter values and allows the user to edit these parameter values. This is important, as a fair amount of manual intervention is required during the parameter estimation process and when setting up initial parameter estimates.

From the user interface, the parameter estimation routine can be started, using the current parameters as initial values. When the estimation routine terminates, the new parameter estimates are passed to the user interface and these become the current parameter set. The software provides a plotting routine, which plots the measured and estimated frequency-response characteristics of the transformer, providing visual feedback of the quality of the current parameter estimates to the user.

Facilities are provided by which the current parameter set can be saved to disk and by which a previously saved parameter set can be loaded from disk. In this way, a parameter

set will not be lost, e.g. if the estimation routine fails, provided that it was saved before the estimation routine was started. Parameter disk-files also provide a convenient way of transporting a parameter set to other programs, e.g. to calculate a response other than the responses used in the estimation procedure.

Chapter 6

Parameter Estimation Results

The aim of the parameter estimation process is to determine the values of the transformer equivalent-circuit model elements, based on a set of measured terminal frequency responses, $\check{\mathbf{g}}_{\mathbf{T}}$. In this chapter, the parameter estimation methodology developed in chapter 5 will be applied to the 16 kVA experimental transformer and the results of the estimation process will be presented. As a first step, the model parameters will be estimated without including any frequency-dependent effects. Once estimates of the linear model parameters are available, these will be used as a basis for the inclusion of frequency-dependent effects. The effect of providing insufficient frequency-response information to the estimation algorithm will also be investigated. Finally, it will be shown that the proposed parameter estimation procedure can be applied to the transformer model suggested by Douglass [17].

6.1 Definition of the Parameter Set

The transformer equivalent-circuit model structure of figure 4.7 has a total of 36 parameters, consisting of 9 capacitances, 6 resistances, 6 self-inductances and 15 mutual inductances. Parameter sub-vectors for the capacitances and resistances are respectively

given by:

$$\boldsymbol{\theta}_C = \begin{bmatrix} C_{a10} & C_{b10} & C_{b12} & C_{b34} & C_{b1} & C_{b2} & C_{b3} & C_{b4} & C_{ab1} \end{bmatrix}^T \tag{6.1}$$

and

$$\boldsymbol{\theta}_R = \begin{bmatrix} R_{a1} & R_{b1} & R_{b2} & R_{b3} & R_{b4} & R_c \end{bmatrix}^T . \tag{6.2}$$

The remaining parameters are contained in the inductance matrix, which is given by:

$$\boldsymbol{L} = \begin{bmatrix} L_{a1} & M_{a1b1} & M_{a1b2} & M_{a1b3} & M_{a1b4} & M_{a1c} \\ M_{a1b1} & L_{b1} & M_{b12} & M_{b13} & M_{b14} & M_{b1c} \\ M_{a1b2} & M_{b12} & L_{b2} & M_{b23} & M_{b24} & M_{b2c} \\ M_{a1b3} & M_{b13} & M_{b23} & L_{b3} & M_{b34} & M_{b3c} \\ M_{a1b4} & M_{b14} & M_{b24} & M_{b34} & L_{b4} & M_{b4c} \\ M_{a1c} & M_{b1c} & M_{b2c} & M_{b3c} & M_{b4c} & L_c \end{bmatrix} . \tag{6.3}$$

In section 4.2 the assumption was made that L_c is virtually ideally coupled to the other self-inductances. Thus, all coupling coefficients involving L_c can be set to a fixed value which approaches unity. L_c serves only to couple the core-loss resistance R_c to the transformer winding inductances and therefore its value can also remain constant. Letting k_c be the coupling coefficient between L_c and the winding self-inductances, the mutual inductances between L_c and the winding self-inductances can be written as:

$$\begin{aligned} M_{a1c} &= k_c\sqrt{L_c L_{a1}}\,, & M_{b1c} &= k_c\sqrt{L_c L_{b1}}\,, \\ M_{b2c} &= k_c\sqrt{L_c L_{b2}}\,, & M_{b3c} &= k_c\sqrt{L_c L_{b3}} \quad \text{and} \\ M_{b4c} &= k_c\sqrt{L_c L_{b4}}\,. \end{aligned} \tag{6.4}$$

The value of L_c can be chosen arbitrarily. A value of 37.5 H was used for L_c, which placed the estimated value of R_c in a numerically convenient range. Once the estimation procedure is completed, R_c is easily referred to either the LV or HV winding, to reflect the core-loss resistance as seen from the transformer terminals. A value of 0.9999 was used for k_c. Thus, the mutual inductances between L_c and the winding self-inductances are determined from the current estimates of the winding self-inductances at each evaluation of $\hat{\mathcal{G}}_{\mathbf{T}}$. This reduces the number of parameters to be estimated in $\boldsymbol{L}$ to 15. As discussed in section 5.5, constraints will be imposed by the estimation algorithm to keep the mutual inductance elements of $\boldsymbol{L}$ within physically feasible bounds. This is done by defining

the coupling coefficients as parameters, rather than directly estimating the mutual inductances. The mutual inductances can then be determined from the estimates of the coupling coefficients and the winding self-inductances (see equation 5.18). The inductance matrix can thus be found from the elements of the following parameter sub-vectors:

$$\boldsymbol{\theta}_L = \begin{bmatrix} L_{a1} & L_{b1} & L_{b2} & L_{b3} & L_{b4} \end{bmatrix}^T \tag{6.5}$$

and

$$\boldsymbol{\theta}_k = \begin{bmatrix} k_{a1b1} & k_{a1b2} & k_{a1b3} & k_{a1b4} & k_{b12} & k_{b13} & k_{b14} & k_{b23} & k_{b24} & k_{b34} \end{bmatrix}^T . \tag{6.6}$$

The complete parameter vector for the linear transformer model contains 30 elements and is given by:

$$\boldsymbol{\theta} = \left[\boldsymbol{\theta}_C^T \mid \boldsymbol{\theta}_R^T \mid \boldsymbol{\theta}_L^T \mid \boldsymbol{\theta}_k^T \right]^T \tag{6.7}$$

If frequency-dependence of the parameters is to be considered, additional parameters are required to define frequency-dependent expressions for the elements of $\boldsymbol{\theta}_R$ and $\boldsymbol{\theta}_L$. These parameters will be introduced in section 6.5.

The elements of $\boldsymbol{\theta}$ vary greatly in magnitude and it is good practice to scale the parameter vector before it is passed to the estimation algorithm, as the accuracy and numerical stability of the estimation procedure is generally improved [105]. This is achieved by multiplying $\boldsymbol{\theta}$ by a diagonal scaling matrix, $\boldsymbol{D}$. The estimation procedure thus estimates the elements of a scaled version of the parameter vector. The parameter scales have to be corrected at each evaluation of the estimated transformer model frequency responses, $(\hat{\mathbf{G}}_\mathbf{T})$, by multiplying the current (estimated) parameter vector by $\boldsymbol{D}^{-1}$ before the responses are evaluated. For the estimation of the transformer model parameters, the following scaling factors were used:

Capacitances: 10^9, i.e. given in nF, except C_{ab1}, which is scaled by 10^{12} (given in pF).
Resistances: 10^{-3} (given in kΩ), except R_{a1}, which is given in Ω.
Inductances: 10^{-3} (given in kH), except L_{a1}, which is given in H.

No scaling is applied to the coupling coefficients. Using the above scaling factors, all parameter values are of the same order of magnitude and are conveniently given in standard engineering units.

6.2 Parameter Constraints

The use of a constrained optimization algorithm in the parameter estimator for the transformer model, makes it possible to include *a priori* knowledge about the parameter values and their relative magnitudes in the estimation process. A basic constraint that is imposed on all parameters is that they are positive. Further, it is possible to constrain all parameters to ranges in which their values are expected to lie. This is particularly useful in the case of the coupling coefficients, which can thus be constrained to a physically feasible range. For the 16 kVA experimental transformer, the following bounds were set for all the coupling factors:

$$0.9970 \leq k \leq 0.99990\,. \tag{6.8}$$

A number suitably close to unity was chosen as the upper limit for k, while the lower limit is based on experience gained during the parameter estimation process. Further constraints can be set when considering the physical layout of the HV winding. L_{b1} and L_{b4} represent the outer layers of the two coils that constitute the HV winding (see figure 4.6). These outer layers are expected to have higher leakage-flux components than the inner winding layers, and are affected by their proximity to the tank walls. The flux distribution in the inner winding layers, which would form the largest part of the winding, is expected to be more uniform. According to this reasoning, the complete HV winding would be represented by two smaller 'outer' inductances (L_{b1} and L_{b4}) and two higher-valued 'inner' inductances (L_{b2} and L_{b3}). This information on the relative magnitude of the HV winding inductances can be included in the parameter estimation process by defining the following inequality constraints:

$$\left.\begin{aligned} L_{b1} &< L_{b2} \\ L_{b4} &< L_{b2} \\ L_{b1} &< L_{b3} \\ L_{b4} &< L_{b3} \end{aligned}\right\} \tag{6.9}$$

6.3 Data Preparation

The PRBS frequency response measurements, from which the transformer model parameters are to be estimated, contain a large number of data points (in the order of 4000 data points per response). To evaluate the transformer model responses at such a high number

of points during the estimation procedure, would require an excessive amount of computing time. Therefore, it is desirable to reduce the amount of measured frequency-response data to a more manageable volume. Decimation of the measured frequency-response data can be achieved by extracting a limited number of logarithmically spaced points from the full measured responses (the measured data contains linearly spaced data points, resulting in an excessive number of points at the high end of the frequency range).

Reduction of the number of data points by extracting a subset of the 'raw', unsmoothed, frequency-response data is not feasible, as the signal-to-noise ratio of the decimated data will increase as the number of data points decreases. This could lead to unwanted bias in the estimated frequency-response characteristics of the transformer. This problem is reduced considerably when the smoothed frequency response measurements are used in the parameter estimation procedure (see section 3.5.2). However, it must be remembered that any bias or variance in the smoothed data will be carried forward to the parameter estimation procedure, thus affecting the accuracy of the parameter estimates.

The smoothed, measured transformer frequency responses, $\check{\mathbf{G}}_{\mathbf{T}}$, were reduced to 200 approximately logarithmically-spaced data points each, by simply extracting data points, at suitable frequencies, from $\check{\mathbf{G}}_{\mathbf{T}}$. In this way, an adequate representation of the measured responses is made available to the parameter estimation procedure, with 50 points per decade across the 10 Hz to 100 kHz frequency range.

6.4 Linear Model Parameters

The parameters of the linear equivalent-circuit transformer model were estimated using the procedure discussed in chapter 5. When applying the linear model, large errors will be made in the low frequency range, as frequency-dependence of the parameters will not have been taken into account. To avoid problems due to such errors, only frequency-response data in the 1 kHz to 100 kHz range was used to estimate the linear model parameters. The initial parameters were determined on a trial-and-error basis, by manually adjusting parameters and observing the effect of the adjustments on the frequency responses of the transformer model. Once a crude approximation of the frequency responses is obtained, the parameter estimation routine is started. The estimation software did not allow arbitrary interruption of the optimization procedure, but by setting a maximum number of iterations as a stop criterion, it is possible to examine the current parameter estimates

at regular intervals during the estimation process. During the initial stages of the estimation process, manual intervention was sometimes required at such points to assist the estimation algorithm, e.g. if it was suspected that the algorithm was converging towards a local minimum of the cost function.

The final, estimated parameter set is shown in table 6.1. The corresponding simulated transformer frequency responses are compared to the measured responses in figures 6.1 to 6.6. The frequency responses obtained by sinusoidal stepped-frequency excitation are given as the reference measurements in these figures, as these are considered to be the most accurate, noise-free frequency response measurements available.

Table 6.1: Parameter estimates for the linear transformer model structure.

Parameter	Value	Parameter	Value	Parameter	Value
C_{a10} [nF]	0.072	R_{b1} [kΩ]	2.02	k_{a1b1}	0.999043
C_{b10} [nF]	0.102	R_{b2} [kΩ]	2.96	k_{a1b2}	0.999051
C_{b12} [nF]	0.164	R_{b3} [kΩ]	2.36	k_{a1b3}	0.999072
C_{b34} [nF]	0.269	R_{b4} [kΩ]	1.27	k_{a1b4}	0.999079
C_{b1} [nF]	0.228	R_c [kΩ]	60.4	k_{b12}	0.999130
C_{b2} [nF]	0.351	L_{a1} [H]	0.358	k_{b13}	0.997584
C_{b3} [nF]	0.411	L_{b1} [kH]	0.144	k_{b14}	0.997907
C_{b4} [nF]	0.187	L_{b2} [kH]	0.322	k_{b23}	0.998343
C_{ab1} [pF]	60	L_{b3} [kH]	0.427	k_{b24}	0.999161
R_{a1} [Ω]	0.0098	L_{b4} [kH]	0.161	k_{b34}	0.999321

In figures 6.1 to 6.4, which show the transformer input impedance frequency responses, it can be seen that good agreement of the measured and simulated responses is obtained in the high frequency range. Below 4 kHz there is a considerable difference between the measured and simulated frequency responses due to frequency-dependence of the inductive and resistive model parameters, which has not been taken into account at this stage. The frequency responses of the voltage transformation ratios (figures 6.5 and 6.6) are not visibly affected by these frequency-dependencies and the simulated results show good agreement with the measured frequency responses in the frequency range between 10 Hz and 60 kHz. Above 60 kHz, the simulated results deviate from the measured frequency responses. This deviation is due to at least one winding resonance below 100 kHz that can not be predicted by the model, as its order is too low. This resonance is also evident at

approximately 60 kHz in the measured responses of $\mathbf{Z}_{Loc}(j\omega)$ in figure 6.1 and $\mathbf{Z}_{Lsc}(j\omega)$ in figure 6.2, although not as prominent as in the measured responses of the voltage transformation ratios. It is very likely that this resonance can be predicted by adding a further section to the representation of the HV winding. However, this was not attempted due to the complexity of the associated parameter estimation procedure.

From the comparison of the measured and simulated transformer frequency responses, it can be concluded that the model structure of figure 4.7, with the parameters of table 6.1, correctly models the transformer frequency responses up to 60 kHz. Further, an investigation of the estimated model parameters reveals a reasonable correlation between the estimated model and the physical construction of the transformer:

(a) The relative magnitudes of the HV and LV winding parameters correspond to values that would be expected from a physical point of view. The LV winding parameters, i.e. L_{a1}, R_{a1} and C_{a10}, are much lower than any of the HV winding parameters and appear to be in proportion to each other. The inter-turn capacitance component of C_{a10} will be lower than the lumped inter-turn capacitances of the HV winding as the LV winding has a much lower number of turns. Note that the capacitance between the LV winding and earth is also included in C_{a10}. The lumped winding self-inductances, resistances and inter-turn capacitances of the HV winding are roughly in proportion for each winding section, i.e. the section with the highest self-inductance (highest number of turns) also has the highest lumped winding resistance and the highest lumped inter-turn capacitance.

(b) In section 6.2 it was suggested that each of the two coils that constitute the HV winding are represented by two self-inductances in the equivalent-circuit model; with the smaller self-inductances representing the outer layers of each coil. While this is reflected by the relative values of the estimated self-inductances for each coil, closer agreement between L_{b1} and L_{b4} as well as between L_{b2} and L_{b3} was expected, i.e. $L_{b1} \approx L_{b4}$ and $L_{b2} \approx L_{b3}$.

(c) The coupling coefficients between the LV winding and all the HV winding sections are similar. This is the expected result, as the HV coils are wound on the outside of the two (parallel connected) LV coils.

It was found that the estimate obtained for C_{ab1} is not reliable. The cost function is insensitive the the value of C_{ab1} in the 10 Hz to 100 kHz frequency range as C_{ab1} does not significantly influence any of the transformer frequency responses in this frequency range. C_{ab1} is not expected to affect any of the transformer frequency responses at frequencies

below 500 kHz [14]. Thus, an accurate estimate of C_{ab1} can only be obtained if frequency-response data above 500 kHz is made available to the estimator.

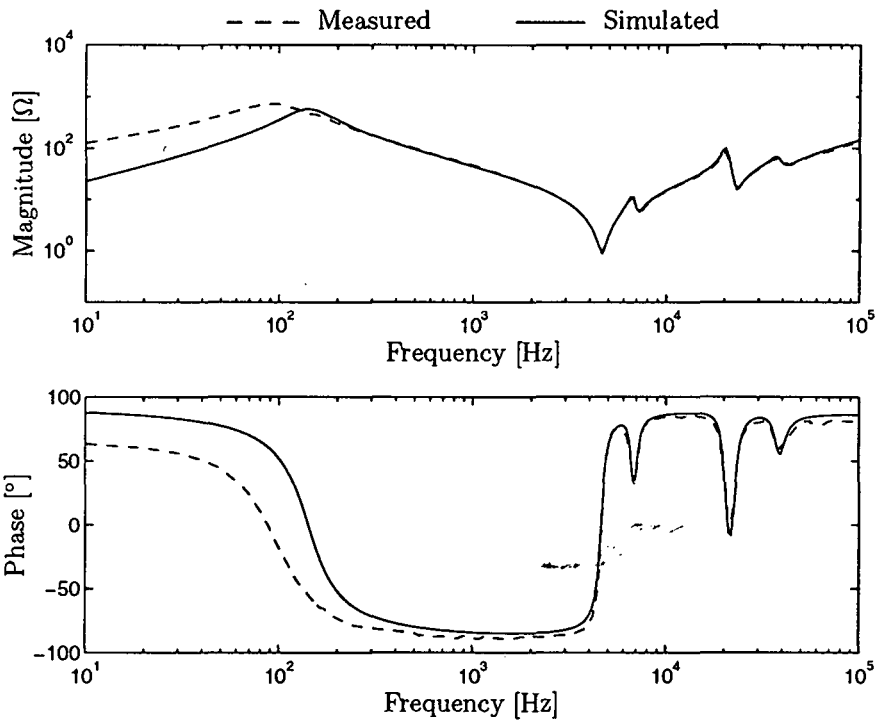

Figure 6.1: Measured and simulated LV open-circuit input impedance frequency response, $\mathbf{Z}_{Loc}(j\omega)$.

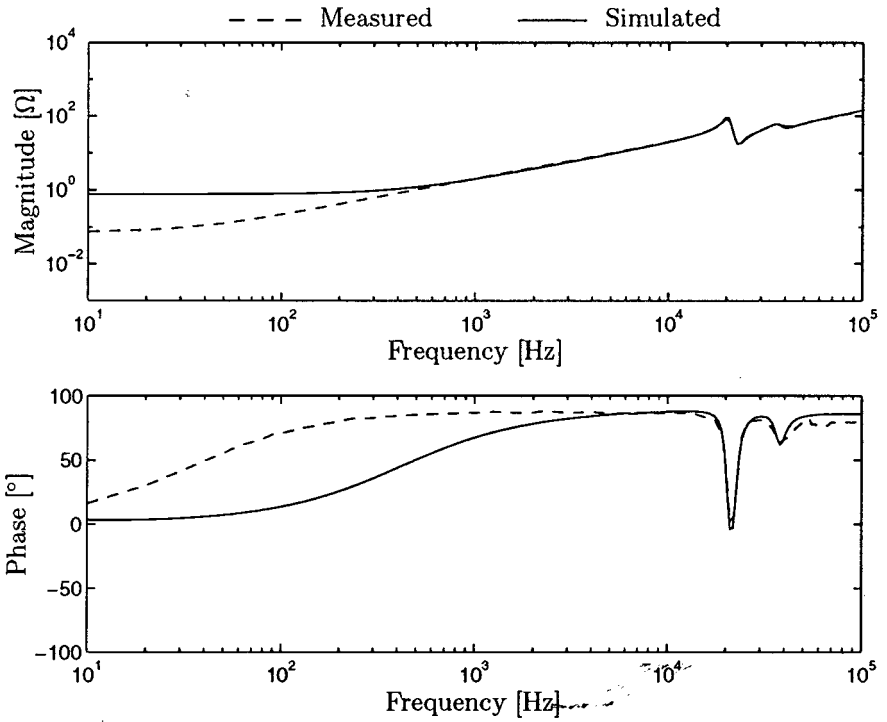

Figure 6.2: Measured and simulated LV short-circuit input impedance frequency response, $\mathbf{Z}_{Lsc}(j\omega)$.

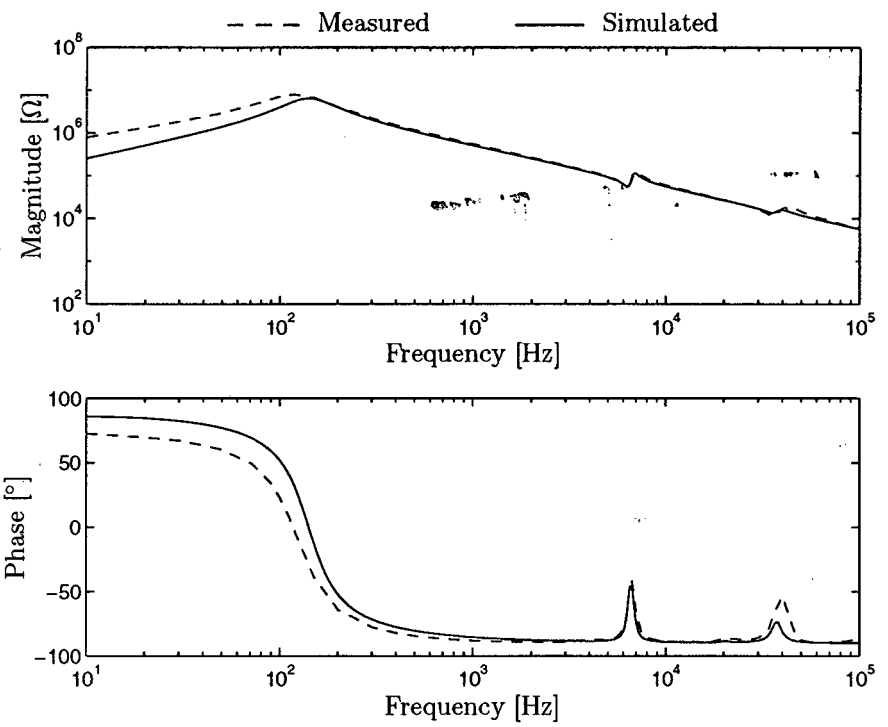

Figure 6.3: Measured and simulated HV open-circuit input impedance frequency response, $\mathbf{Z}_{Hoc}(j\omega)$.

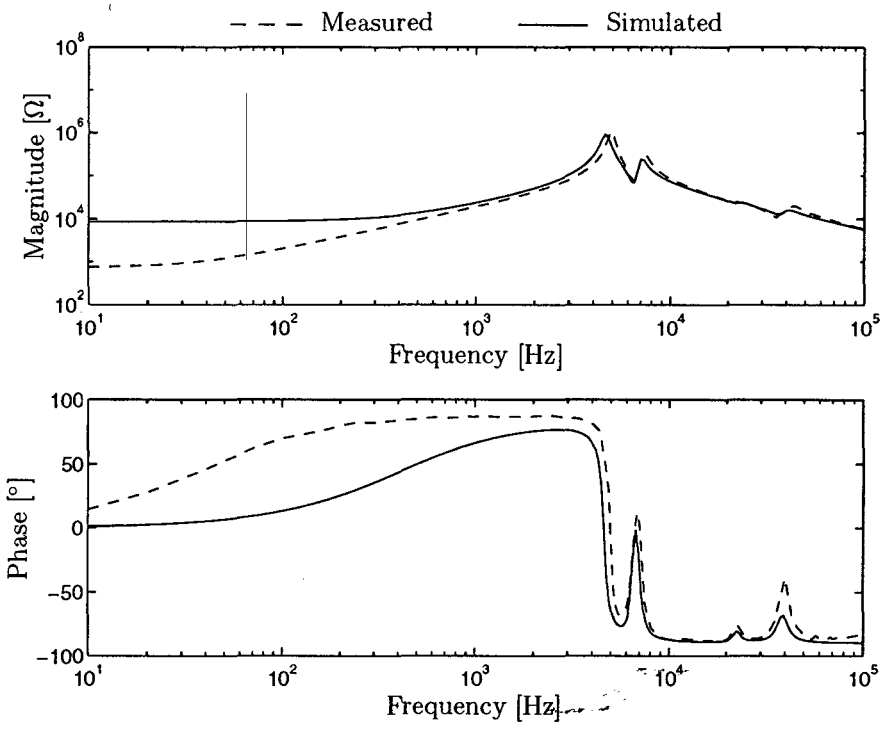

Figure 6.4: Measured and simulated HV short-circuit input impedance frequency response, $\mathbf{Z}_{Hsc}(j\omega)$.

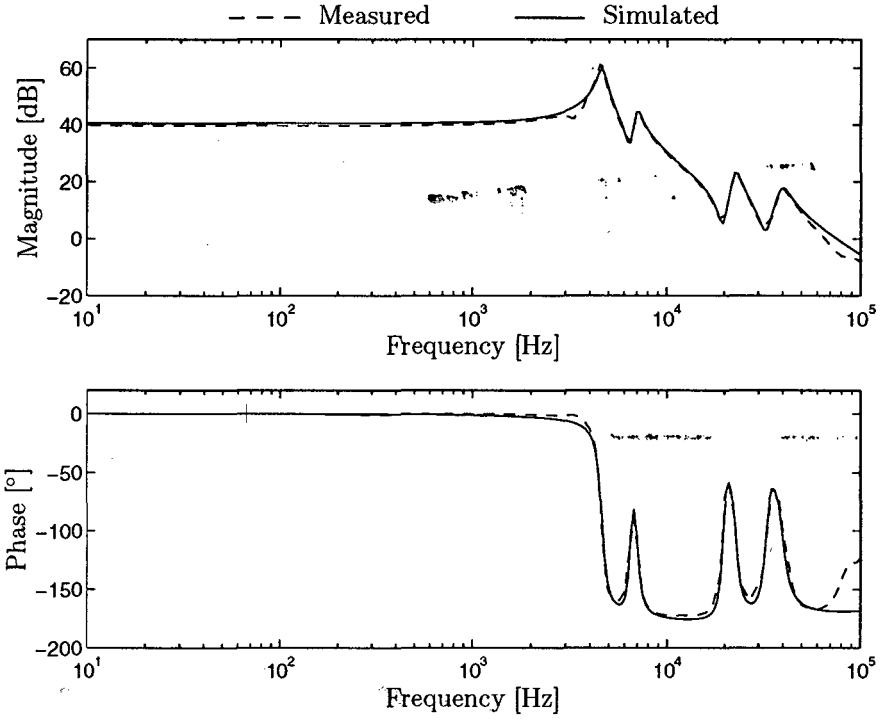

Figure 6.5: Measured and simulated LV–HV voltage transformation ratio frequency response, $\mathbf{H}_{LH}(j\omega)$.

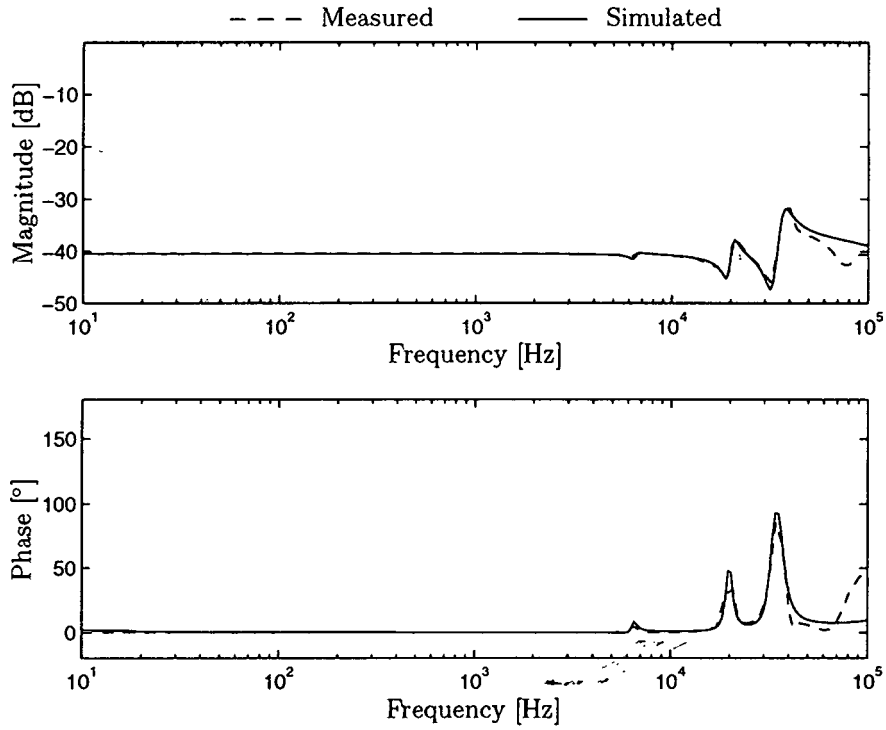

Figure 6.6: Measured and simulated HV–LV voltage transformation ratio frequency response, $\mathbf{H}_{HL}(j\omega)$.

6.5 Frequency-dependent Model Parameters

In the previous section, a set of parameters was estimated for the transformer model, based on the assumption that the transformer behaves linearly. From the results in figures 6.1 to 6.6, it can be seen that this assumption is valid for frequencies above about 4 kHz, but not in the lower frequency range, due to frequency-dependence of the equivalent-circuit model parameters. Frequency-dependence of the resistive and inductive model parameters will be introduced by adjusting the relevant linear parameters, rather than by estimating a completely new set of parameters. This reduces the estimation problem to the estimation of a few parameters describing the frequency-dependence of the resistive and inductive equivalent-circuit model elements.

A problematic aspect of introducing frequency-dependence is that the resistive and inductive equivalent-circuit element values are not only a function of frequency, but are also a function of the excitation level that was used during frequency response measure-

ment. Thus, while the parameter frequency-dependence is expected to follow the same trend for the various frequency responses, the parameters that describe the frequency-dependence functions for each response will have different values. This implies that the frequency-dependence of the equivalent-circuit elements has to be evaluated separately for each response, instead of the simultaneous response evaluation used during the linear parameter estimation process.

Parameter frequency-dependence for the open-circuit and short-circuit input impedance responses is treated differently, as these are respectively dominated by the magnetizing-branch elements and the winding resistances. The open-circuit voltage transformation ratio frequency responses are not affected by parameter frequency-dependence and no separate frequency-dependence functions need to be considered for these responses.

6.5.1 Open-circuit Frequency Responses

The parameter frequency-dependence for the open-circuit input impedance frequency responses is dominated by the magnetizing-branch elements. This means that the core-loss resistance, R_c, and the winding self-inductances are to be expressed as functions of frequency. As discussed in section 4.3.1, the core-loss resistance will be represented by:

$$R_c = \frac{a_{Ro} f}{f + b_{Ro}} . \tag{6.10}$$

If it is assumed that the coupling coefficients between the various winding self-inductances are not frequency-dependent, the complete inductance matrix of the transformer model can be adjusted to compensate for the frequency-dependence of the winding inductances. By applying the frequency-dependence function proposed by Funk and Hantel [95] (see section 4.3.1) to the inductance matrix, the following frequency-dependent expression for $\boldsymbol{L}$ is obtained:

$$\boldsymbol{L}_{non-linear} = a_{Lo} f^{-b_{Lo}} \boldsymbol{L}_{linear} . \tag{6.11}$$

The expressions of equations 6.10 and 6.11 can be used to modify the linear transformer model parameters, so that the frequency-dependent parameter estimation problem reduces to the estimation of only four parameters (a_{Ro}, b_{Ro}, a_{Lo} and b_{Lo}) for each of the two open-circuit input impedance frequency responses. The same estimation procedure, that was applied to the linear model parameters, was applied to estimate a set of frequency-

dependence parameters for each open-circuit input impedance response, although it was not necessary to define any parameter constraints. Further, only the frequency response under consideration was included in the estimation process.

The estimates of the frequency-dependence parameters, for both the HV and LV open-circuit input impedance frequency responses, are given in table 6.2. The corresponding frequency responses are shown in figures 6.7 and 6.8. From these figures it can be seen that, with the inclusion of the frequency-dependence of the magnetizing-branch elements, a very good correlation between the measured and simulated open-circuit input impedance frequency responses is obtained across the 10 Hz to 100 kHz frequency range.

The differences in the frequency-dependence parameters obtained for $\mathbf{Z}_{Loc}(j\omega)$ and $\mathbf{Z}_{Hoc}(j\omega)$ are due to the different excitation levels that were used during the respective frequency response measurements. The peak core flux that could be established during the measurement of $\mathbf{Z}_{Hoc}(j\omega)$ was much lower than that obtained during the measurement of $\mathbf{Z}_{Loc}(j\omega)$. At any given frequency, the elements of $\boldsymbol{L}$ are lower for $\mathbf{Z}_{Hoc}(j\omega)$ than for $\mathbf{Z}_{Loc}(j\omega)$, due to the higher value of b_{Lo}. This is the expected result, as the effective permeability of the core tends to increase with excitation level (for low excitation voltages compared to the transformer rating), as discussed in section 3.7.

Table 6.2: Estimated frequency-dependence parameters for the transformer open-circuit input impedance frequency responses.

Parameter	$\mathbf{Z}_{Loc}(f)$	$\mathbf{Z}_{Hoc}(f)$
a_{Ro}	96.8	101
b_{Ro}	28.9	40.4
a_{Lo}	8.89	7.97
b_{Lo}	0.263	0.357

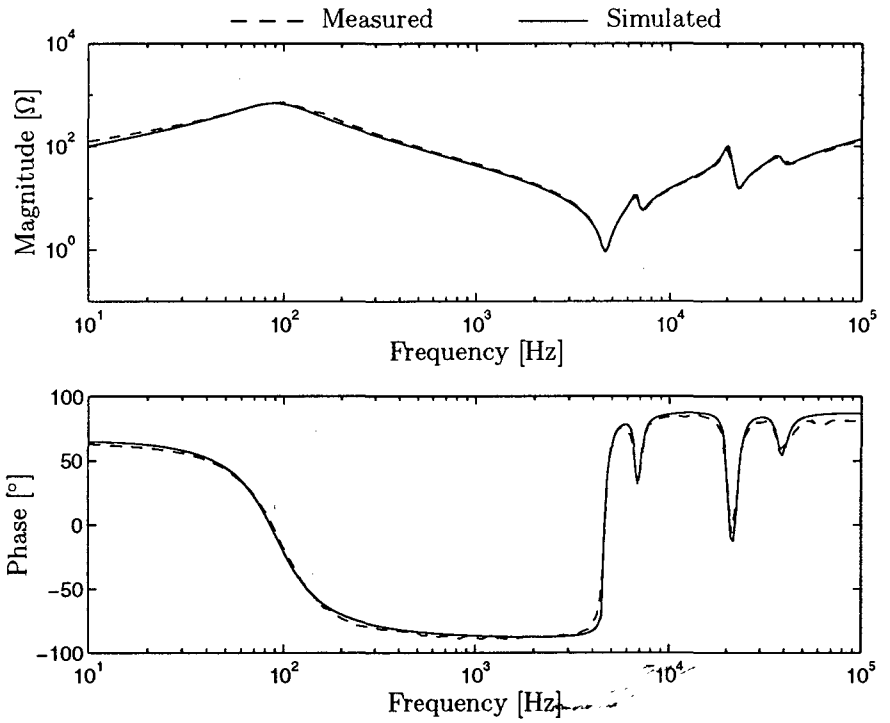

Figure 6.7: Measured and simulated LV open-circuit input impedance frequency response, $\mathbf{Z}_{Loc}(j\omega)$, allowing for frequency-dependence of the magnetizing-branch.

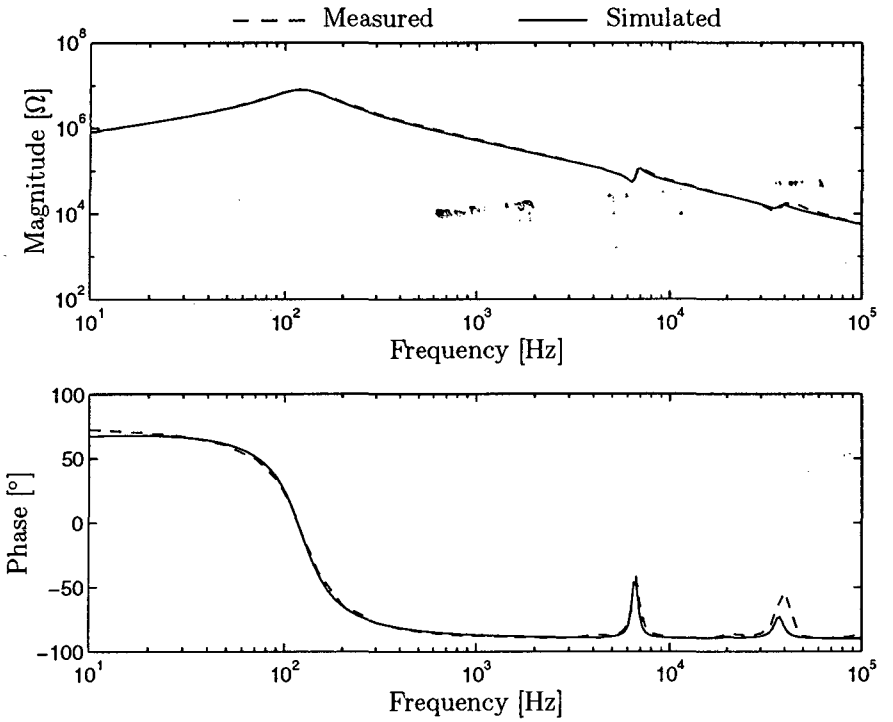

Figure 6.8: Measured and simulated HV open-circuit input impedance frequency response, $\mathbf{Z}_{Hoc}(j\omega)$, allowing for frequency-dependence of the magnetizing-branch.

6.5.2 Short-circuit Frequency Responses

As discussed in section 4.3.2, the transformer winding resistances are a strong function of frequency, primarily due to skin-effect. The winding resistances, together with the leakage-inductances of the windings, dominate the short-circuit input impedance frequency responses of the transformer in the low frequency range. It was also shown in section 4.3.2 that the equivalent leakage inductance of the experimental transformer does not change appreciably with frequency. However, from the result for the linear HV short-circuit input impedance response, shown in figure 6.4, it is clear that the inductive parameters of the transformer model are slightly affected by non-linearities. In figure 6.4 it can be seen that the first resonance peak of $\mathbf{Z}_{Hsc}(j\omega)$ occurs at a higher frequency than that of the measured response, indicating a reduction in the winding self-inductances as a function of frequency. The inductance frequency-dependence function proposed by Funk and Hantel [95] will be applied to account for this reduction in the winding self-inductances:

$$\boldsymbol{L}_{non-linear} = a_{Ls} f^{-b_{Ls}} \boldsymbol{L}_{linear} \,. \tag{6.12}$$

Strictly speaking, a different frequency-dependence function should be defined for the HV and LV winding resistances respectively, as different conductors are used to form each winding. However, it was found that satisfactory results could be obtained by adjusting all the linear winding resistances according to the same function:

$$R_{non-linear} = \frac{R_{linear}}{c_{Rs}} \left[1 + a_{Rs} \left(\frac{f}{10} - 1 \right)^{b_{Rs}} \right] \tag{6.13}$$

Thus, the parameter frequency-dependence for the short-circuit input impedance responses is defined by five parameters (a_{Ls}, b_{Ls}, a_{Rs}, b_{Rs} and c_{Rs}). These parameters were estimated for $\mathbf{Z}_{Lsc}(j\omega)$ and $\mathbf{Z}_{Hsc}(j\omega)$, yielding the results shown in table 6.3. The short-circuit input impedance frequency responses, calculated by including the frequency-dependence of the winding resistances, are shown in figures 6.9 and 6.10 and it can be seen that a good prediction of the measured responses is obtained.

From the parameter estimates shown in table 6.3, it can be seen that for $\mathbf{Z}_{Lsc}(j\omega)$ no adjustment of the winding self-inductances as a function of frequency was required as the frequency-dependence function maintains a value of unity across the frequency range. In the case of $\mathbf{Z}_{Hsc}(j\omega)$, the low value of b_{Lo} causes a slight reduction in the element values of $\boldsymbol{L}$ as the frequency increases, but this is sufficient to correct the location of the first resonance peak of this response. The values of a_{Ls} and b_{Ls} shown in table 6.3 are similar

to the values reported by Funk and Hantel [95], who determined values of a_{Ls} and b_{Ls} for the short-circuit input-impedance frequency responses of a number of transformers.

The estimation results in table 6.3 also show a good agreement between the frequency-dependence parameters of the winding resistances for $\mathbf{Z}_{Lsc}(j\omega)$ and $\mathbf{Z}_{Hsc}(j\omega)$. This indicates that these parameters are primarily frequency-dependent and are not significantly affected by the excitation level that was used during the measurement of the short-circuit input impedance frequency responses.

Table 6.3: Estimated frequency-dependence parameters for the transformer short-circuit input impedance frequency responses.

Parameter	$\mathbf{Z}_{Lsc}(j\omega)$	$\mathbf{Z}_{Hsc}(j\omega)$
a_{Rs}	0.0118	0.0103
b_{Rs}	0.908	0.930
c_{Rs}	12.6	12.4
a_{Ls}	1	1
b_{Ls}	≈ 0	0.0084

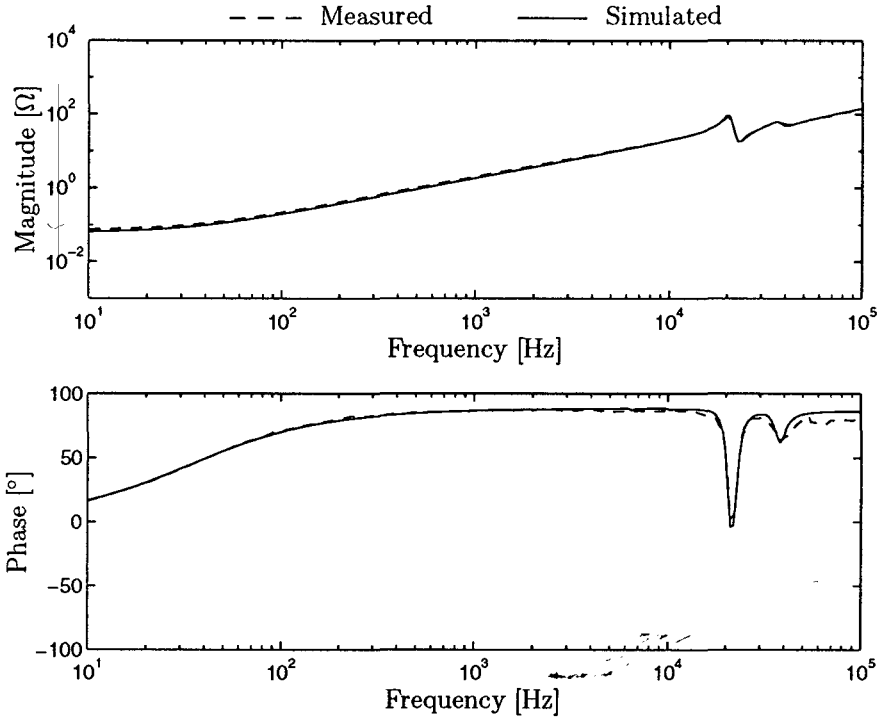

Figure 6.9: Measured and simulated LV short-circuit input impedance frequency response, $\mathbf{Z}_{Lsc}(j\omega)$, including frequency-dependence of the winding resistances.

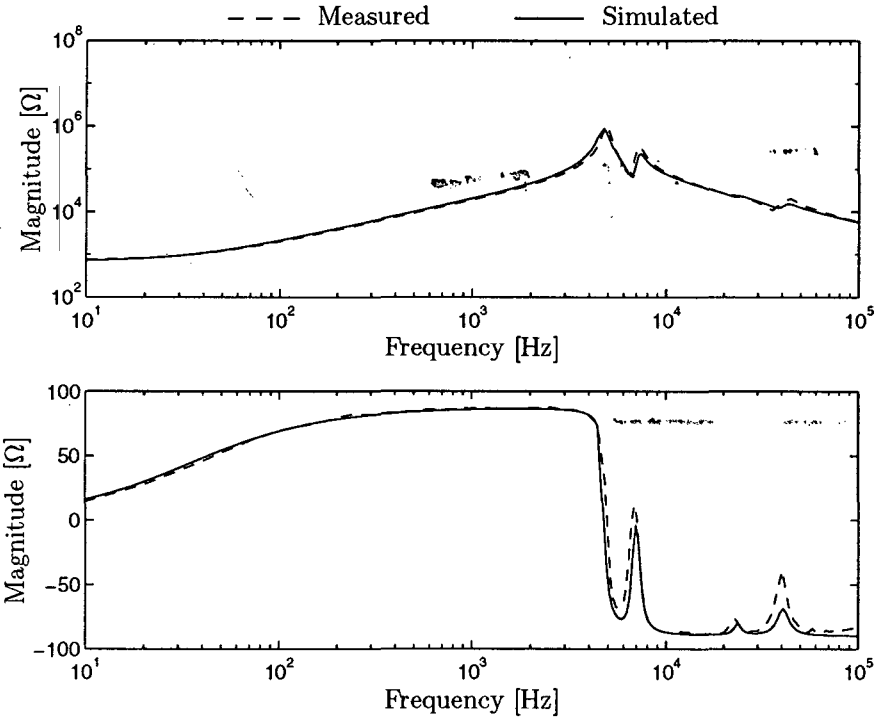

Figure 6.10: Measured and simulated HV short-circuit input impedance frequency response, $\mathbf{Z}_{Hsc}(j\omega)$, including frequency-dependence of the winding resistances.

6.6 Parameter Estimation From One Frequency Response

All six of the available, measured transformer frequency responses, $\check{\mathbf{G}}_{\mathbf{T}}$, were used in the parameter estimation procedure to obtain the results discussed in section 6.4. This is not ideal, as six responses have to be measured and the inclusion of these responses in the parameter estimation procedure represents a considerable computing overhead. The aim of the following example is to confirm the earlier conclusion that more than one frequency response measurement is in fact required to obtain feasible and unique parameter estimates for the transformer model.

Table 6.4 shows a set of parameter estimates obtained for the transformer model, using only the LV open-circuit input impedance frequency responses as reference for the parameter estimation procedure. In all other respects, the estimation procedure was identical to that used to obtain the parameter estimates discussed in section 6.4. Generally, the parameters shown in table 6.4 seem physically feasible and the result is a good simulation of $\mathbf{Z}_{Loc}(j\omega)$, as shown in figure 6.11.

However, when the same parameters are used to predict any of the other transformer

Table 6.4: Parameter estimates for the linear transformer model structure, using only the LV open-circuit input impedance frequency-response data.

Parameter	Value	Parameter	Value	Parameter	Value
C_{a10} [nF]	0.0654	R_{b1} [kΩ]	2.29	k_{a1b1}	0.999174
C_{b10} [nF]	0.125	R_{b2} [kΩ]	2.67	k_{a1b2}	0.999267
C_{b12} [nF]	0.228	R_{b3} [kΩ]	2.44	k_{a1b3}	0.998791
C_{b34} [nF]	0.162	R_{b4} [kΩ]	1.98	k_{a1b4}	0.998857
C_{b1} [nF]	0.177	R_c [kΩ]	60.4	k_{b12}	0.999235
C_{b2} [nF]	0.381	L_{a1} [H]	0.348	k_{b13}	0.999151
C_{b3} [nF]	0.355	L_{b1} [kH]	0.156	k_{b14}	0.997901
C_{b4} [nF]	0.168	L_{b2} [kH]	0.412	k_{b23}	0.998146
C_{ab1} [pF]	60.1	L_{b3} [kH]	0.394	k_{b24}	0.997682
R_{a1} [Ω]	0.019	L_{b4} [kH]	0.113	k_{b34}	0.998894

frequency responses, incorrect results are obtained. Figures 6.12 and 6.13 show the simulated LV short-circuit input impedance and the HV-LV transformation ratio frequency responses respectively, obtained using the parameters of table 6.4. The simulated LV short-circuit input impedance response clearly shows that the first series-parallel resonance pair is incorrectly represented, being under-damped and thus more prominent than the equivalent, measured resonance at that point. In the HV-LV voltage transformation ratio frequency response, the same resonance pair incorrectly appears as a parallel-series resonance pair. This can easily be seen from the reversed phase response of this resonance pair. Thus, table 6.4 represents a set of parameters for the equivalent-circuit transformer model that does not correctly describe all the frequency-response characteristics of the experimental transformer. This result highlights the importance of considering as many frequency responses as possible when validating a transformer model or estimating its parameters.

It was found that the frequency responses predicted by the proposed model are very sensitive to the values of the coupling coefficients. Comparing the coupling coefficient estimates shown in table 6.4 to the estimates shown in table 6.1, it can be seen that the coupling coefficients estimated from one response differ considerably from those estimated from a full set of frequency responses. Reasonably similar values were however obtained for the other parameters. It can thus be concluded that the parameter estimation procedure is unable to reliably resolve the relative values of the coupling coefficients when only the LV open-circuit input impedance frequency response is used as input data. This problem is expected to become more severe as the number of sections used to represent each winding is increased. This raises the following question: How many sections can be added to the model before unique and consistent parameter estimates can no longer be obtained, even when a full set of terminal frequency responses (but no other information) is available? An answer to this question can probably only be found by carrying out a detailed analysis of the transformer model structure. Referring to the analysis presented in section 4.1, it can be seen that this is not a straight-forward matter and was thus not attempted as part of this project.

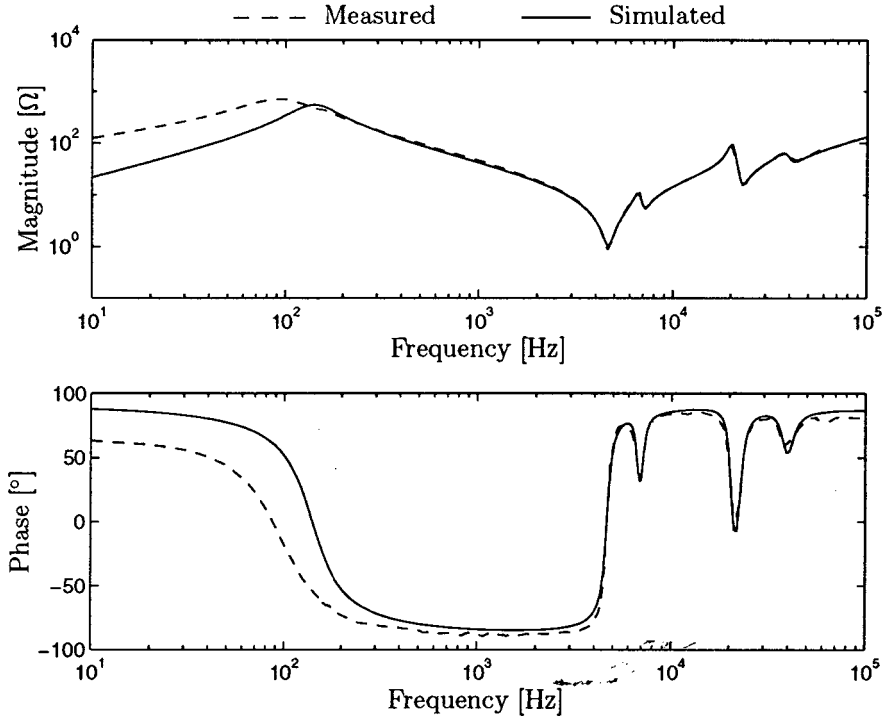

Figure 6.11: LV open-circuit input impedance frequency response, $\mathbf{Z}_{Loc}(j\omega)$, simulated with the parameters of table 6.4.

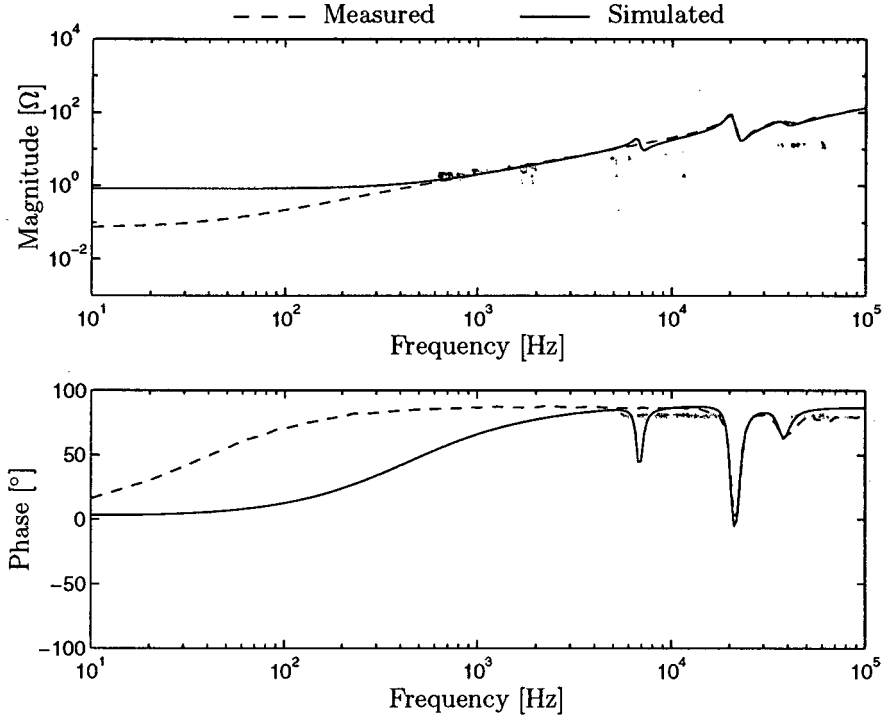

Figure 6.12: LV short-circuit input impedance frequency response, $\mathbf{Z}_{Lsc}(j\omega)$, simulated with the parameters of table 6.4.

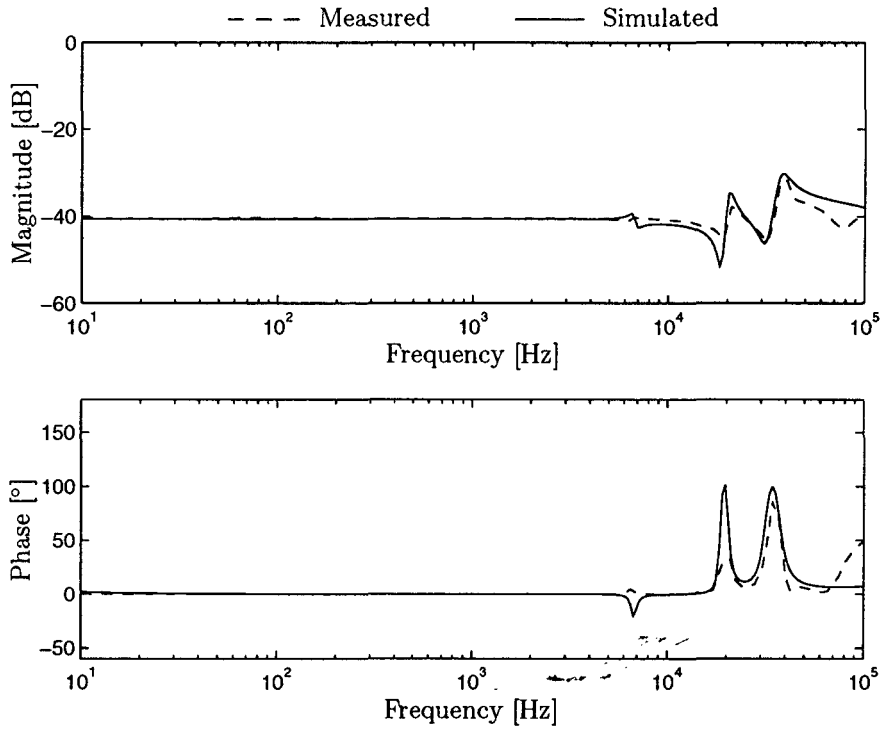

Figure 6.13: HV-LV voltage transformation ratio frequency response, $H_{HL}(j\omega)$. The simulation used the parameters of table 6.4.

6.7 Application of the Parameter Estimator to the Model Proposed by Douglass

In section 2.2.2, the methods developed by Bak-Jensen *et al.* [14] and Islam *et al.* [13] to estimate the parameters of the transformer model proposed by Douglass [17], were discussed. These methods require that the transformer model is represented by a number of reduced sub-circuits, which are each described by a transfer function. The coefficients of these transfer functions are then estimated by applying standard parameter estimation algorithms and finally the equivalent-circuit elements are determined from the estimated transfer-function coefficients.

The aim of this section is to show that the parameter estimation procedure, developed in chapter 5, can also be applied to directly estimate the parameters of the transformer equivalent circuit proposed by Douglass [17] for the 16 kVA test transformer. The com-

plete Douglass equivalent-circuit model is shown in figure 6.14. The model is described by eight parameters, including the ratio $a = N_p/N_s$ of the ideal transformer, so that a parameter vector can be formulated as follows:

$$\boldsymbol{\theta} = \begin{bmatrix} C_s & C_p & C_{ps} & R_{ps} & L_{ps} & k_{Re} & k_{Le} & a \end{bmatrix}^T . \tag{6.14}$$

The transformer model, excluding the ideal transformer, is represented by its nodal admittance matrix (see Appendix A), with all parameters referred to the LV side of the ideal transformer. The HV input impedance responses and the voltage transformation ratio frequency responses are subsequently scaled by the ratio of the ideal transformer so that this ratio can be included as a parameter:

$$\mathbf{Z}_{Hoc}(j\omega) = a^2\mathbf{Z}'_{Hoc}(j\omega)\,, \tag{6.15}$$

$$\mathbf{Z}_{Hsc}(j\omega) = a^2\mathbf{Z}'_{Hsc}(j\omega)\,, \tag{6.16}$$

$$\mathbf{H}_{HL}(j\omega) = \frac{1}{a}\mathbf{H}'_{HL}(j\omega) \quad \text{and} \tag{6.17}$$

$$\mathbf{H}_{LH}(j\omega) = a\mathbf{H}'_{LH}(j\omega)\,, \tag{6.18}$$

where the prime indicates a response that is referred to the LV side of the ideal transformer.

The SQP constrained optimization routine was used to minimize the cost function of the estimator, but no constraints were specified, except to limit all the parameters to a feasible, positive range. An unconstrained optimization routine can be applied with equal success: The BGFS [106, 105] method, implemented by the `fminu` function of the MATLAB Optimization Toolbox [100] was also applied to estimate the parameters of the model proposed by Douglass and yielded results that were virtually identical to those

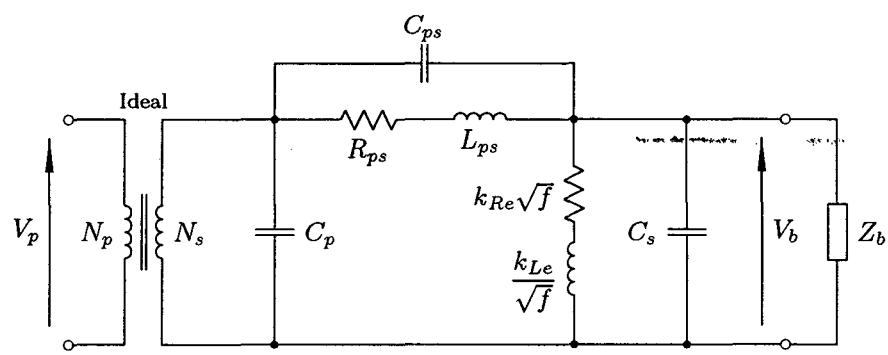

Figure 6.14: Transformer equivalent circuit proposed by Douglass [17], with a frequency-dependent magnetizing branch.

produced by the SQP method.

The stepped-frequency response measurements of the 16 kVA transformer were used to estimate the model parameters. With respect to the estimation procedure, the Douglass model structure has fewer degrees of freedom than the proposed model structure of figure 4.7, so that it was possible to estimate its parameters using only two of the responses in $\mathfrak{S}_{\mathbf{T}}$. Table 6.5 shows the parameter estimates that were obtained for the model, using only $\mathbf{Z}_{Loc}(j\omega)$ and $\mathbf{H}_{LH}(j\omega)$ as input responses. The predicted frequency responses are compared to the measured responses in figures 6.15 to 6.20.

Note that the estimates of C_s and C_{ps} are likely to be poor. The first parallel resonance in $\mathbf{Z}_{Loc}(j\omega)$ occurs when L_e resonates with C_p at a resonant frequency of:

$$f_1 = \frac{1}{2\pi\sqrt{C_p\, k_{Le}/\sqrt{f_1}}}, \tag{6.19}$$

if the effects of the other circuit elements are ignored. Solving for f_1 yields:

$$f_1 = \left[(2\pi)^2\, C_p\, k_{Re}\right]^{\frac{2}{3}}. \tag{6.20}$$

Substituting the estimated values of C_p and k_{Re} in equation 6.20 shows that the first parallel resonant frequency of $\mathbf{Z}_{Loc}(j\omega)$ lies at $f_1 = 109$ Hz, which agrees with the response of $\mathbf{Z}_{Loc}(j\omega)$ shown in figure 6.15 (the same resonance is also visible from the HV terminals, as shown in figure 6.17. The series resonance following the first parallel resonance, is formed by L_{ps} and C_p, with a resonant frequency of approximately:

$$f_2 = \frac{1}{2\pi\sqrt{C_p\, L_{ps}}} = 4\,627 \text{ Hz}, \tag{6.21}$$

Table 6.5: Parameter estimates for the transformer model proposed by Douglass [17].

Parameter	Value	Parameter	Value
C_p [μF]	4.05	R_e [Ω]	$20.7\sqrt{f}$
C_s [nF]	1.75	L_{ps} [mH]	0.292
C_{ps} [nF]	≈ 0	L_e [H]	$5.47/\sqrt{f}$
R_{ps} [Ω]	0.591	N_p/N_s	96.7

which can be seen in figure 6.15 and corresponds with the first peak in the voltage transformation ratio frequency responses. The next resonance that will occur in $\mathbf{Z}_{Loc}(j\omega)$ will be a parallel resonance between C_s and L_{ps}, assuming that C_p can be treated as a short-circuit, as $C_s \ll C_p$. Using the estimated values of C_s and L_{ps}, the resonant frequency of this resonance can be approximated by:

$$f_3 = \frac{1}{2\pi\sqrt{C_s L_{ps}}} = 222 \text{ kHz}, \tag{6.22}$$

which lies above the frequency range that was considered in the parameter estimation process. An accurate estimate of C_s would require that frequency response data in the vicinity of f_3 is available. Thus, it must be concluded that the estimate of C_s given in table 6.5 is not reliable. A similar argument applies to C_{ps}, which is generally considered to have virtually no effect at frequencies below 500 kHz [14]. This is confirmed by the fact that a value of $C_{ps} \approx 0$ was estimated. In contrast to this result, Douglass [17] found C_{ps} values that were more than an order higher than C_s, when determining parameters for two voltage transformer models in the frequency range between 100 Hz and 30 kHz. Thus, the results reported by Douglass suggest that C_{ps} will have a noticeable effect on the transformer frequency responses in the frequency range below 100 kHz. Bak-Jensen *et al.* [14] also reported values of C_{ps} that are higher than C_s. However, their parameter estimation procedure was unable to determine a reliable value for C_s, so that a conclusion on the relative magnitudes of C_s and C_{ps} can not be drawn from their results. The accurate estimation of C_s and C_{ps} for the model proposed by Douglass [17] is an important issue which can not be addressed in the present context, as frequency response data is not available over a sufficiently wide frequency range. However, it is likely that the parameter estimation procedure presented above will yield accurate and reliable estimates of C_s and C_{ps}, provided that a full set of frequency response data is available up to at least 1 MHz.

From the responses shown in figures 6.15 to 6.20 it can be seen that the model proposed by Douglass provides a reasonably good prediction of the frequency responses of the 16 kVA transformer, despite its relative simplicity. The agreement between the measured and predicted frequency responses of the short-circuit input impedances $\mathbf{Z}_{Lsc}(j\omega)$ and $\mathbf{Z}_{Hsc}(j\omega)$ is not as good as for the other responses. The reason for this is that the frequency-dependence of R_{ps}, due to skin-effect, has not been considered. By reducing the value of R_{ps}, a better prediction of the short-circuit responses is obtained at the cost of a poorer prediction of the damping associated with all the winding resonances, except the first parallel resonance in the open-circuit input impedance responses. This result suggests that the transformer model proposed by Douglass can be improved by the addition of a

function to describe the frequency-dependence of R_{ps} (such as the frequency-dependence function proposed by Funk and Hantel [95]).

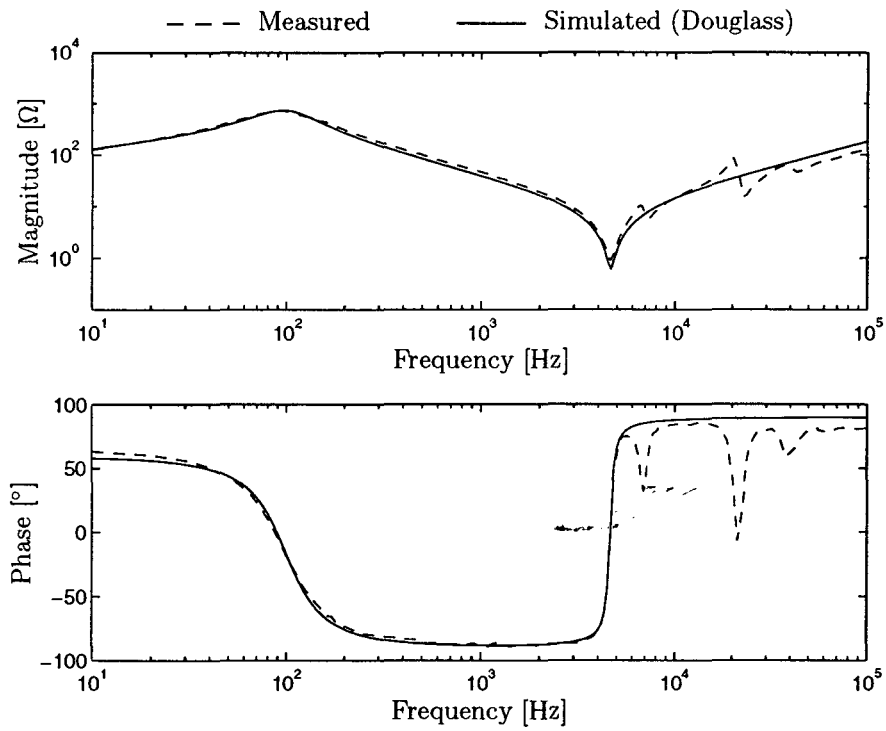

Figure 6.15: Measured and simulated LV open-circuit input impedance frequency response, $\mathbf{Z}_{Loc}(j\omega)$.

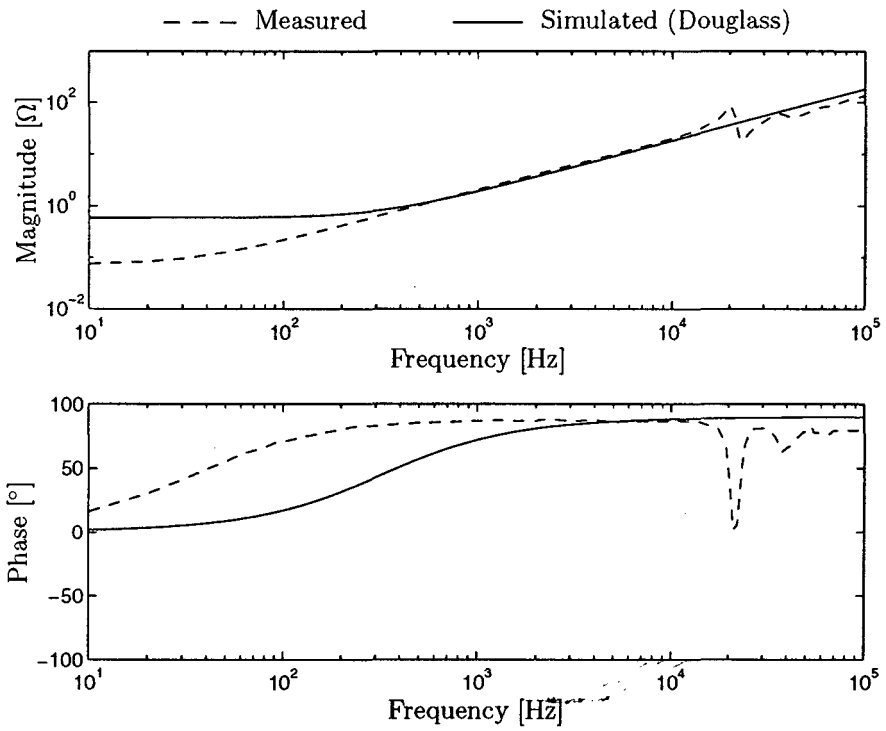

Figure 6.16: Measured and simulated LV short-circuit input impedance frequency response, $\mathbf{Z}_{Lsc}(j\omega)$.

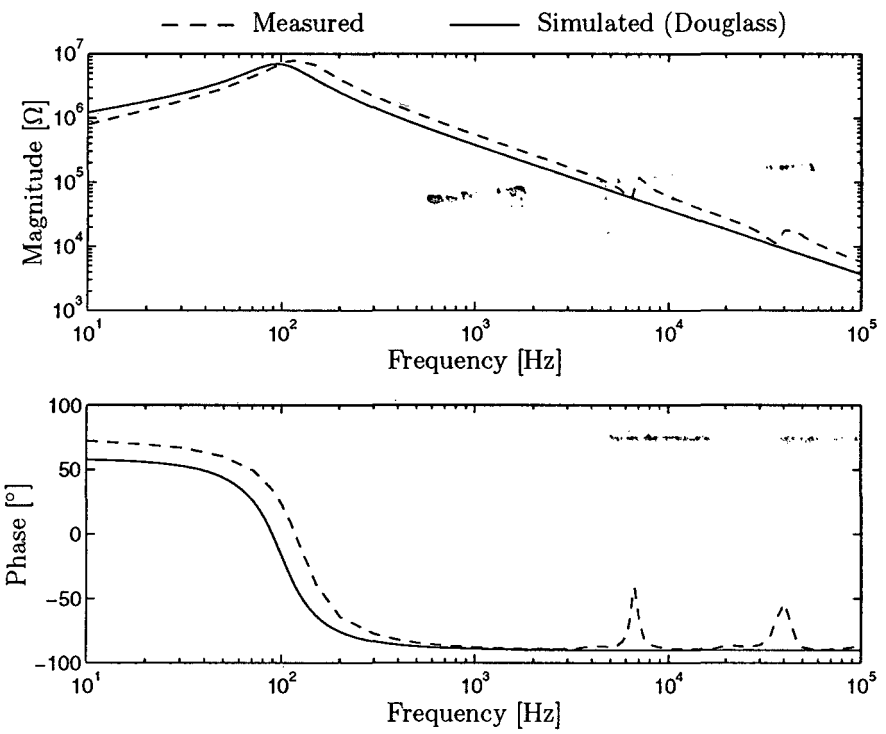

Figure 6.17: Measured and simulated HV open-circuit input impedance frequency response, $\mathbf{Z}_{Hoc}(j\omega)$.

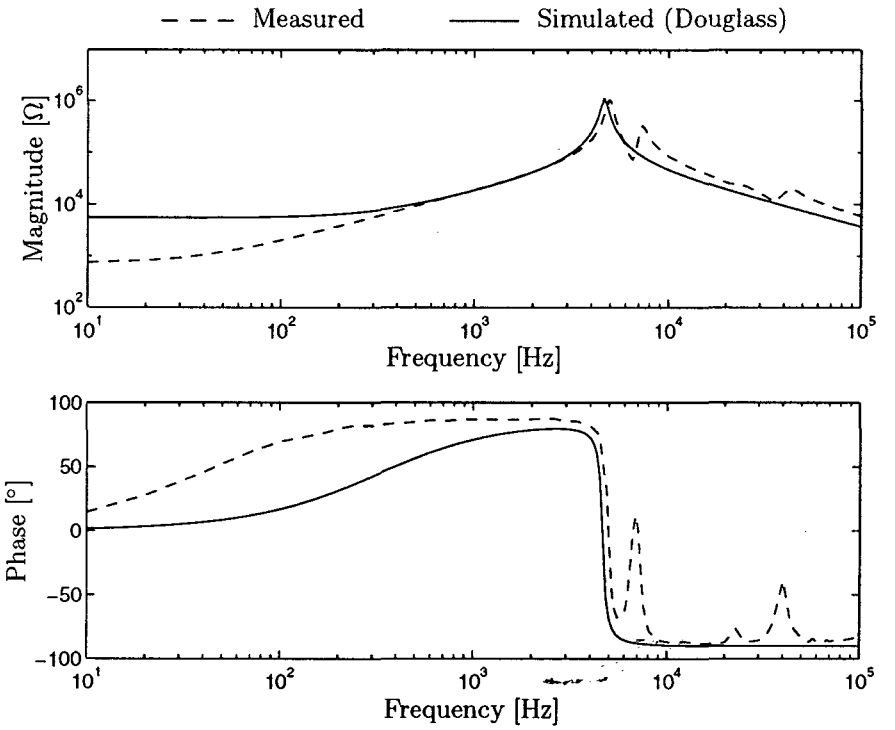

Figure 6.18: Measured and simulated HV short-circuit input impedance frequency response, $\mathbf{Z}_{Hsc}(j\omega)$.

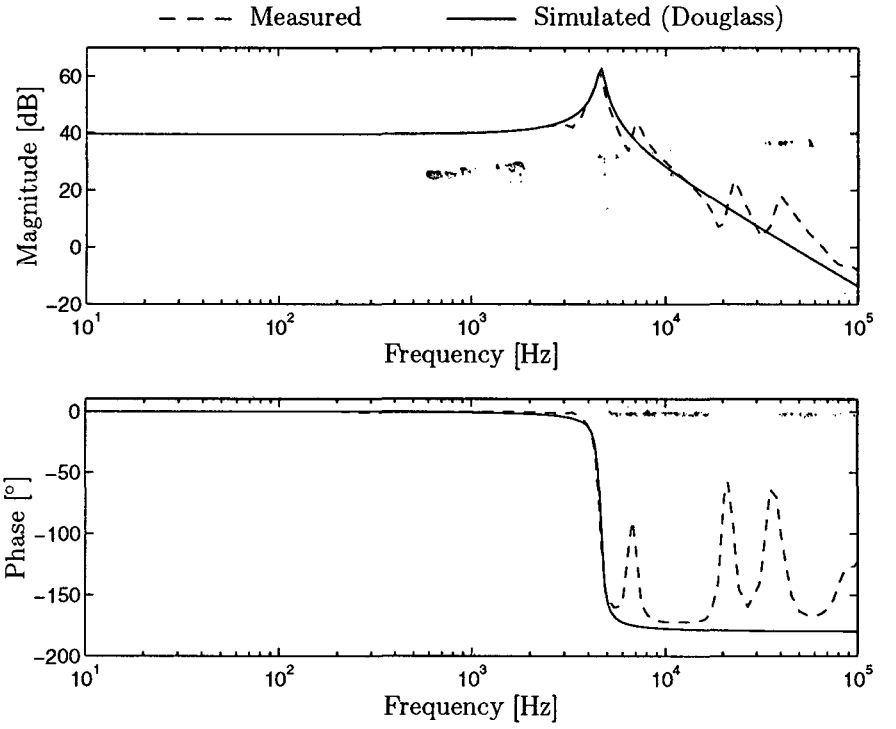

Figure 6.19: Measured and simulated LV–HV voltage transformation ratio frequency response, $\mathbf{H}_{LH}(j\omega)$.

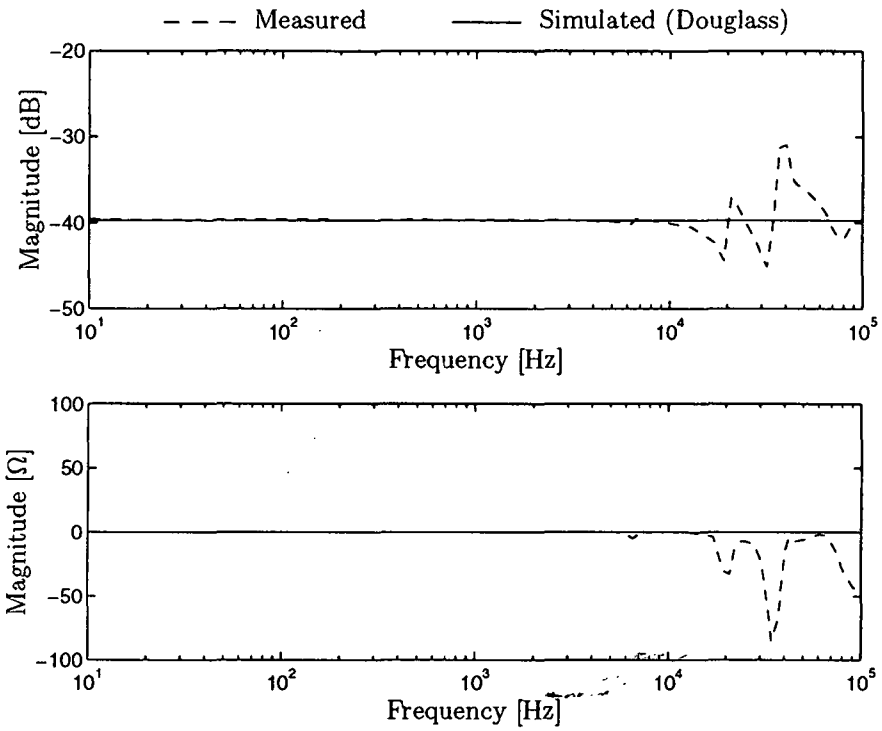

Figure 6.20: Measured and simulated HV–LV voltage transformation ratio frequency response, $\mathbf{H}_{HL}(j\omega)$.

Chapter 7

Model Validation and Application

With the parameters estimated in chapter 6, the proposed lumped-parameter equivalent-circuit transformer model is able to predict the open-circuit and short-circuit frequency responses of the 16 kVA experimental transformer. This chapter aims to further validate the transformer model by demonstrating its ability to predict the frequency-response characteristics of the transformer under loaded conditions and by applying the model for time-domain simulations.

Application of the transformer model, and the associated parameter estimation process, to an 11 kV / 110 V voltage transformer is also presented. The core of this transformer was accessible, which made it possible to measure the 'core-voltage' response (i.e. the frequency response of the voltage induced in a search-coil tightly wound on the transformer core). The core-voltage provides additional frequency responses which can be used to validate the transformer model, especially with respect to the physical significance of the model elements.

7.1 16 kVA, 22 kV / 240 V Distribution Transformer

7.1.1 Frequency-domain Simulations

The frequency response of transformers under loaded conditions is often of interest, particularly in the case where voltage transformers are to be used for voltage harmonic

measurements [17, 28]. The voltage transformation ratio frequency response is a function of the transformer load [17, 14], and the availability of a good transformer model would make it possible to compensate wideband measurements made via the transformer, provided that the load-impedance characteristics are known.

An 11 Ω resistive load was connected to the LV side of the 16 kVA transformer, and the HV–LV voltage transformation ratio frequency response, $\mathbf{H}_{HL}(j\omega)$, was measured using stepped-frequency excitation. The 11 Ω load represents $\frac{1}{3}$ of the transformer full-load rating. The equivalent-circuit transformer model, using the parameters obtained in section 6.4, was used to predict the HV–LV voltage transformation ratio frequency response. Frequency-dependence of the model parameters was not included. The results are presented in figure 7.1 and it can be seen that the measured and simulated results agree well up to 50 kHz. It can thus be concluded that the transformer model can be applied with the transformer under loaded conditions. This result serves as a cross-validation for the transformer model, i.e. validating the model with a response that was not used in the parameter estimation process [74].

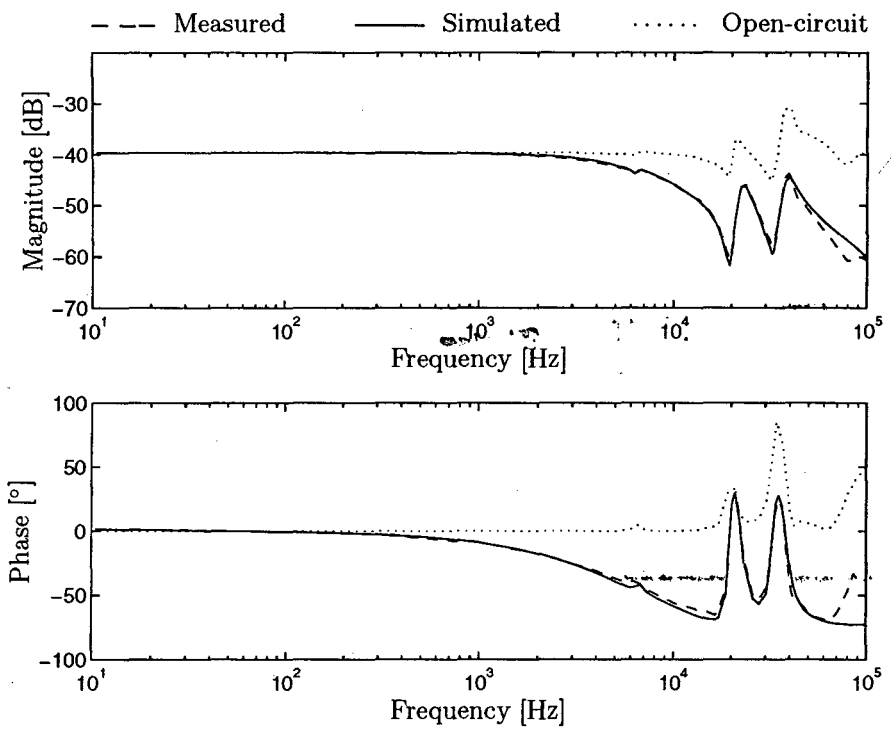

Figure 7.1: Measured and simulated 16 kVA Transformer HV–LV voltage transformation ratio with an 11 Ω resistive load connected to the LV terminals.

7.1.2 Time-domain Simulations

Two estimation steps are performed before the parameters of the transformer equivalent-circuit model is obtained. Firstly, a non-parametric estimation process is applied to the 'raw' frequency-response data to obtain a smoothed version of the transformer frequency responses. The second step is the determination of the model parameters from the smoothed frequency-response data, as described in chapter 6. These steps could lead to errors in the eventual parameter estimates, due to bias introduced by each estimation procedure. However, if it can be shown that the transformer model is able to adequately predict the time-domain response to an unprocessed input signal, it can be concluded that the errors made in the estimation process are within acceptable limits. This section investigates the time-domain response of the transformer model to a number of input signals, to demonstrate the validity of the transformer model and the accuracy of the parameter estimation process.

The time-domain response simulations were carried out by formulating state-space representations of the transformer model and then calculating the model response to a measured input signal, using the `lsim` function provided by the MATLAB Control System Toolbox [108]. The state-equations used in these simulations are given in appendix B. Problems can be expected during time-domain simulations due to the poor condition of the inductance matrix, $\boldsymbol{L}$. The core-loss resistor is included in the equivalent-circuit model by connecting it across a separate inductor, L_c, which is tightly coupled to the winding self-inductances. As a result, $\boldsymbol{L}$ is almost singular. This did not present a problem during the frequency-response simulations, but leads to accumulating numerical errors in the time-domain simulations [36]. The problem can be overcome by applying a solution algorithm that is stable under such conditions [99]. However, the problem can also be solved by improving the condition of $\boldsymbol{L}$ by slightly increasing the value of L_c without adjusting any other elements of $\boldsymbol{L}$. Good results, with no appreciable loss in accuracy, were obtained by increasing L_c from 37.5 H to 38.5 H.

The non-linear behaviour of the inductive and resistive transformer equivalent-circuit elements can not be included in a model intended for time-domain simulations without significantly complicating the model structure (see section 2.1.3). No non-linear effects have thus been included in the model that was used to obtain the time-domain responses discussed below. As discussed in chapter 3, the non-linearities mainly affect the transformer responses in the frequency range below 1 kHz. Thus, the input signals have been chosen in such a way that the transformer will be excited predominantly in the high-

frequency range, i.e. between 1 kHz and 100 kHz, thus limiting errors that will arise from not including non-linearities in the transformer model.

Three sets of time-domain response simulation results for the 16 kVA experimental transformer will be presented here:

(a) The LV terminal voltage response to a PRBS input current applied to the LV terminals, with the HV terminals open-circuit, is shown in figure 7.2. The PRBS input current was generated with $f_c = 200$ kHz and $N = 15$, and is shown in the upper trace of figure 7.2. Note that the complete PRBS signal is not shown for clarity. The lower plot in figure 7.2 compares the calculated time-domain response to the measured response for the same input signal. Figure 7.3 presents an expanded view of the first 200 μs of the simulated and measured signals.

(b) The HV terminal voltage response to a PRBS current applied to the LV terminals, with the HV terminals open-circuit, is shown in figure 7.4. The PRBS input current is shown in the upper trace of figure 7.4 (the PRBS signal parameters are $f_c = 200$ kHz and $N = 15$). The simulated and measured HV voltage responses are compared in the bottom section of figure 7.4. An expanded view of the simulated and measured results is given in figure 7.5.

(c) In many practical applications, the response of transformers to impulse excitation signals is of importance [2, 1]. Figure 7.6 shows the measured and simulated HV terminal voltage response to an impulse voltage applied to the LV terminals. The upper trace of figure 7.6 shows the input voltage, while the measured and simulated responses to the input signal are given in the lower plot.

From the above results it can be seen that the lumped-parameter equivalent-circuit transformer model can be used to obtain accurate time-domain terminal response simulations, with good agreement between the simulated responses and the measured responses to the same input signal. These results confirm the accuracy of the model parameter estimation procedure, as the measured input signals and the measured responses were not subjected to the signal processing steps applied to obtain the transformer frequency responses.

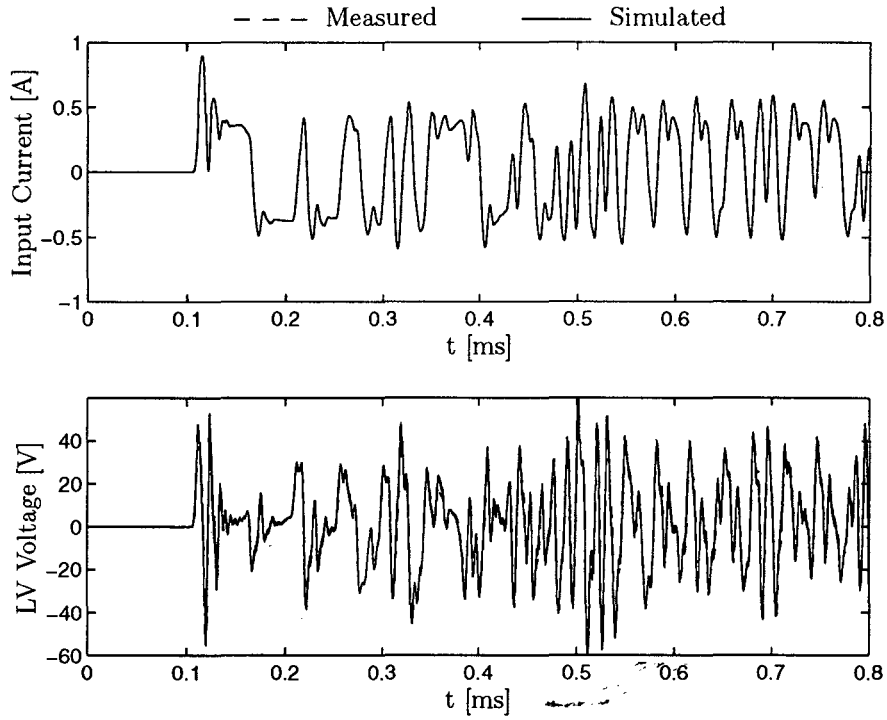

Figure 7.2: Measured and simulated LV terminal response to a PRBS input current.

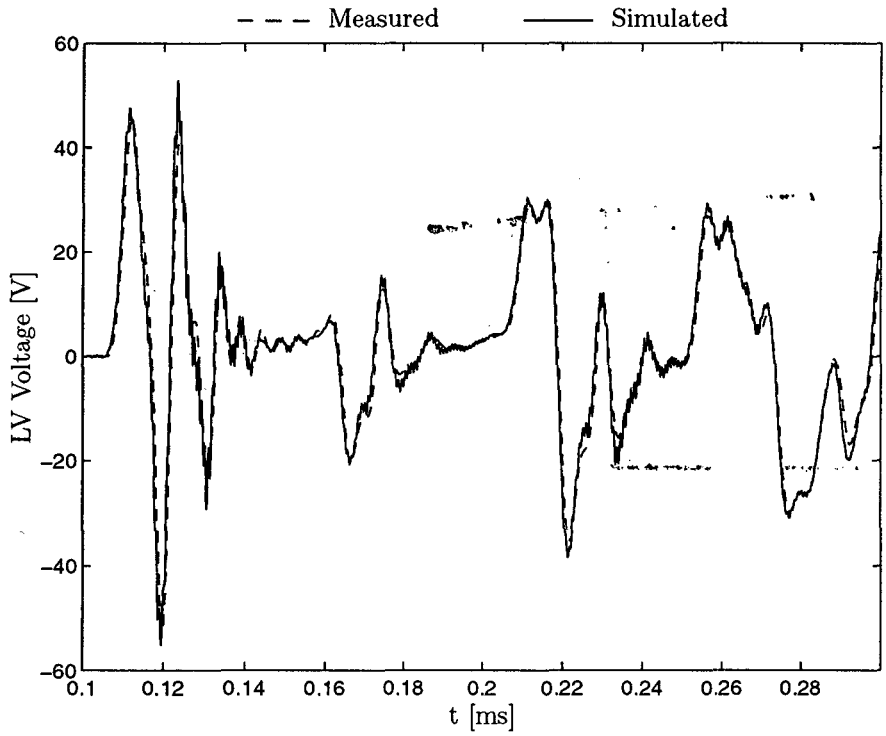

Figure 7.3: Measured and simulated LV terminal response to a PRBS input current. This figure gives an expanded view of the first part of the response shown in figure 7.2.

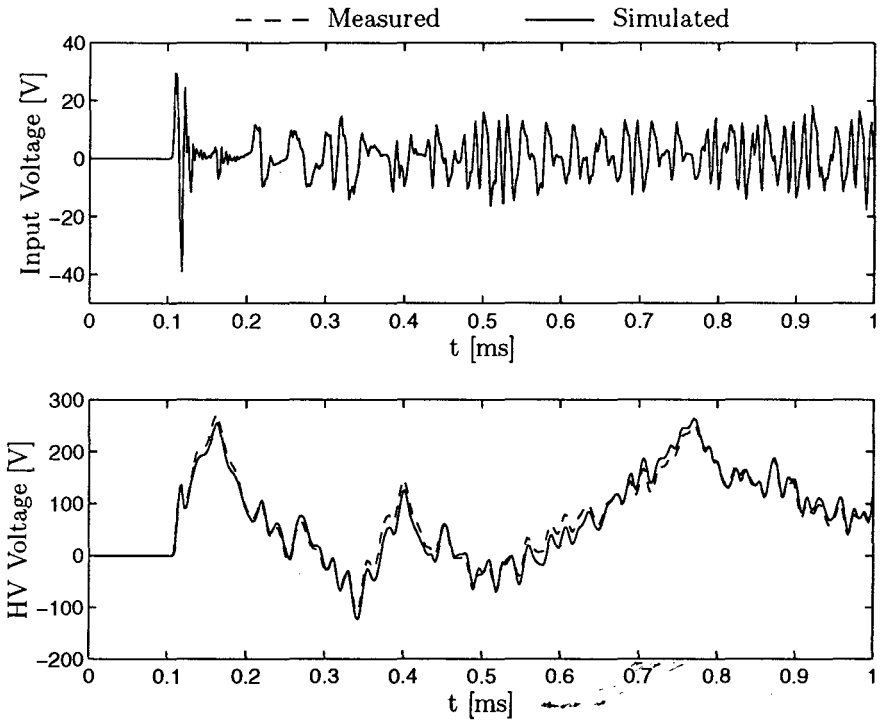

Figure 7.4: Measured and simulated HV terminal response to a PRBS input voltage at the LV terminals.

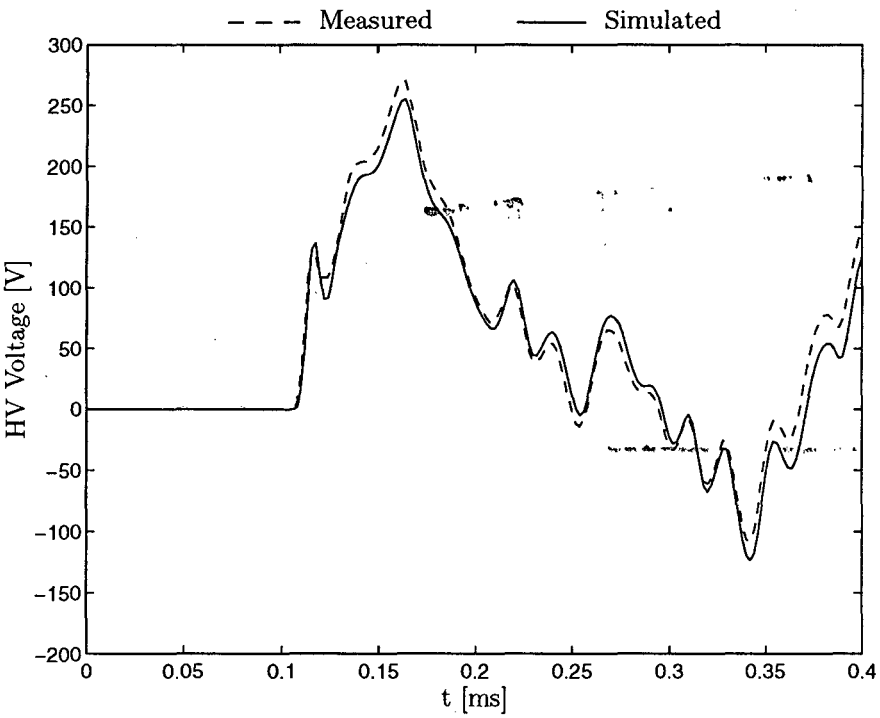

Figure 7.5: Measured and simulated HV terminal response to a PRBS input voltage at the LV terminals. This figure gives an expanded view of the first 400 μs of figure 7.4

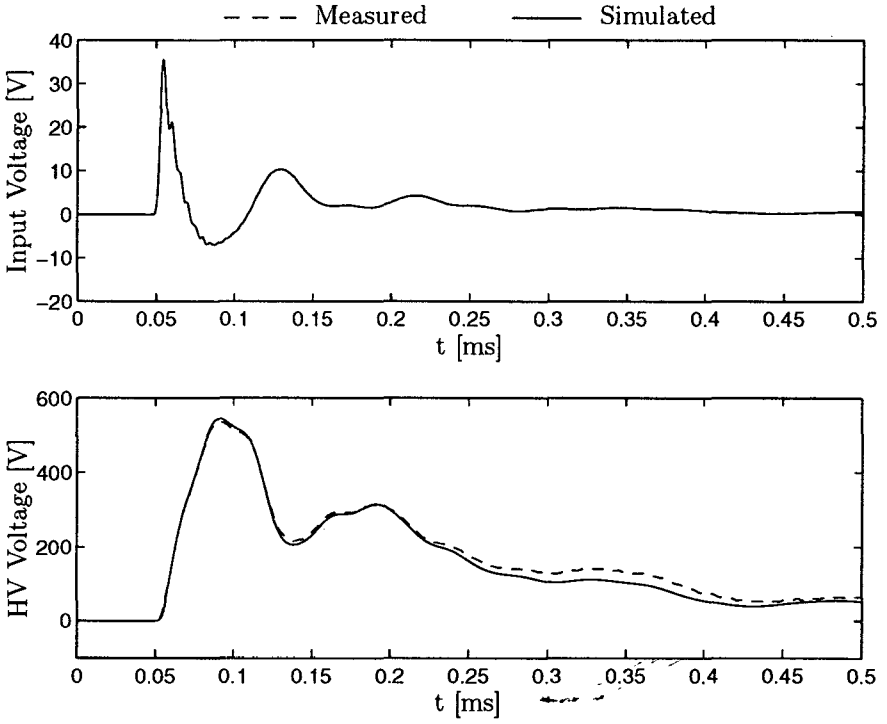

Figure 7.6: Measured and simulated HV terminal response to an impulse input voltage at the LV terminals.

7.1.3 EMTP Implementation

The time-domain transformer response simulations discussed in section 7.1.2 require that a state-space representation of the transformer model is available. However, in most cases it is more convenient to implement the transformer model using a transient simulation program such as the EMTP [36], especially when the model is to form part of a larger system simulation. The lumped-parameter equivalent-circuit structure of the transformer model makes its inclusion in such programs a reasonably simple matter, provided that multiple coupled branches are supported by the software in question.

The simulation results discussed in this section were obtained with the ATP version of the EMTP [109]. The winding self-inductances are represented by a system of mutually coupled branches which also include the winding resistances. The capacitances are included as linear RLC-branches of which only the capacitive component is used. The elements of the inductance matrix, $\boldsymbol{L}$, have to be entered with a high accuracy to ensure that the simulation results will be accurate (a minimum of 5 to 6 significant digits is recommended [36]). As discussed in section 7.1.2, the value of L_c has to be increased slightly to avoid accuracy or numerical instability problems due to ill-conditioning of the

inductance matrix. The full ATP data file for the 16 kVA transformer model is given in appendix C.

ATP can be used to perform both time-domain and frequency-domain simulations. Frequency-domain simulation is available via the `FREQUENCY SCAN` option of ATP and was used to verify that the transformer model data was entered correctly in the ATP data file. The open-circuit LV input impedance and the LV–HV voltage transformation ratio frequency responses, calculated by ATP, are shown in figures 7.7 and 7.8. These results show that the ATP frequency-domain simulation yields correct results for both responses. Below 1 kHz the frequency response prediction for the LV open-circuit input impedance (figure 7.7) is not correct, as the non-linearity of the winding self-inductances and the winding resistances can not easily be included in the ATP model.

ATP was used to calculate the LV terminal voltage response to a PRBS input current at the LV terminals. The current input signal, used to obtain the results shown in figure 7.2, was also used as input signal to the ATP simulation (see appendix C). The measured and simulated time-domain responses are shown in figure 7.9 and it can be seen that a very good simulation of the LV voltage is obtained from ATP.

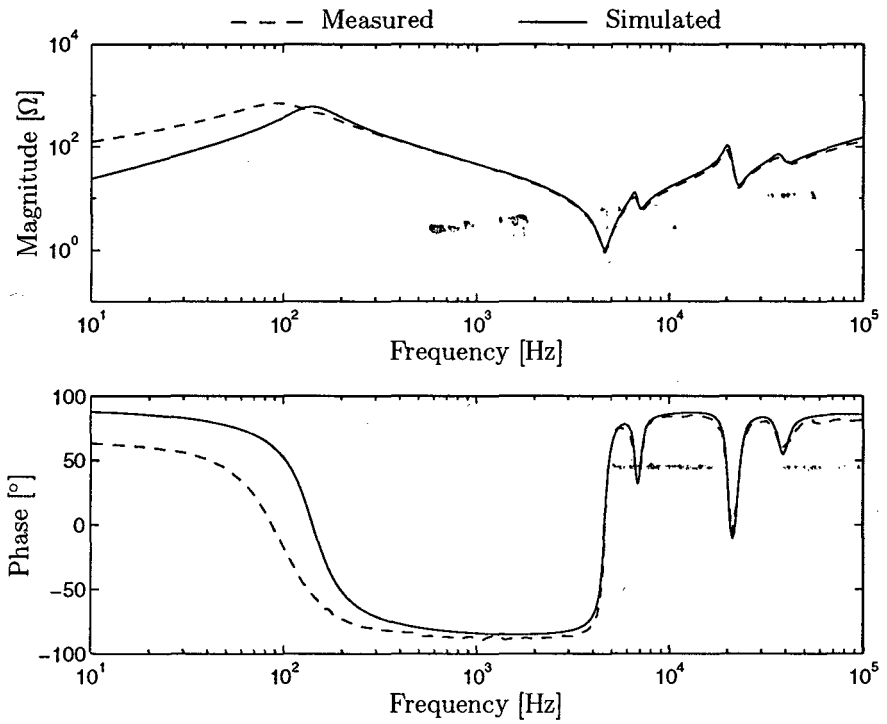

Figure 7.7: LV open-circuit input impedance frequency response, $Z_{Loc}(j\omega)$. The simulated result was calculated by ATP.

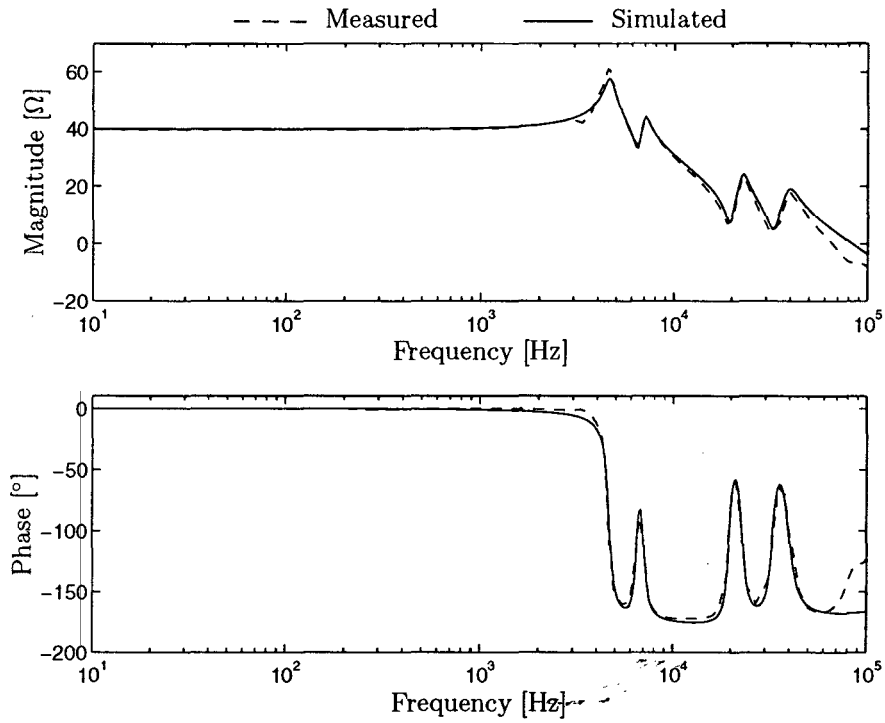

Figure 7.8: LV to HV voltage transformation ratio frequency response, $H_{LH}(j\omega)$. The simulated result was calculated by ATP.

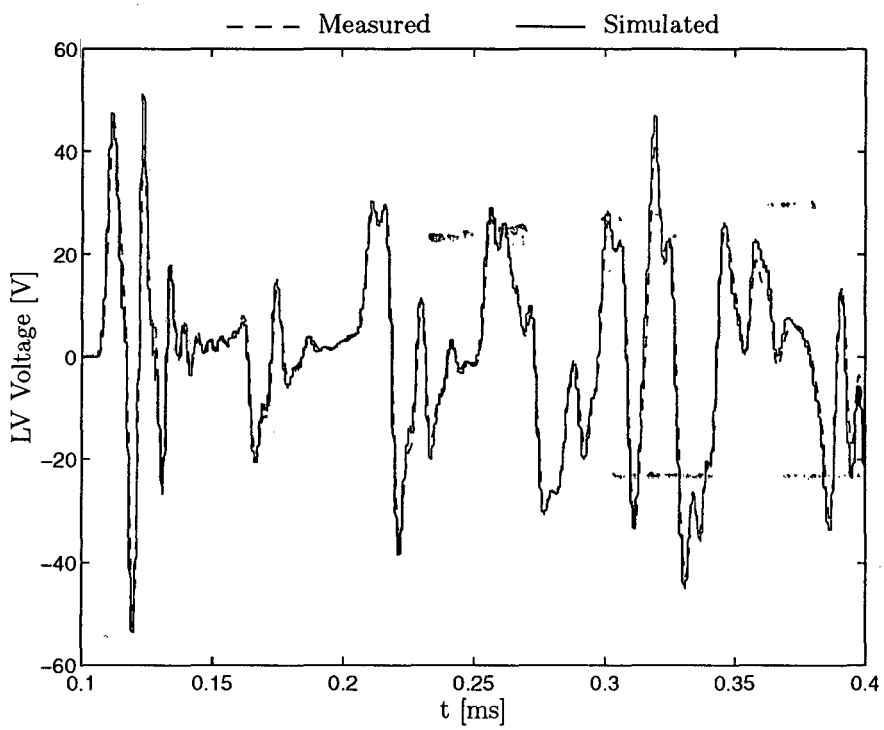

Figure 7.9: LV terminal response to the PRBS input current shown in figure 7.2. The simulated result was calculated by ATP.

7.2 11 kV / 110 V Voltage Transformer

In the previous sections, the development, parameter estimation and validation of the transformer model was carried out with particular reference to the 22 kV / 240 V, 16 kVA experimental transformer. This section aims to demonstrate that the identification procedure can successfully be applied to another two-winding transformer. For this purpose an 11 kV / 110 V voltage transformer was selected. The core of this transformer was accessible, which made it possible to place a number of test turns around the core to measure the frequency response of the core-voltage. The core-voltage is given by:

$$v_e = N_c \frac{d\phi_c}{dt}, \tag{7.1}$$

where N_c represents the number of test turns and ϕ_c is the core flux. This represents a further response signal which can be used to validate the transformer model, as the trend of v_e should correspond to the voltage induced in the coupling inductance, L_c, if the model correctly simulates the transformer.

The high-frequency response of the voltage transformer is complex and at least four major series-parallel resonance pairs can be identified in the frequency range between 1 kHz and 100 kHz. According to the arguments presented in section 4.2, five sections would be required to accurately represent the HV winding. If five HV winding sections are used, the transformer model would be represented by more than 40 parameters, which complicates the parameter estimation process considerably. It was however found that acceptable simulation of the transformer frequency responses can be obtained by applying a model with three or four HV winding sections. Results for both the three and four HV winding section models will be presented.

7.2.1 Three-section HV Winding Model

An equivalent-circuit model with three HV winding sections and a single LV winding section was developed for the 11 kV / 110 V voltage transformer. The model structure is similar to the structure defined for the 16 kVA experimental transformer, with the exception that the HV winding is divided into only three sections. The voltage transformer windings are wound on an E-core, with the HV winding wound over the LV winding on the middle leg of the core. The HV winding thus consists of a single coil, leading to the

lumped inter-layer capacitances C_{b12} and C_{b23} as shown in figure 7.10.

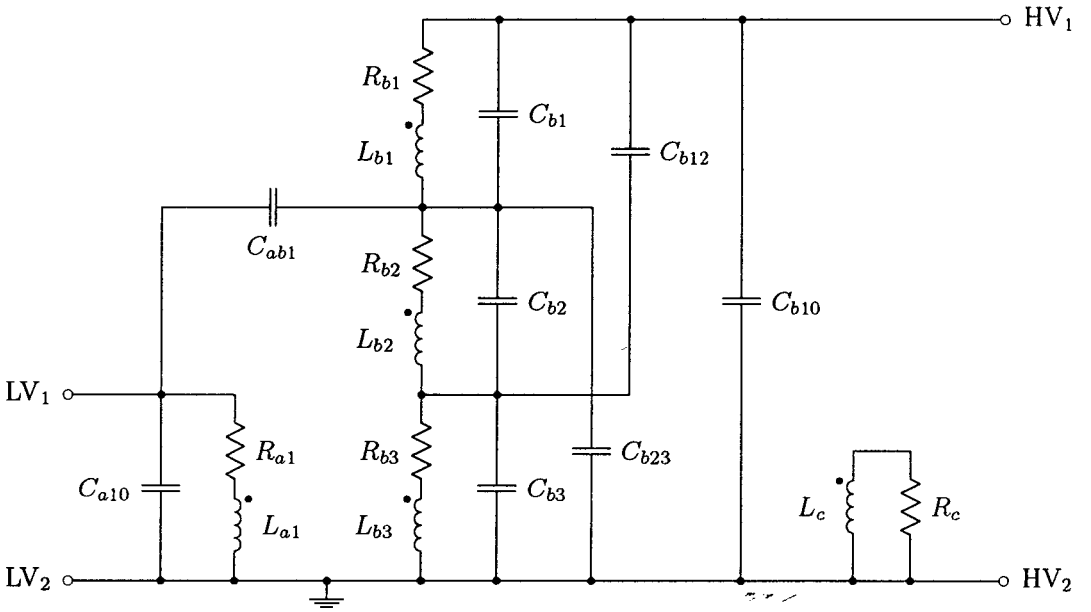

Figure 7.10: Lumped-parameter equivalent-circuit voltage transformer model, using three HV winding sections.

The frequency responses, $\mathfrak{G}_{\mathbf{T}}$, of the 11 kV / 110 V voltage transformer were measured in the frequency range between 100 Hz and 100 kHz by applying PRBS excitation signals. In addition to $\check{\mathfrak{G}}_{\mathbf{T}}$, two responses involving the core-voltage were also measured:

(a) During the measurement of the LV open-circuit input impedance, the response of the search-coil voltage, $\mathbf{V}_{co}$ was also recorded. Defining a transfer-function in terms of the core-voltage and the LV terminal voltage ($\mathbf{V}_{LV}$) as:

$$\mathbf{H}_{Lco}(j\omega) = \frac{\mathbf{V}_{co}(j\omega)}{\mathbf{V}_{LV}(j\omega)}, \tag{7.2}$$

yields a frequency response that can be used to test the validity of the transformer model.

(b) The core-voltage was also measured with the HV winding terminals short-circuited, from which a short-circuit core-voltage frequency response can be defined as:

$$\mathbf{H}_{Lcs}(j\omega) = \frac{\mathbf{V}_{cs}(j\omega)}{\mathbf{V}_{LV}(j\omega)}, \tag{7.3}$$

where $\mathbf{V}_{cs}$ is the search-coil response voltage and $\mathbf{V}_{LV}$ is the LV terminal excitation voltage.

The voltage transformer model parameters were estimated from $\check{\mathfrak{I}}_{\mathbf{T}}$ by applying the parameter estimation procedure discussed in chapters 5 and 6. The resulting parameters are shown in table 7.1. Note that the core-voltage frequency responses, $\mathbf{H}_{Lco}(j\omega)$ and $\mathbf{H}_{Lcs}(j\omega)$ were not used in the parameter estimation process.

Table 7.1: Parameter estimates for the voltage transformer model structure of figure 7.10.

Parameter	Value	Parameter	Value	Parameter	Value
C_{a10} [nF]	0.048	R_{a1} [Ω]	2.58	k_{a1b1}	0.997605
C_{b10} [nF]	0.038	R_{b1} [kΩ]	5.30	k_{a1b2}	0.998107
C_{b12} [nF]	0.081	R_{b2} [kΩ]	5.28	k_{a1b3}	0.998433
C_{b23} [nF]	0.086	R_{b3} [kΩ]	5.00	k_{b12}	0.999145
C_{b1} [nF]	0.150	R_c [kΩ]	59.9	k_{b13}	0.997804
C_{b2} [nF]	0.156	L_{a1} [H]	0.621	k_{b23}	0.998852
C_{b3} [nF]	0.158	L_{b1} [kH]	1.14		
C_{ab1} [pF]	10	L_{b2} [kH]	0.772		
		L_{b3} [kH]	0.264		

The measured and simulated LV open-circuit input impedance frequency responses are shown in figure 7.11 and the corresponding core-voltage responses are given in figure 7.12. The LV short-circuit frequency responses are presented in figures 7.13 and 7.14. (The remaining voltage transformer frequency responses are included in appendix D.) Note that the measured and simulated core-voltage response magnitudes have been normalized to their respective values at 10 Hz to allow comparison of the results. As expected, the three-section HV winding model predicts two series-parallel resonance pairs beyond the first series resonance in $\mathbf{Z}_{Loc}(j\omega)$. From the responses of $\mathbf{Z}_{Loc}$ and $\mathbf{Z}_{Lsc}$ it can be seen that the model predicts a slightly under-damped first resonance pair, while the second pair approximates the response at a point where two closely-spaced resonances are clearly visible from the measured responses. A reasonably good approximation of the measured responses is nevertheless obtained for the high-frequency range. Poor results are obtained below 1 kHz as no frequency-dependence has been taken into account. The predicted core-voltage responses follow the general trend of the measured responses, but it is clear that several winding resonances are not accounted for by the model. However, the correlation between the measured and simulated core-voltage responses does suggest that the model is a good approximation of the physical behaviour of the transformer, but is limited by the number of sections used to represent the HV winding.

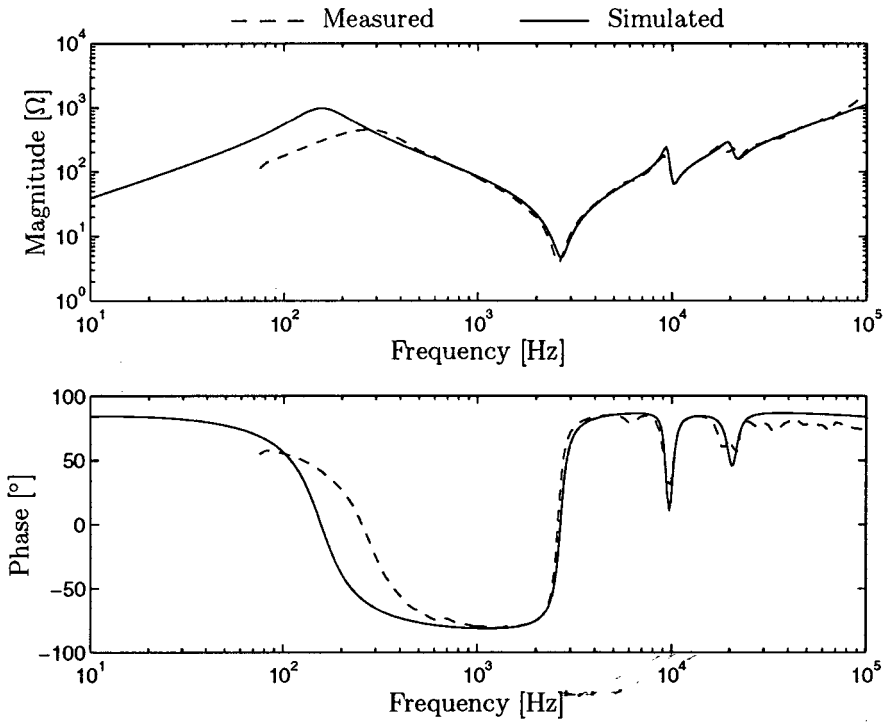

Figure 7.11: Voltage transformer LV open-circuit input impedance frequency response, $\mathbf{Z}_{Loc}(j\omega)$ (Three HV winding sections).

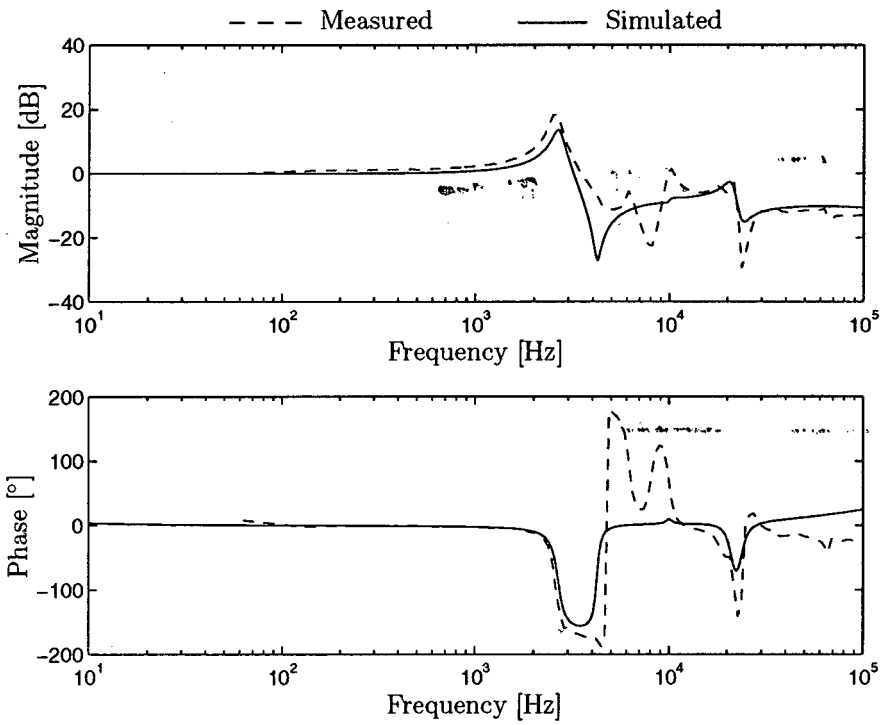

Figure 7.12: Voltage transformer open-circuit core-voltage frequency response, $\mathbf{H}_{Lco}(j\omega)$ (Three HV winding sections).

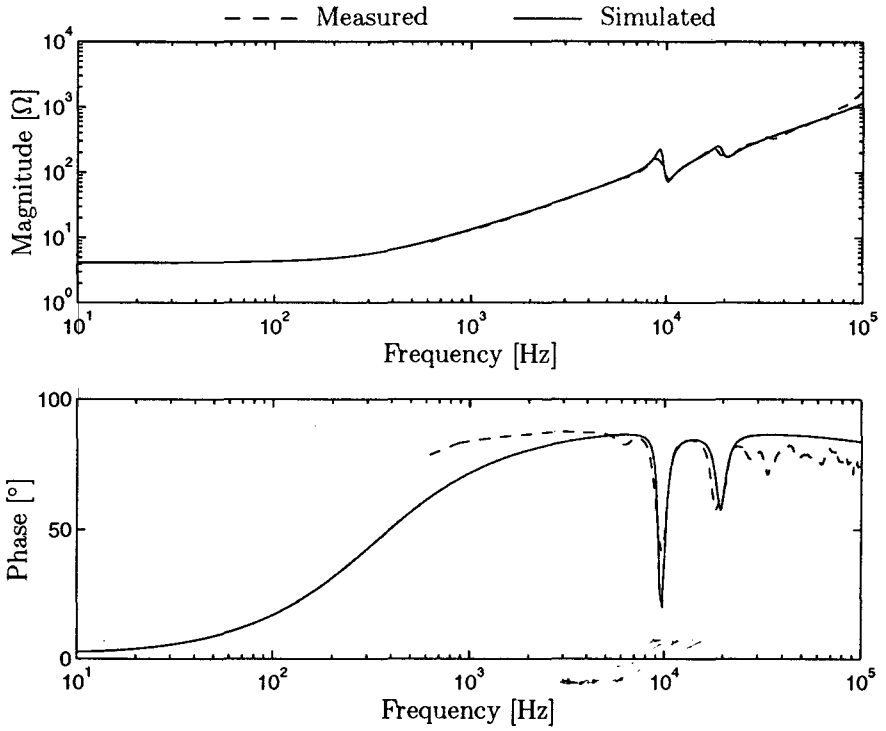

Figure 7.13: Voltage transformer LV short-circuit input impedance frequency response, $\mathbf{Z}_{Lsc}(j\omega)$ (Three-section HV winding model).

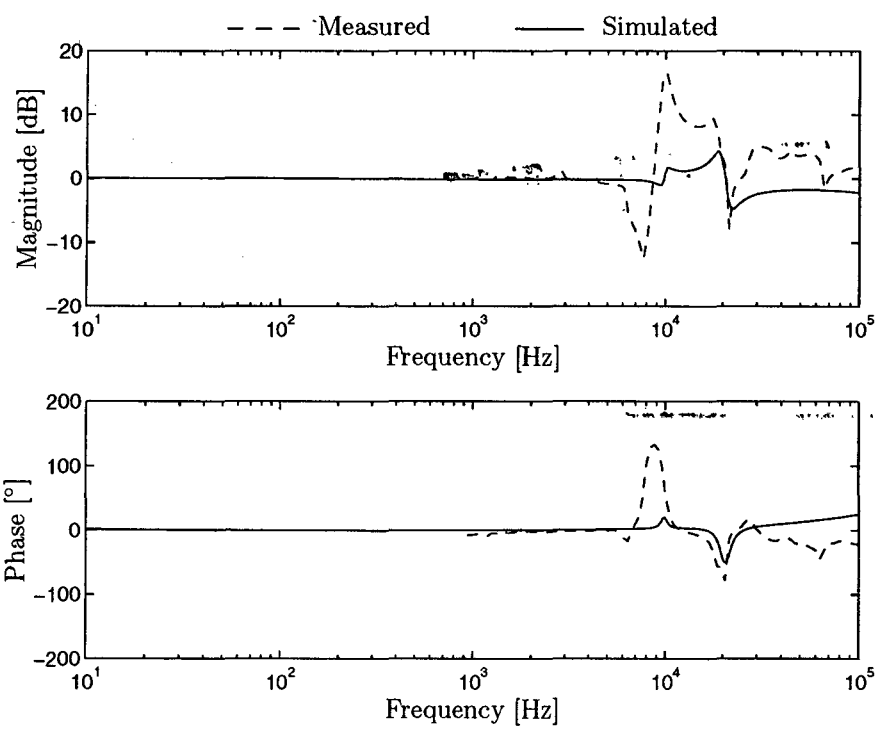

Figure 7.14: Voltage transformer short-circuit core-voltage frequency response, $\mathbf{H}_{Lcs}(j\omega)$ (Three HV winding sections).

7.2.2 Four-section HV Winding Model

From the results discussed in section 7.2.1, in which a transformer model with three HV winding sections was used to predict the voltage transformer frequency responses, it was concluded that more HV winding sections are required to improve the simulated core-voltage frequency-response results. The aim of this section is to show that the predicted core-voltage frequency responses are improved by increasing the number of HV winding sections in the transformer model to four.

The equivalent-circuit model structure (with four HV winding sections) for the 11 kV / 110 V voltage transformer is shown in figure 7.15. This model structure is essentially identical to the structure of the model of the 16 kVA transformer (figure 4.7). As the HV winding consists of a single coil, a further lumped inter-layer capacitance, C_{b23}, has been added. Following the same reasoning, capacitances C_{b13} and C_{b24} were also added. However, very low values were estimated for C_{b13} and C_{b24}, indicating that these capacitances are not required in the model structure. C_{b13} and C_{b24} were subsequently omitted from the model. The location of the inter-winding capacitance, C_{ab1}, was chosen to approximate its physical location with respect to the transformer windings. Estimation of the model parameters was carried out with the frequency response measurements used to obtain the results of section 7.2.1, yielding the parameter estimates shown in table 7.2.

Table 7.2: Parameter estimates for the voltage transformer model structure of figure 7.15.

Parameter	Value	Parameter	Value	Parameter	Value
C_{a10} [nF]	0.017	R_{a1} [Ω]	2.10	k_{a1b1}	0.998516
C_{b10} [nF]	0.034	R_{b1} [kΩ]	2.67	k_{a1b2}	0.997795
C_{b12} [nF]	0.048	R_{b2} [kΩ]	4.95	k_{a1b3}	0.997702
C_{b23} [nF]	0.080	R_{b3} [kΩ]	4.32	k_{a1b4}	0.998202
C_{b34} [nF]	0.084	R_{b4} [kΩ]	3.58	k_{b12}	0.998686
C_{b1} [nF]	0.352	R_c [kΩ]	79.7	k_{b13}	0.999092
C_{b2} [nF]	0.209	L_{a1} [H]	0.690	k_{b14}	0.999131
C_{b3} [nF]	0.434	L_{b1} [kH]	0.822	k_{b23}	0.998974
C_{b4} [nF]	0.201	L_{b2} [kH]	0.203	k_{b24}	0.997777
C_{ab1} [pF]	5	L_{b3} [kH]	0.494	k_{b34}	0.998823
		L_{b4} [kH]	0.281		

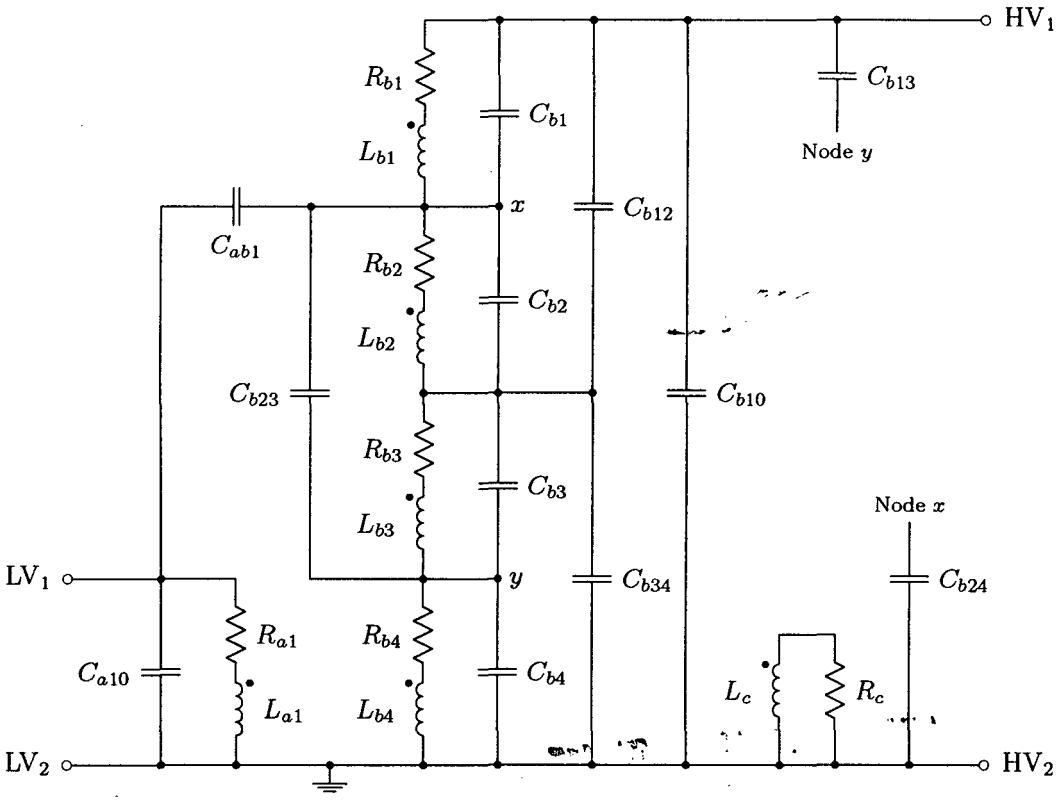

Figure 7.15: Lumped-parameter equivalent-circuit model of the 11 kV / 110 V voltage transformer, using four HV winding sections. Note that C_{b13} and C_{b24} were omitted to form the final model.

The measured and simulated LV open-circuit and short-circuit input-impedance frequency responses are shown in figures 7.16 and 7.18 respectively. The remaining voltage transformer frequency responses are included in appendix D. The simulated frequency responses of $\mathbf{Z}_{Loc}$ and $\mathbf{Z}_{Lsc}$ show only a slight improvement over the results shown in figures 7.11 and 7.13. Apparently, only two high-frequency parallel-series resonance pairs are represented, even though four HV winding sections are employed by the transformer model. This is due to the fact that two sections have been combined to predict the resonance-pair at 10 kHz. The damping of this resonance is predicted accurately by the model, which was not the case when only three HV winding sections were used (cf. figures 7.11 and 7.13). It is possible to adjust the model parameters in such a way that three distinct high-frequency resonance-pairs are represented in $\mathbf{Z}_{Loc}(j\omega)$ and $\mathbf{Z}_{Lsc}(j\omega)$. However, this leads to incorrect prediction of the voltage transformation ratio frequency responses (see section 6.6).

The effect of introducing an additional HV winding section is clear when considering the core-voltage frequency responses, which are given in figures 7.17 and 7.19. With four HV winding sections, the predicted core-voltage responses follow the trend of the measured responses much more closely than was the case when only three HV winding sections were used. From the phase response of $\mathbf{Z}_{Loc}(j\omega)$ it can be seen that several winding resonances exist that are not predicted by the model, notably those at the points indicated by A and B in figure 7.16. These resonances occur at the frequencies where the simulated core-voltage deviates the most from the measured core-voltage response. It can thus be concluded that the correlation between the core-voltage response predicted by the model and the measured core-voltage response will improve as the number of HV winding sections used in the model increases, i.e. as the number of predicted resonances increases. This result also shows that the transformer model provides a good approximation of the electromagnetic behaviour of the transformer and that the 'core-voltage' frequency responses provide an excellent means to validate a transformer model.

While a further increase in the number of sections used to model the HV winding is likely to improve the accuracy of the core-voltage response predictions, this was not attempted for practical reasons. More computing time is required to evaluate the model frequency responses during the estimation procedure, as the complexity of the mathematical description of the model increases with order. Further, a higher number of iterations is required before the estimation procedure converges to a feasible set of parameter estimates, due to the higher number of parameters.

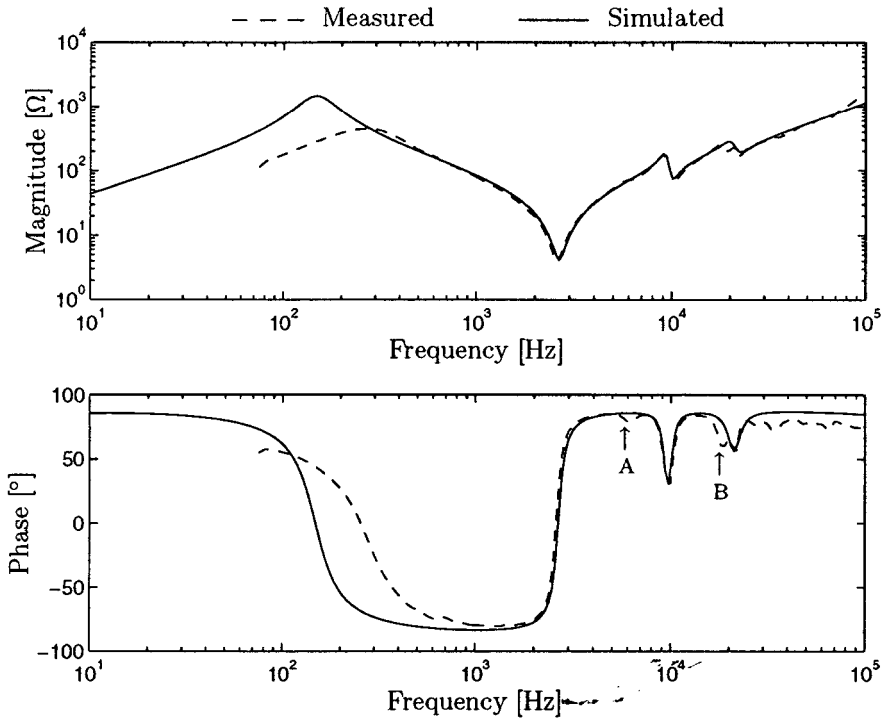

Figure 7.16: Voltage transformer LV open-circuit input impedance frequency response (Four HV winding sections).

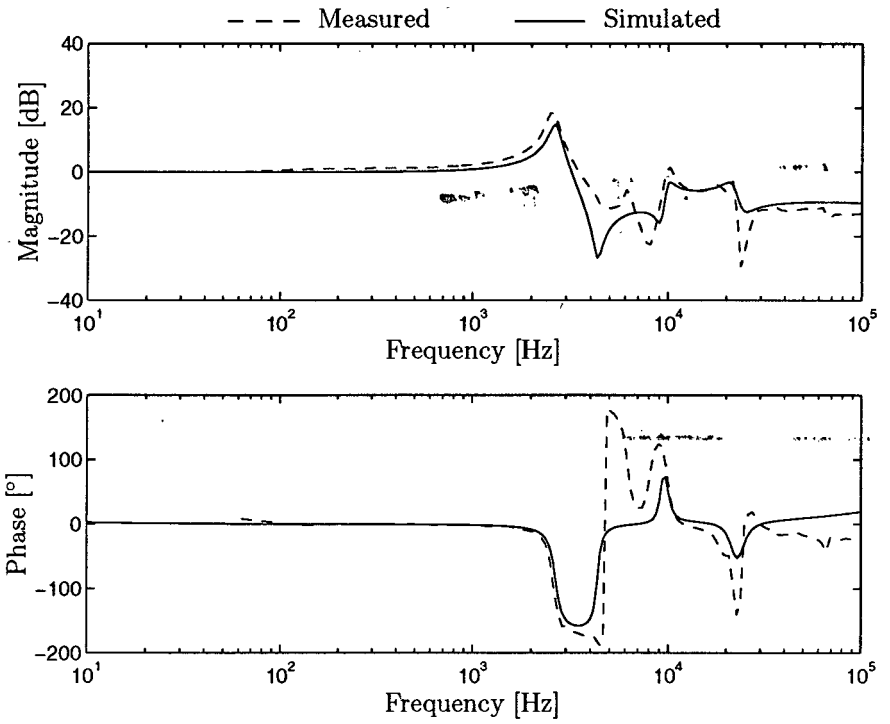

Figure 7.17: Voltage transformer open-circuit core-voltage frequency response, H_{Lco} (Four HV winding sections).

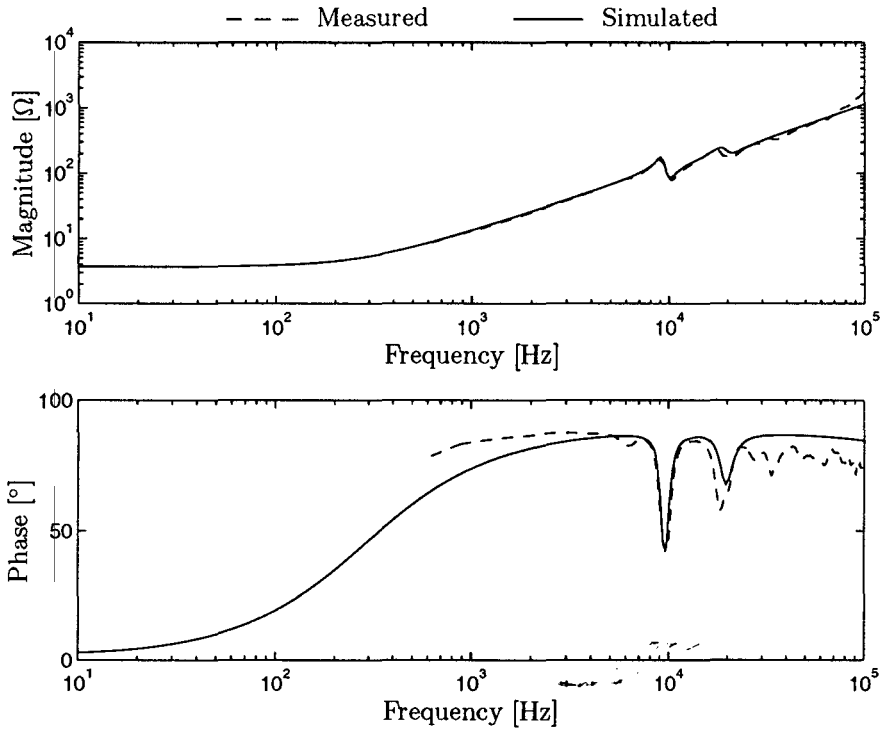

Figure 7.18: Voltage transformer LV short-circuit input impedance frequency response (Four HV winding sections).

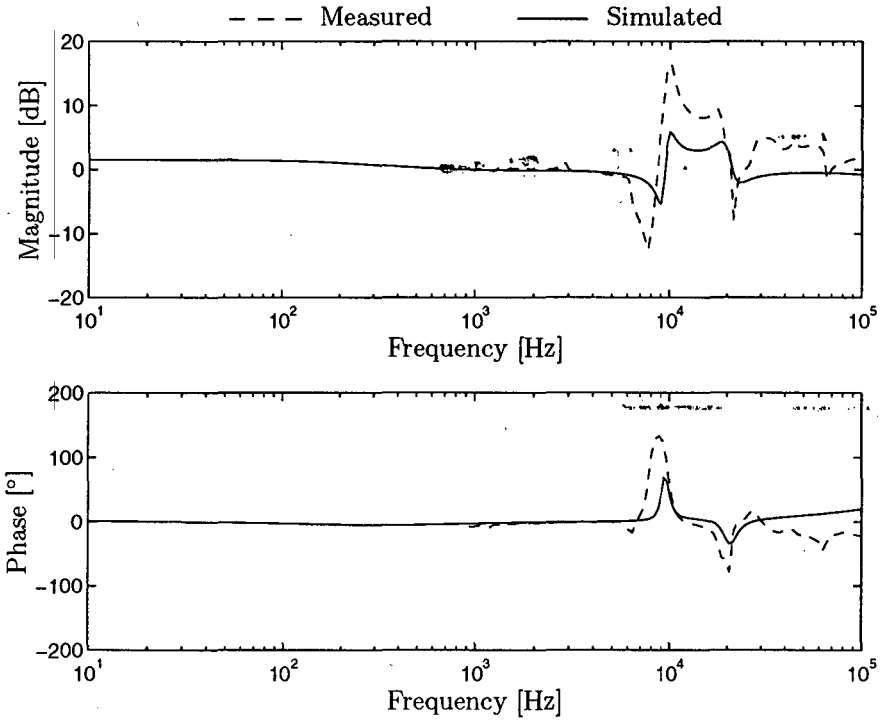

Figure 7.19: Voltage transformer short-circuit core-voltage frequency response, H_{Lcs} (Four HV winding sections).

Chapter 8

Conclusions and Recommendations

The findings of this research project and the key conclusions that were drawn from the results of the experimental and theoretical work, are reviewed in this chapter. Finally, suggestions for further research are discussed.

8.1 Transformer Modelling

An extensive literature survey was conducted to determine whether transformer model structures exist that meet the requirements originally defined in chapter 1 of this dissertation. It was found that:

(a) The order of existing lumped-parameter equivalent-circuit transformer model structures, that are suitable for parameter estimation applications, are too low to make the prediction of the 'minor' winding resonances possible.

(b) A variety of transformer model structures, which have an order that is high enough to predict the 'minor' winding resonances, have been described. However, these model structures are complex and have a high number of parameters, which makes them unsuitable for the application of parameter estimation techniques.

A new wideband, lumped-parameter equivalent-circuit transformer model structure was subsequently proposed to overcome these problems. The development of this model structure was based on physical principles and on the characteristics of measured transformer

frequency responses. The model structure was validated by applying it to simulate a 16 kVA, 22 kV / 240 V single-phase distribution transformer and a 11 kV / 110 V voltage transformer, leading to the following findings:

(a) *Frequency-domain response prediction.* The proposed transformer model provided very accurate predictions of the frequency responses of the two test transformers in the frequency range between 10 Hz and 100 kHz, including prediction of the 'minor' winding resonances. The number of 'minor' resonances that can be represented by the proposed model structure is only limited by the number of sections that are used to represent each of the transformer windings. The model was successfully applied to the simulation of open-circuit and short-circuit frequency responses. It was also shown that the model can be applied to predict the frequency-response characteristics of a loaded transformer.

(b) *Time-domain response prediction.* The proposed transformer model produced excellent results when applied to time-domain simulations in a linear form. For time-domain simulations the non-linear effects of the transformer were ignored. Thus, good results can not be expected if the excitation and response signals contain significant low-frequency components (typically below 1 kHz).

(c) *Representation of non-linear effects.* The proposed transformer model is primarily intended for, but not limited to, frequency-domain application. For this reason, detailed representation of the transformer non-linearities was not desirable, as this would increase the number of model parameters and thus complicate the parameter estimation procedure. It was, however, found that the frequency-dependence of the inductive and resistive elements could be approximated by applying the empirical functions proposed by Funk and Hantel [95] and Bak-Jensen [15]. These functions describe the frequency-dependence of each of the inductive and resistive model elements in terms of two constants. It was found the same constants could be applied to describe the frequency-dependence of a group of model elements, e.g. only two constants are required to model the frequency-dependence of all the winding resistances. Thus the inclusion of frequency-dependent effects in the transformer model did not result in a large increase in the total number of model parameters. The disadvantage of this approach is that the transformer non-linearities are not represented in the time domain, so that the proposed model can only be applied to time-domain simulations in its linear form.

(d) *'Core-voltage' prediction.* The ability of a transformer model to accurately represent the core flux was identified as an excellent means to assess the physical significance

of a transformer model structure. It was found that the proposed transformer model structure provides a good representation of the core flux. This was shown by comparing the voltage induced in a search coil wound on the core of an 11 kV / 110 V voltage transformer, to a simulation of the voltage across the core-loss resistor of the transformer model. Good correlation between the measured and simulated core-voltage responses was obtained under open-circuit and short-circuit conditions. It can thus be concluded that the equivalent-circuit elements of the proposed transformer model structure have a very high degree of physical significance.

8.2 Transformer Frequency Response Measurement

In order to meet the project objectives, a suitable technique to measure the frequency response characteristics of a practical power transformer had to be developed. The measured transformer frequency responses provided information which could be applied during the model development process and were also used as input data to the parameter estimation procedure.

(a) *Excitation signal.* Several excitation signals were considered for application to the transformer frequency response measurements. It was found that stepped-frequency excitation yielded very good, virtually noise-free results, but that a large amount of time is required to complete a single frequency response measurement. The method is also limited by the restricted bandwidth of the signal amplifier and step-up transformer, if these are used. Impulse excitation provides good response measurements at high frequencies (typically above 1 kHz), but at low frequencies, the signal-to-noise ratio of the response signal is too low to provide meaningful results. PRBS excitation signals yielded excellent results across the 10 Hz to 100 kHz frequency range. PRBS signals can be generated at high voltage- or current levels and contain signal energy over a wide bandwidth, which makes them ideal for rapid transformer frequency response measurements. Measurements were performed using both stepped-frequency excitation and PRBS excitation and good agreement between the respective results was consistently obtained.

(b) *Signal processing.* Transformer frequency responses measured with a wideband excitation signal will inevitably contain a certain amount of noise, due to the non-linear properties of the transformer under test, errors introduced by the data acquisition system, which quantifies its input signals in terms of discrete levels, and electro-

magnetically coupled noise from sources external to the test arrangement. During frequency response measurements with PRBS excitation, reasonably high excitation levels could be applied to the transformer under test so that high signal-to-noise ratios could be maintained over a wide frequency range. As a result, the unsmoothed estimates of the transformer frequency responses contained only a relatively small noise component, which could be successfully removed by the application of a simple spectral estimation algorithm, without reducing the accuracy of the frequency response measurement.

(c) *Instrumentation.* During transformer frequency response measurements, it is easy to underestimate the magnitude of the terminal input impedance, particularly in the vicinity of a parallel resonant frequency in the HV input-impedance frequency responses. In the case of the 22 kV / 240 V, 16 kVA test transformer, the HV open-circuit input impedance was found to be of the same order of magnitude as the input impedance of the data-acquisition system (10 MΩ when using a 10:1 probe). Unless the experimental arrangement is designed correctly, large errors will be made during the measurement of the HV input impedance frequency responses, as the current flowing into the transformer terminals is of the same order of magnitude as the current flowing through the input impedance of the data-acquisition system.

8.3 Parameter Estimation

Existing parameter estimation procedures for transformer equivalent-circuit models require that the equivalent circuit is sub-divided into several smaller sub-circuits, each of which is represented by a transfer function [14, 13, 44]. The coefficients of these transfer functions are then estimated, from which the equivalent-circuit parameters are finally determined.

A parameter estimation procedure to determine the parameters of the proposed transformer equivalent-circuit model was developed and implemented. This procedure differs from previously proposed methodologies in that the equivalent-circuit parameters are estimated directly, i.e. without the need to formulate intermediate sub-circuits. Further, several transformer frequency responses are simultaneously evaluated by the estimator. This procedure was found to provide consistent, unique and accurate parameter estimates for the proposed transformer model structure. The following findings are of importance to the application of parameter estimation techniques to transformer models:

(a) *Frequency-domain estimation.* Estimation of the parameters of the proposed transformer model structure was carried out in the frequency domain. It was found that the frequency-domain approach has several distinct advantages that make it preferable to a time-domain estimation procedure:

- The frequency-dependence of the model parameters is simple to represent in the frequency domain.
- A lower number of data points are required, so that fewer evaluations of the model responses are required within each iteration of the estimation procedure.
- In the frequency domain, several responses can be evaluated simultaneously with relative ease, without the need for input data for each required response.

(b) *Constrained minimization of the cost function.* The proposed transformer model consists of a number of mutually coupled inductors. For practical transformers, the following inequality holds for each pair of coupled inductances L_i and L_j:

$$M_{ij} < \sqrt{L_i L_j}\,. \tag{8.1}$$

If a standard, unconstrained optimization algorithm is applied to minimize the cost function during the parameter estimation process, the inequality of equation 8.1 is often violated. A constrained optimization algorithm was successfully applied to minimize the cost function when estimating the parameters of the proposed transformer model. The use of such an optimization procedure makes it possible to constrain all the transformer model parameters to a physically feasible range so that equation 8.1 can be enforced.

(c) *Uniqueness of the parameter estimates.* It was shown that the parameters of the proposed transformer model can not be estimated uniquely from one of the transformer frequency responses alone. Practically it was found that at least four of the transformer frequency responses were required as input data to the estimation procedure to obtain an accurate and consistent solution for the transformer model parameters. However, it is not known how many winding sections can be employed in the model before it is no longer possible to uniquely estimate the model parameters from a set of terminal frequency responses alone.

(d) *Parameter estimation of the transformer model proposed by Douglass.* The parameter estimation procedure that was developed for the proposed transformer model was also successfully applied to estimate the parameters of the equivalent-circuit transformer model proposed by Douglass [17]. It was further shown that a constrained optimization algorithm is not required in this case, as the model suggested by Douglass does

not include any mutually coupled inductances. A minimum of two transformer frequency responses were required as input data to the estimation procedure to obtain accurate results.

(e) *Inter-winding capacitance.* Both the proposed model structure and the transformer model suggested by Douglass [17] include capacitances representing the capacitance between the transformer windings. Realistic estimates of the inter-winding capacitance could not be obtained. The reason for this is that the magnitude of the inter-winding capacitance is too low to have any significant effect on the transformer frequency responses in the 10 Hz to 100 kHz frequency range that was considered in this investigation. Typically, the inter-winding capacitance affects the transformer frequency responses at frequencies above 500 kHz [14].

8.4 Recommendations for Further Research

(a) *Parameter sensitivity to transformer faults and ageing.* One of the intended application areas of the proposed transformer model and the parameter estimation procedure is transformer condition monitoring. By relating changes in the measured transformer frequency responses to changes in the model parameters, conclusive results regarding the nature and location of any internal faults or damage may be obtained. This problem was investigated by Mikkelsen *et al.* [11, 81, 16] and Bak-Jensen *et al.* [6] by applying parameter estimation techniques to the transformer model proposed by Douglass [17]. The use of an improved transformer model is expected to yield more detailed and accurate information from which conclusions regarding the condition of a transformer can be drawn. However, before the proposed transformer model can be applied to practical transformer condition monitoring problems, the sensitivity of the model parameters to a variety of potential faults has to be investigated in detail.

(b) *Extension of the transformer model.* In this dissertation, the modelling of two-winding transformers in the frequency range between 10 Hz and 100 kHz was considered. The validity of the proposed model structure for frequencies above 100 kHz remains to be confirmed. It has been shown that the number of winding resonances that can be predicted by the proposed model is a function of the number of sections that are used to represent the windings. Thus, a logical extension of the model would be to incorporate additional winding sections and then applying it over a wider frequency range. However, what is not known is how many winding sections can be used before it is no longer possible to uniquely estimate the model parameters from terminal

frequency response measurements alone, assuming that the parameter estimation procedure can be carried out practically when a large number of winding sections is used. This is an important question that has to be considered as part of further research projects in order to define the limitations of the model structure when it is used in parameter estimation applications.

It should also be possible to extend the model to include more than two windings. However, extension of the proposed model structure to more than two windings increases the number of model parameters, resulting in a more complicated parameter estimation procedure which is likely to require additional frequency responses as input data as the number of windings increases. In the case of a three-phase transformer, it may be possible to find a way to exploit the similarity of the three primary windings and the three secondary windings respectively, to simplify the parameter estimation process (e.g. by assuming that the three primary and the three secondary windings are identical, so that a reasonably accurate initial parameter estimates are obtained before allowing the parameters of each winding to be adjusted independently by the parameter estimation procedure).

(c) *Transformer model capacitances.* Although a representation of the inter-winding capacitance is included in the proposed transformer model structure, a reliable estimate of this capacitance could not be obtained for any of the models considered during this project. Very low values were obtained for the inter-winding capacitance, which suggests that it only affects the transformer frequency response characteristics significantly at frequencies above 100 kHz. Thus, the location of the inter-winding capacitance within the model structure could not be verified. This problem can be addressed by obtaining frequency response data over a wider frequency range, which can then be used to obtain more reliable estimates of the inter-winding capacitance. A similar uncertainty exists in the significance of C_{ps} in the model proposed by Douglass [17] (see figure 6.14) and its magnitude relative to the other equivalent-circuit capacitances. These problems should be addressed as part of future research, especially in cases where the physical significance of the representation of the inter-winding capacitance is of importance.

(d) *PRBS excitation at high frequencies.* The PRBS source described by Cornelissen [90, 92] was applied for the transformer frequency response measurements described in this dissertation, which required response measurements up to 100 kHz. For transformer FRA testing, the frequency-response characteristics of transformers are typically measured up to frequencies in the order of several MHz [4, 5]. The maximum frequency at which the PRBS source output signal contains useable energy is limited by

the maximum switching frequency of the semiconductor switching elements used to realize the output stage. The maximum frequency up to which Cornelissen's PRBS source can be applied has not been established, mainly due to the limitations of the available data acquisition equipment. This maximum frequency should be determined and if it is found to lie below ≈ 5 MHz, methods should be investigated by which the frequency range of the PRBS source can be extended (keeping in mind that useable signal energy is contained in the side-lobes of the PRBS power spectral density).

Appendix A

Symbolic Nodal Admittance Matrices

Methods by which the nodal admittance matrix of a linear network can be constructed from a topological description of the network, are well documented in the literature [99, 28]. A symbolic, rather than a numeric version of the nodal admittance matrix can be obtained by programming such a method in terms of symbolic element values. Brozio and Vermeulen [102] have shown that this can be achieved by making use of the symbolic mathematics capabilities of MATLAB [3, 110] or *Mathematica* [101]. The string-handling capabilities of the PASCAL programming language also make it a good choice for the implementation of a symbolic nodal admittance matrix construction program. PASCAL allows considerably more flexibility in the formatting of the input and output data than MATLAB or *Mathematica*, while requiring a roughly similar amount of coding for this application. Significantly faster program running times are also obtained. Such a PASCAL program (`MAKEYN`) was implemented to derive the nodal admittance matrices of the transformer equivalent-circuit models described in this dissertation. The program reads a topological description of the network from a file and outputs the nodal admittance matrix of that network in a form that can be read directly by MATLAB.

A.1 Construction of the Nodal Admittance Matrix

Consider an *RLCM* network, consisting of b branches and $n+1$ nodes. The nodes are numbered from 0 to n and the branches are numbered from 1 to b. Node 0 is defined as the reference node. The network will thus have an $n \times n$ nodal admittance matrix, $\boldsymbol{Y}_n$. The construction of $\boldsymbol{Y}_n$ starts by conceptually removing all branches from the network, so that $\boldsymbol{Y}_n = \boldsymbol{0}$. The elements of $\boldsymbol{Y}_n$ are now updated by sequentially adding the relevant entries for each branch [99].

In the `MAKEYN` program, $\boldsymbol{Y}_n$ is represented as an $n \times n$ array of strings:

Listing A.1
```
  var
    Yn = array[1..n,1..n] of string;
```
End of listing A.1

The size of this structure is limited by the available computer memory and by the limitations of the memory model implemented by the compiler. Note that it is always possible to define the structure in terms of memory pointers to increase its size. Using Borland's Turbo Pascal [111], a 20×20 nodal admittance matrix could be defined, with each entry limited to 150 characters in length, which was found to be sufficient for the networks considered in this dissertation.

The PASCAL variable `Yn` is initialized by setting each of its elements to represent an empty string:

Listing A.2
```
  for i := 1 to n do
    begin
      for j := 1 to n do Yn[i,j] := '';
    end;
```
End of listing A.2

Once `Yn` has been initialized, network data is read from an input file. As the transformer equivalent-circuit model is passive, only *RLC* branches and mutual inductances have to be supported. *RLC* branches and mutually coupled branches are treated differently, so that `MAKEYN` has to identify the branch type and then update `Yn` according to the relevant procedure, as shown in figure A.1. Sections A.1.1 and A.1.2 discuss how nodal admittance matrix entries are made for each branch type. `MAKEYN` continues to read input data and to update `Yn` until the end of the data file is reached. Before the completed `Yn` is written to

an output file, `Yn` is formatted so that the output file can be read directly by MATLAB. The correct row and column separators are appended to the element strings and any remaining empty strings are replaced by `'0'`.

A.1.1 *RLC* Branches

Consider the l^{th} network branch, directed from node i to node j, with an admittance y_l. Letting y' denote the existing value of an element of $\boldsymbol{Y}_n$, the elements of $\boldsymbol{Y}_n$ are updated for the l^{th} branch as follows [99, 102]:

$$\begin{aligned} y_{ii} &= y'_{ii} + y_l \\ y_{ij} &= y'_{ij} - y_l \\ y_{ji} &= y'_{ji} - y_l \\ y_{jj} &= y'_{jj} + y_l \end{aligned} \tag{A.1}$$

In general, each y_l thus appears in four places in $\boldsymbol{Y}_n$. However, if $i = 0$ or $j = 0$, i.e. the branch is incident at the reference node, the entry is not made. In the `MAKEYN` program, the above process is applied symbolically. First, a symbolic representation of the admittance of each branch has to be determined in terms of the branch-element designator. For *RLC* branches, with $s = j\omega$:

$$\text{Resistive branches:} \quad y_l = \frac{1}{R_l} \tag{A.2}$$

$$\text{Inductive branches:} \quad y_l = \frac{1}{sL_l} \tag{A.3}$$

$$\text{Capacitive branches:} \quad y_l = sC_l \tag{A.4}$$

The nodes at which a branch is incident, i and j, the element type (R, L or C) and the symbolic element value, or element designator, are read from the data file. Using this information, entries can be made in the symbolic nodal admittance matrix:

Listing A.3

```
case Branch_Type of
  'R'  :  Yn_Entry := '1/' + Designator;
  'L'  :  Yn_Entry := '1/(s*' + Designator +')';
  'C'  :  Yn_Entry := 's*' + Designator;
end;
if i<>0 then Yn[i,i] := Yn[i,i] + '+' + Yn_Entry;
```

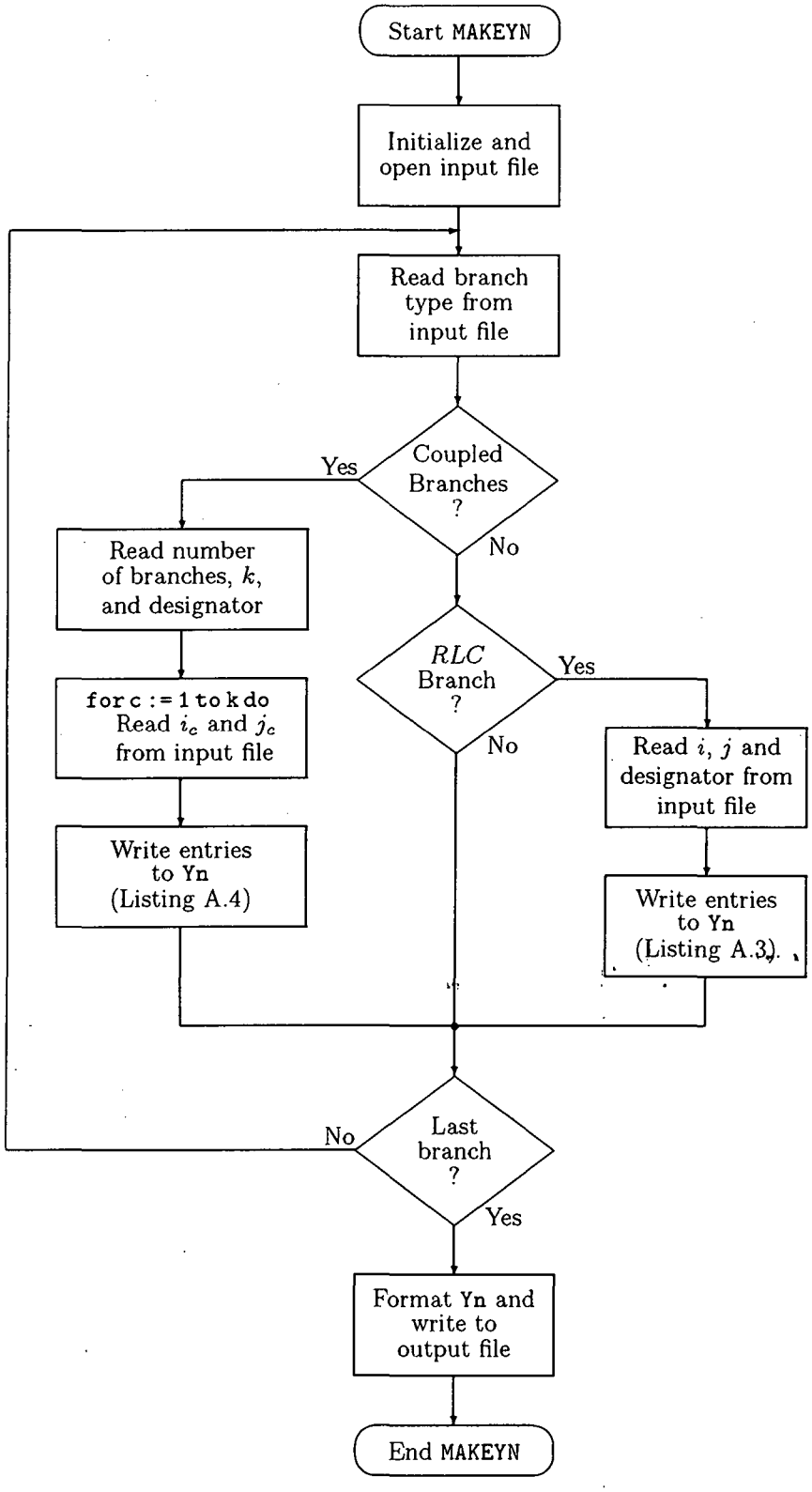

Figure A.1: Flow diagram for the MAKEYN program.

```
  if (i<>0) and (j<>0) then
    begin
      Yn[i,j] := Yn[i,j] + '-' + Yn_Entry;
      Yn[j,i] := Yn[j,i] + '-' + Yn_Entry;
    end;
  if j<>0 then Yn[j,j] := Yn[j,j] + '+' + Yn_Entry;
```

End of listing A.3

A.1.2 Mutually Coupled Branches

A system of k mutually coupled branches is generally represented as follows:

$$\begin{bmatrix} \mathbf{V}_1 \\ \mathbf{V}_2 \\ \vdots \\ \mathbf{V}_k \end{bmatrix} = s \begin{bmatrix} L_{11} & M_{12} & \cdots & M_{1k} \\ M_{21} & L_{22} & \cdots & M_{2k} \\ \vdots & \vdots & \ddots & \vdots \\ M_{k1} & M_{k2} & \cdots & L_{kk} \end{bmatrix} \begin{bmatrix} \mathbf{I}_1 \\ \mathbf{I}_2 \\ \vdots \\ \mathbf{I}_k \end{bmatrix}, \tag{A.5}$$

or

$$\boldsymbol{V}_L = s\boldsymbol{L}\boldsymbol{I}_L\,. \tag{A.6}$$

Equation A.5 can not be included in $\boldsymbol{Y}_n$ directly, but must be expressed in terms of the inverse inductance matrix, $\boldsymbol{\Gamma} = \boldsymbol{L}^{-1}$ [99]:

$$\boldsymbol{I}_L = \tfrac{1}{s}\boldsymbol{\Gamma}\boldsymbol{V}_L\,. \tag{A.7}$$

The system of mutually coupled branches can now be witten in terms of voltage-controlled current sources as illustrated by figure A.2. Assuming that $\boldsymbol{\Gamma}$ is known, k entries have to be

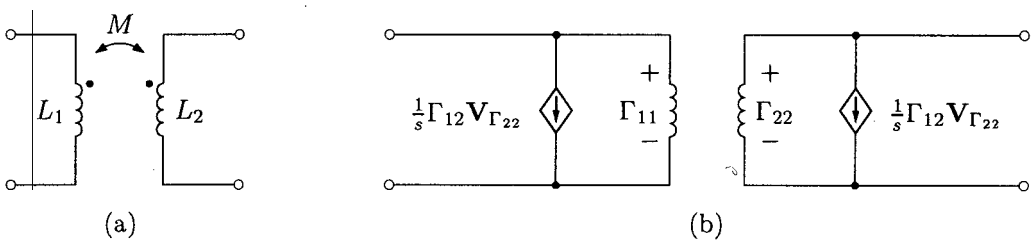

Figure A.2: Representation of mutually coupled branches for inclusion in $\boldsymbol{Y}_n$.

made in $\boldsymbol{Y}_n$ for each branch in the mutually coupled system. The reciprocal self-inductance of the l^{th} branch, Γ_{ll}, directed from node i to node j, is entered as an admittance branch between nodes i and j. Also connected between nodes i and j are $k-1$ voltage-controlled current sources, controlled by the voltages across the reciprocal self-inductances of the other branches that form part of the mutually coupled system. The current source resulting from the coupling of the m^{th} branch (directed from node p to node q) to the l^{th} branch, results in the following entries in $\boldsymbol{Y}_n$:

$$\begin{aligned} y_{ip} &= y'_{ip} + g_m \\ y_{iq} &= y'_{iq} - g_m \\ y_{jp} &= y'_{jp} - g_m \\ y_{jq} &= y'_{jq} + g_m \end{aligned} \tag{A.8}$$

where

$$g_m = \tfrac{1}{s}\Gamma_{lm} \tag{A.9}$$

It is not practical to attempt the inversion of $\boldsymbol{L}$ symbolically, as the resulting expressions are unwieldy (the determinant of $\boldsymbol{L}$ appears in each element of $\boldsymbol{\Gamma}$). The `MAKEYN` program thus constructs the symbolic nodal admittance matrix in terms of $\boldsymbol{\Gamma}$, based on the assumption that $\boldsymbol{\Gamma}$ can be found numerically before its elements are substituted in the symbolic $\boldsymbol{Y}_n$. `MAKEYN` reads the following information from the input file for each set of mutually coupled branches:

(1) The number of coupled branches, k,

(2) the designator that will be used to identify the elements of $\boldsymbol{\Gamma}$, and

(3) k pairs of incident node numbers, i_c and j_c, where $c = 1, 2 \ldots k$, i.e. the incident nodes of each coupled branch are read.

The following listing shows how the nodal admittance matrix entries for mutually coupled branches are made by `MAKEYN`:

Listing A.4

```
for c := 1 to k do
  begin
    str(c,c_string);  (* Convert c to string *)
    Yn_Entry := Designator+'('+c_string+','+c_string+')/s';
    if i[c]<>0 then Yn[i[c],i[c]] := Yn[i[c],i[c]] + '+' + Yn_Entry;
    if (i[c]<>0) and (j[c]<>0) then
```

```
        begin
          Yn[i[c],j[c]] := Yn[i[c],j[c]] + '-' + Yn_Entry;
          Yn[j[c],i[c]] := Yn[j[c],i[c]] + '-' + Yn_Entry;
        end;
      if j[c]<>0 then Yn[j[c],j[c]] := Yn[j[c],j[c]] + '+' + Yn_Entry;
      for r := 1 to k do
        begin
          if r<>c then
            begin
              str(r,r_string);  (* Convert r to string *)
              Yn_Entry := Designator+'('+c_string+','+r_string+')/s';
              if (i[c]<>0) and (i[r]<>0) then
                Yn[i[c],i[r]] := Yn[i[c],i[r]] + '+' + Yn_Entry;
              if (j[c]<>0) and (i[r]<>0) then
                Yn[j[c],i[r]] := Yn[j[c],i[r]] + '-' + Yn_Entry;
              if (i[c]<>0) and (j[r]<>0) then
                Yn[i[c],j[r]] := Yn[i[c],j[r]] + '-' + Yn_Entry;
              if (j[c]<>0) and (j[r]<>0) then
                Yn[j[c],j[r]] := Yn[j[c],j[r]] + '+' + Yn_Entry;
            end;  (* if r<>c *)
        end;  (* for r *)
    end;  (* for c *)
```

End of listing A.4

A.2 Example

The nodal admittance matrix of the proposed transformer model, with four HV winding sections (see figure 4.7), is large and will thus not serve as a good example to demonstrate the operation of the MAKEYN program. Figure A.3 shows a transformer model that is based on the same structure, but uses only one section to represent each winding.

Using the node numbers shown in figure A.3, the MAKEYN input file for this equivalent-circuit model is:

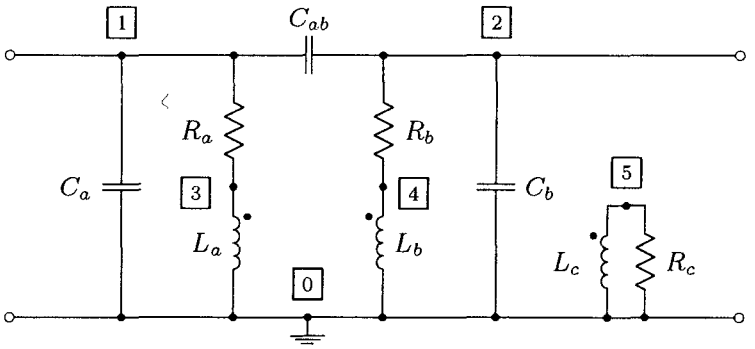

Figure A.3: Transformer equivalent-circuit model with one section per winding.

Type	i	j	Designator
↓	↓	↓	↓
C	1	0	Ca
C	2	0	Cb
C	1	2	Cab
R	1	3	Ra
R	2	4	Rb
R	5	0	Rc
M	3		I ⟵ Three coupled branches.
	3	0	⟵ Coupled branch nodes (3 rows).
	4	0	
	5	0	

The designator I is used to represent the inverse admittance matrix. After running MAKEYN with the above input data, the output file contains the following symbolic representation of $\boldsymbol{Y}_n$, which can be included in a MATLAB file without modification:

```
Yn = [+s*Ca+s*Cab+1/Ra,-s*Cab,-1/Ra,0,0;...
      -s*Cab,+s*Cb+s*Cab+1/Rb,0,-1/Rb,0;...
      -1/Ra,0,+1/Ra+I(1,1)/s,+I(1,2)/s,+I(1,3)/s;...
      0,-1/Rb,+I(2,1)/s,+1/Rb+I(2,2)/s,+I(2,3)/s;...
      0,0,+I(3,1)/s,+I(3,2)/s,+1/Rc+I(3,3)/s];
```

Within MATLAB, s is replaced by $j\omega$ and I is found by numerically inverting the inductance matrix of the transformer model before substitution in the nodal admittance matrix.

Rewriting the MAKEYN output in terms of the inverse inductance matrix Γ, yields the following result for the nodal admittance matrix of the equivalent circuit of figure A.3:

$$\boldsymbol{Y}_n = \begin{bmatrix} sC_a + sC_{ab} + \frac{1}{R_a} & -sC_{ab} & -\frac{1}{R_a} & 0 & 0 \\ -sC_{ab} & sC_b + sC_{ab} + \frac{1}{R_b} & 0 & -\frac{1}{R_b} & 0 \\ -\frac{1}{R_a} & 0 & \frac{1}{R_a} + \frac{1}{s}\Gamma_{11} & \frac{1}{s}\Gamma_{12} & \frac{1}{s}\Gamma_{13} \\ 0 & -\frac{1}{R_b} & \frac{1}{s}\Gamma_{21} & \frac{1}{R_b} + \frac{1}{s}\Gamma_{22} & \frac{1}{s}\Gamma_{23} \\ 0 & 0 & \frac{1}{s}\Gamma_{31} & \frac{1}{s}\Gamma_{32} & \frac{1}{R_c} + \frac{1}{s}\Gamma_{33} \end{bmatrix} \quad \text{(A.10)}$$

Appendix B

State-space Representation of the Transformer Model

B.1 Formulation of the State-equations

A generalised algorithm by which unique and consistent expressions for the state-equations of *RLCM* networks can be obtained is described by Chua and Lin [99]. Provided that the network does not contain loops consisting of independent voltage sources or cutsets consisting of independent current sources, the procedures outlined below can be followed to obtain a state-space representation of an *RLCM* network.

The first step is to construct a topological description of the network under consideration. Kirchoff's current law, applied to each network node, can be expressed as [99]:

$$\boldsymbol{A}^{i'}\boldsymbol{i} = 0\,, \tag{B.1}$$

where $\boldsymbol{A}^{i'}$ and $\boldsymbol{i}$ denote the node-branch incidence matrix and the branch-current vector respectively. An n-node, b-branch network gives rise to a $n \times b$ incidence matrix of the form

$$\boldsymbol{A}^{i'} = [a_{ij}]\,, \tag{B.2}$$

where

$a_{ij} = 1$ if branch j is incident at node i and the positive current direction is defined away from node i,

$a_{ij} = -1$ if branch j is incident at node i and the positive current direction is defined towards node i, and

$a_{ij} = 0$ if branch j is not incident at node i.

The elements of the branch-current vector, $\boldsymbol{i}$ are ordered with respect to the type of network element involved, i.e. sequentially in the order of independent voltage sources, capacitors, resistors, inductors and lastly, independent current sources. Within the capacitive and inductive branch-current groups, the branch-currents can be further ordered to reflect the preferred allocation of state variables.

Equation B.1 is overdetermined. An independent set of equations is obtained by deleting one of the rows of $\boldsymbol{A}^{i'}$, which yields a reduced incidence matrix. The reduced incidence matrix is now transformed to row-echelon form by a series of elementary row operations, and arranged so that the first non-zero entry of each row lies on the diagonal. The result is a reduced incidence matrix in the form

$$\boldsymbol{A}^i = \left[\boldsymbol{A}^i_{\mathcal{T}} | \boldsymbol{A}^i_{\mathcal{L}}\right] , \tag{B.3}$$

where $\boldsymbol{A}^i_{\mathcal{T}}$ and $\boldsymbol{A}^i_{\mathcal{L}}$ denote tree and link partitions for the network. The fundamental cutset matrix of the network, $\boldsymbol{D}^c$, is obtained from the reduced incidence matrix, by applying the following transformation [99]:

$$\boldsymbol{D}^c = \left[\boldsymbol{A}^i_{\mathcal{T}}\right]^{-1} \boldsymbol{A}^i , \tag{B.4}$$

which yields

$$\boldsymbol{D}^c \boldsymbol{i} = 0 , \tag{B.5}$$

where

$$\boldsymbol{D}^c = \left[\begin{array}{cccc|cccc} 1_{E\mathcal{T}} & 0 & 0 & 0 & \boldsymbol{F}_{11} & \boldsymbol{F}_{12} & \boldsymbol{F}_{13} & \boldsymbol{F}_{14} \\ 0 & 1_{C\mathcal{T}} & 0 & 0 & \boldsymbol{F}_{21} & \boldsymbol{F}_{22} & \boldsymbol{F}_{23} & \boldsymbol{F}_{24} \\ 0 & 0 & 1_{R\mathcal{T}} & 0 & \boldsymbol{F}_{31} & \boldsymbol{F}_{32} & \boldsymbol{F}_{33} & \boldsymbol{F}_{34} \\ 0 & 0 & 0 & 1_{L\mathcal{T}} & \boldsymbol{F}_{41} & \boldsymbol{F}_{42} & \boldsymbol{F}_{43} & \boldsymbol{F}_{44} \end{array}\right] , \tag{B.6}$$

and

$$\boldsymbol{i} = \begin{bmatrix} i_{E\mathcal{T}} & i_{C\mathcal{T}} & i_{R\mathcal{T}} & i_{L\mathcal{T}} & i_{J\mathcal{L}} & i_{L\mathcal{L}} & i_{R\mathcal{L}} & i_{C\mathcal{L}} \end{bmatrix}^T . \tag{B.7}$$

The entries in the cutset matrix, $\boldsymbol{D}^c$, are all submatrices containing only ones and zeros. The submatrices denoted by $\mathbf{1}$ are diagonal unit matrices. Subscripts $\mathcal{T}$ and $\mathcal{L}$ indicate tree and link entries respectively, while subscripts E, C, R, L and J indicate the type of branch element, i.e. independent voltage sources, capacitors, resistors, inductors and independent current sources respectively. The RLC branches are characterised by the following relationships:

$$\begin{bmatrix} \boldsymbol{v}_{R\mathcal{T}} \\ \boldsymbol{v}_{R\mathcal{L}} \end{bmatrix} = \begin{bmatrix} \boldsymbol{R}_{\mathcal{T}} & 0 \\ 0 & \boldsymbol{R}_{\mathcal{L}} \end{bmatrix} \begin{bmatrix} \boldsymbol{i}_{R\mathcal{T}} \\ \boldsymbol{i}_{R\mathcal{L}} \end{bmatrix} \quad \text{or} \quad \begin{bmatrix} \boldsymbol{i}_{R\mathcal{T}} \\ \boldsymbol{i}_{R\mathcal{L}} \end{bmatrix} = \begin{bmatrix} \boldsymbol{G}_{\mathcal{T}} & 0 \\ 0 & \boldsymbol{G}_{\mathcal{L}} \end{bmatrix} \begin{bmatrix} \boldsymbol{v}_{R\mathcal{T}} \\ \boldsymbol{v}_{R\mathcal{L}} \end{bmatrix} , \tag{B.8}$$

$$\begin{bmatrix} \boldsymbol{i}_{C\mathcal{T}} \\ \boldsymbol{i}_{C\mathcal{L}} \end{bmatrix} = \begin{bmatrix} \boldsymbol{C}^e_{\mathcal{T}} & \mathbf{0} \\ \mathbf{0} & \boldsymbol{C}^e_{\mathcal{L}} \end{bmatrix} \frac{d}{dt} \begin{bmatrix} \boldsymbol{v}_{C\mathcal{T}} \\ \boldsymbol{v}_{C\mathcal{L}} \end{bmatrix} , \text{ and} \tag{B.9}$$

$$\begin{bmatrix} \boldsymbol{v}_{L\mathcal{T}} \\ \boldsymbol{v}_{L\mathcal{L}} \end{bmatrix} = \begin{bmatrix} \boldsymbol{L}_{\mathcal{T}\mathcal{T}} & \boldsymbol{L}_{\mathcal{T}\mathcal{L}} \\ \boldsymbol{L}_{\mathcal{L}\mathcal{T}} & \boldsymbol{L}_{\mathcal{L}\mathcal{L}} \end{bmatrix} \frac{d}{dt} \begin{bmatrix} \boldsymbol{i}_{L\mathcal{T}} \\ \boldsymbol{i}_{L\mathcal{L}} \end{bmatrix} . \tag{B.10}$$

Matrices $\boldsymbol{R}$, $\boldsymbol{G}$ and $\boldsymbol{C}^e$ are square matrices with branch-element values on the diagonal. The remaining entries in $\boldsymbol{R}$, $\boldsymbol{G}$ and $\boldsymbol{C}^e$ are zero. Matrix $\boldsymbol{L}$ is the inductance matrix which is assumed to be positive definite, i.e. its inverse exists. Given the partitioned cutset matrix $\boldsymbol{D}^c$ and the branch-element matrices, a state-space expression for the network can be obtained in the following form [99]:

$$\dot{\hat{\boldsymbol{x}}} = \boldsymbol{A}\hat{\boldsymbol{x}} + \boldsymbol{B}_1\boldsymbol{u} + \boldsymbol{B}_2\dot{\boldsymbol{u}} , \tag{B.11}$$

where

$$\boldsymbol{A} = \left[\boldsymbol{M}^{(0)}\right]^{-1} \boldsymbol{A}^{(0)} \tag{B.12}$$

$$\boldsymbol{B}_1 = \left[\boldsymbol{M}^{(0)}\right]^{-1} \boldsymbol{B}_1^{(0)} \tag{B.13}$$

$$\boldsymbol{B}_2 = \left[\boldsymbol{M}^{(0)}\right]^{-1} \boldsymbol{B}_2^{(0)} \tag{B.14}$$

and

$$\boldsymbol{M}^{(0)} = \begin{bmatrix} \boldsymbol{C}^e_{\mathcal{T}} + \boldsymbol{F}_{24}\boldsymbol{C}^e_{\mathcal{L}}\boldsymbol{F}^T_{24} & \boldsymbol{0} \\ \boldsymbol{0} & (\boldsymbol{L}_{\mathcal{L}\mathcal{L}} - \boldsymbol{F}^T_{42}\boldsymbol{L}_{\mathcal{T}\mathcal{L}} - \boldsymbol{L}_{\mathcal{L}\mathcal{T}}\boldsymbol{F}_{42} + \boldsymbol{F}^T_{42}\boldsymbol{L}_{\mathcal{L}\mathcal{L}}\boldsymbol{F}_{42}) \end{bmatrix} \tag{B.15}$$

$$\boldsymbol{A}^{(0)} = \begin{bmatrix} -\boldsymbol{F}_{23}\boldsymbol{R}^{-1}\boldsymbol{F}^T_{23} & (-\boldsymbol{F}_{22} + \boldsymbol{R}^{-1}\boldsymbol{F}^T_{33}\boldsymbol{R}_{\mathcal{T}}\boldsymbol{F}_{32}) \\ (\boldsymbol{F}^T_{12} - \boldsymbol{F}^T_{32}\boldsymbol{G}^{-1}\boldsymbol{F}_{33}\boldsymbol{G}_{\mathcal{L}}\boldsymbol{F}^T_{23}) & -\boldsymbol{F}^T_{32}\boldsymbol{G}^{-1}\boldsymbol{F}_{32} \end{bmatrix} \tag{B.16}$$

$$\boldsymbol{B}^{(0)}_1 = \begin{bmatrix} -\boldsymbol{F}_{23}\boldsymbol{R}^{-1}\boldsymbol{F}^T_{13} & (-\boldsymbol{F}_{21} + \boldsymbol{F}_{23}\boldsymbol{R}^{-1}\boldsymbol{F}^T_{33}\boldsymbol{R}_{\mathcal{T}}\boldsymbol{F}_{31}) \\ (\boldsymbol{F}^T_{12} - \boldsymbol{F}^T_{32}\boldsymbol{G}^{-1}\boldsymbol{F}_{33}\boldsymbol{G}_{\mathcal{L}}\boldsymbol{F}^T_{13}) & -\boldsymbol{F}^T_{32}\boldsymbol{G}^{-1}\boldsymbol{F}_{31} \end{bmatrix} \tag{B.17}$$

$$\boldsymbol{B}^{(0)}_2 = \begin{bmatrix} -\boldsymbol{F}_{24}\boldsymbol{C}^e_{\mathcal{L}}\boldsymbol{F}^T_{14} & \boldsymbol{0} \\ \boldsymbol{0} & (-\boldsymbol{F}^T_{42}\boldsymbol{L}_{\mathcal{L}\mathcal{L}}\boldsymbol{F}_{41} + \boldsymbol{L}_{\mathcal{L}\mathcal{T}}\boldsymbol{F}_{41}) \end{bmatrix}. \tag{B.18}$$

The input vector, $\boldsymbol{u}$, contains the independent voltage and current sources:

$$\boldsymbol{u} = \begin{bmatrix} \boldsymbol{v}_E \\ \boldsymbol{i}_J \end{bmatrix} \tag{B.19}$$

The derivative of $\boldsymbol{u}$ appears in equation B.11 and can be eliminated by a change of variables:

$$\boldsymbol{x} = \hat{\boldsymbol{x}} - \boldsymbol{B}_2\boldsymbol{u}\,, \tag{B.20}$$

which yields the standard-form state equations:

$$\dot{\boldsymbol{x}} = \boldsymbol{A}\boldsymbol{x} + \boldsymbol{B}\boldsymbol{u}\,, \tag{B.21}$$

where

$$\boldsymbol{B} = \boldsymbol{B}_1 + \boldsymbol{A}\boldsymbol{B}_2\,. \tag{B.22}$$

For the applications discussed in this dissertation, the output variables of the state-equations are usually one, or more, of the state-variables. In such cases it is straightforward to manually construct the standard-form output equations:

$$\boldsymbol{y} = \boldsymbol{C}\boldsymbol{x} + \boldsymbol{D}\boldsymbol{u}\,. \tag{B.23}$$

B.2 State-equations for the 16 kVA Transformer Model

The state-equations for the 16 kVA transformer model can be constructed by applying the above procedure. Using the node-numbering scheme shown in figure B.1 on page 174, the nodal incidence matrix, $\boldsymbol{A}^{i'}$, for the transformer equivalent circuit (excited by a current source, i_1, at the LV terminals) is given by equation B.28 on page 175. The branch-element matrices, $\boldsymbol{C}^e$, $\boldsymbol{R}$, $\boldsymbol{L}$ and $\boldsymbol{G}$ are given by equations B.29 to B.32, respectively. By applying equations B.15 to B.18, matrices $\boldsymbol{M}^{(0)}$, $\boldsymbol{A}^{(0)}$, $\boldsymbol{B}_1^{(0)}$ and $\boldsymbol{B}_2^{(0)}$ can be found. Up to this point, the derivation of the state-equations could be carried out symbolically [94, 103], to yield the expressions given by equations B.33 to B.36 on page 176. The next step requires inversion of $\boldsymbol{M}^{(0)}$ (equations B.12 to B.14). It is impractical to perform this step symbolically, as the resulting expressions are extremely lengthy and complex. The estimated element values of the 16 kVA transformer equivalent circuit (see table 6.1) are thus substituted in equations B.33 to B.36 before the operations given by equations B.12 to B.14 are carried out. Finally, the state equations are obtained by applying the change of variables given by equation B.20. The resulting state-space matrices for the 16 kVA test transformer, excited by a current source at the LV terminals, are given in equations B.37 to B.40 on page 177.

Output equations for the transformer network are usually straight-forward to formulate. If the LV terminal voltage response to the input current i_1 is required (as was the case for the simulation result shown in figure 7.2), the required output is simply the voltage across C_{a1}, the first state-variable, so that the output equation is:

$$\boldsymbol{y} = \begin{bmatrix} 1 & 0 & 0 & 0 & 0 & 0 & 0 & 0 & 0 & 0 & 0 \end{bmatrix} \boldsymbol{x} \tag{B.24}$$

$$= [v_{C_{a1}}] \, . \tag{B.25}$$

The simulation results shown in figures 7.4 and 7.6 were obtained by exciting the transformer with a voltage source connected to the LV terminals. The state-equations for this case are derived in the same way as for the current-source case. The topological data is similar to that shown on page 175, with the following changes:

(1) The entry for C_{a10} in $\boldsymbol{A}^{i'}$ is replaced by an entry for the voltage source, e_1. (C_{a10} is connected in parallel to the voltage source and will thus not affect the voltage

response of the equivalent circuit.)

(2) The entry for i_1 in $\boldsymbol{A}^{i'}$ is removed.

(3) The row and column associated with C_{a10} in $\boldsymbol{C}^e$ are removed.

With these changes in effect and using the estimated parameters for the 16 kVA transformer model (see table 6.1), the state-space matrices given by equations B.41 to B.44 are obtained (page 178). The simulation results of figures 7.4 and 7.6 show the HV terminal voltage response of the transformer, i.e. the voltage across C_{b10}, for which the output equation was formulated as follows:

$$\boldsymbol{y} = \begin{bmatrix} 1 & 0 & 0 & 0 & 0 & 0 & 0 & 0 & 0 & 0 \end{bmatrix} \boldsymbol{x} \tag{B.26}$$

$$= \left[v_{C_{b10}}\right] . \tag{B.27}$$

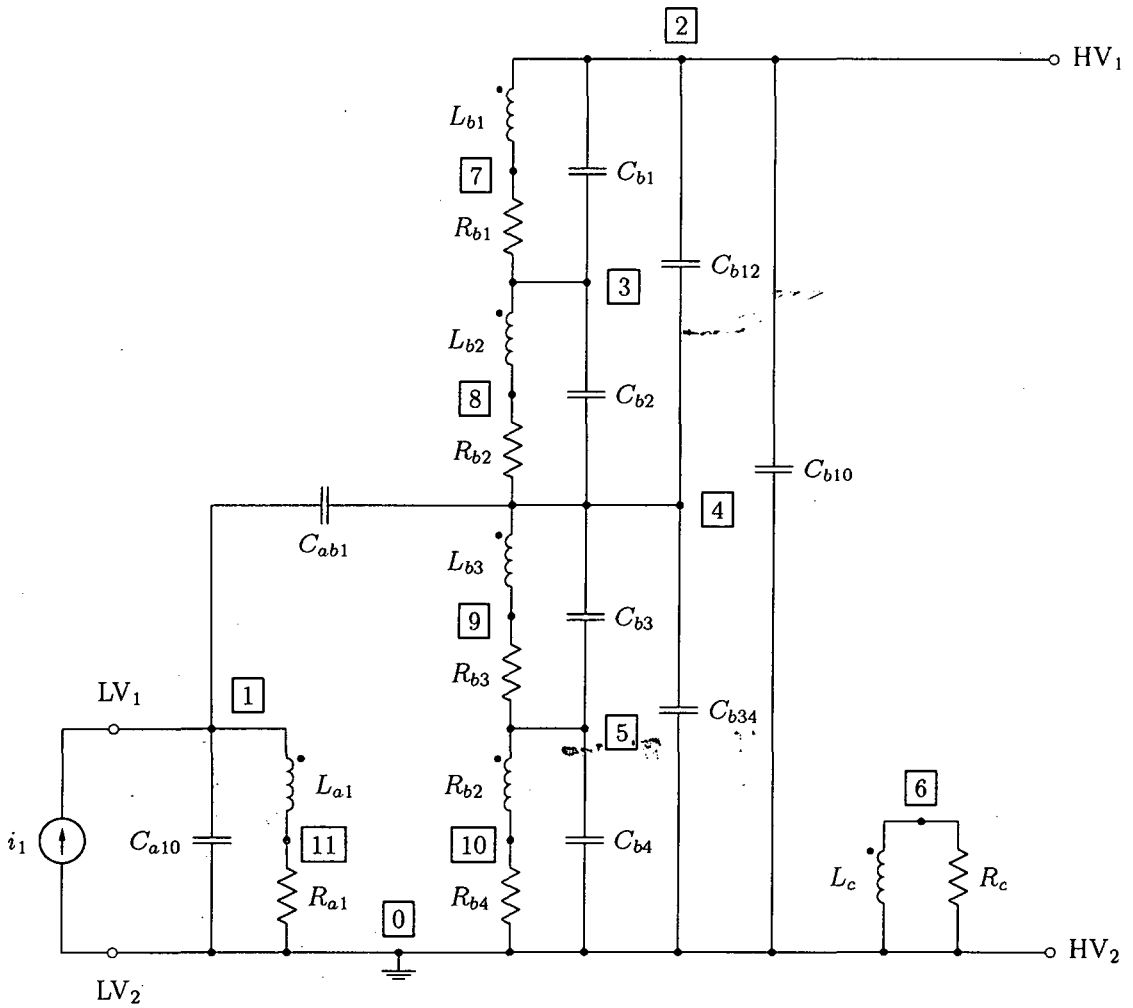

Figure B.1: Transformer equivalent circuit with node numbering for state-space implementation.

$$
\boldsymbol{A}^{i'} = \begin{array}{c} n\downarrow \\ 1 \\ 2 \\ 3 \\ 4 \\ 5 \\ 6 \\ 7 \\ 8 \\ 9 \\ 10 \\ 11 \\ 0 \end{array}
\begin{array}{c}
\begin{array}{ccccccccccccccccccccccc}
C_{a10} & C_{b10} & C_{b12} & C_{b34} & C_{b1} & C_{b2} & C_{b3} & C_{b4} & C_{ab1} & R_{b1} & R_{b2} & R_{b3} & R_{b4} & R_{a1} & R_c & L_{a1} & L_{b1} & L_{b2} & L_{b3} & L_{b4} & L_c & i_1
\end{array} \\
\left[\begin{array}{ccccccccccccccccccccccc}
1 & 0 & 0 & 0 & 0 & 0 & 0 & 0 & 1 & 0 & 0 & 0 & 0 & 0 & 0 & 1 & 0 & 0 & 0 & 0 & 0 & -1 \\
0 & 1 & 1 & 0 & 1 & 0 & 0 & 0 & 0 & 0 & 0 & 0 & 0 & 0 & 0 & 0 & 1 & 0 & 0 & 0 & 0 & 0 \\
0 & 0 & 0 & 0 & -1 & 1 & 0 & 0 & 0 & -1 & 0 & 0 & 0 & 0 & 0 & 0 & 0 & 1 & 0 & 0 & 0 & 0 \\
0 & 0 & -1 & 1 & 0 & -1 & 1 & 0 & -1 & 0 & -1 & 0 & 0 & 0 & 0 & 0 & 0 & 0 & 1 & 0 & 0 & 0 \\
0 & 0 & 0 & 0 & 0 & 0 & -1 & 1 & 0 & 0 & 0 & -1 & 0 & 0 & 0 & 0 & 0 & 0 & 0 & 1 & 0 & 0 \\
0 & 0 & 0 & 0 & 0 & 0 & 0 & 0 & 0 & 0 & 0 & 0 & 0 & 0 & 1 & 0 & 0 & 0 & 0 & 0 & 1 & 0 \\
0 & 0 & 0 & 0 & 0 & 0 & 0 & 0 & 0 & 1 & 0 & 0 & 0 & 0 & 0 & 0 & -1 & 0 & 0 & 0 & 0 & 0 \\
0 & 0 & 0 & 0 & 0 & 0 & 0 & 0 & 0 & 0 & 1 & 0 & 0 & 0 & 0 & 0 & 0 & -1 & 0 & 0 & 0 & 0 \\
0 & 0 & 0 & 0 & 0 & 0 & 0 & 0 & 0 & 0 & 0 & 1 & 0 & 0 & 0 & 0 & 0 & 0 & -1 & 0 & 0 & 0 \\
0 & 0 & 0 & 0 & 0 & 0 & 0 & 0 & 0 & 0 & 0 & 0 & 1 & 0 & 0 & 0 & 0 & 0 & 0 & -1 & 0 & 0 \\
0 & 0 & 0 & 0 & 0 & 0 & 0 & 0 & 0 & 0 & 0 & 0 & 0 & 1 & 0 & -1 & 0 & 0 & 0 & 0 & 0 & 0 \\
-1 & -1 & 0 & -1 & 0 & 0 & 0 & -1 & 0 & 0 & 0 & 0 & -1 & -1 & -1 & 0 & 0 & 0 & 0 & 0 & -1 & 1
\end{array}\right]
\end{array}
\tag{B.28}
$$

$$
\boldsymbol{C}^e = \begin{bmatrix}
C_{a10} & 0 & 0 & 0 & 0 & 0 & 0 & 0 & 0 \\
0 & C_{b10} & 0 & 0 & 0 & 0 & 0 & 0 & 0 \\
0 & 0 & C_{b12} & 0 & 0 & 0 & 0 & 0 & 0 \\
0 & 0 & 0 & C_{b34} & 0 & 0 & 0 & 0 & 0 \\
0 & 0 & 0 & 0 & C_{b1} & 0 & 0 & 0 & 0 \\
0 & 0 & 0 & 0 & 0 & C_{b2} & 0 & 0 & 0 \\
0 & 0 & 0 & 0 & 0 & 0 & C_{b3} & 0 & 0 \\
0 & 0 & 0 & 0 & 0 & 0 & 0 & C_{b4} & 0 \\
0 & 0 & 0 & 0 & 0 & 0 & 0 & 0 & C_{ab1}
\end{bmatrix}
\tag{B.29}
$$

$$
\boldsymbol{R} = \begin{bmatrix}
R_{b1} & 0 & 0 & 0 & 0 & 0 \\
0 & R_{b2} & 0 & 0 & 0 & 0 \\
0 & 0 & R_{b3} & 0 & 0 & 0 \\
0 & 0 & 0 & R_{b4} & 0 & 0 \\
0 & 0 & 0 & 0 & R_{a1} & 0 \\
0 & 0 & 0 & 0 & 0 & R_c
\end{bmatrix}
\tag{B.30}
$$

$$
\boldsymbol{L} = \begin{bmatrix}
L_{a1} & M_{a1b1} & M_{a1b2} & M_{a1b3} & M_{a1b4} & M_{a1c} \\
M_{a1b1} & L_{b1} & M_{b12} & M_{b13} & M_{b14} & M_{b1c} \\
M_{a1b2} & M_{b12} & L_{b2} & M_{b23} & M_{b24} & M_{b2c} \\
M_{a1b3} & M_{b13} & M_{b23} & L_{b3} & M_{b34} & M_{b3c} \\
M_{a1b4} & M_{b14} & M_{b24} & M_{b34} & L_{b4} & M_{b4c} \\
M_{a1c} & M_{b1c} & M_{b2c} & M_{b3c} & M_{b4c} & L_c
\end{bmatrix}
\tag{B.31}
$$

$$
\boldsymbol{G} = \begin{bmatrix}
\frac{1}{R_{b1}} & 0 & 0 & 0 & 0 & 0 \\
0 & \frac{1}{R_{b2}} & 0 & 0 & 0 & 0 \\
0 & 0 & \frac{1}{R_{b3}} & 0 & 0 & 0 \\
0 & 0 & 0 & \frac{1}{R_{b4}} & 0 & 0 \\
0 & 0 & 0 & 0 & \frac{1}{R_{a1}} & 0 \\
0 & 0 & 0 & 0 & 0 & \frac{1}{R_c}
\end{bmatrix}
\tag{B.32}
$$

$$M^{(0)} = \left[\begin{array}{cccccc|c} C_{a10}+C_{ab1} & -C_{ab1} & C_{ab1} & 0 & 0 & & \\ -C_{ab1} & C_{ab1}+C_{b10}+C_{b34}+C_{b4} & -C_{ab1}-C_{b34}-C_{b4} & 0 & -C_{b4} & & \\ C_{ab1} & -C_{ab1}-C_{b34}-C_{b4} & C_{ab1}+C_{b12}+C_{b2}+C_{b34}+C_{b4} & -C_{b2} & C_{b4} & & \mathbf{0} \\ 0 & 0 & -C_{b2} & C_{b1}+C_{b2} & 0 & & \\ 0 & -C_{b4} & C_{b4} & 0 & C_{b3}+C_{b4} & & \\ \hline & & \mathbf{0} & & & & \boldsymbol{L} \end{array}\right] \tag{B.33}$$

$$\boldsymbol{A}^{(0)} = \begin{bmatrix} 0 & 0 & 0 & 0 & 0 & -1 & 0 & 0 & 0 & 0 & 0 \\ 0 & 0 & 0 & 0 & 0 & 0 & 0 & 0 & 0 & -1 & 0 \\ 0 & 0 & 0 & 0 & 0 & 0 & 0 & -1 & 0 & 1 & 0 \\ 0 & 0 & 0 & 0 & 0 & 0 & -1 & 1 & 0 & 0 & 0 \\ 0 & 0 & 0 & 0 & 0 & 0 & 0 & 0 & -1 & 1 & 0 \\ 1 & 0 & 0 & 0 & 0 & -R_{a1} & 0 & 0 & 0 & 0 & 0 \\ 0 & 0 & 0 & 1 & 0 & 0 & -R_{b1} & 0 & 0 & 0 & 0 \\ 0 & 0 & 1 & -1 & 0 & 0 & 0 & -R_{b2} & 0 & 0 & 0 \\ 0 & 0 & 0 & 0 & 1 & 0 & 0 & 0 & -R_{b3} & 0 & 0 \\ 0 & 1 & -1 & 0 & -1 & 0 & 0 & 0 & 0 & -R_{b4} & 0 \\ 0 & 0 & 0 & 0 & 0 & 0 & 0 & 0 & 0 & 0 & -R_c \end{bmatrix} \tag{B.34}$$

$$\boldsymbol{B}_1^{(0)} = \begin{bmatrix} 1 & 0 & 0 & 0 & 0 & 0 & 0 & 0 & 0 & 0 & 0 \end{bmatrix}^T \tag{B.35}$$

$$\boldsymbol{B}_2^{(0)} = \begin{bmatrix} 0 & 0 & 0 & 0 & 0 & 0 & 0 & 0 & 0 & 0 & 0 \end{bmatrix}^T \tag{B.36}$$

State-space matrices for 16 kVA transformer model, current source at LV terminals.

$$\boldsymbol{A} = \begin{bmatrix}
0 & 0 & 0 & 0 & 0 & -7.9723\times10^{9} & 1.3749\times10^{8} & 8.9341\times10^{7} & -2.8062\times10^{8} & -6.1656\times10^{8} & 0 \\
0 & 0 & 0 & 0 & 0 & -6.7034\times10^{8} & -1.2730\times10^{9} & -8.2718\times10^{8} & -4.6171\times10^{8} & -1.0144\times10^{9} & 0 \\
0 & 0 & 0 & 0 & 0 & 2.2683\times10^{8} & -1.5758\times10^{9} & -1.0239\times10^{9} & 1.5624\times10^{8} & 3.4327\times10^{8} & 0 \\
0 & 0 & 0 & 0 & 0 & 1.3749\times10^{8} & -2.6819\times10^{9} & 1.1061\times10^{9} & 9.4700\times10^{7} & 2.0807\times10^{8} & 0 \\
0 & 0 & 0 & 0 & 0 & -2.8062\times10^{8} & 9.4700\times10^{7} & 6.1536\times10^{7} & -1.8654\times10^{9} & 1.2474\times10^{9} & 0 \\
4437.1 & -56.648 & 78.037 & -140.20 & 12.563 & -43.473 & 2.4017\times10^{5} & -6.3390\times10^{4} & 1.0382\times10^{5} & 7.1819\times10^{4} & -1.5337\times10^{5} \\
-118.81 & 4.5074 & -9.1435 & 12.672 & -4.4070 & 1.1641 & -1.6245\times10^{4} & 1.3740\times10^{4} & -236.54 & -5714.6 & 1.2487\times10^{4} \\
21.389 & -5.6932 & 11.082 & -10.025 & 6.5684 & -0.2096 & 9371.5 & -1.5971\times10^{4} & -2061.1 & 7217.9 & -2051.8 \\
-44.086 & -3.1785 & 4.0538 & -0.7748 & 5.6132 & 0.4319 & -203.04 & -2593.8912 & -5733.5 & 4029.8 & 4704.1 \\
-56.648 & 11.685 & -17.378 & 10.201 & -14.864 & 0.5550 & -9111.5 & 1.6873\times10^{4} & 7485.4 & -1.4815\times10^{4} & 5602.5 \\
2.5395 & -0.0928 & 0.1267 & -0.2407 & 0.0149 & -0.0249 & 417.93 & -100.6840 & 183.43 & 117.61 & -3.0889\times10^{4}
\end{bmatrix} \tag{B.37}$$

$$\boldsymbol{B} = \begin{bmatrix} 7.9723\times10^{9} & 0.6703\times10^{9} & -0.2268\times10^{9} & -0.1375\times10^{9} & 0.2806\times10^{9} & 0 & 0 & 0 & 0 & 0 & 0 \end{bmatrix}^{T} \tag{B.38}$$

$$\boldsymbol{x} = \begin{bmatrix} v_{C_{a10}} & v_{C_{b10}} & v_{C_{b12}} & v_{C_{b1}} & v_{C_{b3}} & i_{L_{a1}} & i_{L_{b1}} & i_{L_{b2}} & i_{L_{b3}} & i_{L_{b4}} & i_{L_c} \end{bmatrix}^{T} \tag{B.39}$$

$$\boldsymbol{u} = \begin{bmatrix} i_1 \end{bmatrix} \tag{B.40}$$

State-space matrices for 16 kVA transformer model, voltage source at LV terminals.

$$\boldsymbol{A} = \begin{bmatrix} 0 & 0 & 0 & 0 & 0 & -1.2845\times10^{9} & -8.3469\times10^{8} & -4.3812\times10^{8} & -9.6260\times10^{8} & 0 \\ 0 & 0 & 0 & 0 & 0 & -1.5718\times10^{9} & -1.0214\times10^{9} & 1.4825\times10^{8} & 3.2573\times10^{8} & 0 \\ 0 & 0 & 0 & 0 & 0 & -2.6795\times10^{9} & 1.1076\times10^{9} & 8.9861\times10^{7} & 1.9744\times10^{8} & 0 \\ 0 & 0 & 0 & 0 & 0 & 8.9861\times10^{7} & 5.8391\times10^{7} & -1.8555\times10^{9} & 1.2691\times10^{9} & 0 \\ -56.648 & 78.037 & -140.20 & 12.5630 & -43.4730 & 2.4017\times10^{5} & -6.3390\times10^{4} & 1.0382\times10^{5} & 7.1819\times10^{4} & -1.5337\times10^{5} \\ 4.5074 & -9.1435 & 12.672 & -4.4070 & 1.1641 & -1.6245\times10^{4} & 1.3740\times10^{4} & -236.54 & -5714.6 & 1.2487\times10^{4} \\ -5.6932 & 11.082 & -10.025 & 6.5684 & -0.2096 & 9371.5 & -1.5971\times10^{4} & -2061.1 & 7217.9 & -2051.8 \\ -3.1785 & 4.0538 & -0.7748 & 5.6132 & 0.4319 & -203.04 & -2593.9 & -5733.5 & 4029.8 & 4704.1 \\ 11.685 & -17.3780 & 10.201 & -14.8640 & 0.5550 & -9111.5 & 1.6873\times10^{4} & 7485.4 & -1.4815\times10^{4} & 5602.5 \\ -0.0928 & 0.1267 & -0.2407 & 0.0149 & -0.0249 & 417.93 & -100.68 & 183.43 & 117.61 & -3.0889\times10^{4} \end{bmatrix} \tag{B.41}$$

$$\boldsymbol{B} = \begin{bmatrix} 0 & 0 & 0 & 0 & 4432.9 & -118.55 & 20.999 & -44.257 & -55.870 & 2.5327 \end{bmatrix}^T \tag{B.42}$$

$$\boldsymbol{x} = \begin{bmatrix} v_{C_{b10}} & v_{C_{b12}} & v_{C_{b1}} & v_{C_{b3}} & i_{L_{a1}} & i_{L_{b1}} & i_{L_{b2}} & i_{L_{b3}} & i_{L_{b4}} & i_{L_c} \end{bmatrix}^T \tag{B.43}$$

$$\boldsymbol{u} = \begin{bmatrix} e_1 \end{bmatrix} \tag{B.44}$$

Appendix C

EMTP Implementation of the Transformer Model

The following data files show how the proposed transformer model structure can be implemented in the EMTP. Data files for the 16 kVA, 22 kV / 240 V, single-phase test transformer, using the parameters given in table 6.1, are presented. These data files were created for use with the ATP version of the EMTP and tested with the January 1996 Salford-DBOS release of the program, running under MS-DOS on an IBM-compatible personal computer [109].

The node labelling and the element values that were used to create the data cases are shown in figure C.1 on page 183. For clarity, the self- and mutual inductance values have not been included in figure C.1, however, these can be obtained from the inductance matrix, which is given by (with all elements in H):

$$L = \begin{array}{c} \\ a1 \\ b1 \\ b2 \\ b3 \\ b4 \\ c \end{array} \begin{array}{c} \begin{array}{cccccc} a1 & b1 & b2 & b3 & b4 & c \end{array} \\ \begin{bmatrix} 0.3576444 & 7.1616985 & 10.7253580 & 12.3423966 & 7.5831988 & 3.6618278 \\ 7.1616985 & 143.6851960 & 214.9940672 & 247.0199271 & 151.8179181 & 73.3969840 \\ 10.7253580 & 214.9940672 & 322.2530235 & 370.2157153 & 227.6465639 & 109.9184771 \\ 12.3423966 & 247.0199271 & 370.2157153 & 426.7300908 & 262.0045266 & 126.4878575 \\ 7.5831988 & 151.8179181 & 227.6465639 & 262.0045266 & 161.0845498 & 77.7139791 \\ 3.6618278 & 73.3969840 & 109.9184771 & 126.4878575 & 77.7139791 & 37.50 \end{bmatrix} \end{array}.$$

Note that in the following data files, inductances are given in mH and capacitances are given in μF. Resistances are given in Ω.

C.1 Data File for Frequency-domain Simulations

The following data file shows how the LV open-circuit input impedance frequency response of the 16 kVA transformer can be calculated by ATP, by using the FREQUENCY SCAN option. The equivalent circuit is excited by a 1 A current source at node NODE01 (the LV terminals). The input impedance is then given by the voltage response across C_{a1} (line 18). By changing the location and type of the source (on line 55) and requesting output of the relevant voltage, other frequency responses can be obtained.

```
1   BEGIN NEW DATA CASE
2   C ------------------------------------------------------------------------------
3   C 22kV/240V, 16 kVA SINGLE-PHASE TRANSFORMER
4   C FREQUENCY RESPONSE SIMULATIONS
5   C LV OPEN-CIRCUIT INPUT IMPEDANCE
6   C ------------------------------------------------------------------------------
7   C                         FMINFS  DELFFS  FMAXFS     NPD
8   FREQUENCY SCAN              10.0           1.0E5     100
9   C                  (0=mH)  (0=uF)
10  C DELTAT    TMAX    XOPT    COPT  EPSLIN  TOLMAT  TSTART
11      1E-6       0       0       0
12  C   IOUT   IPLOT  IDOUBL  KSSOUT  MAXOUT    IPUN  MEMSAV    ICAT  NERERG  IPRSUP
13         1       1       1       3       0                      1
14  $VINTAGE, 1
15  C        1         2         3         4         5         6         7         8
16  C 345678901234567890123456789012345678901234567890123456789012345678901234567890
17  C  NODE1 NODE2 NODE3 NODE4<------R------><------L------><------C------>     0
18    NODE01                                                      0.0722E-3   * 2
19    NODE02                                                      0.1022E-3
20    NODE02NODE04                                                0.1638E-3
21    NODE04                                                      0.2685E-3
22    NODE02NODE03                                                0.2281E-3
23    NODE03NODE04                                                0.3510E-3
24    NODE04NODE05                                                0.4110E-3
25    NODE05                                                      0.1871E-3
26    NODE01NODE04                                                60.030E-6
27    NODE06                          60.39E3
28  C                         <------R------><------L------>
29  51NODE01                        0.009798   357.644400733
30  52NODE02NODE03                       0.0  7161.698462583
31                                  2021.43 143685.19595107
32  53NODE03NODE04                       0.0 10725.358005762
33                                       0.0 214994.06721455
34                                  2963.70 322253.02353114
35  54NODE04NODE05                       0.0 12342.396576185
36                                       0.0 247019.92710387
37                                       0.0 370215.71531121
38                                  2354.97 426730.09076669
39  55NODE05                             0.0  7583.198794562
40                                       0.0 151817.91813314
41                                       0.0 227646.56393629
```

```
42                                          0.0 262004.52662276
43                                      1267.81 161084.54979598
44  56NODE06                               0.0  3661.827798873
45                                         0.0 73396.984018946
46                                         0.0 109918.47708910
47                                         0.0 126487.85747294
48                                         0.0 77713.979074762
49                                      0.0001 37500.000000000
50  $VINTAGE, 0
51  BLANK CARD ENDING BRANCH CARDS
52  BLANK CARD ENDING SWITCH CARDS
53  C  1A CURRENT SOURCE AT NODE01
54  C <NODE>ST AMPLITUDE FREQUENCY     PHASE   DEG/SEC              TSTART     TSTOP
55  14NODE01-1   1.41421       1.0       0.0         0                -1.0     100.0
56  BLANK CARD ENDING SOURCE CARDS
57    NODE01NODE02
58  BLANK CARD ENDING OUTPUT VARIABLE REQUESTS
59  BLANK CARD ENDING PLOT CARDS
60  BEGIN NEW DATA CASE
```

C.2 Data File for Time-domain Simulations

The following data file was used to calculate the LV terminal voltage response of the 16 kVA transformer to a PRBS input current at the LV terminals. The input current data, which was sampled in the laboratory, is read from an external file at line 59. By omitting line 59 and adjusting the source card on line 54, any one of the standard ATP sources can be applied instead.

```
1   BEGIN NEW DATA CASE
2   C ------------------------------------------------------------------------------
3   C 22kV/240V, 16 kVA SINGLE-PHASE TRANSFORMER
4   C TIME DOMAIN SIMULATIONS
5   C INPUT DATA IS READ FROM EXTERNAL FILE
6   C Lc IS SET TO 38.5H TO AVOID NUMERICAL PROBLEMS
7   C ------------------------------------------------------------------------------
8   C                  (0=mH)  (0=uF)
9   C DELTAT    TMAX    XOPT    COPT  EPSLIN  TOLMAT  TSTART
10    2.0E-7  0.0010       0       0
11  C   IOUT   IPLOT  IDOUBL  KSSOUT  MAXOUT    IPUN  MEMSAV    ICAT  NERERG  IPRSUP
12        50       1       1       3       0                      1
13  $VINTAGE, 1
14  C        1         2         3         4         5         6         7         8
15  C 345678901234567890123456789012345678901234567890123456789012345678901234567890
16  C  NODE1 NODE2 NODE3 NODE4<------R------><------L------><------C------->     0
17    NODE01                                                  0.0722E-3     2
18    NODE02                                                  0.1022E-3     2
19    NODE02NODE04                                            0.1638E-3
```

```
    NODE04                                                          0.2685E-3
    NODE02NODE03                                                    0.2281E-3
    NODE03NODE04                                                    0.3510E-3
    NODE04NODE05                                                    0.4110E-3
    NODE05                                                          0.1871E-3
    NODE01NODE04                                                    60.030E-6
    NODE06                        60.395E3
C                              <------R-------><------L------->
51NODE01                          0.009798   357.644400733
52NODE02NODE03                         0.0  7161.698462583
                                  2021.43 143685.19595107
53NODE03NODE04                         0.0 10725.358005762
                                       0.0 214994.06721455
                                  2963.70 322253.02353114
54NODE04NODE05                         0.0 12342.396576185
                                       0.0 247019.92710387
                                       0.0 370215.71531121
                                  2354.97 426730.09076669
55NODE05                               0.0  7583.198794562
                                       0.0 151817.91813314
                                       0.0 227646.56393629
                                       0.0 262004.52662276
                                  1267.81 161084.54979598
56NODE06                               0.0  3661.827798873
                                       0.0 73396.984018946
                                       0.0 109918.47708910
                                       0.0 126487.85747294
                                       0.0 77713.979074762
                                    0.0001 38500.000000000
$VINTAGE, 0
BLANK CARD ENDING BRANCH CARDS
BLANK CARD ENDING SWITCH CARDS
C USER DEFINED CURRENT SOURCE, TO BE READ FROM EXTERNAL FILE WITH $INCLUDE BELOW
C <NODE>                                                          TSTART     TSTOP
 1NODE01                                                            -1.0     0.001
BLANK CARD ENDING SOURCE CARDS
  NODE01NODE02
BLANK CARD ENDING OUTPUT VARIABLE REQUESTS
C INCLUDE INPUT DATA FROM EXTERNAL FILE
$INCLUDE FILENAME.EXT
BLANK CARD ENDING PLOT CARDS
BEGIN NEW DATA CASE
```

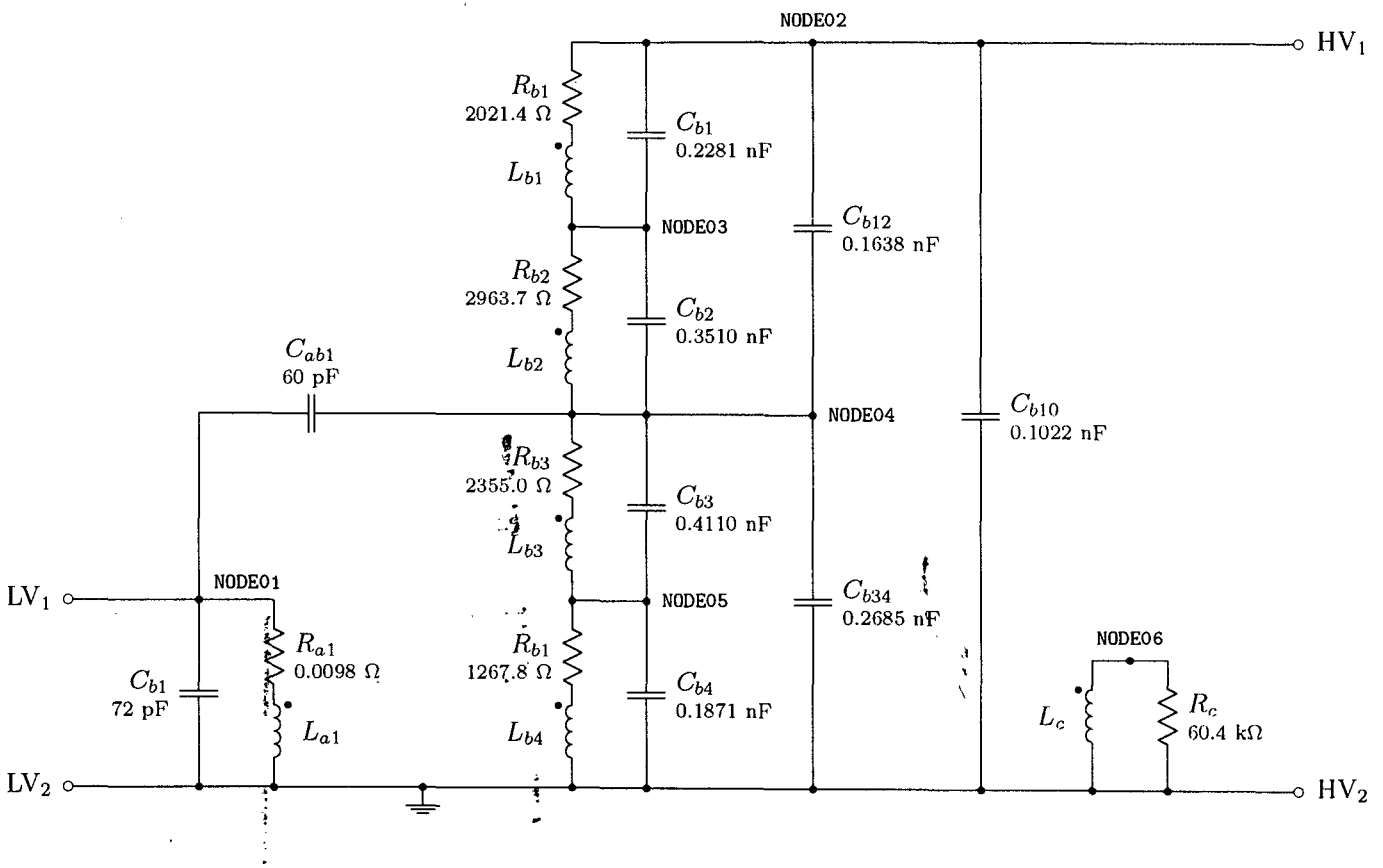

Figure C.1: 16 kVA Transformer equivalent circuit node labelling for ATP implementation.

Appendix D

11 kV / 110 V Voltage Transformer Frequency Responses

This appendix presents additional results for the 11 kV / 110 V voltage transformer model discussed in sections 7.2.1 and 7.2.2. The frequency responses shown below support the accuracy of the parameter estimates that were obtained for the three-section and the four-section HV winding voltage transformer models respectively.

The following measured and simulated frequency responses are shown for both the three-section model and the four-section model, in sections D.1 and D.2 respectively:

(a) HV open-circuit input impedance, $\mathbf{Z}_{Hoc}(j\omega)$.

(b) HV short-circuit input impedance, $\mathbf{Z}_{Hsc}(j\omega)$.

(c) LV–HV voltage transformation ratio, $\mathbf{H}_{LH}(j\omega)$.

(d) HV–LV voltage transformation ratio, $\mathbf{H}_{HL}(j\omega)$.

D.1 Three-Section HV Winding Model

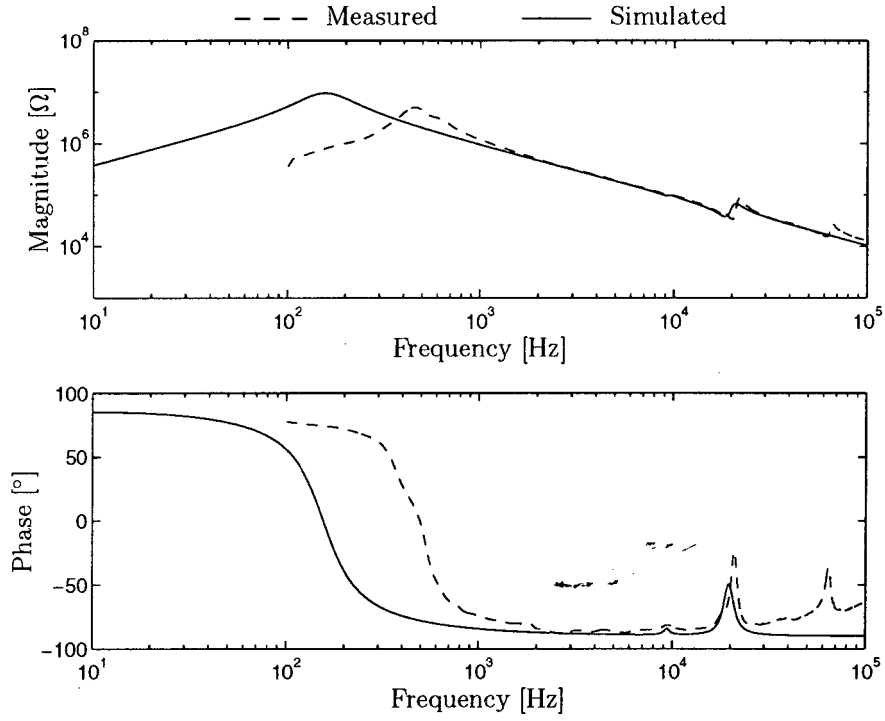

Figure D.1: Measured and simulated HV open-circuit input impedance frequency response, $\mathbf{Z}_{Hoc}(j\omega)$ (three HV winding sections).

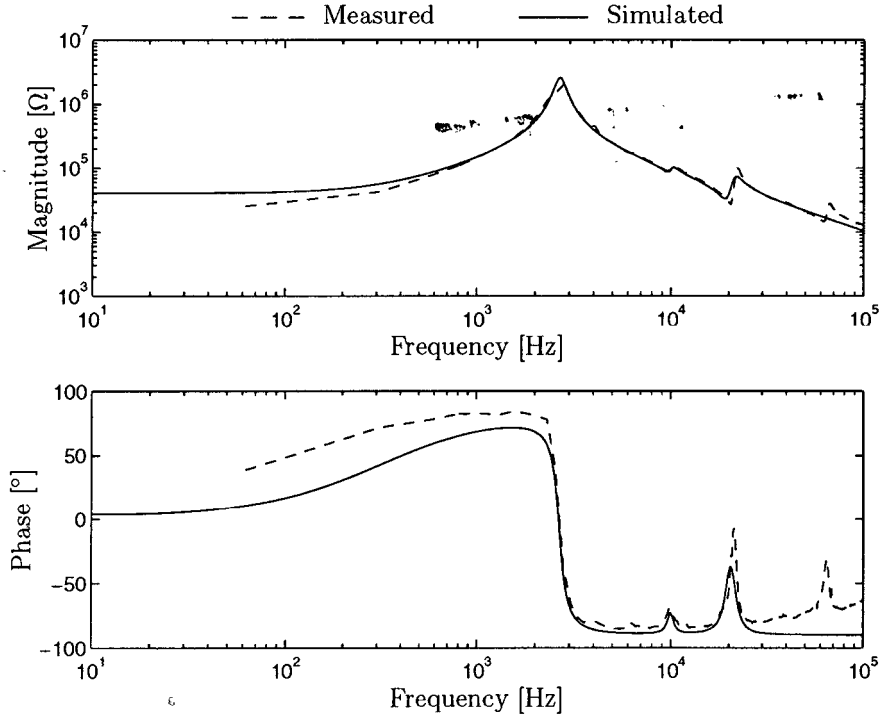

Figure D.2: Measured and simulated HV short-circuit input impedance frequency response, $\mathbf{Z}_{Hsc}(j\omega)$ (three HV winding sections).

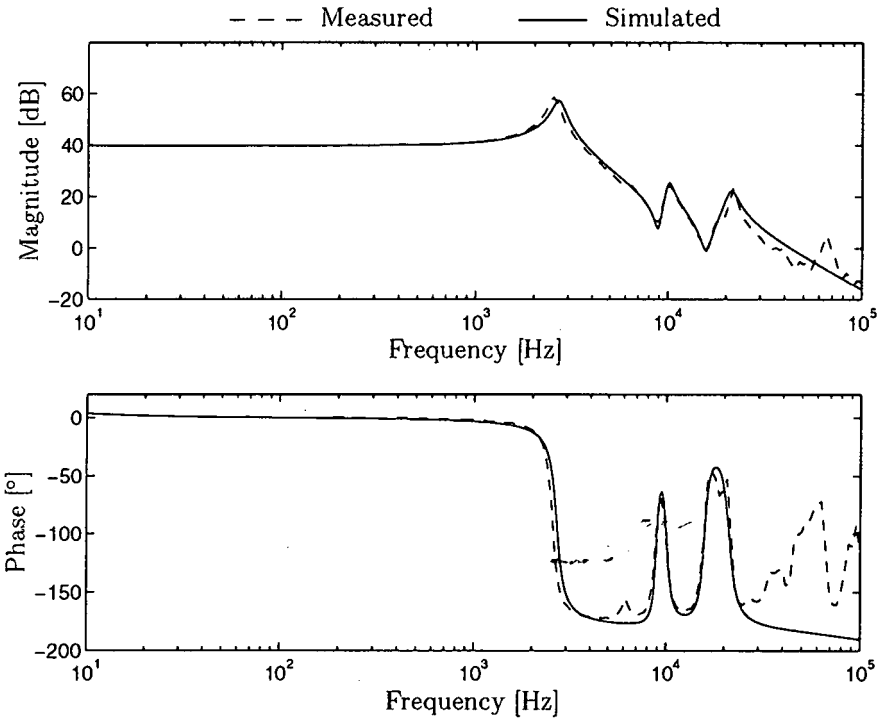

Figure D.3: Measured and simulated LV–HV voltage transformation ratio frequency response, $\mathbf{H}_{LH}(j\omega)$ (three HV winding sections).

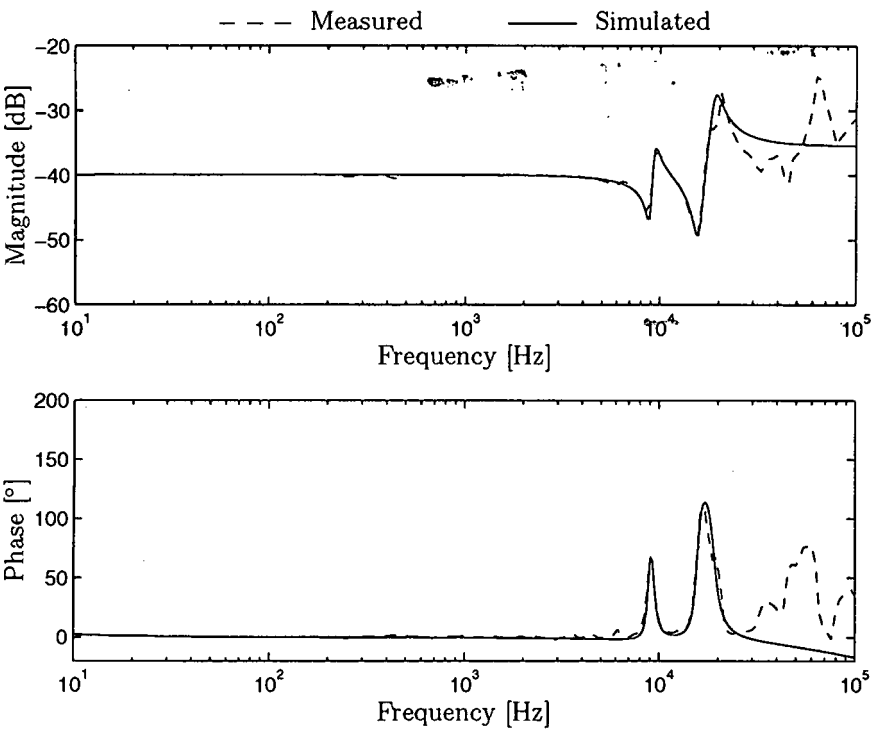

Figure D.4: Measured and simulated HV–LV voltage transformation ratio frequency response, $\mathbf{H}_{HL}(j\omega)$ (three HV winding sections).

D.2 Four-Section HV Winding Model

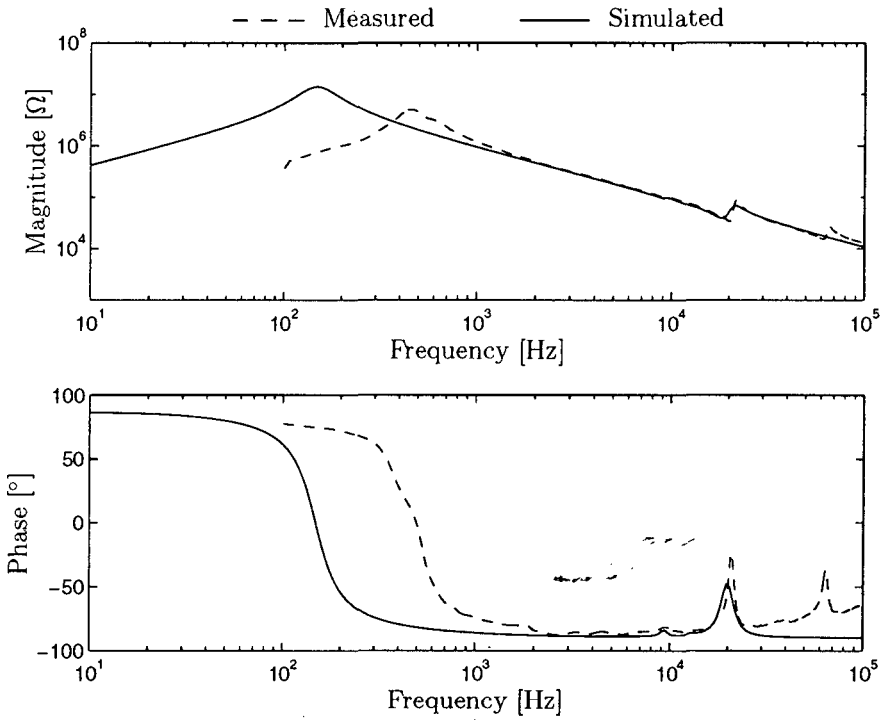

Figure D.5: Measured and simulated HV open-circuit input impedance frequency response, $\mathbf{Z}_{Hoc}(j\omega)$ (four HV winding sections).

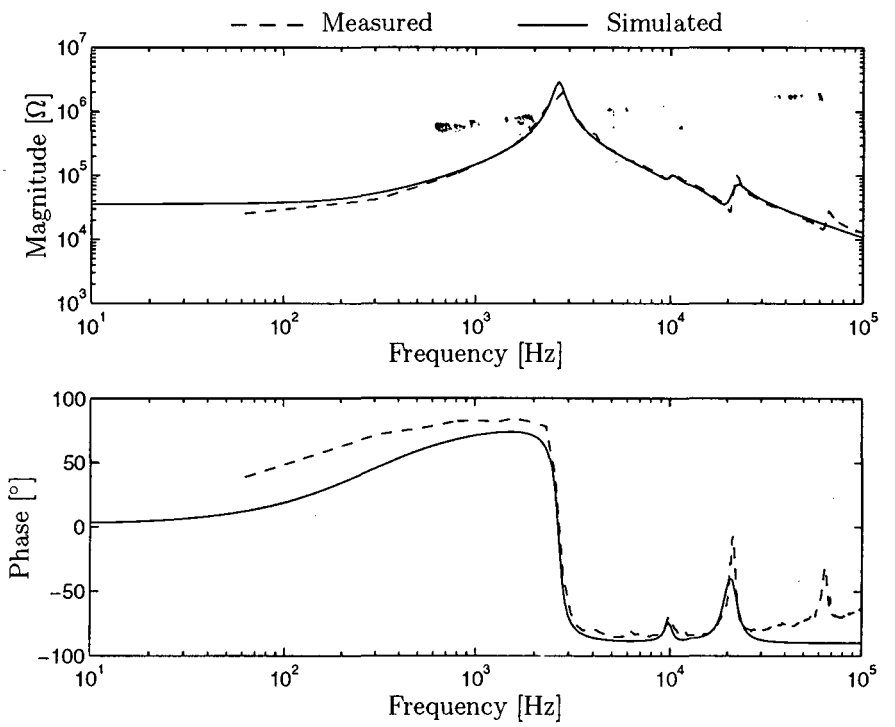

Figure D.6: Measured and simulated HV short-circuit input impedance frequency response, $\mathbf{Z}_{Hsc}(j\omega)$ (four HV winding sections).

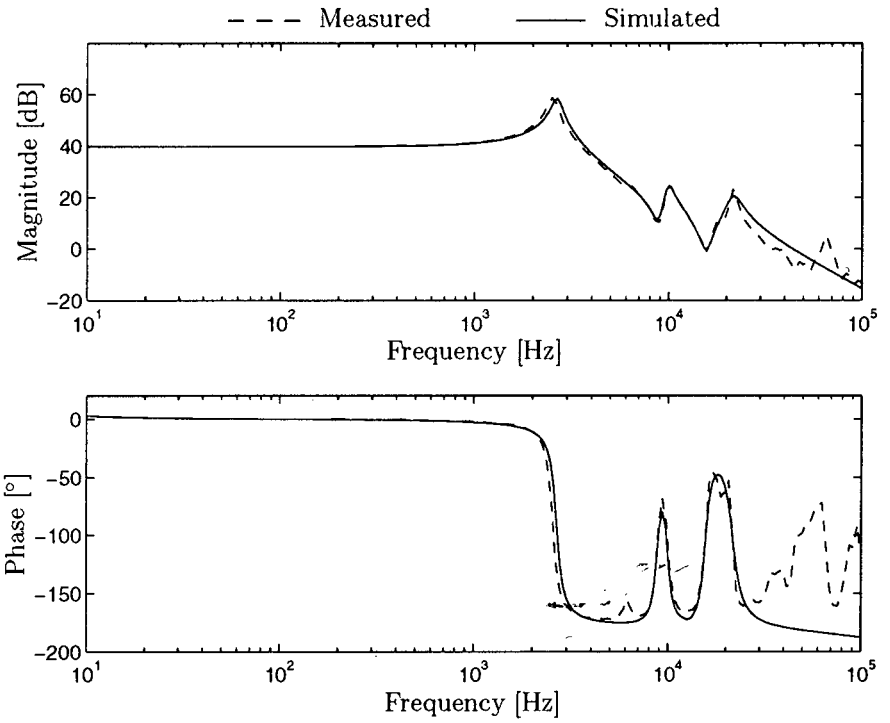

Figure D.7: Measured and simulated LV–HV voltage transformation ratio frequency response, $\mathbf{H}_{LH}(j\omega)$ (four HV winding sections).

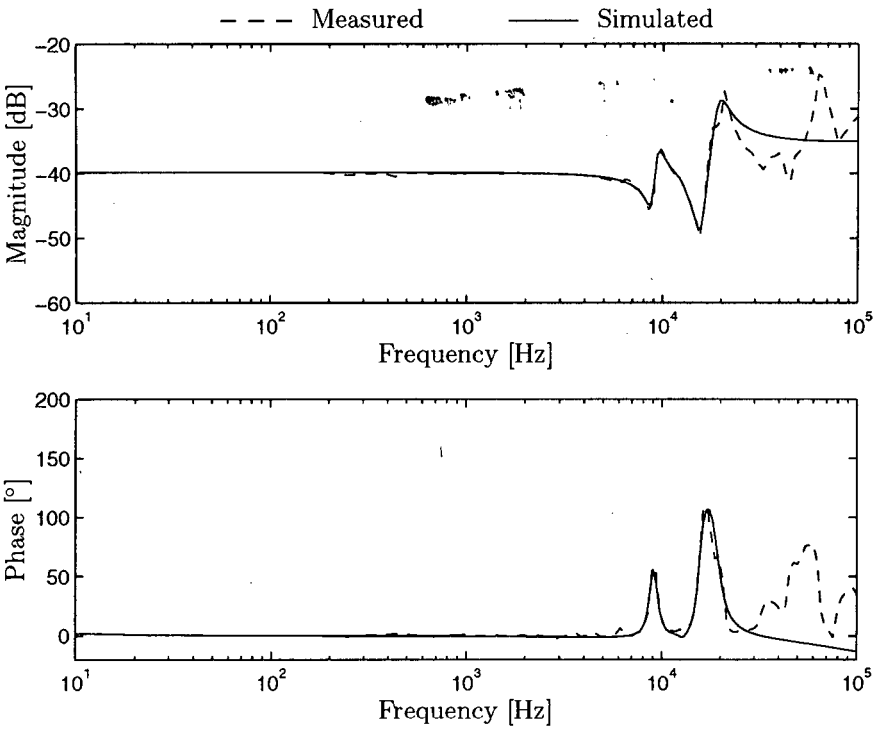

Figure D.8: Measured and simulated HV–LV voltage transformation ratio frequency response, $\mathbf{H}_{HL}(j\omega)$ (four HV winding sections).

References

[1] M. G. Say, *Alternating Current Machines*. Pitman Publishing Ltd., London, 5th ed., 1983, ISBN 0-273-01968-6.

[2] K. Karsai, D. Kerényi and L. Kiss, *Large Power Transformers*. Elsevier Science Publishers B.V., Amsterdam, 1986, ISBN 0-444-99511-0.

[3] The MathWorks, Inc., 24 Prime Park Way, Natick, MA 01760-1500, MATLAB *User's Guide*, 1993.

[4] E. P. Dick and C. C. Erven, "Transformer diagnostic testing by frequency response analysis", *IEEE Transactions on Power Apparatus and Systems*, vol. PAS-97, no. 6, pp. 2144–2150, November 1978.

[5] P. T. M. Vaessen and E. Hanique, "A new frequency response analysis method for power transformers", *IEEE Transactions on Power Delivery*, vol. 7, no. 1, pp. 384–391, January 1992.

[6] J. Bak-Jensen, B. Bak-Jensen and S. D. Mikkelsen, "Detection of faults and ageing phenomena in transformers by transfer functions", *IEEE Transactions on Power Delivery*, vol. 10, no. 1, pp. 308–314, January 1995.

[7] R. Malewski and B. Poulin, "Impulse testing of power transformers using the transfer function method", *IEEE Transactions on Power Delivery*, vol. TPD-3, no. 2, pp. 476–489, April 1988.

[8] A. J. Vandermaar, "Transformer condition monitoring by frequency response analysis", *Proc. 10th International Symposium on High Voltage Engineering*, Montréal, 25–29 August 1997.

[9] T. Leibfried and K. Feser, "Off-line- and on-line-monitoring of power transformers using the transfer function method", *Conference Record of the 1996 IEEE International Symposium on Electrical Insulation*, Montréal, pp. 34–37, 16–19 June 1996.

[10] J. A. Lapworth, P. N. Jarman and I. R. Funnell, "Condition assessment techniques for large power transformers", *IEE Conference Publication No. 406: The Reliability of Transmission and Distribution Equipment*, pp. 85–90, 29–31 March 1995.

[11] S. D. Mikkelsen, J. Bak-Jensen, B. Bak-Jensen and J. Tolstrup Sørensen, "Sensitivity of identified transfer functions in transformer diagnosis", *21st Electrical/Electronic Insulation Conference and Electrical Manufacturing and Coil Winding Exhibition*, Chicago, pp. 533–537, 1993.

[12] S. M. Islam and G. Ledwich, "Locating transformer faults through sensitivity analysis of high frequency modeling using transfer function approach", *Conference Record of the 1996 IEEE International Symposium on Electrical Insulation*, Montréal, pp. 38–41, 16–19 June 1996.

[13] S. M. Islam, K. M. Coates and G. Ledwich, "Identification of high frequency transformer equivalent circuit using MATLAB from frequency domain data", *Proc. 1997 IEEE Industry Applications Conference (32nd IAS Annual Meeting)*, New Orleans, pp. 357–364, 5–9 October 1997.

[14] J. Bak-Jensen, B. Bak-Jensen, S. D. Mikkelsen and C. G. Jensen, "Parametric identification in potential transformer modelling", *IEEE Transactions on Power Delivery*, vol. 7, no. 1, pp. 70–76, January 1992.

[15] B. Bak-Jensen, *Modelling of High Voltage Components*, Ph.D. thesis, Institut for Energiteknik, Aalborg Universiteitscenter, Pontoppidanstraede 101, DK-9220 Aalborg East, Denmark, September 1992, ISBN 87-89179-07-2.

[16] S. D. Mikkelsen, *Diagnosis of the Condition of Electric Components Using Transfer Functions*, Ph.D. thesis, Institut for Energiteknik, Aalborg Universiteitscenter, Pontoppidanstraede 101, DK-9220 Aalborg East, Denmark, December 1992, ISBN 87-89179-08-0.

[17] D. A. Douglass, "Potential transformer accuracy at 60 Hz voltages above and below rating and at frequencies above 60 Hz", *IEEE Transactions on Power Apparatus and Systems*, vol. PAS-100, no. 3, pp. 1370–1375, March 1981.

[18] F. de León and A. Semlyen, "Complete transformer model for electromagnetic transients", *IEEE Transactions on Power Delivery*, vol. 9, no. 1, pp. 231–239, January 1994.

[19] A. Morched, L. Martí and J. Ottevangers, "A high frequency transformer model for the EMTP", *IEEE Transactions on Power Delivery*, vol. 8, no. 3, pp. 1615–1626, July 1993.

[20] S. Chimlaki and J. R. Martí, "Simplified three-phase transformer model for electromagnetic transient studies", *IEEE Transactions on Power Delivery*, vol. 10, no. 3, pp. 1316–1325, July 1995.

[21] R. G. Koch, *The Broadband Modelling of Electromagnetic Voltage Transformers Using Parameter Estimation Techniques*, Master's thesis, Department of Electrical and Electronic Engineering, University of Stellenbosch, South Africa, February 1992.

[22] J. van Rooijen, *A New Wideband Lumped Parameter Model for Magnetic Voltage Transformers*, Master's thesis, Department of Electrical and Electronic Engineering, University of Stellenbosch, South Africa, November 1996.

[23] H. J. Vermeulen, R. G. Koch and W. L. Rawlins, "Frequency-domain characteristics of high-ratio step-up transformers for high voltage test applications", *Proc. 6th International Symposium on High Voltage Engineering*, New Orleans, 28 August – 1 September 1989, Paper 11.02.

[24] R. Malewski and J. Douville, "Measuring properties of voltage and current transformers for the higher harmonic frequencies", *Proc. IEEE Canadian Communications and Power Conference*, Montréal, pp. 327–329, 1976, Paper 76 CH1126-2 REG 7.

[25] H. J. Vermeulen, R. G. Koch and W. L. Rawlins, "Broadband modelling of magnetic voltage transformers through application of parameter estimation techniques", *Proc. 6th International Symposium on High Voltage Engineering*, New Orleans, 28 August – 1 September 1989, Paper 50.12.

[26] G. Olivier, R. P. Bouchard, Y. Gervais and D. Mukhedkar, "Frequeny response of HV test transformers and the associated measurement problems", *IEEE Transactions on Power Apparatus and Systems*, vol. PAS-99, no. 1, pp. 141–146, January 1980.

[27] IEEE Task Force on Harmonics Modeling and Simulation, "Modeling and simulation of the propagation of harmonics in electric power networks, Parts I and II", *IEEE Transactions on Power Delivery*, vol. 11, no. 1, pp. 452–474, January 1996.

[28] J. Arrillaga, D. A. Bradley and P. S. Bodger, *Power System Harmonics*. Wiley-Interscience, John Wiley & Sons Ltd., 1988, ISBN 0-471-90640-9.

[29] G. T. Heydt, *Electric Power Quality.* Stars in a Circle Publications, 2932 SR 26 W, West LaFayette, Indiana 47906, USA, 1994.

[30] J. J. LaForest, R. H. Lasseter, J. Reeve and C. B. Lindh, "Modeling of the DC converter equipment in the carrier band", *IEEE Transactions on Power Apparatus and Systems*, vol. PAS-101, no. 7, pp. 2137–2145, July 1982.

[31] L. Ljung, *System Identification: Theory for the User.* Prentice-Hall, Inc., Englewood Cliffs, New Jersey, 1987, ISBN 0-13-881640-9.

[32] T. Söderström and P. Stoica, *System Identification.* Prentice-Hall International (UK) Ltd., 1988, ISBN 0-13-881236-5.

[33] S. Benda, *Interference-free Electronics.* Studentlitteratur, Chartwell-Bratt Ltd., Lund, Sweden, 1995, ISBN 0-86238-255-6.

[34] L. S. Bobrow, *Elementary Linear Circuit Analysis.* Holt, Rinehart and Winston, Inc., New York, 2nd ed., 1987, ISBN 0-03-007298-0.

[35] A. E. Fitzgerald, C. Kingsley, Jr. and S. D. Umans, *Electric Machinery.* McGraw-Hill Book Company Japan, Ltd., 4th ed., 1983, ISBN 0-07-066286-X.

[36] H. W. Dommel, *EMTP Theory Book.* Microtran Power Systems Analysis Corporation, 1992.

[37] X. Chen, "A three-phase multi-legged transformer model in ATP using the directly-formed inverse inductance matrix", *IEEE Transactions on Power Delivery*, vol. 11, no. 3, pp. 1554–1562, July 1996.

[38] E. P. Dick and W. Watson, "Transformer models for transient studies based on field measurements", *IEEE Transactions on Power Apparatus and Systems*, vol. PAS-100, no. 1, pp. 409–419, January 1980.

[39] F. de León and A. Semlyen, "A simple representation of dynamic hysteresis losses in power transformers", *IEEE Transactions on Power Delivery*, vol. 10, no. 1, pp. 315–321, January 1995.

[40] D. A. Bradley, P. S. Bodger and P. R. Hyland, "Harmonic response tests on voltage transducers for the New Zealand power system", *IEEE Transactions on Power Apparatus and Systems*, vol. PAS-104, no. 7, pp. 1750–1756, July 1985.

[41] G. R. Slemon, *Magnetoelectric Devices: Transducers, Transformers and Machines.* John Wiley & Sons Inc., 1966.

[42] D. A. Douglass, "Current transformer accuracy with asymmetric and high frequency fault currents", *IEEE Transactions on Power Apparatus and Systems*, vol. PAS-100, no. 3, pp. 1006–1011, March 1981.

[43] S.-P. Ladewig, *The Broadband Modelling of Two-winding Transformers*, Master's thesis, Department of Electrical and Electronic Engineering, University of Stellenbosch, South Africa, December 1997.

[44] A. Keyhani, S. W. Chua and S. A. Sebo, "Maximum likelihood estimation of transformer high frequency parameters from test data", *IEEE Transactions on Power Delivery*, vol. 6, no. 2, pp. 858–865, April 1991.

[45] R. C. Dugan, R. Gabrik, J. C. Wright and K. W. Patten, "Validated techniques for modelling shell-form EHV transformers", *IEEE Transactions on Power Delivery*, vol. 4, no. 2, pp. 1070–1078, April 1989.

[46] R. C. Degeneff, "A general method for determining resonances in transformer windings", *IEEE Transactions on Power Apparatus and Systems*, vol. PAS-96, no. 2, pp. 423–430, March 1977.

[47] L. M. Popović, "Analytical expressions for estimating resonant frequencies of machine and transformer windings", *IEEE Transactions on Power Delivery*, vol. 7, no. 3, pp. 1338–1344, July 1992.

[48] P. Chowdhuri, "Calculation of series capacitance for transient analysis of windings", *IEEE Transactions on Power Delivery*, vol. PWRD-2, no. 1, pp. 133–139, January 1987.

[49] B. Heller and A. Veverka, *Surge Phenomena in Electrical Machines.* Iliffe Books Ltd., London, 1968.

[50] W. J. McNutt, T. J. Blalock and R. A. Hinton, "Response of transformer windings to system transient voltages", *IEEE Transactions on Power Apparatus and Systems*, vol. PAS-93, pp. 457–467, March 1974.

[51] F. de León and A. Semlyen, "Reduced order model for transformer transients", *IEEE Transactions on Power Delivery*, vol. 7, no. 1, pp. 361–369, January 1992.

[52] R. J. Galarza, J. H. Chow and R. C. Degeneff, "Transformer model reduction using time and frequency domain sensitivity techniques", *IEEE Transactions on Power Delivery*, vol. 10, no. 2, pp. 1052–1059, April 1995.

[53] R. C. Degeneff, M. R. Gutierrez and M. Vakilian, "Nonlinear, lumped parameter transformer model reduction technique", *IEEE Transactions on Power Delivery*, vol. 10, no. 2, pp. 862–868, April 1995.

[54] K. Heuck, R. Kegel, K. Voußem and K. Brodersen, "Simulation von einpolig-isolierten induktiewen Nieder- und Mittelspannungswandlern", *ETZ Archiv*, vol. 5, no. 6, pp. 189–196, June 1983.

[55] D. J. Wilcox, W. G. Hurley and M. Conlon, "Calculation of self and mutual impedances between sections of transformer windings", *IEE Proceedings*, vol. 136, Part C, no. 5, pp. 308–314, 1989.

[56] D. Wilcox, M. Conlon and W. G. Hurley, "Calculation of self and mutual impedances for coils on ferromagnetic cores", *IEE Proceedings*, vol. 135, Part A, no. 7, pp. 470–476, September 1988.

[57] M. Condon and D. J. Wilcox, "Capacitance calculations in transformer windings", *Proc. 31st Universities Power Engineering Conference*, Iraklio, Greece, pp. 1107–1080, 18–20 September 1996.

[58] R. C. Degeneff, M. R. Gutierrez and P. J. McKenny, "A method for constructing reduced order transformer models from detailed lumped parameter models", *IEEE Transactions on Power Delivery*, vol. 7, no. 2, pp. 649–655, April 1991.

[59] F. de León and A. Semlyen, "Efficient calculation of elementary parameters of transformers", *IEEE Transactions on Power Delivery*, vol. 7, no. 1, pp. 376–383, January 1992.

[60] M. Gutierrez and R. C. Degeneff, "Linear, lumped parameter transformer model reduction technique", *IEEE Transactions on Power Delivery*, vol. 10, no. 2, pp. 853–861, April 1995.

[61] D. J. Leonard and D. J. Wilcox, "Front-end representation of modal transformer models", *Proc. 30th Universities Power Engineering Conference*, London, pp. 289–292, 5–7 September 1995.

[62] D. J. Wilcox and T. P. McHale, "Modified theory of modal analysis for the modelling of multiwinding transformers", *IEE Proceedings*, vol. 139, Part C, no. 6, pp. 505–512, November 1992.

[63] D. J. Wilcox, W. G. Hurley, T. P. McHale and M. Conlon, "Application of modified modal theory in the modelling of practical transformers", *IEE Proceedings*, vol. 139, Part C, no. 6, pp. 513–520, November 1992.

[64] G. R. Slemon, "Equivalent circuits for transformers and machines, including non-linear effects", *IEE Proceedings*, vol. 100, Part IV, pp. 129–143, July 1953.

[65] R. Kegel, K. Heuck and C. Ruchhotz, "Simulation der Frequenzgänge zweipolig isolierter Mittelspannungswandler", *ETZ Archiv*, vol. 6, no. 11, pp. 373–379, 1984.

[66] K. Dettmann, K. Heuck, R. Kegel and E. Waldhaim, "Kompensation von Eigenschwingungen bei hochohmigen Drosselspulen und Spannungswandlern des Mittelspannungsbereiches", *ETZ Archiv*, vol. 5, no. 10, pp. 309–313, October 1983.

[67] D. J. Wilcox, "Theory of transformer modelling using modal analysis", *IEE Proceedings*, vol. 138, Part C, no. 2, pp. 121–128, March 1991.

[68] D. J. Wilcox, M. Condon, D. J. Leonard and T. P. McHale, "Time-domain modelling of power transformers using modal analysis", *IEE Proc. Electrical Power Applications*, vol. 144, no. 2, pp. 77–84, March 1997.

[69] P. T. M. Vaessen, "Transformer model for high frequencies", *IEEE Transactions on Power Delivery*, vol. 3, no. 4, pp. 1761–1768, October 1988.

[70] P. Glaninger, "Modale Parameter der elektrischen Eigenschwingungen von Transformatoren", *ETZ Archiv*, vol. 6, no. 12, pp. 399–405, December 1984.

[71] A. Oğuz Soysal, "A method for wide frequency range modelling of power transformers and rotating machines", *IEEE Transactions on Power Delivery*, vol. 8, no. 4, pp. 1802–1810, October 1993.

[72] A. Oğuz Soysal and A. Semlyen, "Practical transfer function estimation and its application to wide frequency range representation of transformers", *IEEE Transactions on Power Delivery*, vol. 8, no. 3, pp. 1627–1633, July 1993.

[73] R. Caldecott, Y. Liu, S. A. Sebo, D. G. Kasten and S. E. Wright, "Measurement of the frequency dependent impedance of major station equipment", *IEEE Transactions on Power Delivery*, vol. 5, no. 1, pp. 474–480, January 1990.

[74] J. Schoukens and R. Pintleton, *Identification of Linear Systems: A Practical Guideline to Accurate Modeling*. Pergamon Press, 1991, ISBN 0-08-040734-X.

[75] L. Ljung, *System Identification Toolbox.* The MathWorks, Inc., 24 Prime Park Way, Natick, MA 01760-1500, 1982.

[76] I. Kollár, *Frequency Domain System Identification Toolbox.* The MathWorks, Inc., 24 Prime Park Way, Natick, MA 01760-1500, 1994.

[77] K. J. Åström, "Maximum likelihood and prediction error methods", *Automatica*, vol. 16, pp. 551–574, 1980.

[78] A. Keyhani, H. Tsai and A. Abur, "Maximum likelihood estimation of high frequency machine and transformer winding parameters", *IEEE Transactions on Power Delivery*, vol. 5, no. 1, pp. 212–219, January 1990.

[79] C. Bengtsson, "Status and trends in transformer monitoring", *IEEE Transactions on Power Delivery*, vol. 11, no. 3, pp. 1379–1384, July 1996.

[80] N. Prabhakar, V. Kamaraju and B. P. Singh, "Sensitivity analysis of the power transformer windings by transfer function method", *Proc. 10th International Symposium on High Voltage Engineering*, Montréal, 25–29 August 1997.

[81] B. Bak-Jensen and E. Ritchie, "Diagnostic methods and condition monitoring of broken rotor bars, voltage transformers and zinc-oxide arresters", *IEEE International Symposium on Diagnostics for Electrical Machines, Power Electronics and Drives*, Carry-le-Rouet, France, pp. 211–217, 1997.

[82] P. A. Lynn, *An Introduction to the Analysis and Processing of Signals.* Macmillan Publishers Ltd., London, 2nd ed., 1986, ISBN 0-333-34030-2.

[83] S. M. Kay, *Modern Spectral Estimation.* Prentice-Hall, Inc., 1987, ISBN 0-13-598582-X.

[84] C. C. Brozio, J. J. Germishuizen, H. J. Vermeulen and K. J. Cornelissen, "Comparison of excitation methods for power transformer frequency response measurements", *Proc. 7th South African Universities Power Engineering Conference*, Stellenbosch, South Africa, pp. 85–88, 20–21 January 1998.

[85] C. C. Brozio, J. J. Germishuizen and H. J. Vermeulen, "Evaluation of excitation methods for power transformer frequency response measurements", *Proc. 33rd Universities Power Engineering Conference*, Edinburgh, pp. 298–301, 8–10 September 1998.

[86] C. C. Brozio, H. J. Vermeulen and K. J. Cornelissen, "Power transformer frequency response measurement using pseudo-random binary sequence excitation", *Proc. 32nd Universities Power Engineering Conference*, Manchester, pp. 121–124, 10–12 September 1997.

[87] L. Scheltinga and P. T. M. Vaessen, "Digital measurement system for high-voltage impulse tests on transformers", *European Transactions on Electrical Power Engineering*, vol. 2, no. 2, pp. 111–116, March 1992.

[88] J. J. Germishuizen, *Transformer Frequency Response Measurement using Impulse Excitation*, B. Eng. Final-year Project Report, Department of Electrical and Electronic Engineering, University of Stellenbosch, South Africa, November 1997.

[89] W. D. T. Davies, *System Identification for Self-Adaptive Control.* Wiley-Interscience, John Wiley & Sons Ltd., 1970, ISBN 0-471-19885-4.

[90] K. J. Cornelissen, *A Programmable Pseudo-Random Binary Sequence Perturbation Source for* In Situ *Parameter Estimation Applications*, Master's thesis, Department of Electrical and Electronic Engineering, University of Stellenbosch, South Africa, December 1987.

[91] J. van Rooijen and H. J. Vermeulen, "A perturbation source for *in situ* parameter estimation applications", *Proc. International Conference on Industrial Electronics and Instrumentation*, Bologna, Italy, pp. 1819–1823, 5–9 September 1994.

[92] K. J. Cornelissen, C. C. Brozio and H. J. Vermeulen, "A programmable pseudo-random binary sequence generator for system identification applications", *Proc. 32nd Universities Power Engineering Conference*, Manchester, pp. 742–745, 10–12 September 1997.

[93] L. H. Koopmans, *The Spectral Analysis of Time Series.* Academic Press, New York, 1974, ISBN 0-12-419250-5.

[94] H. J. Vermeulen, *Wideband Modelling and* In Situ *Parameter Estimation of a Capacitive Voltage Transformer with Nonlinear Damping*, Ph.D. thesis, Department of Electrical and Electronic Engineering, University of Stellenbosch, South Africa, December 1995.

[95] G. Funk and T. Hantel, "Frequenzabhängigkeit der Betriebsmittel von Drehstromnetzen", *ETZ Archiv*, vol. 9, no. 11, pp. 349–356, November 1987.

[96] P. I. Fergestad and T. Henriksen, "Transient oscillations in multiwinding transformers", *IEEE Transactions on Power Apparatus and Systems*, vol. 93, pp. 500–509, 1974.

[97] P. A. Abetti and F. J. Maginniss, "Fundamental oscillations of coils and windings", *AIEE Transactions*, vol. 73, Part III-A, pp. 1–10, February 1954.

[98] P. A. Abetti and F. J. Maginniss, "Natural frequencies of coils and windings determined by equivalent circuit", *AIEE Transactions*, vol. 72, Part III, pp. 495–504, June 1953.

[99] L. O. Chua and P. Lin, *Computer-Aided Analysis of Electronic Circuits: Algorithms & Computational Techniques.* Prentice-Hall, Inc., Englewood Cliffs, New Jersey, 1975, ISBN 0-13-165415-2.

[100] M. A. Branch and A. Grace, MATLAB *Optimization Toolbox.* The MathWorks, Inc., 24 Prime Park Way, Natick, MA 01760-1500, 1990.

[101] S. Wolfram, *Mathematica, A System for Doing Mathematics by Computer.* Addison-Wesley Publishing Company, Inc., 1988, ISBN 0-201-19334-5.

[102] C. C. Brozio and H. J. Vermeulen, "Computer-aided formulation of network equations in symbolic format, Part I: Network functions", *Proc. 7th South African Universities Power Engineering Conference*, Stellenbosch, South Africa, pp. 93–96, 20–21 January 1998.

[103] H. J. Vermeulen and C. C. Brozio, "Computer-aided formulation of network equations in symbolic format, Part II: State-space representation", *Proc. 7th South African Universities Power Engineering Conference*, Stellenbosch, South Africa, pp. 97–100, 20–21 January 1998.

[104] G. E. Alderson and P. M. Lin, "Computer generation of symbolic network functions – a new theory and implementation", *IEEE Transactions on Circuit Theory*, vol. CT–20, no. 1, pp. 48–56, January 1973.

[105] J. E. Dennis, Jr. and R. B. Schnabel, *Numerical Methods for Unconstrained Optimization and Nonlinear Equations.* Prentice-Hall, Inc., Englewood Cliffs, New Jersey, 1983, ISBN 0-13-627216-9.

[106] L. E. Scales, *Introduction to Non-Linear Optimization.* Macmillan Publishers Ltd., London, 1985, ISBN 0-333-32553-2.

[107] G. L. Nemhauser, A. H. G. Rinnooy Kan and M. J. Todd (Eds.), *Optimization*. Elsevier Science Publishers B.V., Amsterdam, 1989, ISBN 0-444-87284-1.

[108] The MathWorks, Inc., 24 Prime Park Way, Natick, MA 01760-1500, MATLAB *Control System Toolbox*, 1993.

[109] Canadian/American EMTP User Group, Portland, Oregon, *Alternative Transients Program (ATP) Rule Book*, 1995.

[110] The MathWorks, Inc., 24 Prime Park Way, Natick, MA 01760-1500, MATLAB *Symbolic Math Toolbox*, 1994.

[111] Borland International, 1800 Green Hills Road, Scotts Valley, CA 95066-0001, *Turbo Pascal Version 5.0 Users' Guide*, 1988.